Quantitative systems pharmacology modeling of biotherapeutics in oncology

Betts, A.M.

Quantitative systems pharmacology modeling of biotherapeutics in oncology

Alison M. Betts

Cover design: Edgar Stewart Design & Illustration, Concord MA 01742

Printing: Alpha Graphics, Concord MA, U.S.A

ISBN: 978-0-578-89120-0

Quantitative systems pharmacology modeling of biotherapeutics in oncology

Proefschrift

Ter verkrijging van de graad van Doctor aan de Universiteit Leiden,

op gezag van Rector Magnificus prof. dr. ir. H. Bijl,

volgens besluit van het College voor Promoties

te verdedigen op 3 juni 2021

klokke 15:00 uur

Door

Alison Mary Betts

Geboren te Edinburgh, Scotland

Op 4 juli 1972

Promotores:

Prof. dr. P.H. van der Graaf

Prof. dr. J. Burggraaf

Promotiecommissie:

Prof. dr. H. Irth, voorzitter

Prof. dr. J.A. Bouwstra, secretaris

Prof. dr. C. Kloft, University of Berlin

Prof. dr. J.P. Balthasar, University at Buffalo, The State University of New York

Prof. dr. A.D.R. Huitema, Netherlands Cancer Institute

Dr. J.G.C. van Hasselt

The research described in this thesis was performed at Pfizer Worldwide Research & Development, Groton CT, and Cambridge MA, USA.
Publication of this thesis was financially supported by Pfizer, Inc. and Applied BioMath, LLC, Concord MA 01742.

Table of contents

Section I.
Introduction to translational modeling in oncology

Chapter 1

Introduction and scope

1.1 Challenges in oncology drug development

Significant advances have been made in the treatment of cancer in the past decades, with a shift away from cytotoxic drugs, towards more targeted therapies, immune-oncology drugs, cancer vaccines and cell-based treatments. Groundbreaking new therapies have been identified, with a myriad of potential combination therapies possible. Some 50 years since 'the war on cancer' was declared, these are enabling a different era in cancer treatment with declines in mortality and morbidity, less side effects and talk of chronic treatments [1]. Despite these advances, the success rate of oncology drug development remains the lowest among all the therapeutic areas [2] with an overall success rate of only 3.4%, mainly driven by failure in Phase 2 [2].

There are multiple reasons why oncology drug discovery and development are so difficult. First, cancer is an exceptionally heterogeneous and adaptable disease, with massive variability between tumors and within a tumor. At the molecular level, it is likely that no two cancers are identical. In treating cancer, we are therefore treating a multitude of different diseases [1]. This is exacerbated by the fact that patients are entering trials heavily pre-treated with high potential for drug resistance. A 'one size fit all' approach will not work in cancer treatment. Secondly, it is difficult to translate from preclinical data to the clinic to predict efficacy and toxicity [3]. Until recently, efficacy was assumed to be dose related and clinicians would push cancer drugs to the maximum tolerated dose (MTD) in clinical development, which was subsequently defined as the efficacious dose [3]. This assumption may have been possible for small molecule drugs but is much less appropriate for biotherapeutics. The trade-off between efficacy and toxicity has almost always been resolved in the clinic and remains a large source of drug failure.

The workhorse preclinical model in oncology is the mouse xenograft model, which comprises subcutaneous implantation of a human cell line or tumor into immune compromised host mice [4]. The xenograft model represents extreme simplification of human cancer, as it does not account for complexities of tumor metastasis, host immunity, tumor heterogeneity, and the development of treatment resistance that is routinely observed in cancer patients [5]. However, the drug exposure response relationship derived from these models is useful for understanding efficacy and if accompanied by rigorous quantitative analysis such as mathematical modeling, can be used to translate from mouse to human to predict clinical anti-tumor response [6, 7]. Clinically translatable biomarkers are another useful tool likely to improve preclinical to clinical translation, and advances in experimental techniques has made these easier to measure. However, often the biomarkers need to be measured kinetically in tumor tissue, necessitating tumor biopsies from patients, which are still not common path. In vitro to in vivo correlation is thought to be poor, which means that in vitro assays are typically only used for drug screening. A rigorous unifying preclinical to clinical translational framework could facilitate oncology clinical development by better identifying translational strategies, patient selection criteria and appropriate biomarkers to measure [3].

1.2 Biotherapeutic modalities used to treat cancer

Large molecule biotherapeutics in oncology are enabling tumor targeting, activation and re-targeting of the immune system to kill cancer cells, and stimulation of separate immunomodulatory pathways from one molecule. However, the versatility of these molecules brings with it an additional level of complexity, with intricate mechanisms of action and concentration response relationships that are non-intuitive and difficult to predict. In this thesis, different types of biotherapeutic drugs are discussed including monoclonal antibodies (mAbs), antibody drug conjugates (ADCs), T-cell engagers (TCEs) and other bispecific antibodies (bsAbs)- see Figure 1. mAbs have formed the backbone of many successful biotherapeutic modalities for the treatment of cancer. Monospecific mAbs have been used to target specific tumor receptors such as HER-2 and CD20 to inhibit signaling and/or trigger antibody dependent cellular toxicity (ADCC) [8]. This has resulted in first generation mAb drugs in oncology such as trastuzumab and rituximab. More recently, mAbs have been used to target immune checkpoint receptors such as CTLA4 and PD1 on T cells, releasing negative immune regulation of the tumor [9]. This has led to revolutionary new immunotherapy treatments including ipilimumab and pembrolizumab. Although undoubtedly a breakthrough in cancer treatment, immunotherapy still only works well in a minority of patients and for certain cancer types [9]. ADCs are a targeted therapy for cancer treatment, combining a specific mAb to a tumor antigen linked to a potent cytotoxic agent [10]. They make use of the specific binding properties of the antibody to deliver a cytotoxic payload to cancer cells for increased efficacy, whilst minimizing exposure of normal tissues. Brentuximab-vedotin and ado-trastuzumab-emtansine are examples of ADCs on the market for oncology indications. T cell retargeting molecules are bispecific antibodies, or antibody fragments, that bind to CD3 on the surface of T cells and to a tumor associated antigen (TAA) on the tumor cell surface [11]. When both CD3 and the TAA are engaged, the proximity of the T cell and tumor cell results in the formation of an immune synapse, stimulation of the T cell and 'redirection' of cytotoxic activity against the tumor cells. Blinatumomab is a CD19 x CD3 bispecific T cell engager that has received regulatory approval. A second wave of bsAbs are emerging, with tumor selective recruitment and activation of T cells, or more powerful immunomodulation by targeting two distinct immunomodulatory pathways [12].

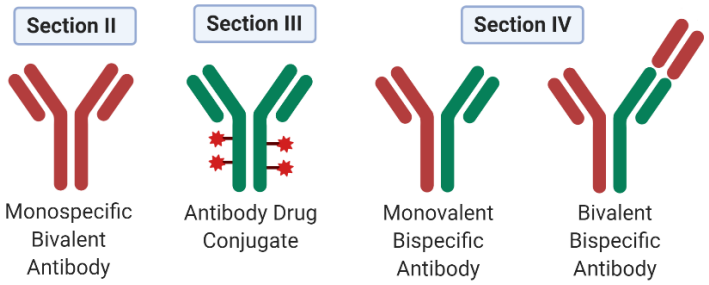

Figure 1: Biotherapeutic drug modalities discussed in different sections of this thesis.

1.3 Mathematical modeling in oncology drug development

To overcome the challenges in oncology drug discovery and development, and to deconvolve the complexities of novel biotherapeutic modalities, innovative approaches are needed. Mathematical modeling is a key tool which has been shown to increase efficiency and effectiveness in drug discovery and development and can be used to facilitate design, selection and preclinical to clinical translation of oncology therapies and to optimize clinical trials [13]. Mathematical modeling can be used to integrate data from disparate sources including literature, preclinical experimental data, and clinical data, to examine the relationships between a drug, the biological system, and the disease process. A quantitative framework is assembled which can provide mechanistic understanding of drug function, enabling optimal experimental design and faster data interpretation. The model framework can be used at early stages to aid in the identification of optimal drug properties for next generation molecules, including optimal target, epitopes, and drug format. Once a lead compound has been selected, the model can be used to translate from preclinical in vitro and in vivo studies to the clinic, to inform clinical study design including prediction of clinical starting dose, efficacious dose, and regimen.

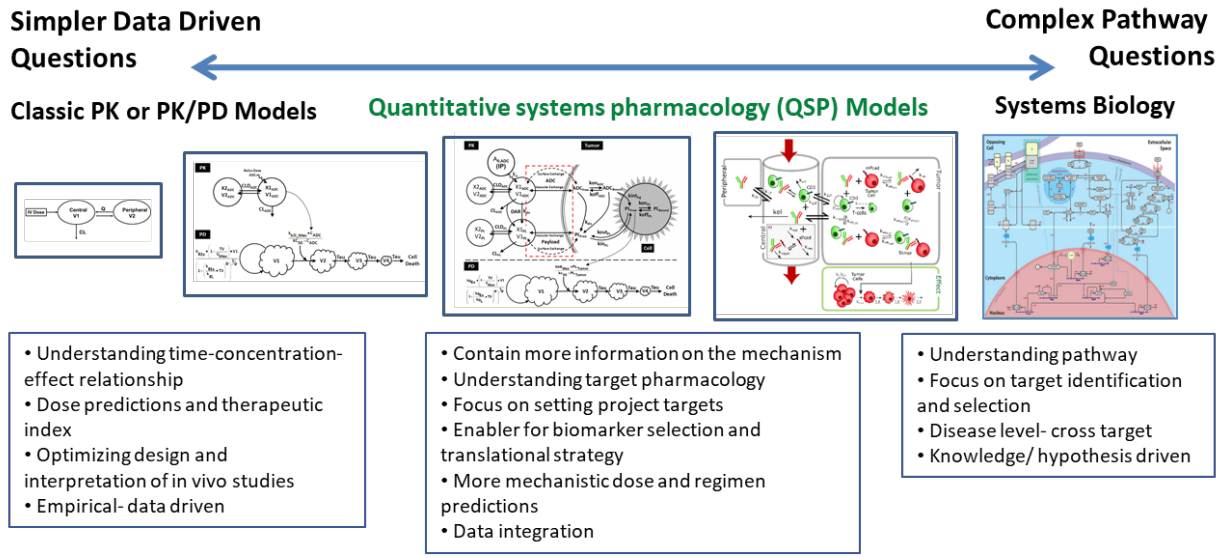

Figure 2: The continuum of mathematical models utilized in drug discovery and development. In this thesis PK, PK/PD and quantitative systems pharmacology models are used, depending on the questions asked and the objective of the modeling. Systems biology modeling was not in the scope of this thesis.

1.4 Scope of this thesis

The aim of this work was to investigate different ways in which mechanistic mathematical modeling and simulation can be used to help with quantitative decision making in oncology drug discovery and development. **Section I** introduces the thesis and its scope. **Section II** focuses on modeling of mAbs, **Section III** on ADCs and **Section IV** on bispecific antibodies. Conclusions and further perspectives are discussed in **Section V**.

Different levels of mathematical modeling were used depending on the questions asked and are introduced in **Chapter 1** (Figure 2). For example, a more statistical population-pharmacokinetic (pop-PK) modeling approach was used for analysis of a large mAb PK dataset with quantitation of variability (**Chapter 2**). Pharmacokinetic/ pharmacodynamic (PK/PD) modeling was used for data driven interpolation of in vitro and in vivo datasets with limited extrapolation (**Chapters 3 & 4**). Quantitative systems pharmacology (QSP) modeling was used to answer more complex mechanistic questions, involving integration of data from disparate sources (literature, in vitro, in vivo and the clinic), linkage of drug pharmacology to biological systems and disease, and multi-scale predictions (**Chapters 4, 5, 6 & 7**).

The scope of this work extends from early drug discovery through to clinical trials, and includes use of modeling and simulation to influence:

- Hypothesis testing
- Interpretation of large datasets to simplify processes, and to avoid unnecessary in vivo studies
- Establishment of in vitro to in vivo correlations
- Preclinical to clinical translational strategies to predict PK and PD
- Competitor differentiation, to ensure that therapeutically beneficial molecules are progressed to clinical studies
- Prediction of optimal clinical doses and regimens
- Precision medicine approaches, including identification of sensitive parameters impacting dose in patients, which could be used as clinical diagnostics and/or to select the optimal patient population.

1.5 Outline of this thesis

In **Chapter 1**, the challenges of oncology drug development are introduced, along with the increasingly diverse array of biotherapeutic modalities being developed to treat cancer. The role of mathematical modeling in the process is discussed.

In **Chapter 2**, pop-PK modeling was used for a meta-analysis of the linear PK of mAbs across different species used in the pharmaceutical industry. This work indicated that linear PK of therapeutic mAbs can be considered a class property, with a typical set of parameters identified across species, with similar values to endogenous IgG. Strategies are presented for predicting linear PK of mAbs with less reliance on cynomolgus monkeys and use of smaller animal or in silico alternatives.

In **Chapter 3**, in vitro to in vivo correlation (IVIVC) was established for ADCs using a PK/PD modeling approach. A comparable efficacy parameter, tumor static concentration (TSC), was derived for in vitro and in vivo experiments and a predictive correlation determined. The methodology established here could potentially be applied to all anti-cancer drugs (large and small molecules). This work has many applications including early triage of ADCs, prevention of unnecessary in vivo studies and saving of resources.

In **Chapter 4,** a PK/PD modeling approach was used for quantitative comparison of a new generation HER2 ADC (PF-06804103) with trastuzumab-DM1 (T-DM1), to ensure efficacy differentiation and as a rationale to pursue clinical development of PF-06804103. This included comparison of TSC values across a range of in vivo tumor models, representing different disease origins (breast, gastric and lung), clinical pathologies such as low-high HER2 expression and resistance to T-DM1. A mechanistic model was developed to describe non-linearity in T-DM1 PK in patients due to binding to shed HER2. A similar model was then used to predict clinical PK for PF-06804103. A translational strategy was proposed to predict clinical efficacy in patients.

In **Chapter 5**, a translational QSP model for ADCs is presented, which was used for preclinical clinical translation of inotuzumab-ozogamicin, a CD22 targeting ADC for the treatment of B cell malignancies. The model predicted progression free survival responses for inotuzumab versus non-Hodgkin's Lymphoma (NHL) that were comparable to observed clinical trial results, demonstrating its utility for predicting efficacy of ADCs. The model was also able to give useful mechanistic insight into optimal dosing regimens and sensitive parameters impacting outcome. This knowledge could be applied to optimize the design of ADCs in the discovery phase of research and/or for selection of predictive diagnostic in the clinic.

In **Chapter 6**, a translational QSP model for T cell retargeting CD3 bsAbs is presented. This model predicts trimolecular complex formation between drug, T cell and tumor cells required to form an immune synapse, which triggers T cell activation and cytotoxicity. The model was used to characterize the PK/PD relationship in mouse tumor models and translated to the clinic to predict clinical efficacious dose. Notably, this model can also be applied at early stages to aid in CD3 bsAb design and candidate selection.

In **Chapter 7**, as a means of a general conclusion to this investigation, mechanistic quantitative pharmacology strategies for the early clinical development of bispecific antibodies (bsAbs) in oncology is presented. This includes use of modeling to understand complexities of bsAbs, impact decision making and aid in clinical translation, trial design, and prediction of regimens and strategies to reduce dose limiting toxicities. BsAbs are an integral component of the current therapeutic research strategy in oncology and explorative preclinical and emerging clinical data indicate potential for enhanced efficacy and reduced systemic toxicity. The strategies discussed could be powerful tools to facilitate clinical success of bsAbs, while decreasing time required for non-clinical development.

References

1. Kamb, A., S. Wee, and C. Lengauer, *Why is cancer drug discovery so difficult?* Nature Reviews Drug Discovery, 2007. **6**(2): p. 115-120.
2. Wong, C.H., K.W. Siah, and A.W. Lo, *Estimation of clinical trial success rates and related parameters.* Biostatistics (Oxford, England), 2019. **20**(2): p. 273-286.
3. Zhu, A.Z., *Quantitative translational modeling to facilitate preclinical to clinical efficacy & toxicity translation in oncology.* Future science OA, 2018. **4**(5): p. FSO306-FSO306.
4. Jung, J., *Human tumor xenograft models for preclinical assessment of anticancer drug development.* Toxicological research, 2014. **30**(1): p. 1-5.

5. Sausville, E.A. and A.M. Burger, *Contributions of Human Tumor Xenografts to Anticancer Drug Development.* Cancer Research, 2006. **66**(7): p. 3351.
6. Rocchetti, M., et al., *Predicting the active doses in humans from animal studies: A novel approach in oncology.* European Journal of Cancer, 2007. **43**(12): p. 1862-1868.
7. Wong, H., et al., *Antitumor Activity of Targeted and Cytotoxic Agents in Murine Subcutaneous Tumor Models Correlates with Clinical Response.* Clinical Cancer Research, 2012. **18**(14): p. 3846.
8. Scott, A.M., J.D. Wolchok, and L.J. Old, *Antibody therapy of cancer.* Nature Reviews Cancer, 2012. **12**(4): p. 278-287.
9. Farkona, S., E.P. Diamandis, and I.M. Blasutig, *Cancer immunotherapy: the beginning of the end of cancer?* BMC medicine, 2016. **14**: p. 73-73.
10. Lambert, J.M. and C.Q. Morris, *Antibody-Drug Conjugates (ADCs) for Personalized Treatment of Solid Tumors: A Review.* Advances in therapy, 2017. **34**(5): p. 1015-1035.
11. Ellerman, D., *Bispecific T-cell engagers: Towards understanding variables influencing the in vitro potency and tumor selectivity and their modulation to enhance their efficacy and safety.* Methods, 2019. **154**: p. 102-117.
12. Dahlén, E., N. Veitonmäki, and P. Norlén, *Bispecific antibodies in cancer immunotherapy.* Therapeutic advances in vaccines and immunotherapy, 2018. **6**(1): p. 3-17.
13. Venkatakrishnan, K., et al., *Optimizing oncology therapeutics through quantitative translational and clinical pharmacology: challenges and opportunities.* Clin Pharmacol Ther, 2015. **97**(1): p. 37-54.

Section II.
Modeling of monoclonal antibodies

Chapter 2

Linear pharmacokinetic parameters for monoclonal antibodies are similar within a species and across different pharmacological targets:

A comparison between human, cynomolgus monkey and hFcRn Tg32 transgenic mouse using a population-modeling approach

Alison Betts, Anne Keunecke, Tamara J. van Steeg, Piet H. van der Graaf, Lindsay B. Avery, Hannah Jones, and Jan Berkhout

MAbs 10(5): 751-64 (2018).

2.1 Abstract

The linear pharmacokinetics (PK) of therapeutic monoclonal antibodies (mAbs) can be considered a class property with values similar to endogenous IgG. Knowledge of these parameters across species could be used to avoid unnecessary *in vivo* PK studies and to enable early PK predictions and pharmacokinetic/pharmacodynamic (PK/PD) simulations. In this work, population-pharmacokinetic (popPK) modeling was used to determine a single set of 'typical' popPK parameters describing the linear PK of mAbs in human, cynomolgus monkey and transgenic mice expressing the human neonatal Fc receptor (hFcRn Tg32), using a rich dataset of 27 mAbs. Non-linear PK was excluded from the datasets and a 2-compartment model was applied to describe mAb disposition. Typical human popPK estimates compared well with data from comparator mAbs with linear PK in the clinic. Outliers with higher than typical clearance were found to have non-specific interactions in an AC-SINS self-association assay, offering a potential tool to screen out these mAbs at an early stage. Translational strategies were investigated for prediction of human linear PK of mAbs, including the use of (1) typical human popPK parameters and (2) allometric exponents from cynomolgus monkey and Tg32 mouse. Each method gave a good prediction of human PK with parameters predicted within 2-fold. These strategies offer alternative options to the use of cynomolgus monkeys for human PK predictions of linear mAbs, based on *in silico* methods (typical human popPK parameters) or using a rodent species (Tg32 mouse) and call into question the value of completing extensive *in vivo* preclinical PK to inform linear mAb PK.

2.2 Introduction

Therapeutic antibodies have come of age as an important class of drugs with over 40 antibody-based therapies approved by the US FDA across multiple indications and many more in clinical trials [1]. Advances in antibody engineering have enabled rapid progress from the first generation of highly immunogenic murine and chimeric antibodies to better tolerated humanized and fully human mAbs. Recently, the variety of antibody-like modalities has evolved further to include Fc-fusion proteins, antibody drug conjugates and bi-specific antibody products. In addition to their exquisite specificity and potency, mAbs are successful therapeutics due to their long pharmacokinetic (PK) half-life [2]. Low clearance of mAbs from the systemic circulation enables them to be administered less frequently than their peptide or small molecule counterparts, which is more convenient for the treatment of chronic diseases.

The PK properties of mAbs are a function of their large size (150kDa), relative polarity, Fc-receptor binding, and specific binding to target antigens. The primary elimination route for mAbs is cellular uptake followed by proteolytic degradation. There are two distinct catabolic pathways for mAbs [3]. The first is a non-specific, linear (first-order) clearance (CL) pathway mediated by fluid-phase pinocytosis or unspecific fluid-phase endocytosis [2]. This common pathway shared by endogenous IgG and therapeutic mAbs operates independently of the specific interaction between a mAb and its pharmacological target. This pathway is not easily saturated at therapeutic doses, and tends to result in linear CL. FcRn functions as a salvage receptor to protect IgG from rapid intracellular catabolism, and is responsible for the long half-life of endogenous IgG and exogenous IgG based therapeutic proteins [4].

The second catabolic pathway is a non-linear (target mediated) CL pathway mediated by the specific interaction between the Fab region of the antibody and its pharmacological target. This pathway is often referred to as target mediated drug disposition (TMDD). Following binding of the mAb to its target on the cell surface, the mAb-antigen complex is internalized and then trafficked via the endosomes to the lysosomes where the complex is degraded. When the target binding is saturated, the relative importance of target binding to overall disposition is diminished and mAb is eliminated by first order process [2]. For mAbs exhibiting this pathway, disposition depends upon the concentration and distribution of the mAb, along with target receptor expression, internalization and turnover rates [5]. Certain mAbs to soluble targets can also undergo TMDD driven by binding of 2 or more mAbs to form multimeric complexes which are rapidly eliminated by phagocytosis. mAbs cleared primarily by TMDD will have dose dependent non-linear elimination. For these mAbs, PK is distinctly different from the catabolism of endogenous IgG, with higher CL and shorter half-life values at lower doses.

The rate and extent of mAb distribution is very slow and depends upon extravasation in tissue, distribution within the particular tissue, and degradation. The convective CL of mAbs from the tissue is thought to be more efficient than the process of convective extravasation, thereby maintaining relatively low mAb concentrations in the interstitial fluid [6, 7]. As a result of this mAbs often have small apparent volumes of distribution [8, 9].

The ability to predict the PK of a drug prior to first in human studies is of utmost importance to reduce attrition in Phase 1. Preclinical testing of mAbs often occurs in a rodent species and non-human primate (NHP) to understand efficacy and toxicity prior to human dosing. Cynomolgus monkey is the preferred strain of NHP for preclinical PK and toxicological studies due to a high genetic similarity with humans and therefore greater likelihood of target antigen sequence homology, comparable binding affinities for cynomolgus monkey vs human FcRn [10], and similar tissue cross reactivity profiles. Cynomolgus monkey is also the preferred species for predicting the PK of mAbs with linear CL in humans: several groups have reported the successful use of fixed allometric exponents to predict CL and volume of distribution of mAbs in human from data in cynomolgus monkey [11-14]. For mAbs which exhibit non-linear CL due to TMDD, scaling of PK is more challenging. In order to take into account the kinetics of mAb binding to its target a mechanistic TMDD model is required, with proper exploration of species differences in target expression and binding [5, 15-17].

In this study, the objective was to complete a comprehensive analysis of the linear PK of therapeutic mAbs using popPK methods. The dataset was composed of 27 Pfizer mAbs where PK had been generated in at least one of three species: human, cynomolgus monkeys and human FcRn Tg32 homozygous transgenic mice. Given that the linear, Fc-mediated elimination is a common pathway shared by both endogenous IgG and therapeutic IgG of mAbs, it was theorized that a single set of ‘typical’ linear PK parameters could be estimated for each species, describing the linear PK of all mAbs in the dataset. PopPK is an ideal technique to investigate this as it can separately estimate variability, including variability between mAbs, between individuals in a given mAb dataset and also random, non-specific error [18]. The resulting ‘typical’ linear PK parameter estimates could be used for designing PK/PD and toxicology studies, dose predictions and viability assessments. For tractable mAbs with linear PK in preclinical species it could forfeit

the requirement for allometric scaling for clinical PK predictions: instead, the typical PK parameters could be used as a substitute until clinical PK is obtained. In addition to cynomolgus monkey, we also studied the potential of a human FcRn Tg32 transgenic mouse model to predict linear PK of mAbs in human. The availability of a rodent model to accurately estimate human PK of mAbs, would enable earlier predictions before cynomolgus monkey data is routinely available. In addition to the single species analysis, a combined analysis was performed on the entire dataset of human, cynomolgus monkey and hFcRn Tg32 transgenic mice and used to estimate allometric coefficients between species. While our primary focus was to explore PK predictions utilizing a variety of species, we also investigated the value of an in vitro assay measuring self-association in predicting the CL of mAbs in the dataset. The analysis herein provides robust strategies for predicting linear human PK of mAbs which could improve throughput for lead drug candidate selection, and potentially increase the overall success while decreasing the time for non-clinical development of mAbs.

2.3 Results

mAb PK dataset and selection of linear dose range

Properties of the mAbs included in this study are summarized in Table 1. Of the 27 mAbs analyzed, 12 were IgG1 and 15 were IgG2; 16 were specific for soluble ligand targets, 9 bound to membrane targets and 2 had both membrane and soluble targets; 16 of the mAbs were fully human, 10 were humanized and 1 was from a human phage display library. All of the mAbs had similar binding Kd values to FcRn and had wild type sequences for the FcRn binding region. For 18 of these mAbs there was clinical PK data available, for 23 mAbs there was cynomolgus monkey PK data and 11 mAbs had PK in hFcRn Tg32 transgenic mouse. As discussed in the materials and methods section, non-linear data was removed from the dataset to enable analysis of linear PK only. This was completed via a combination of visual inspection and application of an algorithm applied to a linear regression of dose and AUC to test for deviation of the slope from 1 (Figure 1). Following removal of non-linear data, the remaining linear dose range and number of dose levels included in the popPK analysis for each mAb are summarized in Table 1.

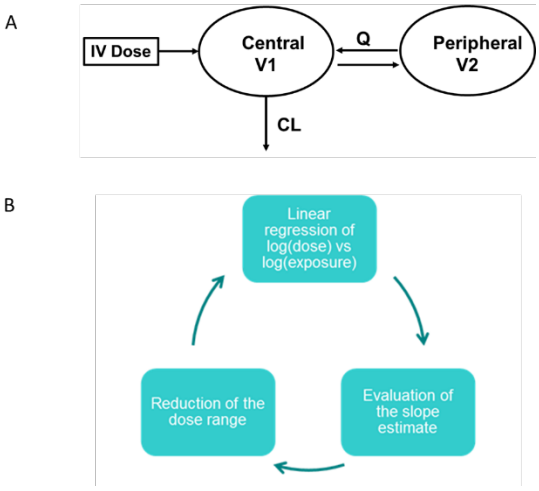

Figure 1: (a) 2-compartment PK model and (b) algorithm to test for linearity of PK data

Table 1: Monoclonal antibodies in this study

mAb number	Ig type	Human or Humanized	Type of mAb target	AC-SINS	Species	Linear dose range (mg/kg)	Dose levels excluded (mg/kg)	Dose levels included
mAb1	IgG2	Human	membrane bound	-	C	2	None	1
mAb2	IgG2	Humanized	soluble	-	C	10- 100	None	3
mAb3	IgG2	Humanized	soluble	3	C, M	1-10, 5	None, None	2, 1
mAb4	IgG2	Human	membrane bound	-	C	1-10	0.01- 0.3	2
mAb5	IgG2	Human	membrane bound	-	H, C	1-15, 5-50	0.5, None	8, 2
mAb6	IgG2	Human	membrane bound	-	H	0.1-15	None	6
mAb7	IgG2	Human	membrane bound	-	H, C	0.2-20, 30-100	None, 3-5	8, 2
mAb8	IgG1	Human	membrane bound	-	C	3-30	0.3	2
mAb9	IgG1	Humanized	soluble	-	H, C	1.5-5, 1-10	0.5, None	2, 2
mAb10	IgG2	Humanized	soluble	-	H, C	1-24, 1-100	0.3, 0.1	6, 3
mAb11	IgG2	Human	soluble	-	C	1- 5	None	2
mAb12	IgG1	Human	soluble	-	H, C	5-600, 2	None	6, 1
mAb13	IgG1	Synthetic	soluble	-	C	2	None	1
mAb14	IgG2	Humanized	soluble	-	H, C	1-18, 3-100	0.3, 0.1-0.3	6, 3
mAb15	IgG2	Humanized	soluble	-	H	1-6	None	3
mAb16	IgG2	Humanized	soluble	-	H, C	0.1-10, 0.8- 16.5	0.01- 0.03, None	4, 3
mAb17	IgG2	Humanized	soluble	-	H, C	1-10, 10-200	0.1- 0.3, None	4, 3
mAb18	IgG1	Human	membrane bound	24	H, C, M	30-120mg, 2-10, 5	None, None, None	3, 2, 1
mAb19	IgG1	Human	membrane bound	17	H, C, M	1-8, 0.5-5, 5	0.5, None, None	4, 2, 1
mAb20	IgG2	Human	membrane bound & sol	0	H, C, M	0.3-10, 1-100, 5	0.03- 0.1, None, None	3, 3, 1
mAb21	IgG1	Human	membrane bound & sol	6	H, C, M	10-800mg, 10-100, 5	1- 3mg, None, None	4, 2, 1
mAb22	IgG2	Human	soluble	1	H, C, M	22-700mg, 0.5-5	7mg, None, None	6, 2
mAb23	IgG1	Humanized	soluble	0	H, C, M	3, 1-100, 5	None, None, None	1, 2, 1
mAb24	IgG1	Humanized	soluble	1	H, C, M	3, 1-100, 5	None, None, None	1, 2, 1
mAb25	IgG1	Human	soluble	10	H, C, M	0.3- 11.25, 50, 5	None, None, None	5, 1, 1
mAb26	IgG1	Human	membrane bound	21	M	5	None	1
mAb27	IgG1	Human	soluble	2	M	5	None	1

H: human, C: cynomolgus monkey, M: Tg32 mouse

Population PK analysis across species

The concentration versus time relationships in Tg32 mouse, cynomolgus monkey, and human mAb datasets were described using a 2-compartmental PK model (Figure 1) with inter-individual variability (IIV) on CL and volume of the central compartment (V1). Residual error was determined per compound and covariance was estimated between CL and V1. This model

adequately captured the PK of all compounds in each species. The PK data for the mAbs in each dataset could be described using a single set of popPK parameters. The parameter estimates for each species are shown in Table 2, with 95% confidence intervals. The popPK estimate of human CL (0.15 mL/h/kg (0.14-0.16)) was in the same range as the CL of endogenous IgG (0.125 mL/h/kg).[19, 20] CL was lowest in humans (0.15 mL/h/kg (0.14-0.16)), followed by cynomolgus monkey (0.27 mL/h/kg (0.24-0.30)) and then Tg32 mouse (0.35 mL/h/kg (0.28- 0.41)). Population estimates of the volumes of distribution in the central (V1) and peripheral (V2) compartments were typically small and approximated plasma volume. The inter-compartmental clearance parameter, Q, varied the most across species and was estimated to be 0.27 mL/h/kg (0.25- 0.30) in human, 1.00 mL/h/kg (0.8-1.20) in cynomolgus monkey and 4.40 mL/h/kg (3.17- 5.62) in Tg32 mouse. Inter-individual variability in V1 was low and moderate-high for CL, which may be expected from the methodology chosen in which PK parameters were estimated for all compounds combined, instead of estimating separate parameters for each compound. Covariance between CL and V1 was low, representing low correlation between the random effects on the parameter estimates. The relative standard error (RSE) was lower than 35% for all parameters representing low uncertainty in parameter estimation.

Results from a jackknife analysis showed consistent estimation of PK parameters without significant influence from removal of one mAb from the dataset at a time. PK parameters from the jackknife analysis with 95% confidence intervals are shown in Supplementary Figure 1. Residual error per compound and diagnostic plots of observed concentration versus individual and population predictions in each species are included in Supplementary Tables 1 and 2 and Supplementary Figures 2 and 3.

Distribution of clearance and volume of distribution of the central compartment

The distribution of CL estimates and the individual estimates of CL (with IIV) for each mAb across species are shown in Figure 2. This plot shows a typical log normal distribution of individual CL estimates. In general CL is lowest in human, followed by cynomolgus monkey and then Tg32 mouse. The distribution of population and individual estimates of V1 for each mAb across species are shown in Figure 3. The estimates of V1 are normally distributed in cynomolgus monkey and human and center on plasma volume (30- 50 mL/kg). Note, more variability was observed in individual estimates of V1 in Tg32 mouse compared with cynomolgus monkey or human. This may have been due to restricted time points in the initial phase of PK sample collection in Tg32 mouse.

Comparison of human population PK parameter estimates with population PK of literature mAbs

In order to put the results into context, popPK parameters determined for the current mAb dataset were compared with therapeutic mAbs with linear CL in clinical studies. 5 fully human, humanized, or chimeric therapeutic mAbs were identified with linear CL in humans and 2-compartment popPK analyses published in the literature. Population estimates of CL, Q, V1 and V2 for the Pfizer mAbs and bevacizumab, infliximab (2 different indications), pertuzumab, rituximab and trastuzumab in human are shown in Table 3. The parameter estimates reported

for the comparator clinical mAbs [19] are very close to the population parameter estimates generated from the analysis of 18 clinical mAbs described herein. An outlier was infliximab for ulcerative colitis, which had a reported mean CL of 0.24 mL/h/kg and Q of 4.25 mL/h /kg, which deviates significantly from the population CL estimates of 0.15 mL/h /kg (0.14- 0.16) and Q estimates of 0.27 mL/h /kg (0.25- 0.3), estimated in this analysis. Figure 4 shows the concentration versus time profiles for the median and 95% prediction interval with observed dose-normalized concentration-time data for the 18 clinical mAbs in this study and the 5 clinical therapeutic mAbs (bevacizumab, infliximab, pertuzumab, rituximab and trastuzumab).

Table 2: Single species popPK parameter estimates for mAbs with linear CL

		Human (n=18)		Cynomolgus Monkey (n=23)		Tg32 hFcRn Transgenic Mouse (n=11)	
Parameter	**Unit**	**Value (95%-CI)**	**RSE (%)**	**Value (95%-CI)**	**RSE (%)**	**Value (95%-CI)**	**RSE (%)**
CL	mL/h/kg	0.15 (0.14-0.16)	3.03	0.27 (0.24-0.30)	5.22	0.35 (0.28-0.41)	9.06
V1	mL/kg	46.31 (45.14-47.48)	1.29	39.29 (37.16-41.41)	2.76	59.28 (54.65-63.90)	3.98
Q	mL/h/kg	0.27 (0.25-0.30)	5.12	1.00 (0.80-1.20)	10.33	4.40 (3.17-5.62)	14.24
V2	mL/kg	31.47 (28.63-34.31)	4.60	27.56 (24.83-30.29)	5.05	60.54 (52.80-68.29)	6.53
IIV CL	-	0.48 (0.43-0.53)	5.29	0.38 (0.31-0.46)	9.48	0.41 (0.29-0.53)	15.34
COV CL-V1	-	0.09 (0.07-0.10)	11.48	0.09 (0.05-0.13)	23.28	0.11 (0.04-0.18)	33.55
IIV V1	-	0.09 (0.08-0.11)	6.66	0.10 (0.07-0.13)	14.90	0.12 (0.07-0.18)	23.91

Table 3: Comparison of typical popPK parameter estimates in human with test set of clinical mAbs with linear PK

		Human	Literature clinical mAbs					
Parameter	**Unit**	**Value (95% CI)**	**Bevacizumab**	**Infliximab AS**	**Infliximab UC**	**Pertuzumab**	**Rituximab**	**Trastuzumab**
CL	mL/h/kg	**0.15** (0.14 – 0.16)	0.12	0.16	0.24	0.13	0.15	0.13
V1	mL/kg	**46.31** (45.14 – 47.48)	38.0	43.7	47.0	39.1	42.6	42.1
Q	mL/h/kg	**0.27** (0.25 – 0.3)	0.35	1.02	4.25	0.33	0.39	0.29
V2	mL/kg	**31.47** (28.63 – 34.31)	39.4	42.0	59.0	30.9	52.0	68.4

CL: clearance from the central compartment, **V1:** volume of the central compartment, **Q:** inter-compartment distribution clearance, **V2:** volume of the peripheral compartment. **RSE (%):** relative standard error, calculated as standard error of estimation / estimated value x 100%. **95% CI:** 95% confidence interval calculated from the standard error. **IIV:** inter-individual variability. **COV CL-V1:** covariance between clearance and volume. Residual errors per compound for Table 2 are shown in **Supplementary Table 1**. **AS:** ankylosing spondylitis; **UC:** ulcerative colitis

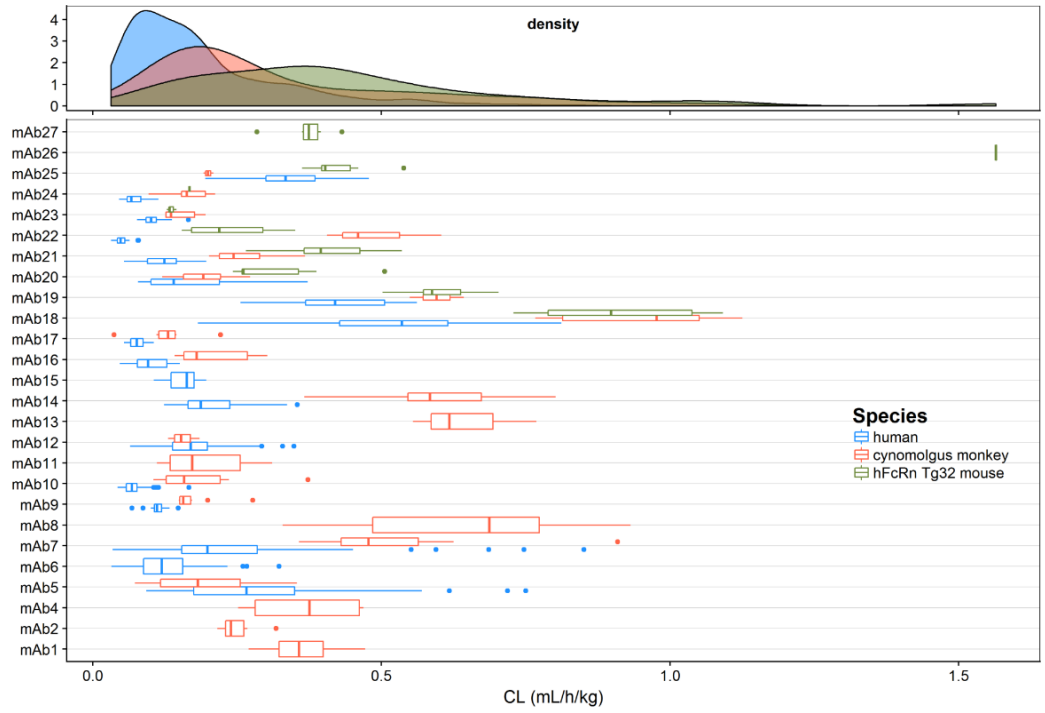

Figure 2: Distribution of population and individual mAb estimates (with variability) of clearance (CL) in the combined human, cynomolgus monkey and hFcRn Tg32 mouse dataset

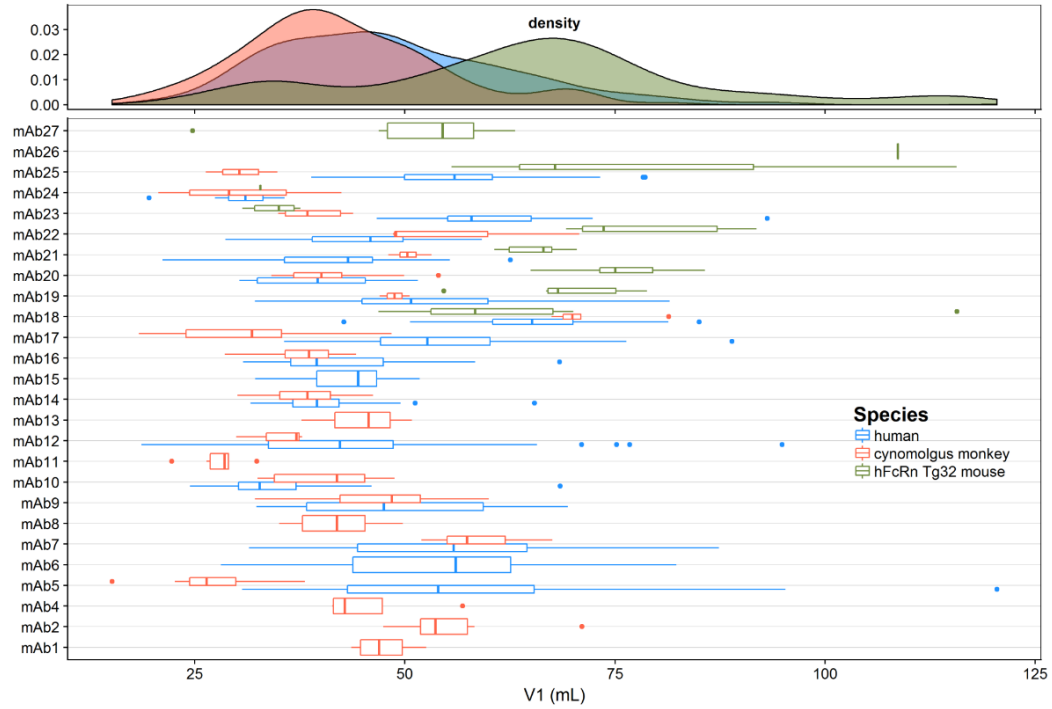

Figure 3: Distribution of population and individual mAb estimates (with variability) of volume of distribution of the central compartment (V1) in the combined human, cynomolgus monkey and hFcRn Tg32 mouse dataset

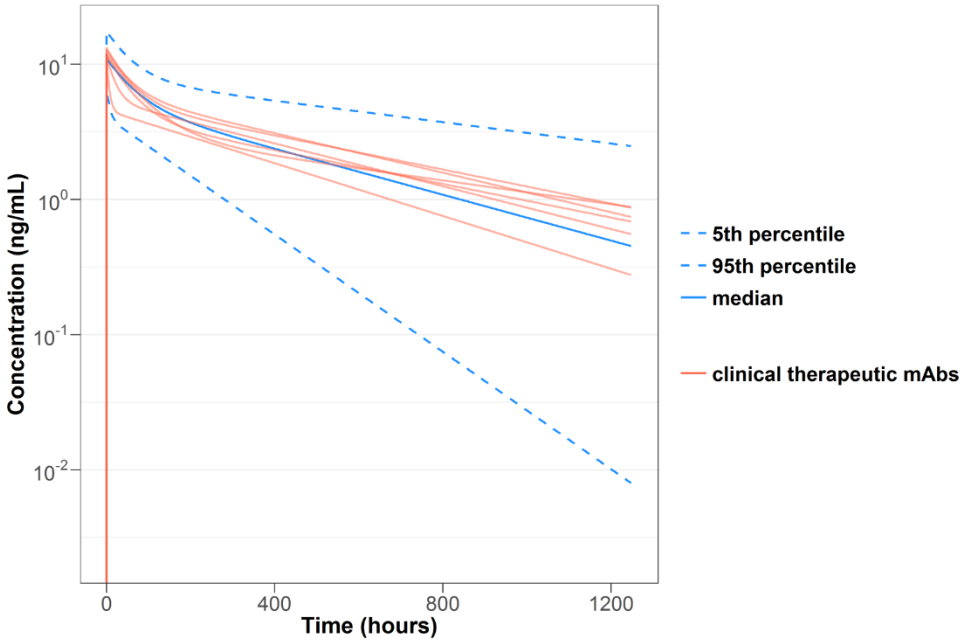

Figure 4: Median, 5th and 95th percentiles of 200 bootstrap samples with the combined species PK model using the observed dose-normalized concentration (ng/mL) vs. time (hours) data for all the mAbs in this study. The red lines indicate the concentration vs. time profile of the 5 clinical therapeutic mAbs (bevacizumab, infliximab (for both ankylosing spondylitis and ulcerative colitis), pertuzumab, rituximab and trastuzumab).

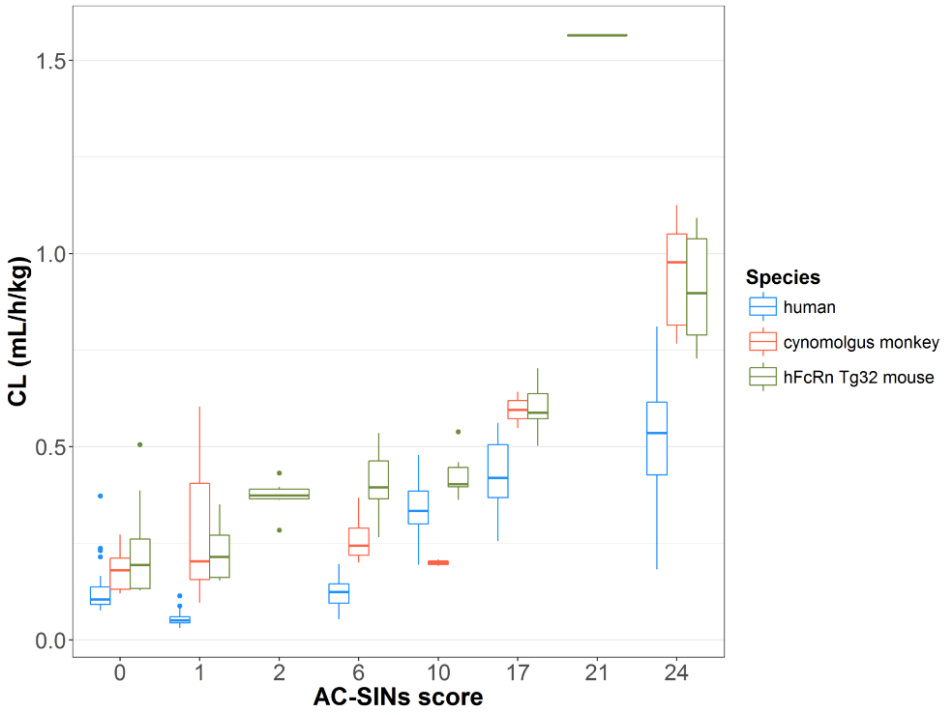

Figure 5: Clearance vs. AC-SINS score for a subset of 11 mAbs in the dataset in human, cynomolgus monkey and hFcRn Tg32 mouse.

Clearance outliers and correlation with non-specific interactions

Four of the mAbs in the human dataset had CL values 2-fold higher than the population estimate of 0.15 mL/h/kg (0.14-0.16) (Table 5). In order to investigate possible non-specific (off-target) binding properties, a subset of the mAbs in the dataset (n=11) were studied using an in vitro affinity capture self-interaction nanoparticle spectroscopy (AC-SINS) assay. This assay assesses self-association, which is often coupled with other poor physicochemical characteristics, including non-specific interactions. AC-SINS uses gold nanoparticles pre-coated with anti-human Fc polyclonal antibodies to capture test mAbs. Self-interactions of immobilized mAbs lead to clustering of the gold nanoparticles, which is measured by a shift in absorbance due to changes in their optical properties [21]. The 11 mAbs studied had AC-SINS scores ranging from 0-24 (Table 1). A plot of CL (mL/h/kg) vs. AC-SINS score for each species is shown in Figure 5. An increase in CL was observed with an increase in AC-SINS scores in all species. This data suggests that non-specific interactions leading to off-target binding may result in faster clearance than predicted by the popPK estimates.

Combined analysis and estimation of allometric exponents

The Tg32 mouse and human datasets, cynomolgus monkey and human datasets and datasets from all three species were combined. 2-compartment human PK parameters were estimated in the combined datasets and allometric exponents to scale the PK parameters from preclinical species to human (Table 4). The human popPK estimates of CL, Q, V1 and V2 in the combined datasets were similar to those estimated previously (Table 2). The estimated allometric exponent for scaling Tg32 mouse CL to human was 0.9 (0.88- 0.92), cynomolgus monkey CL to human was 0.81 (0.77- 0.85) and all preclinical data CL to human was 0.89 (0.87- 0.91). Volumes of distribution from central and peripheral compartments in general scaled with an allometric exponent of approximately 1. Population estimates of the allometric exponent for Q were between 0.57 and 0.67 for Tg32 mouse, cynomolgus monkey and all species.

Linear mAb human PK prediction strategies

Different methods were applied to predict human PK of the mAbs in this dataset. Note, a limitation to this analysis is that there was no separate test dataset to validate the inter-species scaling.

1. **Use of 'typical' PK parameters for human**
   Simulations of the popPK estimates of CL, Q, V1 and V2 estimated from the human dataset, compared with observed clinical PK profiles for the individual mAbs are shown in Figure 6. Root mean square errors (RMSEs) between observed and predicted data are shown in Table 5. Only 4 out of 18 mAbs have RMSEs of >100%, indicating that the human popPK parameters can adequately predict PK for the majority of mAbs in the dataset.

2. **Use of allometric exponents estimated from Tg32 mouse or cynomolgus monkey**
   For every mAb in the dataset with both Tg32 mouse data and human data (n=8), mouse 2-compartment PK parameters were scaled to human using the allometric exponents estimated for Tg32 mouse and presented in Table 4. This process was also completed for every mAb in

the dataset with both cynomolgus monkey and human data (n=16). Simulations of the scaled PK parameters of CL, Q, V1 and V2 estimated from the Tg32 mouse dataset, cynomolgus monkey dataset or the population values estimated from the human dataset, are compared with observed clinical PK for individual mAbs and are shown in Figure 7. RMSEs between observed and predicted data are shown in Tables 6 and 7 for Tg32 mouse and cynomolgus monkey, respectively. In Table 8, RMSEs are compared across different prediction methods: use of human popPK parameters or allometric exponents estimated for Tg32 mouse or cynomolgus monkey. The best prediction method (determined by the lowest RMSE) is indicated for each mAb.

Table 4: Combined species PK parameter estimates for mAbs with linear CL

Combined Datasets		**Tg32 Mouse, Cyno and Human (n=27 mAbs)**		**Cyno and Human (n=23 mAbs)**		**Tg32 Mouse and Human (n=23 mAbs)**	
Parameter	**Unit**	**Value (95%-CI)**	**RSE (%)**	**Value (95%-CI)**	**RSE (%)**	**Value (95%-CI)**	**RSE (%)**
CL	mL/h/kg	0.16 (0.15-0.16)	2.86	0.15 (0.14-0.16)	2.90	0.15 (0.14-0.16)	2.97
V1	mL/kg	45.19 (44.08-46.31)	1.26	45.89 (44.75-47.03)	1.27	46.41 (45.26-47.56)	1.26
Q	mL/h/kg	0.28 (0.25-0.31)	5.06	0.29 (0.26-0.32)	5.08	0.28 (0.25-0.31)	4.97
V2	mL/kg	30.81 (28.15-33.46)	4.40	31.14 (28.61-33.68)	4.15	32.17 (29.31-35.04)	4.55
CL: α	-	0.89 (0.87-0.91)	1.16	0.81 (0.77-0.85)	2.22	0.90 (0.88-0.92)	1.24
V1: β	-	0.98 (0.97-0.99)	0.54	1.04 (1.02-1.06)	0.87	0.97 (0.96-0.98)	0.55
Q: γ	-	0.67 (0.63-0.71)	2.87	0.57 (0.48-0.67)	8.36	0.67 (0.64-0.70)	2.19
V2: δ	-	0.95 (0.93-0.98)	1.28	1.07 (1.03-1.11)	2.02	0.93 (0.91-0.94)	0.84
IIV CL	-	0.47 (0.43-0.52)	4.61	0.45 (0.41-0.50)	4.64	0.47 (0.42-0.52)	5.00
COV CL-V1	-	0.08 (0.06-0.10)	11.25	0.08 (0.06-0.10)	10.82	0.08 (0.07-0.10)	10.83
IIV V1	-	0.11 (0.09-0.12)	6.26	0.10 (0.09-0.11)	6.44	0.10 (0.08-0.11)	6.31

CL: clearance from the central compartment, **V1:** volume of the central compartment, **Q:** inter-compartment distribution clearance, **V2:** volume of the peripheral compartment. **%RSE:** relative standard error, calculated as standard error of estimation / estimated value x 100% **95% CI:** 95% confidence interval calculated from standard error. **α, β, γ, and δ:** allometric exponents estimated for CL, V1, Q and V2 respectively, to scale from the preclinical species to human using the equation:

$$Y_{human\ predicted} = Y_{species} * \left(\frac{BW_{human}}{BW_{species}}\right)^{\alpha,\beta,\gamma\ or\ \delta}$$

IIV: inter-individual variability. **COV CL-V1:** covariance between clearance and volume. Residual errors per compound are shown in **Supplementary Table 2**. For each combined dataset the total 'n' includes n=18 mAbs with clinical data, n=23 mAbs with cyno data, and n=11 mAbs with Tg32 mouse data.

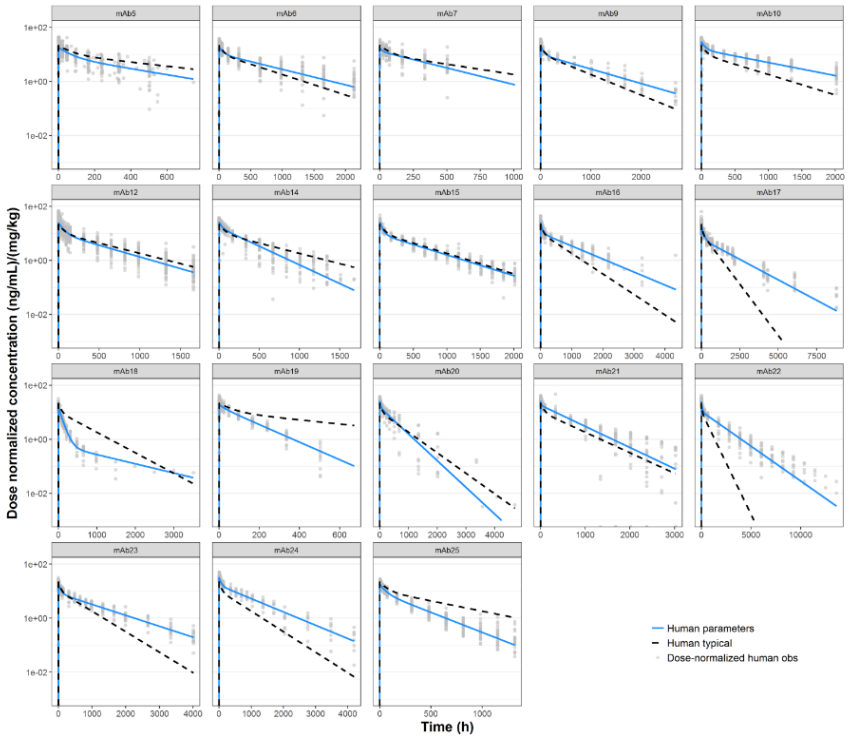

Figure 6: Predicted human PK profiles using 'typical' human popPK parameter estimates (**dashed line**), compared with observed (individual) dose normalized human PK data (symbols) and profiles from fitting human data for individual mAbs (**blue line**).

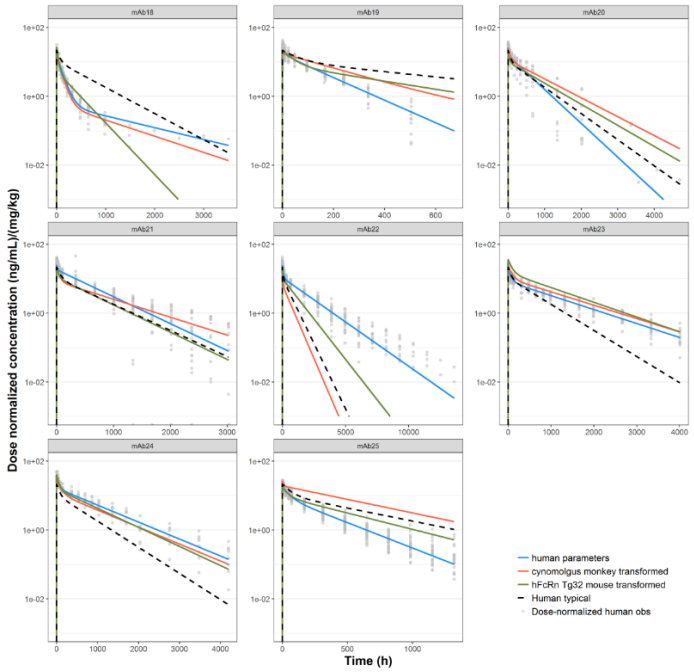

Figure 7: Predicted human PK profiles using (a) allometric exponents estimated for Tg32 mouse (**green line**), (b) allometric exponents estimated for cynomolgus monkey (**red line**) and (c) 'typical' human popPK parameter estimates (**dashed line**). Simulated data are compared with observed (individual) dose normalized human PK data (symbols) and profiles from fitting human data for individual mAbs (**blue line**).

Table 5: Comparison of observed human PK parameters for individual mAbs with 'typical' human popPK parameter estimates.

	CL (mL/h/kg)	V1 (mL/kg)	Q (mL/h/kg)	V2 (mL/kg)	%RMSE
Human PopPK	0.15	46.31	0.27	31.47	-
Observed Human PK					
mAb5	0.26	54.50	0.30	33.29	50.6
mAb6	0.12	52.58	0.32	31.76	23.1
mAb7	0.21	57.04	0.68	16.38	31.4
mAb9	0.12	46.58	0.37	40.47	24.7
mAb10	0.07	34.62	0.25	24.39	53.8
mAb12	0.17	40.49	0.25	32.75	18.2
mAb14	0.18	38.51	0.31	15.70	32.8
mAb15	0.17	39.11	0.43	44.99	19.7
mAb16	0.10	40.23	0.36	42.42	41.6
mAb17	0.09	48.30	0.19	64.89	54.2
mAb18	0.46	65.98	0.20	167.77	361.6
mAb19	0.46	52.18	0.19	6.41	121.9
mAb20	0.14	39.54	0.39	20.48	33.5
mAb21	0.10	40.07	0.80	14.00	54.8
mAb22	0.05	41.67	0.29	42.73	111.8
mAb23	0.11	54.96	0.33	49.29	39.7
mAb24	0.07	31.37	0.21	22.75	78.4
mAb25	0.32	55.76	0.32	27.73	104.1

Table 6: Comparison of observed human PK parameters for individual mAbs and predicted human pharmacokinetic parameters determined by allometric scaling from hFcRnTg32 mouse.

mAb Number	Human PK	CL (mL/h/kg)	V1 (mL/kg)	Q (mL/h/kg)	V2 (mL/kg)	%RMSE
mAb18	Observed	0.46	66.01	0.19	166.77	114.4
mAb18	Predicted	0.45	37.34	0.51	56.69	
mAb19	Observed	0.46	52.19	0.18	5.98	47.4
mAb19	Predicted	0.28	44.71	0.47	43.87	
mAb20	Observed	0.14	39.56	0.38	20.51	66.6
mAb20	Predicted	0.14	57.46	0.61	36.56	
mAb21	Observed	0.1	40.57	0.74	13.33	60.9
mAb21	Predicted	0.16	48.85	0.5	33.85	
mAb22	Observed	0.05	41.7	0.29	42.72	83.1
mAb22	Predicted	0.1	51.2	0.8	42.49	
mAb23	Observed	0.11	54.92	0.33	49.14	137.6
mAb23	Predicted	0.06	27.42	0.14	26.41	
mAb24	Observed	0.07	31.39	0.21	22.72	24.3
mAb24	Predicted	0.08	24.93	0.22	28.29	
mAb25	Observed	0.32	55.83	0.32	27.63	47.7
mAb25	Predicted	0.22	59.27	0.43	33.05	

CL: clearance from the central compartment, **V1:** volume of the central compartment, **Q:** inter-compartment distribution clearance, **V2:** volume of the peripheral compartment. **%RMSE**: percent root mean square error.

Table 7: Comparison of observed human PK parameters for individual mAbs and predicted human pharmacokinetic parameters determined by allometric scaling from cynomolgus monkey.

mAb number	Human PK	CL (mL/h/kg)	V1 (mL/kg)	Q (mL/h/kg)	V2 (mL/kg)	%RMSE
mAb5	Observed	0.26	54.51	0.3	32.97	143.5
mAb5	Predicted	0.1	27.09	0.37	21.65	.
mAb7	Observed	0.21	57.02	0.69	16.43	43.5
mAb7	Predicted	0.28	58.88	0.83	70.31	.
mAb9	Observed	0.12	46.58	0.37	40.43	20.9
mAb9	Predicted	0.09	51.18	0.15	60.19	.
mAb10	Observed	0.07	34.62	0.25	24.38	36.7
mAb10	Predicted	0.11	46.63	0.17	27.36	.
mAb12	Observed	0.17	40.49	0.25	32.75	78.4
mAb12	Predicted	0.08	36.37	0.18	40.05	.
mAb14	Observed	0.18	38.52	0.31	15.72	50
mAb14	Predicted	0.29	40.93	0.34	18.56	.
mAb16	Observed	0.1	40.23	0.36	42.43	23.7
mAb16	Predicted	0.12	35.98	0.28	38.08	.
mAb17	Observed	0.09	48.3	0.19	64.89	135.2
mAb17	Predicted	0.07	38.09	0.44	13.91	.
mAb18	Observed	0.46	65.98	0.2	167.69	40
mAb18	Predicted	0.58	72.13	0.21	134.53	.
mAb19	Observed	0.46	52.18	0.19	6.39	67.9
mAb19	Predicted	0.26	56.93	0.02	15.17	.
mab20	Observed	0.14	39.53	0.39	20.51	55
mAb20	Predicted	0.1	42.3	0.3	33.58	.
mAb21	Observed	0.1	40.07	0.8	14	61.3
mAb21	Predicted	0.13	47.35	0.51	54.07	.
mAb22	Observed	0.05	41.67	0.29	42.73	146.5
mAb22	Predicted	0.26	54.23	0.57	61.06	
mAb23	Observed	0.11	54.96	0.33	49.28	46.7
mAb23	Predicted	0.08	43.34	0.21	38.39	.
mAb24	Observed	0.07	31.37	0.21	22.75	31.9
mAb24	Predicted	0.08	35.94	0.14	28.98	.
mAb25	Observed	0.32	55.76	0.32	27.73	237.2
mAb25	Predicted	0.09	38.48	1.39	13.08	.

CL: clearance from the central compartment, **V1:** volume of the central compartment, **Q:** inter-compartment distribution clearance, **V2:** volume of the peripheral compartment. **%RMSE**: percent root mean square error.

Table 8: Comparison of model prediction RMSE (%) across different methods: use of human PopPK parameters, allometric scaling from Tg32 mouse, and allometric scaling from cynomolgus monkey. The best prediction method (determined by lowest RMSE) is indicated for each mAb.

	Prediction method/ RMSE %			
mAb Number	**Human PopPK**	**Tg32 mouse allometric scaling**	**Cyno allometric scaling**	**Best**
mAb5	50.6	.	143.5	Human
mAb6	23.1	.	.	.
mAb7	31.4	.	43.5	Human
mAb8	.	.	.	.
mAb9	24.7	.	20.9	Cyno
mAb10	53.8	.	36.7	Cyno
mAb11	.	.	.	.
mAb12	18.2	.	78.4	Human
mAb13	.	.	.	.
mAb14	32.8	.	50	Human
mAb15	.	.	.	.
mAb16	41.6	.	23.7	Cyno
mAb17	54.2	.	135.2	Human
mAb18	361.6	114.4	40	Cyno
mAb19	121.9	47.4	67.9	Tg32
mAb20	33.5	66.6	55	Human
mAb21	54.8	60.9	61.3	Human
mAb22	111.8	83.1	146.5	Tg32
mAb23	39.7	137.6	46.7	Human
mAb24	78.4	24.3	31.9	Tg32
mAb25	104.1	47.7	237.2	Tg32

2.4 Discussion

In this study we report a meta-analysis of the linear PK of mAbs across different species used in the pharmaceutical industry. Data on Pfizer mAbs were available from historical studies in human or cynomolgus monkey. In addition, for a subset of mAbs, PK data were available in transgenic mice expressing the human neonatal Fc receptor (Tg32 homozygous hFcRn mice). The hFcRn Tg32 mouse model was chosen over wild type (WT) mouse as mAb PK is often variable in WT mouse with poor predictability to human, which may be due to species differences in binding of human mAbs to mouse FcRn [22, 23]. Following cellular uptake of mAbs exhibiting linear CL, FcRn functions as a salvage receptor to protect IgG from rapid intracellular catabolism. The hFcRn transgenic mouse (Jackson Laboratory) is null for the α chain mFcRn and contains 1 or 2 transgenes of hFcRn, hemizygous or homozygous, respectively [24]. The homozygous Tg32 strain is used in this study with an hFcRn promoter. Avery *et al.* show that mAb CL in hFcRn homozygous mouse correlates with human PK (r^2=0.83, r=0.91) better than NHP (r^2=0.67, r=0,82) [23].

Population PK analysis across species

The long half-life of endogenous and exogenous IgG in conjunction with small volumes of distribution, results in the characteristic bi-exponential decline of mAb concentration-time profiles following IV administration. As such, a 2-compartmental PK model was shown to best describe the data. PopPK analysis is a useful tool that has been used for mAbs to quantify typical disposition characteristics and sources of variability within study populations [19, 25]. The advantage of popPK analysis is that it can be used to simultaneously evaluate PK data from all studies and individuals available. We made use of it in this analysis to create a dataset representing a range of mAbs with linear CL but differences in number of doses, subjects, data points and subject characteristics. A review of the literature performed by Dirks *et al.* showed that the popPK of different mAbs was similar despite differences in their pharmacological target and the fact that they were studied in different patient populations and disease states [19]. PopPK analysis is often used to study the inter-subject variability of mAb PK and to explore covariates of this variability. Body weight/ surface area are the most commonly identified covariates found to influence the PK of mAbs [9, 19, 26, 27]. The impact of other demographic factors including age, sex, ethnicity, body size, genetic polymorphisms, concomitant medications, immune status and multiple other patient specific details have also been considered [28]. In this analysis popPK was used to understand and quantify the variability in linear mAb PK. The inter-individual variability represents both inter-mAb and inter-subject variability, as we sought to estimate a single set of PK parameters across mAbs.

The popPK parameters estimated are presented in Table 2. These values represent typical 2-compartment PK estimates for mAbs with linear elimination in human, cynomolgus monkey and Tg32 mouse. Knowledge of typical parameter estimates of linear mAb PK *a priori* can be very useful in understanding and optimizing the PK/PD of a therapeutic mAb. They can be used at early stages to simulate the behavior of a mAb with 'typical' PK and to inform project teams on the benefit of extending PK half-life by altering affinity to FcRn. In animal PK studies they can be used to inform initial parameter estimates for PK/PD modeling and for simulations to optimize *in vivo* study designs. The parameters can be used as part of a strategy to predict PK in the clinic (as will be discussed later in this article). They could also be used as informative priors for a Bayesian data analysis or to construct parameter uncertainty distributions for clinical trial simulations.

Comparison of human population PK parameter estimates with population PK of literature mAbs

In order to put the human popPK parameter estimates for our dataset into context, they were compared with population estimates for therapeutic mAbs reported to have linear PK in the scientific literature (Table 3). Five relevant mAbs were found including bevacizumab, pertuzumab and trastuzumab which are humanized mAbs and infliximab and rituximab which are chimeric mAbs. In addition, different popPK estimates were considered for infliximab in patients with ankylosing spondylitis (AS) and ulcerative colitis (UC).

Estimates of V1 and V2 were similar for the 5 different mAbs and consistent with the population PK parameters estimated herein (Table 3). In a review of therapeutic mAb popPK parameters reported by Dirks and Meibohm [19], which included the 5 mAbs in Table 3, the estimate of V1 was 3.1 (2.4- 5.5) L, which is equivalent to 44.3 (34.3- 78.6) mL/kg assuming a 70 kg body weight in human, and very similar to the popPK estimate of V1 in this report of 46.3 (45.1- 47.5) mL/kg.

The value of the volume of distribution at steady state (Vss) can be calculated from the sum of V1 and V2. The population estimates for V1 (46.3 mL/kg) and V2 (31.5 mL/kg) in this analysis result in a calculated Vss of 77.8 mL/kg or, 5.4 L assuming a 70 kg individual. Data from early IgG metabolism studies in humans [20] indicates that the mean serum IgG concentration and the total body IgG pool were 12 g/L and 1.06 g/kg respectively, which for a 70 kg person equates to a volume of distribution of 6.2 L for IgG. In summary, the estimates of both central and peripheral volumes in the analysis reported herein appear to be consistent with published popPK of therapeutic mAbs with linear PK [19]. In addition, calculated Vss is close to endogenous IgG.

The values of CL for the 5 mAbs from the literature varied from 0.12- 0.24 mL/h/kg and were similar to the popPK estimate for CL (0.15 (0.14- 0.16) mL/h/kg). The CL of infliximab in UC patients (0.24 mL/h/kg) was out with the popPK range and also different to the CL of infliximab in AS patients (0.16 mL/h/kg). Variation in infliximab CL across patient populations could be due to a number of different factors. Elevated inflammatory status in UC could contribute to higher CL due to a higher whole body turnover rate and increased nonspecific proteolytic degradation rate [2, 29]. In addition, CL of infliximab has also been shown to be affected by concomitant medication as well as immunogenicity [29]. In the analysis by Dirks and Meibohm the population CL value for therapeutic mAbs ranged between 0.2-0.5 L/day (0.12- 0.3 mL/h/kg assuming a 70 kg individual). This range encompasses the popPK estimate of CL reported here (0.15 mL/h/kg). In addition, assuming a volume of distribution of 6.2 L and an elimination half-life of 21 days for IgG (which doesn't include IgG3) the CL of endogenous IgG is approx. 0.21L/day or 0.125 mL/h/kg [20].

The population estimate of the inter-compartmental CL (Q) was in general consistent with the 5 literature mAbs, again with exception of Infliximab for UC. The median Q estimated in the Dirks and Meibohm analysis was 0.79 L/day (0.47 mL/h/kg) [19]. Our value was slightly lower at 0.27 (0.25-0.3) mL/h/kg, but both are consistent with slow transfer of mAbs between the central and peripheral compartments.

Clearance outliers and correlation with non-specific interactions

Closer inspection of the human analysis indicated that 12 of the 18 mAbs studied had individual CL values within 2-fold of the population estimate of CL (0.075- 0.3 mL/h/kg). Of the remaining 6 mAbs, 3 had CL < 0.075 mL/h/kg (mAb10, mAb22 and mAb24) and 3 had CL >0.3 mL/h/kg (mAb18, mAb19 and mAb25). Unexpected high CL of mAbs is particularly undesirable as it can lead to an increased clinical dose requirement and may limit clinical utility. Higher CL of the mAbs in this dataset was not associated with an alteration in FcRn binding as all mAbs in this dataset had similar FcRn Kd values [23].

One potential mechanism that can contribute to faster than expected CL of mAbs is off-target binding [30]. The mechanism of this non-specificity has not been fully elucidated but could be in part due to hydrophobicity/ positive charged patches on mAbs [31]. To test this, an *in vitro* high throughput assay measuring non-specific binding was implemented and used to identify mAbs with increased risk of having fast CL in humans [32]. An affinity capture self-interaction nanoparticle spectroscopy, or AC-SINS, assay was used to screen 11 of the mAbs in the dataset. An AC-SINS score of >11 has been associated with high self-association [32]. The AC-SINS scores for the subset of mAbs tested from this dataset ranged from 0 to 24, with 3 mAbs exhibiting higher than typical CL having scores of 11-24. A correlation was observed with AC-SINS score and

mAb CL across all species (Figure 5). This trend has been observed previously with a larger dataset of mAbs [32] and suggests that the AC-SINS assay is a useful screening tool to de-select mAbs that have the potential for fast clearance in humans.

Predicting human PK

Previous predictions of linear PK of mAbs in the clinic have been completed by single species scaling from cynomolgus monkey assuming allometric principles. Many examples of this type of scaling are available in the literature. The first comprehensive review of mAb CL prediction was completed by Ling *et al.* in 2009. Their study of 14 mAbs indicated that for mAbs with linear kinetics, CL in humans could be reasonably predicted from monkey data using simplified allometry with a fixed exponent. The optimal exponents were estimated to be 0.85 for soluble antigens and 0.9 for membrane based antigens [13]. In a similar analysis of 13 mAbs with linear CL, Deng *et al.* showed that simple allometric scaling of CL in cynomolgus monkey with an exponent of 0.85 provided a good estimate of human CL [11]. Dong *et al.* also concluded that single species monkey PK predicted human PK of mAbs with linear CL within 2.3 fold [12]. Oitate *et al.* demonstrated that both human CL and Vss could be predicted reasonably well from monkey data alone using simple allometry with exponents of 0.79 on CL for soluble target antigens and 0.96 on CL for membrane target antigens [14]. The exponent for prediction of Vss was close to 1 in each case.

In all examples cited, the allometric exponent for prediction of mAb CL is > 0.75, which is the standard exponent value used for interspecies scaling of small molecule drugs. This value was derived from the observation that basal metabolic rates and passive renal filtration could be scaled by body weight with an exponent of 0.75. This has been qualified by several groups in the interspecies scaling for prediction of small molecule drug CL [33, 34]. Given the mechanisms of CL of small molecules are governed by oxidative metabolism and renal CL, an exponent of 0.75 makes sense. For mAbs, CL is driven by proteolysis and therefore allometric exponents may be more dependent on proteolytic rates across species.

In this study, datasets of Tg32 mouse and human PK, cynomolgus monkey and human PK, and all three species PK were combined to estimate allometric exponents to scale preclinical data to human. The estimated allometric exponent for scaling Tg32 mouse CL to human was 0.90 (0.88-0.92), cynomolgus monkey CL to human was 0.81 (0.77- 0.85) and all preclinical data CL to human was 0.89 (0.87- 0.91). The exponents required to predict cynomolgus monkey data to human were in agreement with the literature examples. The hFcRn Tg32 mouse data was encouraging as it predicted well to human, and provides a potential species to replace cynomolgus monkey for human PK predictions of mAbs [23]. Volumes of distribution from central and peripheral compartments in general scaled with an allometric exponent of 1, similar to literature analyses. This was the first time that popPK methods had been used to estimate allometric exponents as a parameter within the model. This is a useful method as it facilitates separation of true parameter estimates from variability.

Another benefit of this analysis was that the use of 2-compartmental PK models enabled prediction of human PK profiles as well as PK parameters. The human predicted profiles were compared with 2 -compartmental fits to the observed human data for each mAb and RMSEs were calculated between observed and predicted parameters to assess prediction accuracy. Two approaches were taken: first of all the popPK parameter estimates from the human analysis were

used to simulate a 'typical' human profile. This was compared with profiles generated for each of the 18 individual mAbs in human. This method gave good prediction accuracy, with 14/18 mAbs with RMSEs <100%, indicating that the human popPK parameters were able to predict the human PK for the majority of mAbs in the dataset. This approach assumes that the CL mechanisms for these therapeutic mAbs are the same as each other and endogenous IgG i.e. non-specific linear catabolic CL. 3 out of the 4 mAbs with RMSEs greater than 100% had high AC-SINS scores, indicating potential for rapid CL due to non-specific binding. The second approach was to predict human PK using allometric exponents determined from Tg32 mouse and cynomolgus monkey. For this approach, CL mechanisms need not be the same as each other or endogenous IgG but must be consistent across species. Again, this method gave a good prediction of human PK with RMSEs between observed and predicted data < 100% for 6/8 of the mAbs scaled from Tg32 mouse to human and 12/16 of the mAbs scaled from cynomolgus monkey to human.

In summary, good prediction accuracy was obtained using human 'typical' popPK parameters as an estimate of human PK or via scaling using allometric exponents from Tg32 mouse or cynomolgus monkey (Table 8). All of these methods are simple and easy to use. The use of allometric exponents from cynomolgus monkey is a common approach to linear mAb PK prediction which is widely understood across the pharmaceutical industry. However, the use of human popPK parameters as a base case scenario is more statistically informed than the allometric scaling approach. This is because the human popPK analysis is informed by rigorous analysis of rich datasets- from both this study and also literature studies on the popPK of mAbs in human [19]. Single species scaling using allometric exponents requires preclinical PK on individual mAbs which is often only generated in low 'n' of 2-3 animals. Projection therefore relies on a small number of animals whose profile may be affected by assay specificities, inter-animal variability and immunogenicity, to name a few. The strategies presented herein call into question the value of completing extensive *in vivo* preclinical PK for mAbs with linear CL and encourage refinement of PK strategies consistent with 3Rs. The '3Rs' refers to the reduction, refinement and replacement of animal use in research, testing and teaching [35]. This analysis provides alternatives to the use of cynomolgus monkey for PK prediction including allometric scaling from Tg32 mouse or use of human popPK parameters as a replacement to animal based methods. As such, it has the potential to reduce the numbers of cynomolgus monkey PK studies completed. Use of the AC-SINS assay can also be used to screen out mAbs with high CL due to non-specific binding/self-association.

MAbs with non-linear PK due to target mediated CL mechanisms were not included in this analysis. Modeling of such data is routinely performed using a Michaelis-Menten (M-M) model with linear first order elimination complemented by a non-linear pathway described using Vmax and Km parameters. Alternatively, a more mechanistic TMDD model can be used which incorporates target properties. Previous work has shown that the TMDD approach is more reliable for human projections, as it can capture differences in target properties between species and disease populations [5, 15, 17]. Since both the M-M and TMDD models require parameterization of the linear CL pathway, the parameters presented herein are a useful guide. Such models have a tendency for over-parameterization, and prior knowledge of typical linear PK parameters across species reduces the need for their estimation.

In conclusion, the popPK analysis completed on 27 Pfizer mAbs in human, cynomolgus monkey or Tg32 mouse showed that a single set of typical linear PK parameters could be estimated across species. These parameters will be useful to inform initial parameters for PK/PD modeling and for simulations to optimize *in vivo* and first in human study designs. In addition, different translational strategies were investigated for prediction of human linear PK of mAbs. Use of 'typical' human PK parameters gave good prediction accuracy for the majority of the mAbs in this study. Allometric exponents were estimated within the popPK model and also gave good predictions, from both Tg32 mouse or cynomolgus monkey to human. The strategies presented herein offer methods to predict linear human PK of mAbs with less reliance on cynomolgus monkey PK and use of smaller animal or *in silico* alternatives.

2.5 Materials and Methods

mAb PK dataset

For this study a dataset was compiled consisting of in-house historical individual concentration versus time data following intravenous (IV) administration of 27 Pfizer mAbs in human, cynomolgus monkey or hFcRn Tg32 transgenic mice. All procedures performed in animals were in accordance with regulations and established guidelines and were reviewed and approved by Pfizer's Institutional Animal Care and Use Committee. Research on human samples was conducted in accordance with all applicable Pfizer policies, including IRB/ IEC approval. Data for 18/ 27 mAbs was available in healthy human volunteers or patients and consisted of single dose IV PK, at multiple dose levels with n=3-24 individuals/ dose level. In cynomolgus monkey, single dose IV PK data was available for 23/ 27 mAbs, administered at 1-3 dose levels with n=2 monkeys/ dose. In hFcRn Tg32 transgenic mice, 11 /27 mAbs were administered as previously described [23] at a single IV dose of 3.5 mg/kg (1 mAb) or 5mg/kg (10 mAbs) with n=5-6 mice per mAb. For the marketed mAbs, popPK estimates were obtained from the literature [19].

Data inclusion and exclusion criteria: selection of linear dose range

Non-linear data was removed from the datasets, where target mediated drug disposition or factors such as immunogenicity were contributing to the overall CL. First, a visual analysis of the data was performed to check for non-linearity, then an algorithm was applied to a linear regression of dose and AUC (Figure 1) to test for deviation of the slope from 1, and the dataset was reduced accordingly. For Tg32 mouse, all PK data was at doses ≥3.5 mg/kg and was included in the analysis. Table 1 provides details of the linear dose range, number of dose levels that were used in the popPK analysis and the non-linear dose levels removed.

PK model

mAb PK following IV administration was described by a 2-compartment disposition model with first-order elimination from the central compartment. The structural model was parameterized in terms of CL, central volume of distribution (V1), peripheral volume of distribution (V2) and inter-compartmental clearance (Q). Random effects were included as exponential terms reflecting log normal distributions of model parameters. The residual variability was implemented by proportional error model per compound. Goodness-of-fit was determined using the minimum value of the objective function defined as minus twice the log likelihood. For nested

models, a decrease of 3.84 points in the objective function (MVOF; corresponding to $P < 0.01$ in a chi-squared distribution) by adding an additional parameter was considered significant. The goodness-of-fit was also investigated by visual inspection of the plots of individual predictions and the diagnostic plots of (weighted) residuals.
The PK model was applied to each species separately (single species PK analysis) or to a combination of two or three species together (combined species PK analysis). The combined species PK analysis used allometric scaling on all PK parameters by a scaling exponent based on bodyweight. For humans the available bodyweights were used, for cynomolgus monkey and hFcRn Tg32 transgenic mice a bodyweight of 3 kg and 0.02 kg, respectively was assumed.

Computation

Individual concentration-time data from all subjects for all mAbs were pooled into a single dataset for pop PK analysis using nonlinear mixed effect modeling with the NONMEM software system (Version 7.3, ICON Development Solutions) using ADVAN3 and subroutine 4 and PsN (version 4.6.0) [36] [37]. Gfortran version 4.6.0 was used as a compiler. Parameters were estimated using the first-order conditional estimation method with interaction between the two levels of stochastic effects (FOCEI).

Model validation

The robustness of the final combined species PK model was evaluated using resampling techniques of a bootstrap method. The bootstrap method involves repeated random sampling of subjects in the dataset. The original dataset is replaced to produce another dataset of the same size, but with a different combination of subjects and compounds. Resampling was repeated 200 times. The obtained PK parameters from the bootstrap sets that produced successful minimization and convergence were used to simulate the concentration time profiles after a single dose of 1 mg/kg for a typical human subject of 70 kg.
In the visual predictive check (VPC), the observation versus time profile was simulated 1000 times by means of Monte Carlo simulations. In a Monte Carlo simulation, random values are drawn from the distributions of the identified random effects. Subsequently, the median and 5 and 95 percentiles of the dependent variables were calculated for each time and plotted together with the observations. A jackknife analysis was also completed with the combined species PK model to test robustness of model predictions. In this type of analysis one mAb is omitted from the total dataset at a time to test the influence of that mAb on the resulting predictions.

AC-SINS

The affinity capture self-interaction nanoparticle spectroscopy method was implemented as previously described [21, 32].

PK prediction methods

To predict the human PK of mAbs in this dataset:

1. **Using 'typical' PK parameters for human**
   Clinical data, available for 18 mAbs in the dataset, was fit individually using a 2 compartment PK model as described previously. Individual values of CL, V1, Q and V2 were determined for each mAb, and PK profiles were simulated using fitted parameters.

These were compared to simulated profiles using the human popPK values of CL, V1, Q and V2 and root mean square error (RMSE) values calculated using the following equation:

$$\sqrt{\frac{\sum_{t=1}^{n}\left(x_{1,t}-x_{2,t}\right)^{2}}{n}}$$

Where n= number of predictions, χ is predicted or observed value

2. **Using allometric exponents estimated from Tg32 mouse or cynomolgus monkey**
   For every mAb in the dataset with both Tg32 mouse data and human data (n=8), or cynomolgus monkey and human data (n=16), preclinical species PK parameters were scaled to human using estimated allometric exponents (Table 4).
   First, the individual Tg32 mouse data for each mAb were fit to a 2-compartment PK model (n=8) as described previously. Individual mAb values of CL, V1, Q and V2 were then scaled to human using the estimated allometric exponents for Tg32 mouse presented in Table 4. PK profiles were simulated using the scaled parameters. These were compared with the individual values of CL, V1, Q and V2 estimated for each individual mAb in human, described in section 1 above, and RMSEs calculated as before.
   This process was also completed for every mAb in the dataset with both cynomolgus monkey and human data (n=16).

2.6 Acknowledgements

The authors are grateful to the following individuals for their contributions to this work:
Steve Penn, Rohit Yadav, Shraddah Desal, Christine Ditondo, Denise O'Hara, Mengmeng Wang, Mania Kavosi, Jeffrey Kurz, Minlei Zhang, Laura Danner, Angela Hernandez, Cynthia Filliettaz, Katie McGinn, Amy King, Laura Lin, Abhinav Tiwari, Fei Hua and Steve Martin.

References

1. Mould, D.R. and B. Meibohm, *Drug Development of Therapeutic Monoclonal Antibodies.* BioDrugs, 2016. **30**(4): p. 275-93.
2. Ryman, J.T. and B. Meibohm, *Pharmacokinetics of Monoclonal Antibodies.* CPT Pharmacometrics Syst Pharmacol, 2017. **6**(9): p. 576-588.
3. Tabrizi, M.A., C.M. Tseng, and L.K. Roskos, *Elimination mechanisms of therapeutic monoclonal antibodies.* Drug Discov Today, 2006. **11**(1-2): p. 81-8.
4. Junghans, R.P. and C.L. Anderson, *The protection receptor for IgG catabolism is the beta2-microglobulin-containing neonatal intestinal transport receptor.* Proc Natl Acad Sci U S A, 1996. **93**(11): p. 5512-6.
5. Betts, A.M., et al., *The application of target information and preclinical pharmacokinetic/pharmacodynamic modeling in predicting clinical doses of a Dickkopf-1 antibody for osteoporosis.* J Pharmacol Exp Ther, 2010. **333**(1): p. 2-13.

6. Baxter, L.T., et al., *Physiologically based pharmacokinetic model for specific and nonspecific monoclonal antibodies and fragments in normal tissues and human tumor xenografts in nude mice.* Cancer Res, 1994. **54**(6): p. 1517-28.
7. Ferl, G.Z., A.M. Wu, and J.J. DiStefano, 3rd, *A predictive model of therapeutic monoclonal antibody dynamics and regulation by the neonatal Fc receptor (FcRn).* Ann Biomed Eng, 2005. **33**(11): p. 1640-52.
8. Lobo, E.D., R.J. Hansen, and J.P. Balthasar, *Antibody pharmacokinetics and pharmacodynamics.* J Pharm Sci, 2004. **93**(11): p. 2645-68.
9. Wang, W., E.Q. Wang, and J.P. Balthasar, *Monoclonal antibody pharmacokinetics and pharmacodynamics.* Clin Pharmacol Ther, 2008. **84**(5): p. 548-58.
10. Neuber, T., et al., *Characterization and screening of IgG binding to the neonatal Fc receptor.* MAbs, 2014. **6**(4): p. 928-42.
11. Deng, R., et al., *Projecting human pharmacokinetics of therapeutic antibodies from nonclinical data.* mAbs, 2014. **3**(1): p. 61-66.
12. Dong, J.Q., et al., *Quantitative prediction of human pharmacokinetics for monoclonal antibodies: retrospective analysis of monkey as a single species for first-in-human prediction.* Clin Pharmacokinet, 2011. **50**(2): p. 131-42.
13. Ling, J., et al., *Interspecies scaling of therapeutic monoclonal antibodies: initial look.* J Clin Pharmacol, 2009. **49**(12): p. 1382-402.
14. Oitate, M., et al., *Prediction of Human Pharmacokinetics of Therapeutic Monoclonal Antibodies from Simple Allometry of Monkey Data.* Drug Metabolism and Pharmacokinetics, 2011. **26**(4): p. 423-430.
15. Dua, P., E. Hawkins, and P.H. van der Graaf, *A Tutorial on Target-Mediated Drug Disposition (TMDD) Models.* CPT Pharmacometrics Syst Pharmacol, 2015. **4**(6): p. 324-37.
16. Mager, D.E. and W.J. Jusko, *General pharmacokinetic model for drugs exhibiting target-mediated drug disposition.* J Pharmacokinet Pharmacodyn, 2001. **28**(6): p. 507-32.
17. Singh, A.P., et al., *Quantitative prediction of human pharmacokinetics for mAbs exhibiting target-mediated disposition.* AAPS J, 2015. **17**(2): p. 389-99.
18. Ette, E.I. and P.J. Williams, *Population pharmacokinetics I: background, concepts, and models.* Ann Pharmacother, 2004. **38**(10): p. 1702-6.
19. Dirks, N.L. and B. Meibohm, *Population pharmacokinetics of therapeutic monoclonal antibodies.* Clin Pharmacokinet, 2010. **49**(10): p. 633-59.
20. Waldmann, T.A. and W. Strober, *Metabolism of immunoglobulins.* Prog Allergy, 1969. **13**: p. 1-110.
21. Liu, Y., et al., *High-throughput screening for developability during early-stage antibody discovery using self-interaction nanoparticle spectroscopy.* MAbs, 2014. **6**(2): p. 483-92.
22. Ober, R.J., et al., *Differences in promiscuity for antibody-FcRn interactions across species: implications for therapeutic antibodies.* Int Immunol, 2001. **13**(12): p. 1551-9.
23. Avery, L.B., et al., *Utility of a human FcRn transgenic mouse model in drug discovery for early assessment and prediction of human pharmacokinetics of monoclonal antibodies.* MAbs, 2016. **8**(6): p. 1064-78.
24. Roopenian, D.C., G.J. Christianson, and T.J. Sproule, *Human FcRn transgenic mice for pharmacokinetic evaluation of therapeutic antibodies.* Methods Mol Biol, 2010. **602**: p. 93-104.

25. Davda, J.P., et al., *A model-based meta-analysis of monoclonal antibody pharmacokinetics to guide optimal first-in-human study design.* MAbs, 2014. **6**(4): p. 1094-102.
26. Bai, S., et al., *A guide to rational dosing of monoclonal antibodies.* Clin Pharmacokinet, 2012. **51**(2): p. 119-35.
27. Wang, D.D., et al., *Fixed dosing versus body size-based dosing of monoclonal antibodies in adult clinical trials.* J Clin Pharmacol, 2009. **49**(9): p. 1012-24.
28. Gill, K.L., et al., *A Bottom-Up Whole-Body Physiologically Based Pharmacokinetic Model to Mechanistically Predict Tissue Distribution and the Rate of Subcutaneous Absorption of Therapeutic Proteins.* AAPS J, 2016. **18**(1): p. 156-70.
29. Feagan, B.G., et al., *The challenge of indication extrapolation for infliximab biosimilars.* Biologicals, 2014. **42**(4): p. 177-83.
30. Hotzel, I., et al., *A strategy for risk mitigation of antibodies with fast clearance.* MAbs, 2012. **4**(6): p. 753-60.
31. Notkins, A.L., *Polyreactivity of antibody molecules.* Trends Immunol, 2004. **25**(4): p. 174-9.
32. Avery, L.B., et al., *Establishing in vitro in vivo correlations to screen monoclonal antibodies for physicochemical properties related to favorable human pharmacokinetics.* MAbs, 2017: p. 0.
33. Hosea, N.A., et al., *Prediction of human pharmacokinetics from preclinical information: comparative accuracy of quantitative prediction approaches.* J Clin Pharmacol, 2009. **49**(5): p. 513-33.
34. Tang, H., et al., *Interspecies prediction of human drug clearance based on scaling data from one or two animal species.* Drug Metab Dispos, 2007. **35**(10): p. 1886-93.
35. Russell, W.M.S.B., R.L., *The Principles of Humane Experimental Technique*. 1959, London: Methuen.
36. Beal S, S.L., Boeckmann A, Bauer RJ. *NONMEM User's Guides.* 1989-2009.
37. Lindbom, L., P. Pihlgren, and E.N. Jonsson, *PsN-Toolkit--a collection of computer intensive statistical methods for non-linear mixed effect modeling using NONMEM.* Comput Methods Programs Biomed, 2005. **79**(3): p. 241-57.

Supplementary Material

Supplementary Figure 1: PK parameters from jackknife analysis using the combined species PK model. Error bars show the 95% confidence intervals, omitting one mAb from the total dataset at a time. Gray areas represent 95% confidence intervals from the full model.

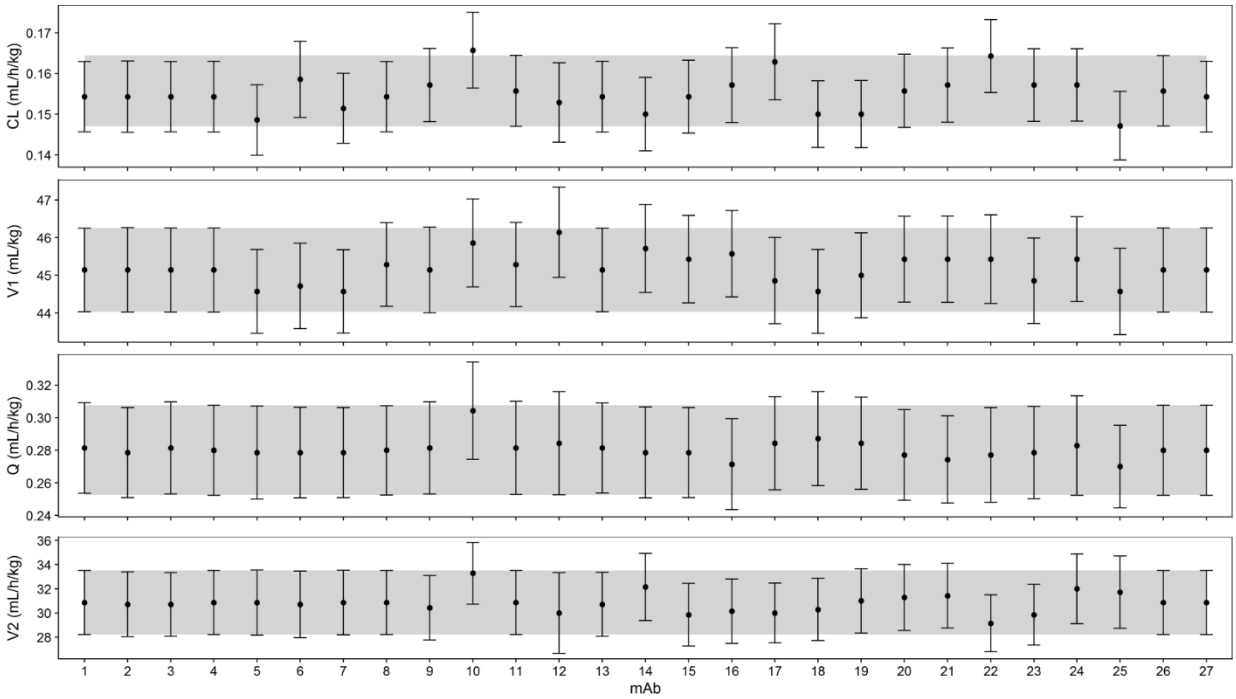

Supplementary Figure 2: Goodness of fit plots of the combined species PK model. The dashed blue line is the line of identity; the red solid line indicates a (Loess) smoother of the observations. GOF plots are paneled by species (1=human; 2= Cynomolgus monkey; 3= Tg32 hFcRn Mouse)

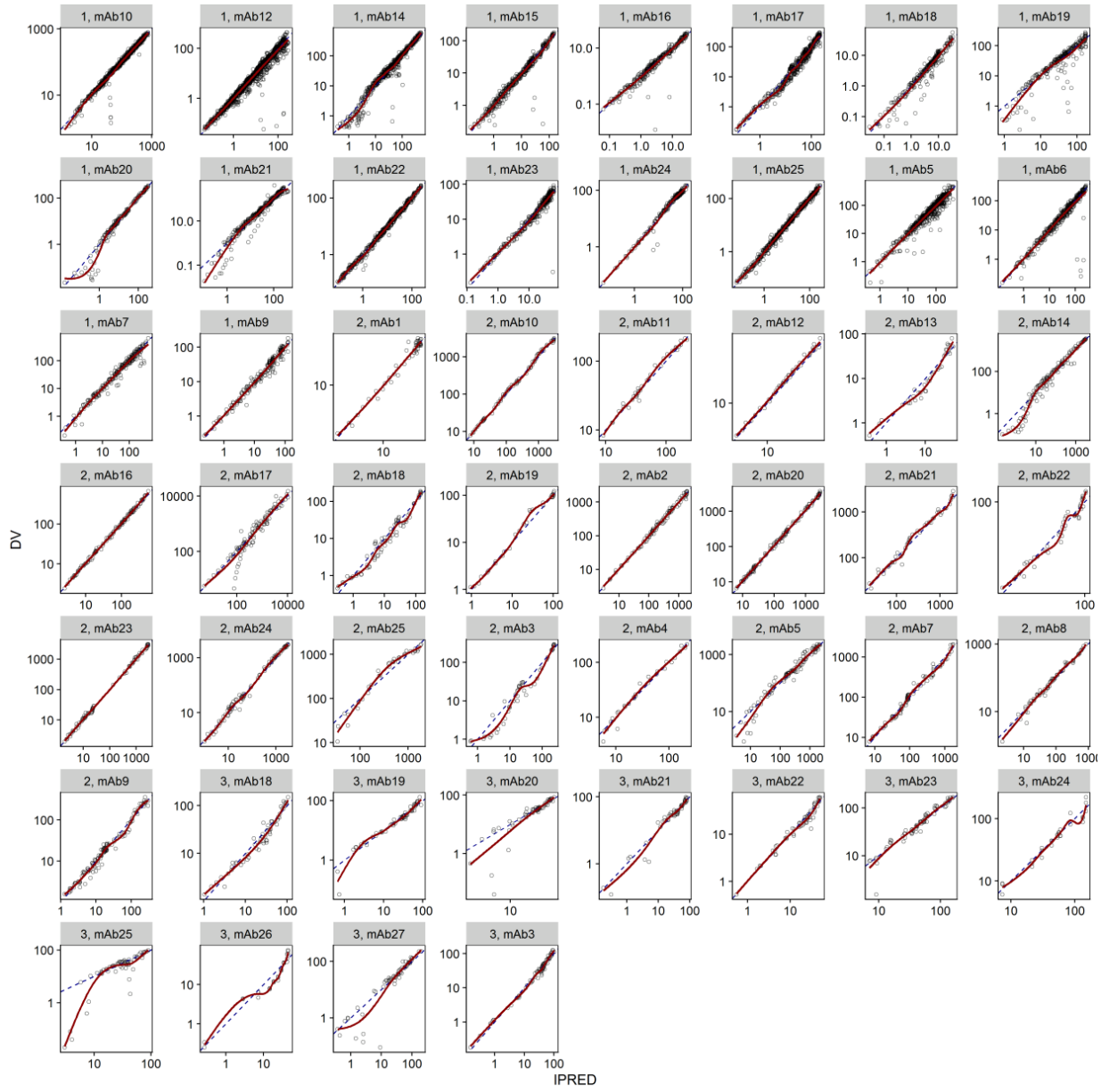

Supplementary Figure 3: Visual predictive plots (VPC) of the combined species PK model. The black circles represent the dose normalized concentrations and the blue line the observed median. The black line represents the predicted median, the dashed red lines represent the 5th and 95th percentiles of the observations. The gray area represents the 90% prediction interval. (A) human (B) Cynomolgus monkey; (C) Tg32 hFcRn Mouse.

3A

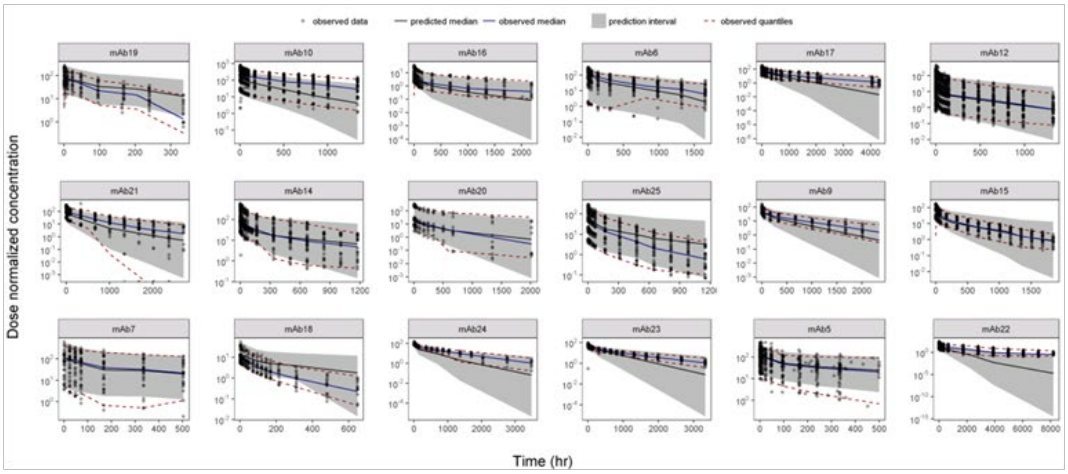

3B

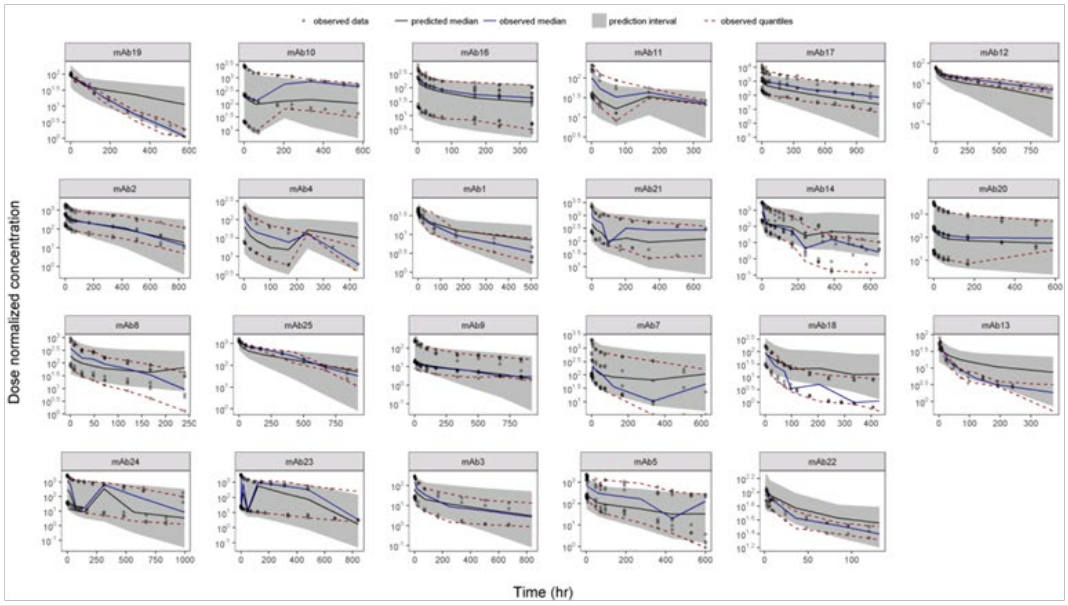

3C

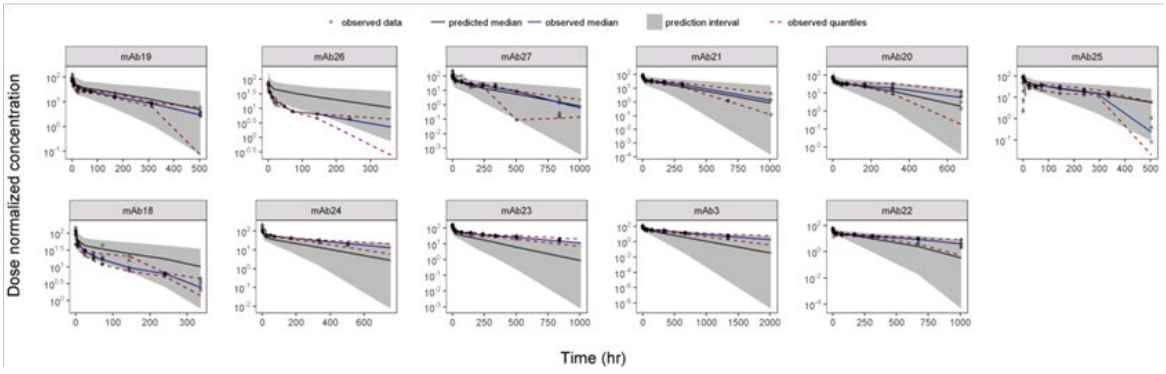

Supplementary Table 1: Residual error (ε) per compound for the single species PopPK analysis

	Human (n=18)		Cynomolgus Monkey (n=20)		Tg32 hFcRn Mouse (n=11)	
Parameter	**Value (95%-CI)**	**%RSE**	**Value (95%-CI)**	**%RSE**	**Value (95%-CI)**	**%RSE**
ε-mAb1			0.0343 (0.0225-0.046)	17.5		
ε-mAb2			0.018 (0.0126-0.0233)	15.1		
ε-mAb3			0.165 (0.136-0.193)	8.87	0.0207 (0.0142-0.0271)	15.9
ε-mAb4			0.0236 (0.00155-0.0457)	47.7		
ε-mAb5	0.0734 (0.0615-0.0853)	8.29	0.115 (0.0497-0.18)	28.9		
ε-mAb6	0.0561 (0.0412-0.0711)	13.6				
ε-mAb7	0.0708 (0.0453-0.0962)	18.3	0.085 (-0.0172-0.187)	61.4		
ε-mAb8			0.0214 (0.00694-0.0359)	34.5		
ε-mAb9	0.0482 (0.0367-0.0597)	12.2	0.0492 (0.0183-0.08)	32.0		
ε-mAb10	0.0213 (0.00364-.0389)	42.3	0.00617 (0.00391-0.00844)	18.7		
ε-mAb11			0.0179 (0.00725-0.0285)	30.3		
ε-mAb12	0.0670 (0.0552-0.0788)	8.98	0.00745 (0.00366-0.0112)	26.0		
ε-mAb13			0.172 (0.128-0.216)	13.1		
ε-mAb14	0.0776 (0.0590-0.0962)	12.2	0.167 (0.0941-0.24)	22.3		
ε-mAb15	0.0459 (0.0294-0.0624)	18.3				
ε-mAb16	0.0453 (0.0286-0.0619)	18.8	0.00494 (0.00358-0.0063)	14.1		
ε-mAb17	0.0868 (0.0693-0.104)	10.3	0.231 (-0.0875-0.549)	70.4		
ε-mAb18	0.0716 (0.0212-0.122)	36.0	0.138 (0.107-0.168)	11.3	0.0706 (0.0384-0.103)	23.3
ε-mAb19	0.119 (0.0971- 0.140)	9.22	0.0288 (0.0175-0.0401)	20.1	0.0492 (0.0157-0.0827)	34.7
ε-mAb20	0.0958 (0.0681-0.123)	14.7	0.0073 (0.00462-0.00997)	18.7	0.095 (0.0201-0.17)	40.3
ε-mAb21	0.153 (0.0383-0.267)	38.2	0.0328 (0.0219-0.0437)	16.9	0.0778 0.0245-0.131)	34.9
ε-mAb22	0.0219 (0.0157-0.0281)	14.4	0.0104 (0.00843-0.0124)	9.7	0.0309 (0.0171-0.0446)	22.7
ε-mAb23	0.0376 (0.0287-0.0466)	12.2	0.0114 (0.00638-0.0164)	22.5	0.0554 (0.0121-0.0987)	39.8

ε-mAb24	0.0263 (0.0114-0.0412)	28.8	0.0362 (0.0145-0.058)	30.7	0.0446 (0.0295-0.0596)	17.2
ε-mAb25	0.0284 (0.0203-0.0365)	14.6	0.0727 (-0.00115-0.147)	51.8	0.176 (0.127-0.226)	14.4
ε-mAb26					0.11 (0.0978-0.122)	5.68
ε-mAb27					0.208 (0.0344-0.382)	42.6

(supplementary to Table 2).

Supplementary Table 2: Residual error (ε) per compound for the combined species PopPK analysis (supplementary to Table 4).

Combined Datasets	**Tg32 Mouse, Cyno and Human**		**Cyno and Human**		**Tg32 Mouse and Human**	
Parameter	**Value (95%-CI)**	**%RSE**	**Value (95%-CI)**	**%RSE**	**Value (95%-CI)**	**%RSE**
ε-mAb1	0.0295 (0.0143-0.0448)	26.4	0.0365 (0.026-0.047)	14.7		
ε-mAb2	0.017 (0.0104-0.0237)	20	0.0193 (0.014-0.0247)	14.2		
ε-mAb3	0.0714 (0.0339-0.109)	26.8	0.175 (0.147-0.204)	8.41	0.0209 (0.0141-0.0278)	16.6
ε-mAb4	0.0387 (-0.00215-0.0795)	53.9	0.0207 (0.00204-0.0393)	46.0		
ε-mAb5	0.0839 (0.0672-0.101)	10.2	0.0768 (0.0646-0.0889)	8.07	0.0733 (0.0613-0.0853)	8.33
ε-mAb6	0.0559 (0.041-0.0707)	13.5	0.0563 (0.0413-0.0713)	13.6	0.0563 (0.0413-0.0713)	13.6
ε-mAb7	0.073 (0.0387-0.107)	24	0.0757 (0.0412-0.11)	23.2	0.0706 (0.0453-0.0958)	18.3
ε-mAb8	0.0406 (0.0213-0.0599)	24.3	0.018 (0.0056-0.0304)	35.2		
ε-mAb9	0.0457 (0.0328-0.0586)	14.4	0.0504 (0.0359-0.0648)	14.6	0.0481 (0.0365-0.0597)	12.3
ε-mAb10	0.0199 (0.0039-0.0359)	41	0.0197 (0.00369-0.0357)	41.5	0.0219 (0.00394-0.0399)	41.8
ε-mAb11	0.0199 0.00384-0.0359)	41.2	0.0182 (0.00583-0.0305)	34.6		
ε-mAb12	0.0644 (0.053-0.0758)	9.01	0.0652 (0.0536-0.0767)	9.02	0.0661 (0.0545-0.0776)	8.96
ε-mAb13	0.122 (0.0835-0.161)	16.2	0.192 (0.143-0.241)	13.0		
ε-mAb14	0.103 (0.0767-0.129)	12.9	0.0872 (0.0683-0.106)	11.0	0.078 (0.0597-0.0963)	12
ε-mAb15	0.0465 (0.03-0.063)	18.1	0.0455 (0.0289-0.0622)	18.7	0.0456 (0.0292-0.062)	18.4
ε-mAb16	0.0375 (0.0233-0.0518)	19.4	0.0366 (0.0226-0.0505)	19.5	0.0455 (0.0289-0.0621)	18.6

ε-mAb17	0.116 (0.0663-0.166)	21.8	0.105 (0.0646-0.145)	19.6	0.0852 (0.0678-0.103)	10.4
ε-mAb18	0.0803 (0.0438-0.117)	23.2	0.0882 (0.046-0.13)	24.4	0.0708 (0.0275-0.114)	31.2
ε-mAb19	0.1 (0.0816-0.119)	9.55	0.107 (0.0836-0.13)	11.1	0.105 (0.0842-0.125)	9.99
ε-mAb20	0.066 (0.043-0.089)	17.8	0.0582 (0.0355-0.081)	19.9	0.096 (0.0675-0.124)	15.1
ε-mAb21	0.127 (0.044-0.209)	33.3	0.137 (0.0407-0.233)	35.8	0.143 (0.0465-0.239)	34.4
ε-mAb22	0.0232 (0.0176-0.0288)	12.3	0.0211 (0.0154-0.0268)	13.8	0.0226 (0.0168-0.0283)	13
ε-mAb23	0.0346 0.0268-0.0424)	11.5	0.0338 (0.0259-0.0417)	11.9	0.039 (0.0299-0.0481)	11.9
ε-mAb24	0.0326 (0.019-0.0462)	21.3	0.0291 (0.0165-0.0416)	22	0.0285 (0.015-0.042)	24.1
ε-mAb25	0.0449 (0.0304-0.0595)	16.5	0.0293 (0.0211-0.0375)	14.3	0.0422 (0.0283-0.056)	16.8
ε-mAb26	0.132 (0.118-0.145)	5.42			0.113 (0.104-0.121)	3.64

Section III.
Modeling of antibody drug conjugates

Chapter 3

Establishing in vitro–in vivo correlation for antibody drug conjugate efficacy:

a PK/PD modeling approach

Dhaval K. Shah, Frank Loganzo, Nahor Haddish-Berhane, Sylvia Musto, Hallie S. Wald, Frank Barletta, Judy Lucas, Tracey Clark, Steve Hansel, Alison Betts

Journal of Pharmacokinetics and Pharmacodynamics 45(2): 339-349 (2018).

3.1 Abstract

The objective of this manuscript was to establish in vitro–in vivo correlation (IVIVC) between the in vitro efficacy and in vivo efficacy of antibody drug conjugates (ADCs), using a PK/PD modeling approach. Nineteen different ADCs were used to develop IVIVC. In vitro efficacy of ADCs was evaluated using a kinetic cell cytotoxicity assay. The cytotoxicity data obtained from in vitro studies was characterized using a novel mathematical model, parameter estimates from which were used to derive an in vitro efficacy matrix for each ADC, termed as 'in vitro tumor static concentration' ($TSC_{in\ vitro}$). $TSC_{in\ vitro}$ is a theoretical concentration at continuous exposure of which the number of cells will neither increase nor decrease, compared to the initial cell number in the experiment. The in vivo efficacy of ADCs was evaluated using tumor growth inhibition (TGI) studies performed on human tumor xenograft bearing mice. The TGI data obtained from in vivo studies was characterized using a PK/PD model, parameter estimates from which were used to derive an in vivo efficacy matrix for each ADC, termed as 'in vivo tumor static concentration' ($TSC_{in\ vivo}$). $TSC_{in\ vivo}$ is a theoretical concentration if one were to maintain in the plasma of a tumor bearing mouse, the tumor volume will neither increase nor decrease compared to the initial tumor volume. Comparison of the $TSC_{in\ vitro}$ and $TSC_{in\ vivo}$ values from 19 ADCs provided a linear and positive IVIVC. The Spearman's rank correlation coefficient for $TSC_{in\ vitro}$ and $TSC_{in\ vivo}$ was found to be 0.82. On average $TSC_{in\ vivo}$ was found to be ~ 27 times higher than $TSC_{in\ vitro}$. The reasonable IVIVC for ADCs suggests that in vitro efficacy data was correctly able to differentiate ADCs for their in vivo efficacy. Thus, IVIVC can be used as a tool to triage ADC molecules in the discovery stage, thereby preventing unnecessary scaling-up of ADCs and waste of time and resources. An ability to predict the concentration of ADC that is efficacious in vivo using the in vitro data can also help in optimizing the experimental design of preclinical efficacy studies. As such, the novel PK/PD modeling method presented here to establish IVIVC for ADCs holds promise and should be evaluated further using diverse set of cell lines and anticancer agents.

3.2 Introduction

In vitro cytotoxicity assay and murine models of human tumor xenograft are the most widely used experimental systems in the discovery and preclinical development of oncology drugs. The routinely used in vitro cytotoxicity assays (usually performed in a 96-well plate format) not only provides a high throughput way to triage anticancer molecules in the discovery setting, but also provide a point estimate of a given molecule's potency for the chosen cell line i.e. IC50 or IC90. The human tumor xenografts transplanted into immune-compromised mice are the regularly used preclinical animal models to evaluate the efficacy of novel anticancer agents in vivo. These animal models not only help triage molecules based on their integrated pharmacokinetics (PK) and potency profile, but also provide some quantification of a given molecule's potency for inhibiting tumor growth in a given xenograft model (e.g. T/C ratio). Although both of these experimental approaches, i.e. in vitro cytotoxicity assay and murine tumor xenografts, are very informative in their own ways to help define a drug's potency and efficacy; there are only a handful of reports which have integrated the information from these two systems to establish in vitro-in vivo correlation (IVIVC) for the efficacy of chemotherapeutic drugs.

One of the reasons for the lack of efforts in establishing IVIVC for anticancer drug efficacy may be the different efficacy matrix that both the in vitro and the in vivo systems provide. The results from in vitro cytotoxicity assays are processed to usually represent the efficacy of a drug in the form of ICx (i.e. the concentration of the drug that causes X% reduction in the cell viability of the treatment group compared to the control group), at a certain period of time after the start of the treatment. Whereas the results from the in vivo tumor growth inhibition (TGI) studies are usually processed to provide the efficacy of a drug in the form of either minimum efficacious dose (MED), area under the drug concentration-time curve (AUC) at MED, or T/C ratio. Thus, because of the different units used to express the efficacy, it would be very difficult to compare the efficacy parameters obtained from an in vitro experimental system to the ones obtained from an in vivo system. This manuscript strives to demonstrate the use of pharmacokinetic-pharmacodynamic (PK/PD) modeling approach to derive a comparable efficacy parameter from the in vitro and in vivo experimental systems, in order to help establish IVIVC for the efficacy of anticancer drugs, using antibody drug conjugates (ADCs) as model therapeutic agents.

Here we have evaluated the in vitro cytotoxicity of 19 different ADCs using a kinetic cytotoxicity assay [1], where the viability of cancer cells was determined at multiple time points after incubation with various concentrations of ADCs. The viable cell number vs. time profile obtained from in vitro experiments was fitted by a semi-mechanistic PK/PD model to derive the secondary parameter for IVIVC, tumor static concentration (TSC). The TSC value derived from in vitro kinetic cytotoxicity assay ($TSC_{in\ vitro}$) is a theoretical concentration of the drug in a cell culture well, at continuous exposure of which the number of viable cells in the well will neither increase nor decrease compared to the starting cell number. To enable in vivo PK/PD modeling, the PK of all 19 ADCs that were tested in vitro, was determined in mice. A multiple dose TGI study was conducted for each of the 19 ADCs, in a murine human tumor xenograft model developed using the same cell line that was used for the in vitro cytotoxicity assay. The TGI data was modeled using a semi-mechanistic PK/PD model, and TSC was derived from the estimated parameters. The TSC value derived from TGI data ($TSC_{in\ vivo}$) is the theoretical concentration of a drug if one were to maintain in the plasma of a tumor bearing mouse, the tumor volume will neither increase nor decrease compared to the initial tumor volume of the experiment. The $TSC_{in\ vitro}$ and $TSC_{in\ vivo}$ values derived for each ADC were correlated to help establish the IVIVC for the efficacy of ADCs.

3.3 Methods

In vitro kinetic cytotoxicity assay

Her2 expressing N87 gastric carcinoma cells were seeded into 96-well cell culture plates for 24 hours before the ADC treatment. Cells were treated with 10 different 3-fold serially diluted ADC concentrations in duplicate. Replicate plates of treated cells were incubated for 1, 2, 3, 6, and 8 days to obtain time-course of drug effect. On the specified harvest day, 30 µl of Cell Titer Glo® One Solution Assay reagent (Promega Cat # G3581) was added to the cells and incubated for 0.5 hours at room temperature while shaking and protecting from light. After incubation, the luminescence was measured on a Victor plate reader (Perkin Elmer, Waltham, MA). Relative cell viability was determined as percentage of untreated control. In a parallel set of plates, a linear

standard curve of N87 cell number vs. relative luminescence units (RLU) was generated to convert the RLU of experimental samples into cell number for kinetic analyses.

Modeling the in vitro cytotoxicity data

The viable cell number versus time profiles obtained from in vitro kinetic cytotoxicity assays was modeled using the semi-mechanistic PK/PD model displayed in Figure-1. The PD model used here is developed by combining the two widely used mathematical models for characterizing the efficacy of chemotherapeutic drugs, the signal distribution model developed by Lobo and Balthasar [1] and the cell distribution model developed by Simeoni *et al.* [2,3]. As described in Figure-1, the model assumes that the presence of drug in the cell culture well ($C_{in\ vitro}$) initiates a concentration dependent nonlinear killing signal ($K1_{kill}$), which imparts its effect on cancer cells ($K4_{kill}$) following a transduction delay characterized by Tau_S. In the absence of drug, the cells are allowed to grow exponentially (K_g) until they reach a plateau ($Cell_{Maximum}$). Once the growing cancer cells in the well responds to the killing signal ($K4_{kill}$), a part of them is shuttled to the non-growing cell compartments, from where the cells are destined to die following a transduction delay characterized by Tau_C. The model equations are provided below:

$$\frac{dK1_{kill}}{dt} = \frac{1}{Tau_S} \bullet \left(\frac{K_{max\_in\_vitro} \bullet C_{in\_vitro}^{\gamma}}{IC_{50\_in\_vitro}^{\gamma} + C_{in\_vitro}^{\gamma}} - K1_{kill} \right) ;\ IC = 0 \quad (1)$$

$$\frac{dK2_{kill}}{dt} = \frac{1}{Tau_S} \bullet (K1_{kill} - K2_{kill}) ;\ IC = 0 \quad (2)$$

$$\frac{dK3_{kill}}{dt} = \frac{1}{Tau_S} \bullet (K2_{kill} - K3_{kill}) ;\ IC = 0 \quad (3)$$

$$\frac{dK4_{kill}}{dt} = \frac{1}{Tau_S} \bullet (K3_{kill} - K4_{kill}) ;\ IC = 0 \quad (4)$$

$$\frac{dCell_1}{dt} = Kg \bullet \left(1 - \frac{Cell_{Total}}{Cell_{Maximum}}\right) \bullet Cell_1 - K4_{kill} \bullet Cell_1 ;\ IC = Cell_{initial} \quad (5)$$

$$\frac{dCell_2}{dt} = K4_{kill} \bullet Cell_1 - \frac{1}{Tau_C} \bullet Cell_2 ;\ IC = 0 \quad (6)$$

$$\frac{dCell_3}{dt} = \frac{1}{Tau_C} \bullet (Cell_2 - Cell_3) ;\ IC = 0 \quad (7)$$

$$\frac{dCell_4}{dt} = \frac{1}{Tau_C} \bullet (Cell_3 - Cell_4) ;\ IC = 0 \quad (8)$$

$$Cell_{Total} = Cell_1 + Cell_2 + Cell_3 + Cell_4 \quad (9)$$

Above, $K1_{kill}$, $K2_{kill}$, $K3_{kill}$ and $K4_{kill}$ are the killing signal compartments, and $Cell_1$, $Cell_2$, $Cell_3$, and $Cell_4$ are the cell number compartments. $K_{max\_in\_vitro}$ is the maximum rate at which the drug can kill the cells and $IC_{50\_in\_vitro}$ is the drug concentration at which the kill rate is half of the maximum. IC refers to initial conditions of the differential equations.

The viable cell number versus time profiles generated for the control and all the concentration groups of a given ADC were fitted simultaneously by the model, using the naïve pool approach in the software Monolix® (v3.2, Paris, France - SAEM algorithm). For all the fittings the slope

coefficient γ was fixed to 1 and the residual error was described using the constant error model. The $TSC_{in\ vitro}$ value for each compound was calculated using the following equation, which is derived from the equation 5:

$$TSC_{in\ vitro} = \frac{Kg \bullet IC_{50\_in\_vitro}}{K_{max\_in\_vitro} - Kg} \quad (10)$$

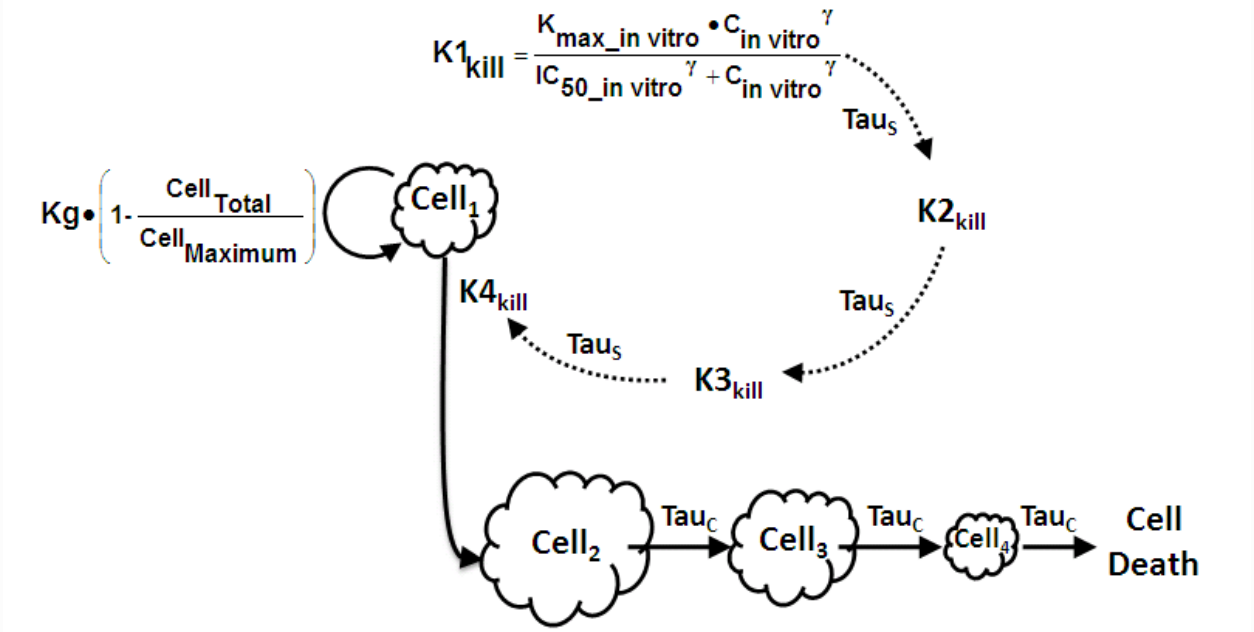

Figure 1: A schematic diagram demonstrating the mathematical model used to characterize in vitro kinetic cytotoxicity data. Please refers to the '*Modeling the In Vitro Cytotoxicity Data*' subsection in the '*Methods*' section for more details about the symbols and structure of the model.

Mouse PK of ADCs

All procedures using mice were approved by the Pfizer Institutional Animal Care and Use Committees and conducted according to established Animal Use Protocols. Female athymic (nu/nu) mice, 6-8 weeks of age, were obtained from Charles River Laboratories (Wilmington, MA) and housed in the vivarium at Pfizer Inc, Pearl River, NY. Mouse blood (10 µL) was collected serially from mice (n=3) for up to 336 h after a single 3 mg/kg dose of each ADC. Quantitation of the ADC concentrations in mouse plasma was achieved using ligand binding assays (ELISA or Gyros Immunoassay). In general, ADC was captured using a commercial polyclonal Anti-Human IgG (Fc specific) antibody, and the bound ADC was detected using a biotinylated polyclonal anti-payload antibody (Pfizer, Inc.). The limit of quantitation (LOQ) for the ligand binding assays was 80-100 ng/mL.

The plasma concentration vs. time profiles of each ADC in mouse was characterized using a two compartmental model with linear clearance from the central compartment. The model equations are provided below:

$$\frac{dX1_{ADC}}{dt} = -\frac{CL_{ADC}}{V1_{ADC}} \bullet X1_{ADC} - \frac{CLD_{ADC}}{V1_{ADC}} \bullet X1_{ADC} + \frac{CLD_{ADC}}{V2_{ADC}} \bullet X2_{ADC}; IC = Dose_{ADC} \quad (11)$$

$$\frac{dX2_{ADC}}{dt} = \frac{CLD_{ADC}}{V1_{ADC}} \bullet X1_{ADC} - \frac{CLD_{ADC}}{V2_{ADC}} \bullet X2_{ADC}; IC = 0 \quad (12)$$

Above, $X1_{ADC}$ and $X2_{ADC}$ are the amount of ADC in the central and peripheral compartment. $V1_{ADC}$ and $V2_{ADC}$ are the ADC volumes of distribution in the central and peripheral compartment. CL_{ADC} is the clearance of ADC from the central compartment and CLD_{ADC} is the distributive clearance between the central and peripheral compartments (see Fig 2). The model was fitted to the data using the weighting scheme of $1/(Y\hat{})^2$, by the software WinNonlin (version 5.2, Pharsight Corp., Mountain View, CA). Here Y^ refers to model predicted concentrations.

TGI studies in mouse xenografts

All procedures using mice were approved by the Pfizer Institutional Animal Care and Use Committees and conducted according to established Animal Use Protocols. Female athymic (nu/nu) mice, 6-8 weeks of age, were obtained from Charles River Laboratories (Wilmington, MA) and housed in the vivarium at Pfizer Inc, Pearl River, NY. Mice were injected subcutaneously with ~7.5 million N87 (gastric cancer cell line) tumor cells in 50% matrigel and the tumor was allowed to grow. Once the tumor volume reached 200-400 mm^3, animals were divided into 4 groups (6 to 10 mice per group) for each ADC. Animals were intravenously administered with saline (vehicle group) or ADC at 1,3 and 10 mg/kg dose levels (treatment groups), at the dosing regimen of Q4d x 4 starting on Day 1 after the randomization. All ADCs were dosed based on antibody (mAb) content. Tumors were measured at least once a week up to at least 41 days after dosing. The tumor volume was calculated using the following formula: Tumor volume in mm^3 = 0.5 x (tumor $width^2$) × (tumor length) [4]. The LOQ for the tumor measurement was 40 mm^3.

Modeling the TGI Data

The tumor volume vs. time data obtained from TGI studies was fitted using the PK/PD model displayed in Figure-2. As mentioned in the '*Mouse PK of ADCs*' section, the plasma PK of ADC was characterized using the standard 2 compartment model with linear elimination from the central compartment. The PD effect of ADC was characterized using a semi-mechanistic (modified cell distribution) model, which we have published earlier [5,6]. Equations for the PD model are provided below:

$$\frac{dV1}{dt} = \frac{k_{g_{Exponential}} \bullet \left(1 - \frac{TV}{V_{Max}}\right) \bullet V1}{\left(1 + \left(\frac{k_{g_{Exponential}}}{k_{g_{Linear}}} \bullet TV\right)^{\psi}\right)^{1/\psi}} - \frac{k_{kill\_Max} \bullet C_{ADC}}{KC_{50} + C_{ADC}} \bullet V1 \; ; IC = V_{Initial} \quad (13)$$

$$\frac{dV2}{dt} = \frac{k_{kill\_Max} \bullet C_{ADC}}{KC_{50} + C_{ADC}} \bullet V1 - \frac{V2}{Tau}\ ; IC = 0 \quad (14)$$

$$\frac{dV3}{dt} = \frac{(V2 - V3)}{Tau}; IC = 0 \quad (15)$$

$$\frac{dV4}{dt} = \frac{(V3 - V4)}{Tau}; IC = 0 \quad (16)$$

$$TV = V1 + V2 + V3 + V4 \quad (17)$$

Above, V1 is the growing tumor volume compartment whereas V2, V3, V4 are the non-growing tumor volume transit compartments. TV is the total tumor volume and $V_{initial}$ is the initial tumor volume. The tumor growth function is adapted from Simeoni *et al.* [2], where initially the tumor is allowed to grow according to an exponential growth rate $k_{gExponential}$ that switches to the linear growth rate $k_{gLinear}$ based on the total tumor volume and switching coefficient ψ. In order to account for the plateau observed at higher tumor volumes, a saturation function was added to the tumor growth term used by Simeoni *et al.* C_{ADC} is the ADC concentration in the plasma, k_{kill_Max} is the maximum rate at which the drug can kill the tumor, and KC_{50} is the drug concentration at which the kill rate is half of the maximum. The transit delay between the non-growing tumor compartments is described by Tau.

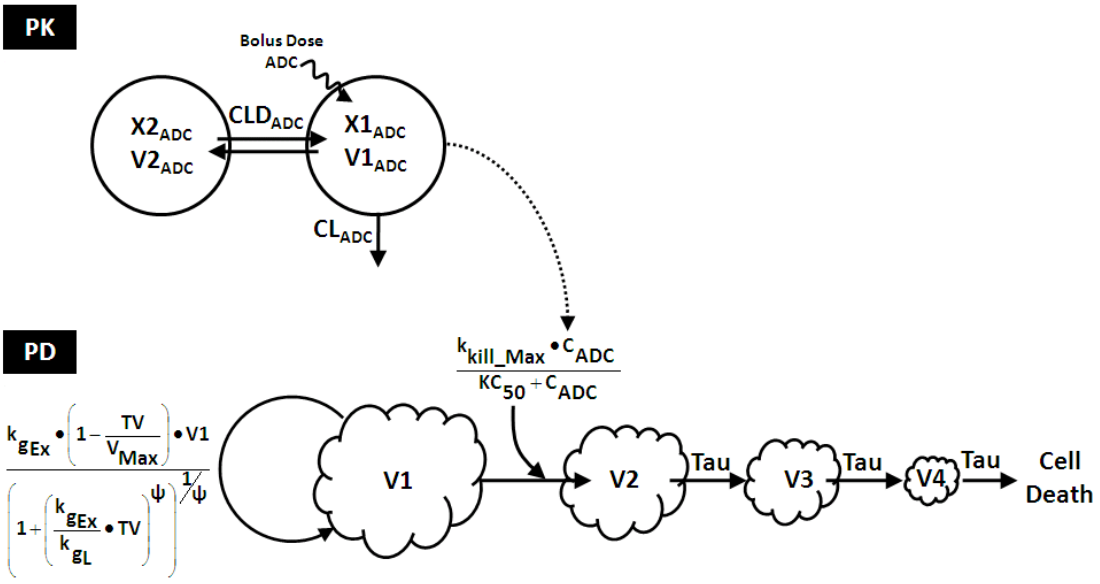

Figure 2: The PK/PD model used to characterize the TGI data for ADCs. Please refers to the '*Modeling the TGI Data*' subsection in the '*Methods*' section for more details about the symbols and structure of the model.

In order to fit the PK/PD model to TGI data generated for each ADC, a sequential parameter estimation method was followed, where the PK parameters were first estimated using the naïve pooling approach and then they were fixed to estimate the PD parameters using the population approach. This two-stage approach was preferred over the joint population PK/PD approach because the detailed information about the PK of ADC in each animal involved in the PD study

was not available. While estimating the PD parameters, initially the tumor growth parameters and inter-individual variability (IIV) for them were estimated from just the control group data. Subsequently, the IIV of the growth parameters and V_{max} were fixed, followed by estimation of both the growth and drug effect parameters simultaneously using the software Monolix® (v3.2, Paris, France - SAEM algorithm). The residual error was characterized using additive, proportional or, additive + proportional error models. The quality of the model fittings was assessed by considering weighted residual plot, observations against individual predictions (iPRED) and population predictions (PRED) plots, AIC and BIC values, and confidence in the parameter estimates (i.e. CV%).

The $TSC_{in\ vivo}$ value for each compound was calculated using the following equation, which is derived from the equation 13:

$$TSC_{in_{vivo}} = \frac{k_{g_{Exponential}} \bullet KC_{50} \bullet \left(1 - \frac{V_{initial}}{V_{max}}\right)}{k_{kill_{Max}} \bullet \left(1 + \left(\frac{k_{g_{Exponential}}}{k_{gLinear}} \bullet V_{initial}\right)^{\varphi}\right)^{\frac{1}{\varphi}} - k_{g_{Exponential}} \bullet \left(1 - \frac{V_{initial}}{V_{max}}\right)} \quad (18)$$

Equation 18 can be further simplified by considering whether $\left(\frac{k_{g_{Exponenial}}}{k_{g_{Linear}}} \bullet V_{Initial}\right)$ is ≤1 or >1. If $\left(\frac{k_{g_{Exponenial}}}{k_{g_{Linear}}} \bullet V_{Initial}\right)$ is ≤1 equation 18 reduces to:

$$TSC_{in\_vivo} = \frac{k_{g_{Exponential}} \bullet KC_{50}}{k_{kill\_Max} - k_{g_{Exponential}}} \quad (19)$$

and if $\left(\frac{k_{g_{Exponential}}}{k_{g_{Linear}}} \bullet V_{Initial}\right)$ is >1 equation 18 reduces to:

$$TSC_{in\_vivo} = \frac{k_{g_{Linear}} \bullet KC_{50}}{k_{kill\_Max} \bullet V_{Initial} - k_{g_{Linear}}} \quad (20)$$

Please refer to Haddish-Berhane *et al.* [6] for detailed derivation of abovementioned simplified equations and for the discussion about pathophysiological meaning behind the simplifications.

Establishing IVIVC using $TSC_{in\ vitro}$ and $TSC_{in\ vivo}$

The $TSC_{in\ vitro}$ and $TSC_{in\ vivo}$ values for each ADC was plotted on a scatter plot and observed for any trends or outliers. The data was analyzed to find out the relationship between $TSC_{in\ vitro}$ and $TSC_{in\ vivo}$ and, to determine the Spearman's rank correlation coefficient, since it is a nonparametric statistical test that does not assume normal distribution for variables. The relationship between $TSC_{in\ vitro}$ and $TSC_{in\ vivo}$ was established by fitting the data to the power model, using the software WinNonlin (version 5.2, Pharsight Corp., Mountain View, CA):

$$TSC_{in_{vivo}} = A \bullet TSC_{in_{vitro}}{}^{B}$$

3.4 Results

In Vitro Kinetic Cytotoxicity Assay

A representative in vitro 'cell number vs. time' profile obtained at various concentrations of one of the 19 ADCs (i.e. trastuzumab-DM1 or T-DM1) is displayed in Figure-3A. As shown in the Figure-3A for T-DM1, for most of the ADCs tested, it was observed that the effect of the ADC on cell viability started after a delay of ~1 day. For most of the ADCs the concentration-effect profile was very steep, and the range of concentrations between which the effect of the ADC varied from almost no effect to the maximum effect was very narrow. For example, as shown in the Figure-3A, at the concentration of 0.46 nM the effect of T-DM1 on cell viability was as low as the control group, whereas at the concentration of 4.12 nM the effect was as high as 1000 nM. It was also observed that it took as many as 6 days before the efficacious concentrations of ADC were able to kill most of the cancer cells in the well, suggesting a gradual and not sudden rate of cell death after exposure to ADC's killing signal. Apart from one of the ADCs, all the ADCs were able to kill the cancer cells in the well at the concentration range tested.

Modeling the In Vitro Cytotoxicity Data

Figure-3B shows a representative model fitting of the in vitro 'viable cell number vs. time' data generated using T-DM1, in the form of 'model predicted cell number vs. observed cell number' plot. Representative parameter estimates from the model fitting shown in Figure-3B are provided in the Table-1. The model did a reasonably good job in fitting the data for most of the ADCs, except for one ADC that did not show any killing. Table-3 provides the calculated (using equation 10) $TSC_{in\ vitro}$ values for the 19 ADCs tested. For the ADC that did not show any killing, the TSC value was assumed to be greater than the highest concentration tested i.e. 1000 nM.

Table 1: Parameter estimates obtained from fitting the model shown in Figure-1 to the in vitro 'viable cell number versus time' data generated following T-DM1 treatment.

Parameter	Estimate	% RSE	Unit
Kg	1.05	4	Day^{-1}
$Cell_{Maximum}$	25300	4	Unit less
Tau_C	0.199	43	Day
Tau_S	0.302	9	Day
$K_{max\_in\_vitro}$	1.62	3	Day^{-1}
$IC^{\gamma}_{50\_in\_vitro}$	3.04	8	nM
γ	1	Fixed	Unitless
$TSC_{in\ vitro}$	5.6	Derived	nM

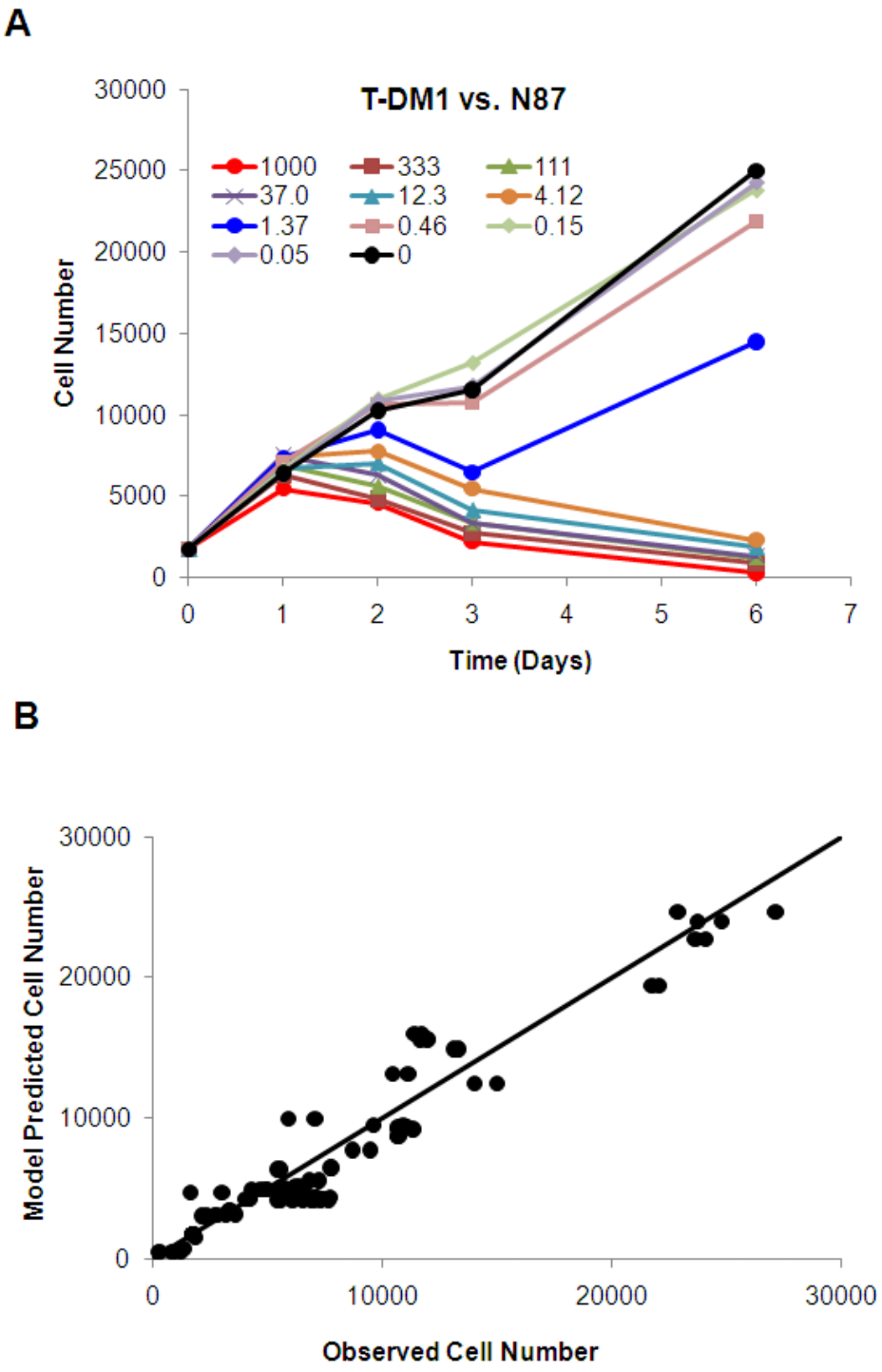

Figure 3: (A) The figure displays 'viable cell number vs. time' profiles generated after incubating different concentrations of Trastuzumab-DM1 with N87 cells. **(B)** The quality of model fitting to the data displayed in the panel A is demonstrated as a plot of 'Model predicted cell number vs. Observed cell number'.

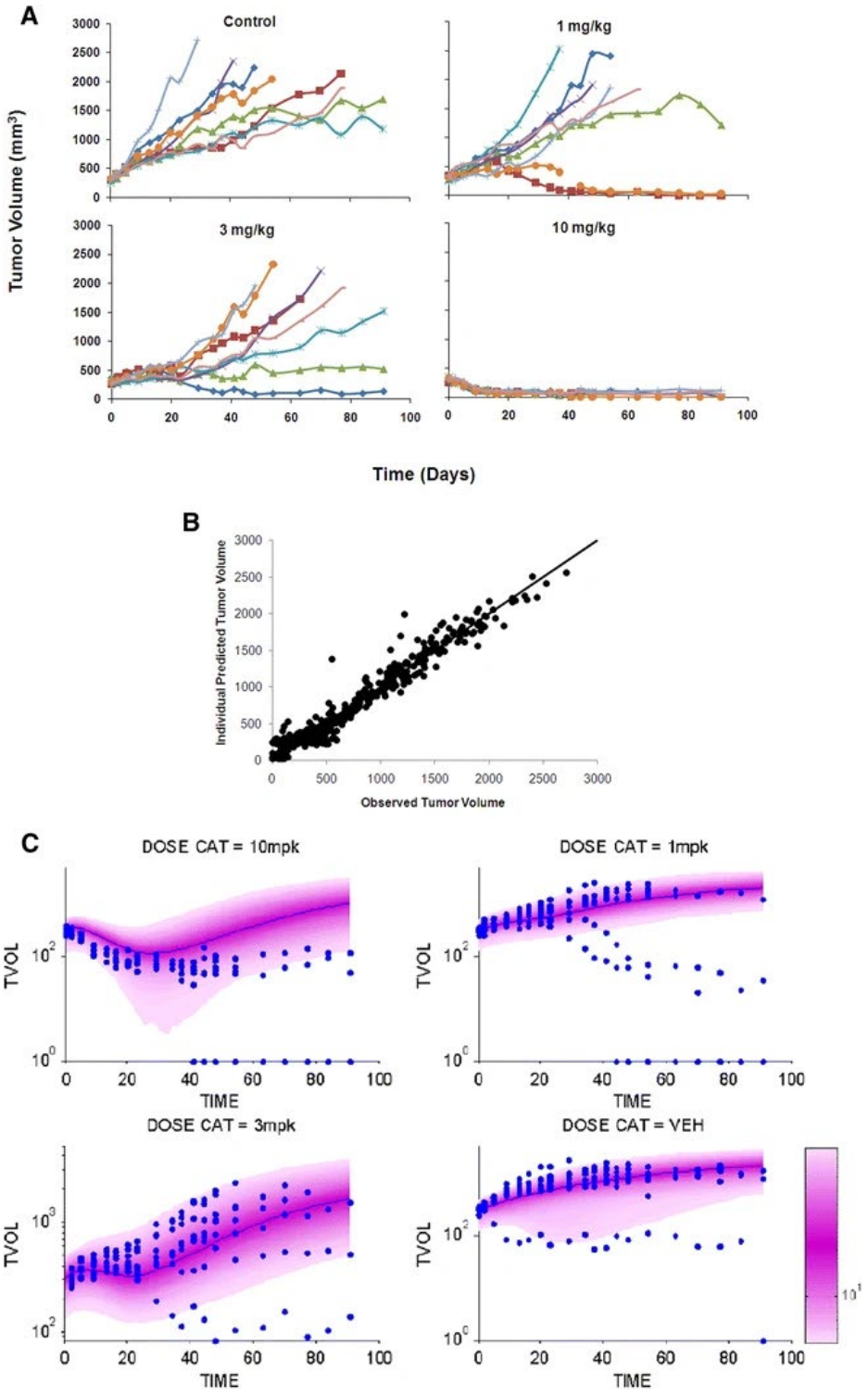

Figure 4: (A) The TGI data obtained after administration of different doses of Trastuzumab-DM1 into N87 xenografts bearing mice. **(B)** The quality of PK/PD model fitting to the TGI data displayed in panel **a** is demonstrated as a plot of 'Individual model predicted tumor volume versus observed tumor volume'. **(C)** The visual predictive check (VPC) for model fitting of T-DM1 TGI data. The symbols represent observed data and the shaded region represent 90% confidence interval

Modeling the Data from TGI Studies in Mouse Xenografts

Figure-4A shows representative tumor volume vs. time profiles obtained from the TGI study conducted in N87 xenografts using one of the ADCs, T-DM1. As demonstrated in the figure for T-DM1, all the ADCs showed a dose dependent response profile. Figure-4B displays the 'observed tumor volume vs. individual predicted tumor volume' profile obtained from the model fitting of the data presented in Figure-4A. Parameter estimates from the model fitting of T-DM1 TGI data are provided in Table-2. As evident from the Figure-4B and Table-2, the model did a reasonably good job in fitting the TGI data for T-DM1. The model also performed well for the characterization of TGI data for all the other ADCs tested (data not shown). The $TSC_{in\ vivo}$ values calculated for T-DM1 and other ADCs, using equations 19 or 20, are reported in Table-3.

Table 2: Parameter estimates obtained from fitting the model shown in Figure-2 to the TGI data generated in N87 xenografts following T-DM1 treatment.

Parameter	Estimate	%RSE	Unit
$k_{g_{Exponenial}}$	0.0732	11	Day^{-1}
$k_{g_{Linear}}$	37.9	17	$mm^3 \bullet Day^{-1}$
V_{Max}	4.22E+03	18	mm^3
Tau	1.36	16	Day
k_{kill_Max}	0.405	38	Day^{-1}
KC_{50}	131	48	µg/mL
ψ	20	Fixed	Unit less
$TSC_{in\ vivo}$	28.9	Derived	µg/mL
$IIV\_k_{g_{Exponenial}}$	0.47	38	Unitless
$IIV\_k_{g_{Linear}}$	0.781	27	Unitless

IIV: interindividual variability

Establishing IVIVC using $TSC_{in\ vitro}$ and $TSC_{in\ vivo}$

Figure-5 depicts the plot generated to correlate $TSC_{in\ vitro}$ and $TSC_{in\ vivo}$, which shows a linear trend between the two variables. The Spearman's rank correlation coefficient between $TSC_{in\ vitro}$ and $TSC_{in\ vivo}$ was found to be 0.82. The ADC that did not show any killing in the in vitro assay (gray symbol in the figure) was considered outlier for building the IVIVC. When this outlier was included for analysis the Spearman's rank correlation coefficient was found to be 0.85. Fitting of the power model to the data (excluding the outlier) that demonstrates a linear and positive relationship between $TSC_{in\ vitro}$ and $TSC_{in\ vivo}$ provided the slope value of 26.8 (CV%=15.2) and an exponent of 0.83 (CV%=9.82); with the weighted correlation coefficient (R^2) value of 0.81.

Table 3: $TSC_{in\ vitro}$ and $TSC_{in\ vivo}$ values derived for each ADC to establish IVIVC.

ADC ID	$TSC_{in\ vitro}$, nM (%RSE)	$TSC_{in\ vivo}$, nM (% RSE)
ADC1	0.23 (9.01)	7.18 (19.5)
ADC2	0.51 (9.31)	11.0 (21.2)
ADC3	0.61 (9.54)	32.7 (11.6)
ADC4	0.62 (9.45)	92.2 (12.3)
ADC5	0.66 (21.2)	14.2 (37.1)
ADC6	0.93 (17.2)	33.5 (34.1)
ADC7	1.12 (12.5)	43.3 (23.1)
ADC8	1.45 (9.66)	41.3 (24.2)
ADC9	2.18 (9.17)	47.9 (57.1)
ADC10	2.56 (20.7)	525 (97)
ADC11	3.10 (17.3)	1160 (63.2)
ADC12	4.08 (15.2)	83.3 (12.1)
ADC13	4.69 (14.1)	135 (144)
ADC14 (Trastuzumab-DM1)	5.60 (16.3)	193 (65.5)
ADC15	12.13 (19)	256 (112)
ADC16	15.26 (11.1)	840 (119)
ADC17	26.25 (29)	441 (71.2)
ADC18	29.64 (19.9)	296 (52.3)
ADC19	> 1000 (NA)	1138 (64.7)

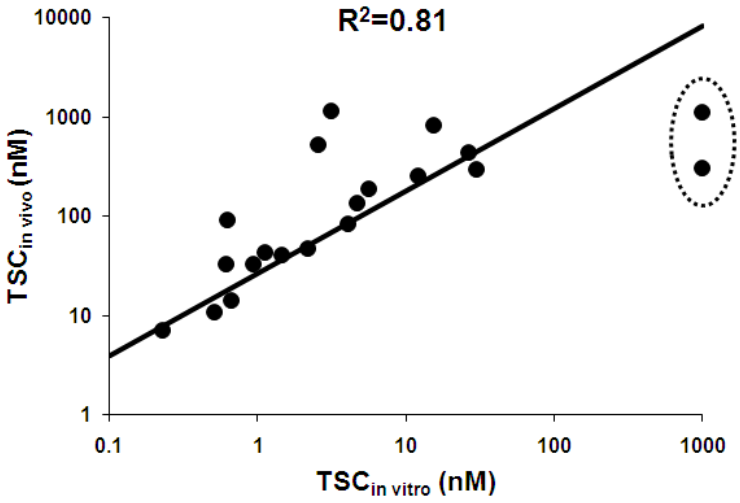

Figure 5: The figure demonstrates the positive linear relationship observed between $TSC_{in\ vitro}$ and $TSC_{in\ vivo}$, which was used to generate the IVIVC. The gray circle highlights the ADC that was an outlier.

3.5 Discussion

IVIVC is generally defined as a predictive mathematical relationship between an in vitro property of the drug and an in vivo response. It is a very routinely sought after and used methodology in the drug discovery and development programs at pharmaceutical industries (e.g. IVIVC between in vitro dissolution and the in vivo absorption rate of a drug from the dosage form). In oncology drug discovery and development programs, scientists have been trying to establish IVIVC between the in vitro sensitivity/resistance of a chemotherapeutic drug and it's in vivo response (preclinical/clinical) [7-10]. However, the majority of these IVIVC studies have based their conclusions on the observation of trends rather than the use of quantitative methods, and most studies have used dichotomous definitions (responsive vs. resistant) of in vitro or in vivo (preclinical/clinical) activity based on largely invalidated cutoff values of efficacy measures [7,10,8,9]. As such, most of the IVIVCs developed for oncology drugs are non-predictive, and overall correlation rates are reported as % of true positive, true negative, false positive, and false negative correlations.

Here we have used mathematical PK/PD modeling to derive a predicative IVIVC between the in vitro and in vivo efficacy of ADCs, which are novel anticancer agents. The success or failure of an effort to establish IVIVC for oncology drugs depend on the quality of experimental models, protocols, and endpoints used to generate the data. Consequently, for our IVIVC study we have conduct a detailed kinetic in vitro and in vivo experiments and have integrated all the available data using mathematical modeling. In the past, a large number of the reported IVIVC are generated using clonogenic in vitro assays that use colorimetric endpoints (e.g. MTT) to infer the

in vitro potency of anticancer drugs (e.g. IC50), and TGI studies in murine xenograft models of human tumors that use changes in tumor volume to infer in vivo potency of the drug (e.g. T/C%). However, the point estimates used for these past IVIVCs do not contain complete information about the time course of a drug's response, and could also change based on the time chosen to determine the particular endpoint (e.g. IC50 and T/C values can be different based on the time point chosen to calculate them). To overcome this issue, we have employed TSC as an integrated endpoint to conduct IVIVC, which is a secondary parameter derived from the model estimates.

While conducting an in vitro time course study to assess the effect of anticancer agents on cell viability is better than a single time point study, correctly integrating the data from the time course study is equally important [10,1]. For example, despite conducting a time course study on the effect of anticancer agents on cell viability, Furukawa *et al.* [10] have reported their data without any kind of integration. This could have been easily accomplished with the use of a mathematical model that can characterize all the data simultaneously [1]. Accordingly, we have not only conducted detailed time course study to investigate the effect of ADCs on cell viability, but we have also integrated all the in vitro data for each ADC simultaneously using a novel mathematical model. The parameter estimates from this model were further used to derive $TSC_{in\ vitro}$. The in vivo efficacy of each ADC was evaluated in xenograft models, where TGI studies were conducted after administering 3 different doses of ADCs, and the data from in vivo studies was integrated using a widely used PK/PD model [2,3]. However, similar to T/C values, just the parameter estimates from the mathematical model cannot be compared with the in vitro results. Thus, $TSC_{in\ vivo}$ was derived from the parameter estimates of the PK/PD model to use it as a variable for correlation with $TSC_{in\ vitro}$.

As reported in Table-3 and Figure-5 and based on the Spearman's rank correlation coefficient value of 0.82, it can be deduced that there was a good positive correlation between $TSC_{in\ vitro}$ and $TSC_{in\ vivo}$. These data suggest that the in vitro studies were correctly able to rank ADCs in terms of in vivo potency. Of note, the estimated value for the ratio of $TSC_{in\ vivo}$ to $TSC_{in\ vitro}$ for all the ADCs was ~27 (the slope of the power model fitted to the linear relationship between $TSC_{in\ vivo}$ and $TSC_{in\ vitro}$), which imply that in order to achieve tumor stasis in vivo ~27 fold higher concentrations of ADC need to be maintained in the plasma of tumor bearing mouse compared to the ADC concentration in the cell culture media. This observation is consistent with the fact that tumor concentrations of antibodies/ADCs can be considerably lower than the plasma concentrations, requiring a higher plasma concentration to achieve tumor concentrations similar to the cell culture media concentration. The IVIVC established in this manuscript can help an ADC discovery and development project team triage the ADCs based on their relative potency and can help the team make go/no-go decisions about a particular ADC based on the expected plasma concentration required to achieve stasis. Thus, the triaging based on IVIVC can save a lot of time, resources, and animals by preventing unnecessary scale-up of ADCs and unnecessary in-vivo experiments. The ability to predict in vivo stasis concentration based on the in vitro experiment can also help scientists design an optimal dosing regimen with suitable doses.

It is important to point out that for conducting IVIVC the same cell line was used for the in vitro and in vivo experiment. So, it remains to be seen whether the in vitro rank ordering of ADCs and IVIVC would hold up if different cell lines were used to conduct the analysis. Also, for one of the

ADCs there was no efficacy observed in vitro, however there was a marginal efficacy in vivo. This could occur because the in vitro cell culture medium provides a different biological milieu than the in vivo system, where the chances of an ADC being digested by a different mechanism and locally releasing the payload in the tumor may be a factor. Nonetheless, the ADC with IC50 value of >1000 nM had a very high $TSC_{in\ vivo}$ value as well, implying the weak efficacy in vitro is aptly translated to a weak efficacy in vivo. All the ADCs tested had payloads with similar mechanisms of action, and the IVIVC approach presented here should also be verified using payloads with diverse mechanism of action. Here we have assumed that nominal concentrations of ADC in the media remain the same, however it is well known that payload may fall off ADCs in the media. So, ideally one should account for the decreasing ADC concentrations in the media while modeling the in vitro data, but it becomes too laborious to measure ADC concentrations in all wells at each time point. Hence, we have assumed the constant concentration of ADC in media.

The IVIVC approach established in this manuscript also showcases the tremendous potential of PK/PD modeling in integrating the available in vitro and in vivo data. Without such tools it would not have been possible to integrate all the in vitro and in vivo data to come up with one single variable representing the efficacy of a molecule in each experimental setting, which can be compared with each other to establish IVIVC. It is hypothesized that the methodology to establish IVIVC presented here can be applied to all anticancer therapeutic drugs. Since this approach accounts for in vitro and in vivo PK of the molecules and associates this PK with the observed efficacy of the molecules, it helps in establishing a relationship that purely depends on compounds' potency. Thus, one should be able to establish IVIVC for any class of anticancer agents (e.g. small molecule or large molecule) using any of the available cancer cell lines. However, one has to keep in mind that this approach assumes that the cancer cells behaves similarly during in vitro and in vivo experiments, which may not always be true. One can also conduct the kinetic in vitro experiment with toxicity prone tissue cells (e.g. liver or bone marrow cells) to generate a toxicity matrix similar to $TSC_{in\ vitro}$, which can help in generating an in vitro therapeutic index that could provide a better parameter for triaging anticancer drugs at the discovery stage.

In summary, here we have presented a novel methodology to establish IVIVC for anticancer drugs, which uses PK/PD modeling to integrate the information obtained from the experimental data. The in vitro potency was represented as $TSC_{in\ vitro}$ and the in vivo potency was represented as $TSC_{in\ vivo}$. Data from 19 different ADCs was used to establish the IVIVC between $TSC_{in\ vitro}$ and $TSC_{in\ vivo}$, which provided a very good positive correlation evident from the Spearman's rank correlation coefficient value of 0.82. Establishing IVIVC for oncology drugs provides a tremendous savings in terms of time and resources, along with an ability to triage correct molecules based on their potency in the discovery or early drug development stage. The PK/PD modeling approach to establish IVIVC presented here should be verified by employing a diverse set of anticancer drugs and cell lines.

References

1. Lobo ED, Balthasar JP (2002) Pharmacodynamic modeling of chemotherapeutic effects: application of a transit compartment model to characterize methotrexate effects in vitro. AAPS pharmSci 4 (4):E42. doi:10.1208/ps040442
2. Simeoni M, Magni P, Cammia C, De Nicolao G, Croci V, Pesenti E, Germani M, Poggesi I, Rocchetti M (2004) Predictive pharmacokinetic-pharmacodynamic modeling of tumor growth kinetics in xenograft models after administration of anticancer agents. Cancer research 64 (3):1094-1101
3. Yang J, Mager DE, Straubinger RM (2010) Comparison of two pharmacodynamic transduction models for the analysis of tumor therapeutic responses in model systems. The AAPS journal 12 (1):1-10. doi:10.1208/s12248-009-9155-7
4. Tomayko MM, Reynolds CP (1989) Determination of subcutaneous tumor size in athymic (nude) mice. Cancer chemotherapy and pharmacology 24 (3):148-154
5. Shah DK, Haddish-Berhane N, Betts A (2012) Bench to bedside translation of antibody drug conjugates using a multiscale mechanistic PK/PD model: a case study with brentuximab-vedotin. Journal of pharmacokinetics and pharmacodynamics 39 (6):643-659. doi:10.1007/s10928-012-9276-y
6. Haddish-Berhane N, Shah DK, Ma D, Leal M, Gerber HP, Sapra P, Barton HA, Betts AM (2013) On translation of antibody drug conjugates efficacy from mouse experimental tumors to the clinic: a PK/PD approach. Journal of pharmacokinetics and pharmacodynamics 40 (5):557-571. doi:10.1007/s10928-013-9329-x
7. Fiebig HH, Maier A, Burger AM (2004) Clonogenic assay with established human tumour xenografts: correlation of in vitro to in vivo activity as a basis for anticancer drug discovery. European journal of cancer 40 (6):802-820. doi:10.1016/j.ejca.2004.01.009
8. Johnson JI, Decker S, Zaharevitz D, Rubinstein LV, Venditti JM, Schepartz S, Kalyandrug S, Christian M, Arbuck S, Hollingshead M, Sausville EA (2001) Relationships between drug activity in NCI preclinical in vitro and in vivo models and early clinical trials. British journal of cancer 84 (10):1424-1431. doi:10.1054/bjoc.2001.1796
9. Voskoglou-Nomikos T, Pater JL, Seymour L (2003) Clinical predictive value of the in vitro cell line, human xenograft, and mouse allograft preclinical cancer models. Clinical cancer research : an official journal of the American Association for Cancer Research 9 (11):4227-4239
10. Furukawa T, Kubota T, Watanabe M, Takahara T, Yamaguchi H, Takeuchi T, Kase S, Kodaira S, Ishibiki K, Kitajima M, et al. (1992) High in vitro-in vivo correlation of drug response using sponge-gel-supported three-dimensional histoculture and the MTT end point. International journal of cancer Journal international du cancer 51 (3):489-498

Supplementary Material

Supplementary Table 1: Parameter estimates obtained by fitting the model shown in Figure 1 to the in vitro 'viable cell number vs. time' data generated following incubation of N87 cells with different ADCs.

ADC-1

Parameter	Estimate	%RSE	Unit
Kg	5.93E-01	3	Day^{-1}
$Cell_{Maximum}$	2.13E+05	3	Unit less
Tau_C	0.979	14	Day
Tau_S	0.184	12	Day
$K_{max\_in\_vitro}$	2.49	6	Day^{-1}
$IC^{\gamma}_{50\_in\_vitro}$	0.729	2	nM
γ	1	Fixed	Unit less

ADC-2

Parameter	Estimate	%RSE	Unit
Kg	5.52E-01	4	Day^{-1}
$Cell_{Maximum}$	2.54E+05	6	Unit less
Tau_C	0.55	19	Day
Tau_S	0.162	9	Day
$K_{max\_in\_vitro}$	1.07	0	Day^{-1}
$IC^{\gamma}_{50\_in\_vitro}$	0.474	4	nM
γ	1	Fixed	Unit less

ADC-3

Parameter	Estimate	%RSE	Unit
Kg	3.73E-01	6	Day^{-1}
$Cell_{Maximum}$	3.21E+05	12	Unit less
Tau_C	0.231	24	Day
Tau_S	0.0187	41	Day
$K_{max\_in\_vitro}$	1.17	1	Day^{-1}
$IC^{\gamma}_{50\_in\_vitro}$	1.3	2	nM
γ	1	Fixed	Unit less

ADC-4

Parameter	Estimate	%RSE	Unit
Kg	3.75E-01	6	Day^{-1}
$Cell_{Maximum}$	4.12E+05	15	Unit less
Tau_C	0.36	19	Day
Tau_S	0.0463	11	Day
$K_{max\_in\_vitro}$	1.03	0	Day^{-1}
$IC^{\gamma}_{50\_in\_vitro}$	1.09	1	nM
γ	1	Fixed	Unit less

ADC-5

Parameter	Estimate	%RSE	Unit
Kg	9.66E-01	3	Day^{-1}
$Cell_{Maximum}$	2.33E+05	3	Unit less
Tau_C	0.256	39	Day
Tau_S	0.35	10	Day
$K_{max\_in\_vitro}$	1.72	5	Day^{-1}
$IC^{\gamma}_{50\_in\_vitro}$	0.517	5	nM
γ	1	Fixed	Unit less

ADC-6

Parameter	Estimate	%RSE	Unit
Kg	8.69E-01	3	Day^{-1}
$Cell_{Maximum}$	2.20E+05	2	Unit less
Tau_C	3.60E-01	37	Day
Tau_S	0.341	7	Day
$K_{max\_in\_vitro}$	1.72	8	Day^{-1}
$IC^{\gamma}_{50\_in\_vitro}$	0.907	1	nM
γ	1	Fixed	Unit less

ADC-7

Parameter	Estimate	%RSE	Unit
Kg	8.56E-01	3	Day^{-1}
Cell Maximum	2.55E+04	5	Unit less
Tau_C	1.02	18	Day
Tau_S	0.253	8	Day
$K_{max\_in\_vitro}$	3.01	7	Day^{-1}
$IC^{\gamma}_{50\_in\_vitro}$	2.81	7	nM
γ	1	Fixed	Unit less

ADC-8

Parameter	Estimate	%RSE	Unit
Kg	0.928	3	Day^{-1}
Cell Maximum	26500	3	Unit less
Tau_C	1.06	14	Day
Tau_S	0.201	6	Day
$K_{max\_in\_vitro}$	2.21	3	Day^{-1}
$IC^{\gamma}_{50\_in\_vitro}$	2	6	nM
γ	1	Fixed	Unit less

ADC-9

Parameter	Estimate	%RSE	Unit
Kg	0.843	3	Day^{-1}
Cell Maximum	2.58E+04	3	Unit less
Tau_C	1.05	10	Day
Tau_S	1.38E-01	8	Day
$K_{max\_in\_vitro}$	3.32	5	Day^{-1}
$IC^{\gamma}_{50\_in\_vitro}$	6.42	5	nM
γ	1	Fixed	Unit less

ADC-10

Parameter	Estimate	%RSE	Unit
Kg	3.87E-01	6	Day^{-1}
Cell Maximum	3.71E+05	12	Unit less
Tau_C	0.0351	168	Day
Tau_S	0.0297	16	Day
$K_{max\_in\_vitro}$	0.676	5	Day^{-1}
$IC^{\gamma}_{50\_in\_vitro}$	1.91	10	nM
γ	1	Fixed	Unit less

ADC-11

Parameter	Estimate	%RSE	Unit
Kg	4.81E-01	7	Day^{-1}
Cell Maximum	4.44E+04	9	Unit less
Tau_C	1.78E-01	19	Day
Tau_S	0.0434	34	Day
$K_{max\_in\_vitro}$	1.14	2	Day^{-1}
$IC^{\gamma}_{50\_in\_vitro}$	3.25	12	nM
γ	1	Fixed	Unit less

ADC-12

Parameter	Estimate	%RSE	Unit
Kg	0.984	4	Day^{-1}
Cell Maximum	2.80E+04	3	Unit less
Tau_C	2.22E-01	60	Day
Tau_S	2.69E-01	18	Day
$K_{max\_in\_vitro}$	1.51E+00	3	Day^{-1}
$IC^{\gamma}_{50\_in\_vitro}$	2.18E+00	8	nM
γ	1	Fixed	Unit less

ADC-13

Parameter	Estimate	%RSE	Unit
Kg	6.31E-01	3	Day^{-1}
$Cell_{Maximum}$	3.81E+05	3	Unit less
Tau_C	0.347	27	Day
Tau_S	0.224	6	Day
$K_{max\_in\_vitro}$	0.857	2	Day^{-1}
$IC^{\gamma}_{50\_in\_vitro}$	1.68	3	nM
γ	1	Fixed	Unit less

ADC-14

Parameter	Estimate	%RSE	Unit
Kg	1.05	4	Day^{-1}
$Cell_{Maximum}$	25300	4	Unit less
Tau_C	0.199	43	Day
Tau_S	0.302	9	Day
$K_{max\_in\_vitro}$	1.62	3	Day^{-1}
$IC^{\gamma}_{50\_in\_vitro}$	3.04	8	nM
γ	1	Fixed	Unit less

ADC-15

Parameter	Estimate	%RSE	Unit
Kg	1	3	Day^{-1}
$Cell_{Maximum}$	2.57E+04	4	Unit less
Tau_C	1.58E+00	15	Day
Tau_S	0.0564	11	Day
$K_{max\_in\_vitro}$	1.23	1	Day^{-1}
$IC^{\gamma}_{50\_in\_vitro}$	2.79	9	nM
γ	1	Fixed	Unit less

ADC-16

Parameter	Estimate	%RSE	Unit
Kg	5.05E-01	3	Day^{-1}
$Cell_{Maximum}$	2.54E+05	5	Unit less
Tau_C	0.747	18	Day
Tau_S	0.0928	12	Day
$K_{max\_in\_vitro}$	0.731	1	Day^{-1}
$IC^{\gamma}_{50\_in\_vitro}$	6.83	4	nM
γ	1	Fixed	Unit less

ADC-17

Parameter	Estimate	%RSE	Unit
Kg	5.99E-01	3	Day^{-1}
$Cell_{Maximum}$	3.68E+05	3	Unit less
Tau_C	0.488	22	Day
Tau_S	0.197	11	Day
$K_{max\_in\_vitro}$	0.73	4	Day^{-1}
$IC^{\gamma}_{50\_in\_vitro}$	5.74	9	nM
γ	1	Fixed	Unit less

ADC-18

Parameter	Estimate	%RSE	Unit
Kg	6.12E-01	2	Day^{-1}
$Cell_{Maximum}$	3.70E+05	2	Unit less
Tau_C	0.436	35	Day
Tau_S	0.226	22	Day
$K_{max\_in\_vitro}$	0.72	2	Day^{-1}
$IC^{\gamma}_{50\_in\_vitro}$	5.23	6	nM
γ	1	Fixed	Unit less

Supplementary Table 2: Parameter estimates obtained by fitting the model shown in Figure-2 to the TGI data generated in N87 xenografts following administration of different ADCs.

ADC-1

Parameter	Estimate	%RSE	Unit
$k_{g\ Exponential}$	0.102	7	Day^{-1}
$k_{gLinear}$	28.6	9	$mm^3 \bullet Day^{-1}$
V_{Max}	4.16E+03	22	mm^3
Tau	1.68	6	Day
k_{kill_Max}	0.174	4	Day^{-1}
KC_{50}	1.01	0	µg/mL
ψ	20	Fixed	Unit less
$IIV\_k_{g\ Exponential}$	0.266	94	Unit less
$IIV\_k_{g\ Linear}$	0.393	23	Unit less

ADC-2

Parameter	Estimate	%RSE	Unit
$k_{g\ Exponential}$	0.0745	6	Day^{-1}
$k_{gLinear}$	51.8	14	$mm^3 \bullet Day^{-1}$
V_{Max}	2.01E+03	8	mm^3
Tau	1.34	7	Day
k_{kill_Max}	0.212	6	Day^{-1}
KC_{50}	3.04	17	µg/mL
ψ	20	Fixed	Unit less
$IIV\_k_{g\ Exponential}$	0.222	70	Unit less
$IIV\_k_{g\ Linear}$	0.478	23	Unit less

ADC-3

Parameter	Estimate	%RSE	Unit
$k_{g\ Exponential}$	0.138	7	Day^{-1}
$k_{gLinear}$	58.5	8	$mm^3 \bullet Day^{-1}$
V_{Max}	3.82E+03	17	mm^3
Tau	5.01	2	Day
k_{kill_Max}	0.585	1	Day^{-1}
KC_{50}	15.9	7	µg/mL
ψ	20	Fixed	Unit less
$IIV\_k_{g\ Exponential}$	0.186	58	Unit less
$IIV\_k_{g\ Linear}$	0.322	23	Unit less

ADC-4

Parameter	Estimate	%RSE	Unit
$k_{g\ Exponential}$	0.236	7	Day^{-1}
$k_{gLinear}$	64.3	8	$mm^3 \bullet Day^{-1}$
V_{Max}	3.05E+03	10	mm^3
Tau	3.22	3	Day
k_{kill_Max}	0.975	0	Day^{-1}
KC_{50}	59	8	µg/mL
ψ	20	Fixed	Unit less
$IIV\_k_{g\ Exponential}$	0.349	>100	Unit less
$IIV\_k_{g\ Linear}$	0.357	24	Unit less

ADC-5

Parameter	Estimate	%RSE	Unit
$k_{g\ Exponential}$	0.0636	13	Day^{-1}
$k_{gLinear}$	61.4	18	$mm^3 \bullet Day^{-1}$
V_{Max}	3.95E+03	5	mm^3
Tau	1	0	Day
k_{kill_Max}	0.135	6	Day^{-1}
KC_{50}	2.39	26	µg/mL
ψ	20	Fixed	Unit less
$IIV\_k_{g\ Exponential}$	0.467	28	Unit less
$IIV\_k_{g\ Linear}$	0.548	24	Unit less

ADC-6

Parameter	Estimate	%RSE	Unit
$k_{g\ Exponential}$	0.0982	14	Day^{-1}
$k_{gLinear}$	23.2	12	$mm^3 \bullet Day^{-1}$
V_{Max}	4.68E+03	45	mm^3
Tau	3.44	6	Day
k_{kill_Max}	0.537	17	Day^{-1}
KC_{50}	37.9	22	µg/mL
ψ	20	Fixed	Unit less
$IIV\_k_{g\ Exponential}$	0.34	62	Unit less
$IIV\_k_{g\ Linear}$	0.54	24	Unit less

ADC-7

Parameter	Estimate	%RSE	Unit
$k_{g\ Exponential}$	0.111	5	Day^{-1}
$k_{gLinear}$	64.8	9	$mm^3 \bullet Day^{-1}$
V_{Max}	3.77E+03	33	mm^3
Tau	2.63	6	Day
k_{kill_Max}	0.308	8	Day^{-1}
KC_{50}	11.6	17	µg/mL
ψ	20	Fixed	Unit less
$IIV\_k_{g\ Exponential}$	0.114	>100	Unit less
$IIV\_k_{g\ Linear}$	0.359	26	Unit less

ADC-8

Parameter	Estimate	%RSE	Unit
$k_{g\ Exponential}$	0.138	5	Day^{-1}
$k_{gLinear}$	61.6	8	$mm^3 \bullet Day^{-1}$
V_{Max}	3.77E+03	33	mm^3
Tau	3.94	5	Day
k_{kill_Max}	0.292	7	Day^{-1}
KC_{50}	6.9	19	µg/mL
ψ	20	Fixed	Unit less
$IIV\_k_{g\ Exponential}$	0.114	>100	Unit less
$IIV\_k_{g\ Linear}$	0.359	26	Unit less

ADC-9

Parameter	Estimate	%RSE	Unit
$k_{g\ Exponential}$	0.16	16	Day^{-1}
$k_{gLinear}$	48.7	13	$mm^3 \bullet Day^{-1}$
V_{Max}	5.01E+03	26	mm^3
Tau	5.11	5	Day
k_{kill_Max}	0.265	13	Day^{-1}
KC_{50}	7.36	23	µg/mL
ψ	20	Fixed	Unit less
$IIV\_k_{g\ Exponential}$	0.715	50	Unit less
$IIV\_k_{g\ Linear}$	0.553	23	Unit less

ADC-10

Parameter	Estimate	%RSE	Unit
$k_{g\ Exponential}$	0.254	15	Day^{-1}
$k_{gLinear}$	79.7	8	$mm^3 \bullet Day^{-1}$
V_{Max}	2.77E+03	12	mm^3
Tau	2.84	8	Day
k_{kill_Max}	0.403	29	Day^{-1}
KC_{50}	59.9	45	µg/mL
ψ	20	Fixed	Unit less
$IIV\_k_{g\ Exponential}$	0.594	>100	Unit less
$IIV\_k_{g\ Linear}$	0.359	24	Unit less

ADC-11

Parameter	Estimate	%RSE	Unit
$k_{g\ Exponential}$	0.113	13	Day^{-1}
$k_{gLinear}$	61.5	9	$mm^3 \bullet Day^{-1}$
V_{Max}	4.38E+03	16	mm^3
Tau	1.1	16	Day
k_{kill_Max}	0.236	25	Day^{-1}
KC_{50}	189	40	µg/mL
ψ	20	Fixed	Unit less
$IIV\_k_{g\ Exponential}$	0.575	31	Unit less
$IIV\_k_{g\ Linear}$	0.45	24	Unit less

ADC-12

Parameter	Estimate	%RSE	Unit
$k_{g\ Exponential}$	0.12	9	Day^{-1}
$k_{gLinear}$	31.4	8	$mm^3 \bullet Day^{-1}$
V_{Max}	4.19E+03	23	mm^3
Tau	4.41	4	Day
k_{kill_Max}	0.78	0	Day^{-1}
KC_{50}	86.6	5	µg/mL
ψ	20	Fixed	Unit less
$IIV\_k_{g\ Exponential}$	0.365	75	Unit less
$IIV\_k_{g\ Linear}$	0.382	23	Unit less

ADC-13

Parameter	Estimate	%RSE	Unit
$k_{g\ Exponential}$	0.11	20	Day^{-1}
$k_{gLinear}$	23.4	14	$mm^3 \bullet Day^{-1}$
V_{Max}	4.37E+03	7	mm^3
Tau	3.44	6	Day
k_{kill_Max}	0.148	18	Day^{-1}
KC_{50}	21.8	44	µg/mL
ψ	20	Fixed	Unit less
$IIV\_k_{g\ Exponential}$	0.5	Fixed	Unit less
$IIV\_k_{g\ Linear}$	0.791	24	Unit less

ADC-14

Parameter	Estimate	%RSE	Unit
$k_{g\ Exponential}$	0.0732	11	Day^{-1}
$k_{gLinear}$	37.9	17	$mm^3 \bullet Day^{-1}$
V_{Max}	4.22E+03	18	mm^3
Tau	1.36	16	Day
k_{kill_Max}	0.405	38	Day^{-1}
KC_{50}	131	48	µg/mL
ψ	20	Fixed	Unit less
$IIV\_k_{g\ Exponential}$	0.47	38	Unit less
$IIV\_k_{g\ Linear}$	0.781	27	Unit less

ADC-15

Parameter	Estimate	%RSE	Unit
$k_{g\ Exponential}$	0.219	18	Day^{-1}
$k_{gLinear}$	15.9	26	$mm^3 \bullet Day^{-1}$
V_{Max}	2.27E+03	14	mm^3
Tau	0.999	29	Day
k_{kill_Max}	0.126	42	Day^{-1}
KC_{50}	52.3	91	µg/mL
ψ	20	Fixed	Unit less
$IIV\_k_{g\ Exponential}$	0.182	>100	Unit less
$IIV\_k_{g\ Linear}$	1.22	23	Unit less

ADC-16

Parameter	Estimate	%RSE	Unit
$k_{g\ Exponential}$	0.0934	8	Day^{-1}
$k_{gLinear}$	38.1	13	$mm^3 \bullet Day^{-1}$
V_{Max}	3.42E+03	21	mm^3
Tau	2.52	15	Day
k_{kill_Max}	0.225	55	Day^{-1}
KC_{50}	177	84	µg/mL
ψ	20	Fixed	Unit less
$IIV\_k_{g\ Exponential}$	0.283	39	Unit less
$IIV\_k_{g\ Linear}$	0.748	26	Unit less

ADC-17

Parameter	Estimate	%RSE	Unit
$k_{g\ Exponential}$	0.0844	12	Day^{-1}
$k_{gLinear}$	54.9	12	$mm^3 \bullet Day^{-1}$
V_{Max}	4.24E+03	21	mm^3
Tau	0.999	5	Day
k_{kill_Max}	0.175	25	Day^{-1}
KC_{50}	70.9	48	µg/mL
ψ	20	Fixed	Unit less
$IIV\_k_{g\ Exponential}$	0.483	27	Unit less
$IIV\_k_{g\ Linear}$	0.516	24	Unit less

ADC-18

Parameter	Estimate	%RSE	Unit
$k_{g\ Exponential}$	0.266	12	Day^{-1}
$k_{gLinear}$	81.4	10	$mm^3 \bullet Day^{-1}$
V_{Max}	2.57E+03	9	mm^3
Tau	6.36	5	Day
k_{kill_Max}	0.353	3	Day^{-1}
KC_{50}	14.5	10	µg/mL
ψ	20	Fixed	Unit less
$IIV\_k_{g\ Exponential}$	0.533	>100	Unit less
$IIV\_k_{g\ Linear}$	0.479	23	Unit less

ADC-19

Parameter	Estimate	%RSE	Unit
$k_{g\ Exponential}$	0.133	10	Day^{-1}
$k_{gLinear}$	70.6	12	$mm^3 \bullet Day^{-1}$
V_{Max}	5.19E+03	20	mm^3
Tau	0.819	22	Day
k_{kill_Max}	0.192	14	Day^{-1}
KC_{50}	75.7	29	µg/mL
ψ	20	Fixed	Unit less
$IIV\_k_{g\ Exponential}$	0.402	29	Unit less
$IIV\_k_{g\ Linear}$	0.657	23	Unit less

Chapter 4

Use of translational modeling and simulation for quantitative comparison of PF-06804103, a new generation HER2 ADC, with Trastuzumab-DM1

Alison Betts, Tracey Clark, Paul Jasper, John Tolsma, Piet H. van der Graaf, Edmund I. Graziani, Edward Rosfjord, Matthew Sung, Dangshe Ma and Frank Barletta

Journal of Pharmacokinetics and Pharmacodynamics 47(5): 513-526 (2020).

4.1 Abstract

A modeling and simulation approach was used for quantitative comparison of a new generation HER2 antibody drug conjugate (ADC, PF-06804103) with trastuzumab-DM1 (T-DM1). To compare preclinical efficacy, the pharmacokinetic (PK)/ pharmacodynamic (PD) relationship of PF-06804103 and T-DM1 was determined across a range of mouse tumor xenograft models, using a tumor growth inhibition (TGI) model. The tumor static concentration (TSC) was assigned as the minimal efficacious concentration. PF-06804103 was concluded to be more potent than T-DM1 across cell lines studied. TSCs ranged from 1.0- 9.8 μg/mL (n=7) for PF-06804103 and from 4.7-29 μg/mL (n= 5) for T-DM1. Two experimental models which were resistant to T-DM1, responded to PF-06804103 treatment. A mechanism-based target mediated drug disposition (TMDD) model was used to predict the human PK of PF-06804103. This model was constructed and validated based on T-DM1 which has non-linear PK at doses administered in the clinic, driven by binding to shed HER2. Non-linear PK is predicted for PF-06804103 in the clinic and is dependent upon circulating HER2 extracellular domain (ECD) concentrations. The models were translated to human and suggested greater efficacy for PF-06804103 compared to T-DM1. In conclusion, a fit-for-purpose translational PK/PD strategy for ADCs is presented and used to compare a new generation HER2 ADC with T-DM1.

4.2 Introduction

Human epidermal growth factor receptor 2 (HER2) over-expression in cancer patients is a genetic alteration that promotes cancer cell proliferation and survival, resulting in increased tumor growth and poor clinical outcome in the absence of HER2 targeted therapy [1, 2]. HER2+ cancers account for approximately 20% of all breast cancers [1, 2]. Trastuzumab, a monoclonal antibody (mAb) which specifically targets HER2, has revolutionized treatment as one of the first non-hormonal medicines for breast cancer [3].

ADCs are a targeted therapy for cancer treatment, combining a specific mAb to a tumor antigen linked to a potent cytotoxic agent [4]. The aim for this type of therapeutic is to target the cytotoxic drug to tumor cells, thus maximizing efficacy while minimizing systemic toxicity due to normal tissue exposure. In 2013, the anti-HER2 ADC T-DM1 was approved, offering greater potential efficacy and enhanced survival by conjugation of a cytotoxic payload (DM1) to trastuzumab [5]. However, both trastuzumab and T-DM1 are only efficacious in patients with high HER2 expression and patients are acquiring resistance [6, 7]. As such there remains a need for improved HER2 therapies to reach a broader spectrum of patients and reduce risk of disease recurrence.

PF-06804103 is a new generation HER2 ADC with an auristatin microtubule inhibitor payload (Aur-101) conjugated to an anti-HER2 IgG1 mAb via a site specific mcValCitPABC cleavable linker [8]. Although both PF-06804103 and T-DM1 are anti-HER2 ADCs, they differ in their linker-payloads and their conjugation chemistry, which has a significant effect on their mechanism of action [9-12]. T-DM1 has a maytansine derived payload (DM1) which is linked via a stable

thioether linker to native lysines on trastuzumab. The conjugation method results in a heterogeneous mixture of conjugates with an average of 3.0- 3.6 drugs per antibody, and a range of 0- 6. Upon binding to HER2, T-DM1 undergoes receptor mediated internalization and trafficking from the endosomes to the lysosomes. In the lysosome T-DM1 undergoes proteolytic degradation, which releases the cytotoxic DM1-linker-lysine-metabolite (lysine-MCC-DM1). This metabolite must be actively transported from the lysosome in order to reach its intra-cellular site of action [13].

The payload of PF-06804103 is conjugated to specific cysteines on the anti-HER2 mAb which have been mutated at fixed locations. This results in production of a homogeneous ADC, with a fixed drug to antibody ratio (DAR) of 4.0. PF-06804103 is also internalized upon binding to HER2, and cleavage of the protease linker results in release of the Aur-101 payload in the endosomes. This is sufficiently permeable to diffuse out of the endosomes and into the nucleus. Unlike T-DM1, the permeability of the released payload means it can enter adjacent cells and mediate cell death, a process referred to as bystander effect [14]. This has been demonstrated in xenograft models in mouse where PF-06804103 enables potent tumor activity in non-HER2 amplified breast cancer and heterogeneous low HER2 models, where T-DM1 is ineffective. The site-specific conjugation method used in PF-06804103 should enable greater stability with more consistent efficacy and the bystander effect should enable treatment of patients with more heterogeneous tumors and lower HER2 expression. Differences in linker-payload chemistry of PF-06804103 compared to T-DM1 should also impede mechanisms of resistance specific to lysine-MCC-DM1, including impaired lysosomal degradation or enhanced efflux [15, 16].

In this manuscript, mathematical modeling and simulation is used as a tool to quantitatively compare PF-06804103 and T-DM1, in terms of their PK and efficacy. A modeling-based method is provided to assess efficacious concentration of PF-06804103 and T-DM1 across preclinical cell line xenograft (CLX) and patient derived xenograft (PDX) studies in mouse. A mechanistic TMDD model is applied to account for variation in shed HER2 and to describe T-DM1 non-linearity in patients. A similar model is then used to predict clinical PK for PF-06804103. A fit-for-purpose translational strategy is proposed to predict clinical efficacy in patients.

4.3 Methods

Compounds

PF-06804103 was synthesized at Pfizer as described [8]. Trastuzumab-maytansinoid conjugate was synthesized at Pfizer and is structurally similar to trastuzumab emtansine (T-DM1) with similar in vitro potency and in vivo efficacy [8]. It is comprised of an anti-HER2 trastuzumab antibody covalently bound to DM1 through a bifunctional linker. Conjugation was conducted as described previously [4].

Animal studies

All animal studies were approved by the Pfizer Institutional Animal Care and Use Committee according to established guidelines.

PF-06804103 In vivo mouse and cynomolgus monkey PK studies

PF-06804103 was administered as a single intravenous (IV) bolus dose of 3 mg/kg to female athymic nu/nu mice (n=4/dose). Blood samples were collected pre-dose and at 0.083, 6, 24, 48, 96 168 and 336 h post dose. PF-06804103 was administered to cynomolgus monkey as multiple IV bolus doses, given every 3 weeks for a total of 3 doses at 3 mg/kg, 6 mg/kg (both n=3 males, n=3 females) and at 12 mg/kg (n=5 males, n=5 females). Blood samples were collected pre-dose and at 0.083, 6, 24, 72, 168, 336 and 504 h post-dose.

PF-06804103 Assay

Quantitation of ADC (mAb with at least one drug molecule conjugated) concentrations in plasma collected from female athymic nu/nu mice and cynomolgus monkeys following administration of PF-06804103 (or T-DM1) was achieved using Gyrolab™ (Gyros Protein Technologies, Uppsala, Sweden). Isolation and detection of ADC concentrations from biological matrix was carried out with streptavidin coupled micro columns located on Bioaffy™200 compact discs (CDs), an integrated nanoliter scale immunoassay device, within Gyrolab™. Plasma calibration standards, quality control samples and plasma study samples were all diluted to the minimum required dilution (MRD) and loaded onto the CDs. For measurement of ADC, a sheep anti-human IgG (Binding Site, San Diego, CA) reagent was used for capture and an internally generated mouse anti-payload reagent for detection. Fluorescence of analyte was measured using a laser embedded within the workstation. All data was processed using Watson v7.4 LIMS with a 1/Y*2 weighting.

In vivo mouse xenograft studies

Mouse efficacy studies were completed in 4 CLX models (JIMT-1, BT474 and HCC-1954 derived from breast cancers, N87 derived from gastric cancer) and 4 PDX models (24312 and 144580 derived from breast, 37622 from lung and GA3109 from gastric tumors). Female athymic nude mice (Nude, Stock No: 002019) were obtained from the Jackson Laboratory (Farmington, CT). For the CLX models, nude mice were injected subcutaneously in the flank with suspensions of 1 $x10^6$ N87 cells, 5 $x10^6$ JIMT-1 cells, 5 $x10^6$ HCC-1954 cells or 10 $x10^6$ BT474 cells in 50% Matrigel (BD Biosciences, Franklin Lakes, NJ). For the PDX models, tumor fragments were subcutaneously passaged in vivo from animal to animal in nude mice. Mice were randomized into study groups when tumors reached approximately 150 to 300 mm^3. Either phosphate buffered saline (PBS, Gibco, Cat#14190-144, as vehicle), PF-06804103, or T-DM1 were administered IV at different doses starting on day 0 for a total of four doses, 4 days apart (Q4d x4). Dose levels administered in each tumor model are shown in Table 2 for PF-06804103 and Table 3 for T-DM1. Tumors were measured at least weekly with a calibrator (Mitutoyo, Aurora, Illinois) and the tumor mass was

calculated as volume = (width X width X length)/2. These studies have been described previously [8].

PK/PD modeling in mouse

1. **Pharmacokinetics of PF-06804103 and T-DM1 in mouse and PF-06804103 in Cynomolgus monkey**

The PK of PF-06804103 in non-tumor bearing mouse following a single IV dose of 3mg/kg and in cynomolgus monkey following multiple dose IV administration at 3, 6 and 12 mg/kg Q3W x 3 were characterized using a 2-compartment PK model with linear elimination from the central compartment (Figure 1a). T-DM1 PK in mouse was taken from the literature, where it was linear across the dose range studied (0.3- 15 mg/kg) [17].

2. **Tumor growth inhibition PK/PD in xenograft mouse as a function of PF-06804103 or T-DM1 concentration**

The mouse xenograft PK/PD relationship was established by relating PF-06804103 (or T-DM1) plasma concentration in mouse to measured xenograft tumor size data using a tumor growth inhibition model (Figure 1b; [18]). The mouse PK parameters derived above were fixed in the subsequent PD modeling of the xenograft mouse data. The presented model is a modified version of the model by Simeoni *et al.* [19]. Briefly, the unperturbed tumor growth was fitted first using individual animal growth data from the vehicle control group, using a logistic model describing linear (k_g) and exponential (k_{gEx}) growth. The measured initial tumor volume in each animal was used for the initial conditions (*v0*). V1 -V4 are the tumor volume in the growth compartment and

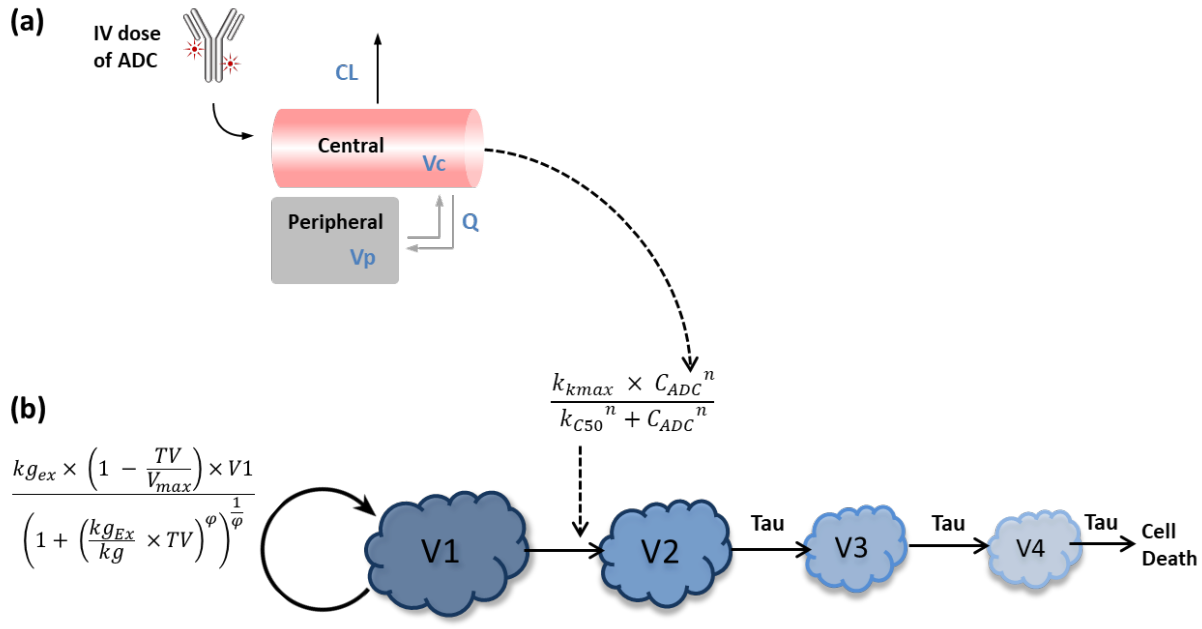

Figure 1: PK/PD model used for the mouse tumor growth inhibition modeling. **(a)** 2-compartmental linear PK model is linked to **(b)** a model of tumor growth inhibition. Please refer to Tables 1 and 2 for description of the model parameters.

three transduction compartments, respectively. *TV is* the total tumor volume (mm^3). The inter-individual variability of the growth parameters and the maximum tumor volume (V_{max}) obtained from the unperturbed growth model were then fixed in the simultaneous estimation of growth and drug effect parameters from the complete tumor volume data set. τ is the transduction time, k_{kmax} is the maximum kill rate, kc_{50} is the concentration of PF-06804103 or T-DM1 in the plasma at half the maximal kill rate, n is the hill co-efficient and ψ is the constant for switching from exponential to linear growth patterns. ψ was fixed to a value of 20 in all cases [19]. C_{ADC} is equivalent to free ADC plasma concentration, as no shed HER2 ECD was detected in mouse. Equations 1 - 6 describe the tumor growth inhibition modeling.

1. $k_{kill} = \frac{k_{kmax} \times {C_{ADC}}^n}{{kc_{50}}^n + {C_{ADC}}^n}$
2. $\frac{dV_1}{dt} = \frac{k_{gEx} \times \left(1 - \frac{TV}{V_{max}}\right) \times V_1}{\left(1 + \left(\frac{k_{gEx}}{k_g} \times TV\right)^{\psi}\right)^{1/\psi}} - k_{kill} \times V_1$
3. $\frac{dV_2}{dt} = k_{kill} \times V_1 - \frac{V_2}{\tau}$
4. $\frac{dV_3}{dt} = \frac{V_2 - V_3}{\tau}$
5. $\frac{dV_4}{dt} = \frac{V_3 - V_4}{\tau}$
6. $TV = V_1 + V_2 + V_3 + V_4$

Initial conditions: *TV(t=0) = V1(t=0) = v0; V2(t=0) = V3(t=0) = V4(t=0) = 0*

Calculation of TSC

TSC was defined as the concentration of PF-06804103 or T-DM1 where tumor growth and death rates are equal and tumor volume remains unchanged. This PK/PD derived parameter combines the growth pattern information and the drug effect, providing insight on the efficacy of the ADC. See equation 7 for TSC calculation. An 80% confidence interval on TSC was calculated using parametric bootstrap by resampling from the estimated parameters using a log-normal distribution.

7. $TSC = \frac{k_{gEx} \times {k_{C50}}^n \times \left(1 - \frac{V_0}{V_{max}}\right)}{\left(k_{kmax} \times \left(1 + \left(\frac{kg_{Ex}}{kg} \times V_0\right)^{\varphi}\right)^{\frac{1}{\varphi}} - kg_{Ex} \times \left(1 - \frac{V_0}{V_{max}}\right)\right)^{\frac{1}{n}}}$

Modeling: All modeling was performed using Monolix software v2016 (Paris, France) using the solver for stiff ordinary differential equations. The quality of the model fitting was assessed using: Diagnostic plots: (a) plots of observations versus population/ individual predictions and

comparison with line of unity, (b) plots of weighted residuals versus time/concentration and check for systematic deviation from zero, (c) visual predictive checks of observations and predictions for all individuals at each dose level to check for goodness of fit [20]. Diagnostic criteria: (a) reasonable precision of the parameter estimates (RSE/ CV%) (b) lack of correlation between model predicted parameters (<0.95) (c) lack of shrinkage (η-) as a check for model over-parameterization (<40%) (d) reduction in objective function values and/or Akaike and Schwarz criterion for model comparison (e) Condition numbers (included in Tables 2 and 3). As a rule of thumb, condition number should be less than 10^{Npar} where Npar is the number of parameters estimated in the model for a well-defined model with respect to the information in the data [21]. However, as with all these diagnostic checks, the condition number cannot be taken in isolation, and must be interpreted with respect to all the other criteria.

Clinical PK predictions

To predict the human PK for PF-06804103 a TMDD model [22] was constructed, incorporating binding to serum HER2 and subsequent clearance of the complex into a standard 2-compartmental PK model. The extracellular domain (ECD) of HER2 is known to shed from the trans-membrane receptor at high levels in the target patient population (metastatic breast cancer) [23]. The presence of shed target is hypothesized to drive non-linear clearance of T-DM1. The TMDD model was initially used to fit the non-linear PK of T-DM1 observed in patients at doses administered in the clinic [24]. The model describes linear, catabolic clearance of T-DM1 (CL), as well as shedding of HER2 ECD (*kshed*), degradation of HER2 ECD (*kdeg*), binding of T-DM1 to HER2 ECD (K_D, k_{on} and k_{off}) and elimination of the complex ($kel_{ADC\text{-}ECD}$). The model structure is shown in Figure 3. The concentration of HER2 ECD was initially set to 20 ng/mL (0.2 nM) which is above the normal upper limit in healthy females (15 ng/mL), and above the median in metastatic breast cancer patients [25]. To improve the individual fit at each dose level, ECD concentration was varied between 16 and 28 ng/mL. Patients with higher ECD concentrations had more rapid clearance due to TMDD and varying the ECD concentrations enabled better description of the slope of the PK curves observed. The k_{on} and K_D of T-DM1 were fixed in the model at 61.3 $nM^{-1}day^{-1}$ and 0.1 nM, respectively [26]. The binding of T-DM1 to HER2 was assumed to be the same for HER2 ECD and transmembrane domain. *kshed, kdeg* and $kel_{ADC\text{-}ECD\ complex}$ were all estimated in the model fitting process.

The model was then applied to predict the human PK of PF-06804103. The 2-compartment linear parameters were scaled from cynomolgus monkey population PK parameters using allometric scaling exponents of 1 for volumes and 0.9 for clearance parameters [27]. The binding of PF-06804103 to HER2 was incorporated into the model and assumed to be the same for HER2 ECD and transmembrane domain. The rate of HER2 shedding, HER2 degradation and the clearance of the complex were set to that estimated from the model used to fit T-DM1 PK data in patients. To investigate the impact of HER2 ECD concentrations on PK/PD, simulations were also performed at low (2ng/ml) and high (750ng/ml) HER2 ECD concentrations, representing the range of concentrations reported across 78 healthy females and 100 patients with metastatic breast

cancer [25]. Equations 8- 11 describe the TMDD modeling. C_{ADC} is the free ADC concentration in the central compartment (nM), C_{ADC_per} is the ADC concentration in peripheral (i.e. tissue) compartment (nM), C_{ECD} is the HER2 ECD concentration (nM) and C_{ADC_ECD} is the ADC- ECD complex (nM). *In(t)* is the infusion rate of the drug in nM/h, based on a MW of the drug of 150 kDa; the infusion duration was 1 hour. Model simulations were performed in Berkeley Madonna v8.3.18 and the model code is included in the Supplementary Material.

Equations:

8. $\frac{dC_{ADC}}{dt} = In\,(t) - \left(\frac{CL}{Vc} \times C_{ADC}\right) - \left(\frac{Q}{Vc} \times C_{ADC}\right) + \left(\frac{Q}{Vp} \times C_{ADC\_per} \times \frac{Vp}{Vc}\right) - (kon \times C_{ADC} \times C_{ECD}\,) + \left(koff\ \times C_{ADC\_ECD}\right)$
9. $\frac{dC_{ADC\_per}}{dt} = \left(\frac{Q}{Vc} \times C_{ADC} \times \frac{Vc}{Vp}\right) - \left(\frac{Q}{Vp} \times C_{ADC\_per}\right)$
10. $\frac{dC_{ECD}}{dt} = kshed_{HER2\_ECD} - \left(kdeg_{HER2\_ECD}\ \times C_{ECD}\right) - (kon \times C_{ADC} \times C_{ECD}) + \left(\ koff\ \times C_{ADC\_ECD}\right)$
11. $\frac{dC_{ADC\_ECD}}{dt} = (kon \times C_{ADC} \times C_{ECD}) - \left(koff\ \times C_{ADC\_ECD}\right) - \left(kel_{ADC\_ECD}\ \times C_{ADC\_ECD}\right)$

Initial conditions: C_{ADC} *(t=0) =* C_{ADC_per} *(t=0) =* C_{ADC_ECD} *(t=0) = 0;* C_{ECD} *(t=0) = 0.206 nM*

Clinical PK/PD predictions

The PD parameters estimated from mouse xenograft studies (Table 2 for PF-06804103 and Table 3 for T-DM1) were integrated with the predicted human PK parameters (Table 4) to project clinical efficacy (tumor regression) following Q3w x4 dosing of PF-06804103 at 1 mg/kg and T-DM1 at 3.6 mg/kg (clinical dose). It was assumed that mouse PD parameters translate directly to human (including initial tumor volumes). Due to the growth rate difference between xenograft models and clinical tumors, the predictions that achieve stasis using mouse xenograft PD parameters are assumed to be minimally efficacious in human, achieving greater than stable disease [18]. This method has been tested previously for T-DM1 and resulted in accurate predictions of efficacious dose in the clinic [18].

4.4 Results

PF-06804103 PK in mouse and cynomolgus monkey

To determine the PK/PD relationship in mouse, PK was determined separately following IV administration of PF-06804103 at 3mg/kg and described using a 2-compartment linear model. To inform PF-06804103 clinical PK predictions, PK was determined in cynomolgus monkey following multiple dose IV administration at 3, 6 and 12 mg/kg Q3W x 3. The PK was linear in monkey across the dose range studied and could be described using a 2-compartment PK model. This was

expected as there is no shed HER2 ECD in cynomolgus monkey. The terminal half-life in monkey was approximately 7 days. The 2-compartment model parameters in mouse and cynomolgus monkey are shown in Table 1.

Table 1: Mouse and cynomolgus monkey PK parameters for PF-06804103

Parameter (unit)[a]	Description	Mouse[b]	Cynomolgus monkey[c] (CV %)
Vc (mL/kg)	Central compartment volume	61.0	38.1 (3)
CL (mL/day/kg)	Clearance	22.8	7.2 (5)
Vp (mL/kg)	Peripheral compartment volume	56.2	20.2 (7)
Q (mL/day/kg)	Inter-compartmental clearance	35.0	19.2 (18)

[a]Macro-constants conversion to micro-constants: kel= CL/Vc; k12=Q/Vc; k21= Q/Vp. [b]PK of PF-06804103 was determined in mouse following single IV administration at 3mg/kg. Mean PK values were fitted to a 2-compartment model (no % CV derived). [c]PK of PF-06804103 was determined in cynomolgus monkey following IV administration on day 1 at 3, 6, or 12 mg/kg. A 2-compartment population PK model was used to fit the cynomolgus monkey data with *Omega V1* = 0.0589 (48), *Omega CL* = 0.22 (16) and proportional error= 0.131 (7).

PF-06804103 and T-DM1 PK/PD relationship in mouse tumor xenograft models

The ability of PF-06804103 and T-DM1 to regress tumors was studied in a range of CLX and PDX experimental mouse tumor models. The mouse PK parameters were integrated with the tumor volume data over time following different dose levels of drug to describe the ADC concentration versus response relationship. The model described the differences in growth rates observed across the tumor models. It described the delay between drug administration and tumor cell killing due to signal transduction. The different tumor models had varying susceptibilities to drug effect which are observed as differences in potency (kc_{50}) and kill rate (k_{kmax}) of PF-06804103 and T-DM1 across models. PD parameters determined for PF-06804103 in 7 mouse xenograft models (3 CLX and 4 PDX) are shown in Table 2 and goodness of fit plots are shown in Supplementary Figure 1. PD parameters for T-DM1 across 3 CLX models in mouse are shown in Table 3.

Comparison of PF-06804103 and T-DM1 efficacy using TSC values

Minimal efficacious concentration (*Ceff*) in mouse xenograft models was defined as the concentration required for tumor stasis (TSC). PF-06804103 and T-DM1 TSC values with 80% confidence intervals across a range of CLX/PDX are shown in Figure 2. Mean TSC of PF-06804103 was 4.3 µg/ml across 7 studies, with a range of 1.0 – 9.8 µg/mL. Mean TSC of T-DM1 was 15.8 µg/mL across 3 studies, with range of 4.7 – 29 µg/mL. JIMT-1 and 144580 mouse tumor models did not respond to T-DM1 and TSCs could not be determined in these models (> 50µg/mL).

Table 2: PF-06804103 estimated PD model parameters (CV %) and derived TSC values [80% confidence intervals] in 3 CLX and 4 PDX mouse models

Parameter (unit)	Description	JIMT-1 CLX (Breast)	N87 CLX (Gastric)	BT474 CLX (Breast)	24312 PDX (Breast)	37622 PDX (NSCLC)	144580 PDX (Breast)	GA3109 PDX (Gastric)
Doses (mg/kg)	IV Q4d x 4	0, 0.25, 0.5, 1	0, 0.3, 1, 3	0, 0.5, 1.5	0, 1.5, 3, 6	0, 0.3, 1, 3	0, 1.5, 3, 6	0, 1, 3
k_{gEx} (day^{-1})	Exponential growth rate	0.0883 (8)	0.068 (8)	0.0442 (65)	0.023 (12)	0.0559 (9)	0.0461 (8)	0.115 (6)
k_g ($mm^3\ day^{-1}$)	Linear growth rate	47.5 (23)	26.8 (14)	78.5 (23)	24.4 (15)	68.4 (22)	395 (65)	57.2 (9)
V_{max} (mm^3)	Maximum growth rate	4.08E+03 (15)	4.60E+03 (20)	5.28E+03 (23)	5.00E+03 (-)	3.84E+03 (13)	5.92E+03 (16)	7.07E+03 (26)
τ (day)	Transduction time	2.23 (6)	2.54 (6)	3.04 (16)	1.66 (1)	3.32 (5)	9 (5)	5.81 (2)
k_{kmax} (day^{-1})	Maximum kill rate	0.703 (9)	0.15 (5)	0.998 (209)	0.721 (0)	0.362 (13)	0.516 (13)	1.24 (2)
kc_{50} (μg mL^{-1})	Concentration at half maximal kill	10.6 (9)	1.24 (16)	31.5 (236)	15.8 (5)	4.19 (19)	25.8 (16)	14.7 (6)
n	--	2.4 (12)	1 (-)	1 (-)	2.6 (-)	1.3 (7)	2.4 (21)	2.5 (6)
ψ	--	20 (-)	20 (-)	20 (-)	20 (-)	20 (-)	20 (-)	20 (-)
Omega k_{gEx}		0.401 (12)	0.271 (-)	2.59 (17)	0.373 (-)	0.372 (-)	0.359 (-)	0.25 (-)
Omega k_g		1.23 (14)	0.666 (-)	0.717 (23)	0.0441 (-)	0.789 (-)	1.3 (-)	0.316 (-)
Additive error		13.4 (12)	34.9 (7)	106 (6)	19.1 (6)	35.8 (3)	63.4 (4)	18.3 (4)
Proportional error		0.118 (6)	0.055 (12)	-	0.227 (6)	0.0755 (8)	0.0648 (11)	0.188 (5)
Condition number		2.4E+03	1.5	2.7E+03	2.7E+03	87	85	2.7E+04
TSC (μg mL^{-1}) [80% CI]	Tumor static concentration	4.8 [4.2, 5.5]	1.0 [0.8, 1.4]	3.0 [-]	4.3 [3.8, 4.6]	1.2 [0.8, 1.5]	9.8 [8.0, 12.0]	5.8 [5.3, 6.2]

Table 3: T-DM1 estimated PD model parameters (CV %) and derived TSC values [80% confidence intervals] for 3 CLX models in mouse (N87, BT474 and HCC-1954)

Parameter (unit)	Description	JIMT-1 CLX (Breast)	N87 CLX (Breast)	BT474 CLX (Gastric)	144580 PDX (Breast)	HCC-1954 CLX (Breast)
Doses (mg/kg)	IV Q4d x 4	6	0, 1, 3, 10	0, 1, 3, 10	6	0, 0.3, 1, 3
k_{gEx} (day^{-1})	Exponential growth rate	No Response	0.0732 (11)	0.0575 (46)	No Response	0.0918 (8)
k_g ($mm^3\ day^{-1}$)	Linear growth rate		37.9 (17)	77.4 (20)		40.7 (6)
V_{max} (mm^3)	Maximum tumor volume		4.22E+03 (18)	5.28E+03 (23)		3.18E+03 (27)
τ (day)	Transduction time		1.36 (16)	2.4 (7)		1 (8)
k_{kmax} (day^{-1})	Maximum kill rate		0.405 (38)	1.38 (91)		0.319 (7)
kc_{50} (μg mL^{-1})	Concentration at half maximal kill		131 (48)	311 (110)		8.63 (10)
n	--		1 (-)	1.01 (4)		1.5 (-)
ψ	--		20 (-)	20 (-)		20 (-)
Omega k_{gEx}			0.47 (-)	2.26 (15)		0.371 (-)
Omega k_g			0.781 (-)	0.917 (16)		0.274 (-)
Additive error			66.8 (6)	30 (-)		14.4 (10)
Proportional error			0.0727 (12)	0.157 (5)		0.0754 (8)
Condition number			250	9E+05		27
TSC (μg mL^{-1}) [80% CI]	Tumor static concentration		29 [13, 67]	14 [2.4, 57]		4.7 [4.0, 5.6]

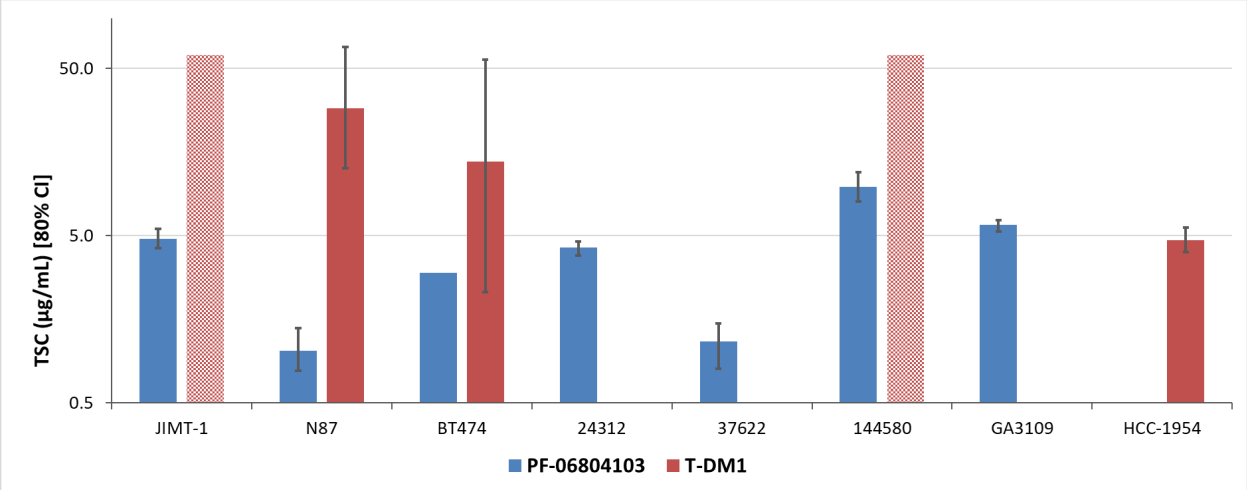

Figure 2: PF-06804103 and T-DM1 TSCs across mouse tumor xenograft models. T-DM1 was not responsive in JIMT-1 and 144580 mouse tumor xenograft models (TSC values > 50 µg/mL). This is represented on the plot as hatched bars. The error bars represent 80% confidence intervals on TSC values.

Clinical PK modeling of T-DM1 using a TMDD model

T-DM1 exhibits non-linear PK in the clinic, which is hypothesized to be due to binding to shed HER2 extracellular domain (ECD). A mechanistic TMDD model was developed to describe the clinical PK of T-DM1, which accounts for shedding of HER2 ECD into the serum, binding of T-DM1 to the ECD and subsequent clearance of the T-DM1-ECD complex (Figure 3). The TMDD model parameters for T-DM1 are shown in Table 4 and the model fit to T-DM1 phase 1 clinical data [24] is shown in Figure 4a.

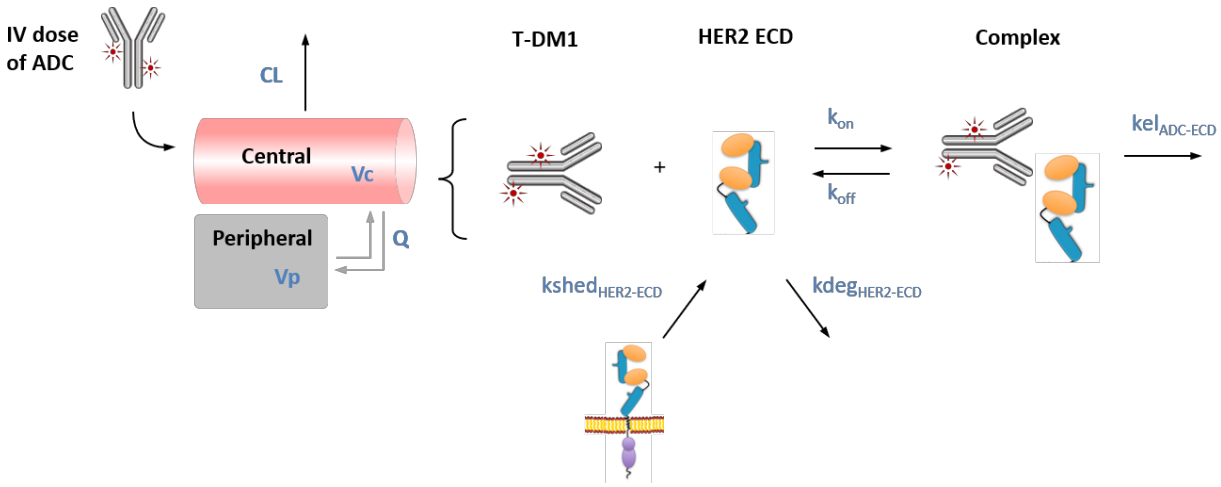

Figure 3: Target mediated drug disposition (TMDD) model used to describe clinical PK of T-DM1 and to predict clinical PK of PF-06804103. Please refer to Table 4 for description of the model parameters.

Table 4: TMDD model parameters for T-DM1 in the clinic and predicted clinical PK of PF-06804103 following IV infusion of 1 hour

Parameter (unit)	Description	T-DM1	Predicted PF-06804103
Vc (mL/kg)	Central compartment volume	37	38.1
CL (mL/day/kg)	Clearance	7.2	5.52
Vp (mL/kg)	Peripheral compartment volume	30	20.2
Q (mL/day/kg)	Inter-compartmental clearance	12	14.9
[a]K_D (nM)	HER2 binding affinity	0.1	
[b]$kshed_{HER2\text{-}ECD}$ (nM day^{-1})	Rate constant for HER2 shedding	6.65	
$kdeg_{HER2\text{-}ECD}$ (day^{-1})	Rate constant for HER2 degradation	33.3	
$kel_{ADC\text{-}ECD\ complex}$ (day^{-1})	Elimination rate constant of the HER2-ADC complex	32.6	
HER2 ECD (ng/mL)/(nM[c])	Concentration of serum HER2 ECD	16-28/ 0.16- 0.28	20 /0.2

[a]$K_D = k_{off}/k_{on}$ [b]$kshed_{HER2\text{-}ECD} = kdeg_{HER2\text{-}ECD}$ x ECD (t=0) [c]Molecular weight of the HER2 ECD is 100kDa.

Clinical PK projections for PF-06804103

The TMDD model developed for T-DM1 was applied to predict the human PK of PF-06804103. The 2- compartment linear IV PK parameters were scaled from cynomolgus monkey PK parameters (as described above, Table 1). The K_D was measured for PF-06804103, and all other parameters were estimated in the T-DM1 model. The predicted TMDD model IV PK parameters for PF-06804103 are shown in Table 4. The predicted PK profiles for PF-06804103 in the clinic following multiple dose administration of 0.15 mg/kg to 3 mg/kg IV Q3W x 4 are shown in Figure 4b. Non-linear PK is predicted over this dose range with a predicted clearance of 33.6 mL/d/kg and elimination half-life of 1.0 day at the lowest simulated dose of 0.15 mg/kg, and a predicted clearance of 7.8 mL/d/kg with terminal half-life of 4.9 days at a dose of 3.0 mg/kg. These PK predictions are assuming a free drug assay. If a total assay is used (which measures free and bound drug) then the PK at each dose level would be as predicted for the high dose of 3.0 mg/kg.

Predicted PF-06804103 concentration versus time profiles following an IV dose of 1mg/kg Q3W x4 in patients with low (2.0ng/ml), medium (20ng/ml) and high (750ng/ml) serum HER2 ECD concentrations are shown in Figure 4c. This figure indicates an inverse correlation between serum HER2 ECD concentration and PF-06804103 exposure. This relationship has also been observed for trastuzumab in clinical studies [6].

(a)

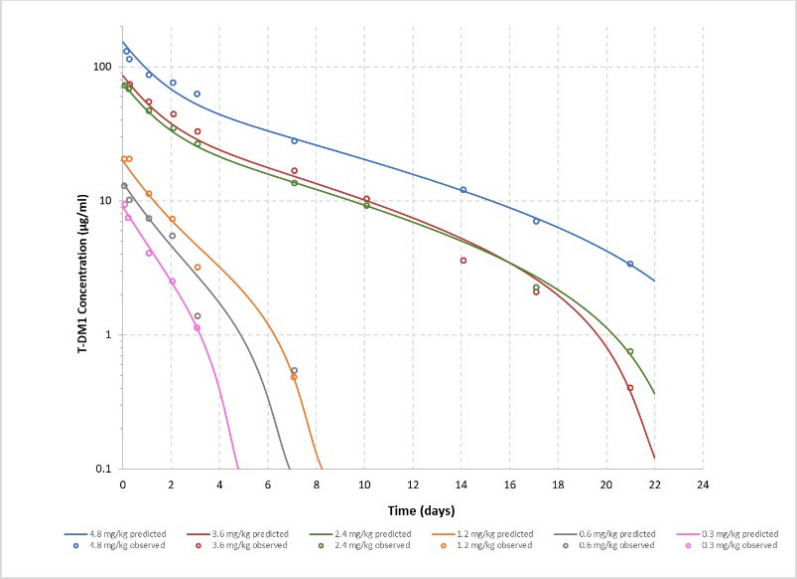

(b)

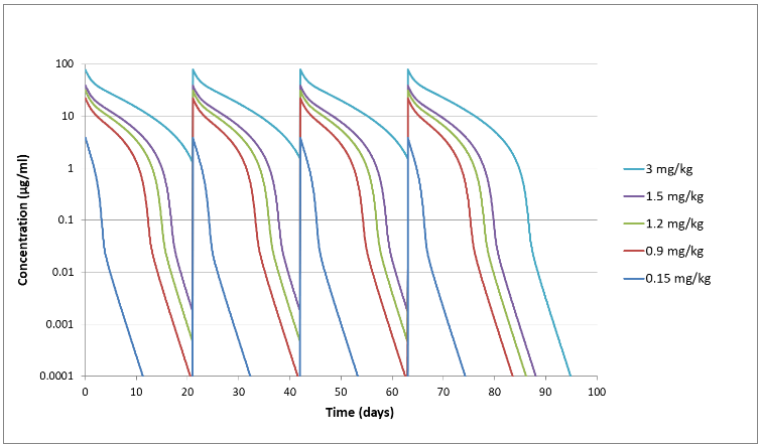

(c)

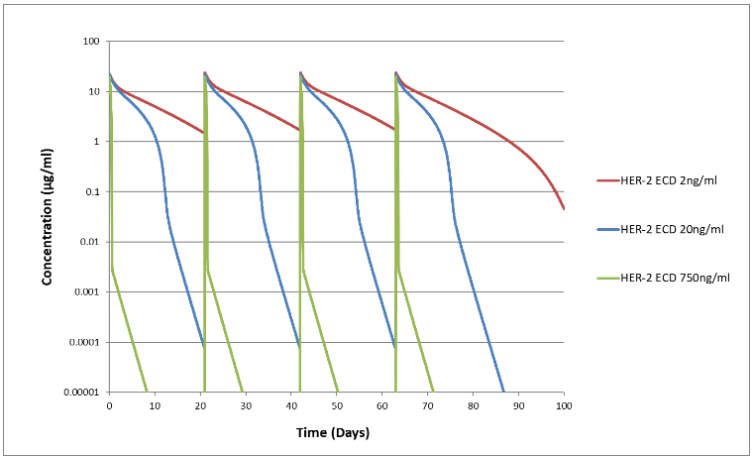

Figure 4: (a) TMDD model fit to T-DM1 Phase 1 clinical PK data (single dose administration) [24] **(b)** PK predictions for PF-06804103 using TMDD model (free drug concentrations) from 0.15- 3 mg/kg IV Q3W x 4 **(c)** PK predictions for PF-06804103 following an IV dose of 1mg/kg Q3W x 4 to patients with low, medium and high HER2 ECD concentrations. These HER2 ECD concentrations are within the reported range for healthy females (low) and patients with advanced breast cancer (medium and high).

Clinical PK/PD predictions for PF-06804103 and comparison with T-DM1

The clinical PK estimates from the TMDD model and the mouse PD model parameter estimates were integrated to simulate PF-06804103 and T-DM1 efficacy in the clinic. This approach assumes that ADC plasma concentrations are a good surrogate marker for the target site concentration that drives response and that mouse PD parameters translate directly to the clinic. Predicted efficacy of T-DM1 following 3.6mg/kg Q3W x 4 IV dose administrations and PF-06804103 following 1mg/kg Q3W x 4 dose administrations are shown in Figures 5a and 5b, respectively. For T-DM1, N87 and BT474 models predict tumor stasis and HCC-195 predict tumor regression at 3.6mg/kg Q3W in the clinic. For PF-06804103, 144580 predicts tumor re-growth, N87 predicts tumor stasis and JIMT-1, BT474, 24312, 37622 and GA3109 all predict tumor regression at 1mg/kg Q3W.

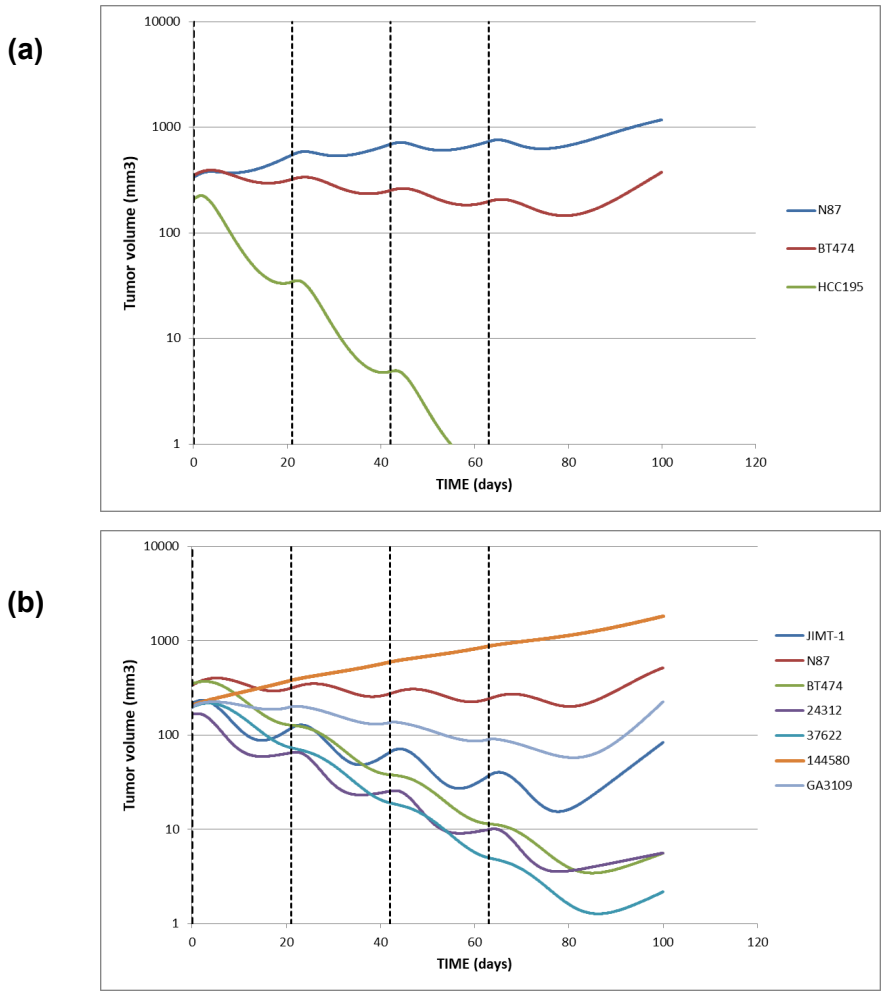

Figure 5: Translation of preclinical PK/PD model to the clinic for each tumor cell line model studied preclinically. Predicted efficacy of **(a)** T-DM1 following a 3.6mg/kg Q3W dose and **(b)** PF-06804103 following a 1mg/kg Q3W dose to cancer patients. The dashed vertical lines represent dosing times. The response in different cell lines is thought to be representative of response in individual patients.

4.5 Discussion

In this work we present the modeling and simulation strategy used to compare a new generation HER2 ADC (PF-06804103) with T-DM1, to ensure efficacy differentiation and as a rationale to pursue clinical development of PF-06804103. HER2 remains an exciting target to prosecute for oncology indications as it is clinically validated, with efficacy of HER2 targeted therapies established for breast and gastric patients that have HER2 amplification/ over-expression. In addition, recent data suggests that HER2 is over-expressed in a variety of other tumor types such as colon, bladder and biliary cancers, opening the door to new potential oncology indications for anti-HER2 therapies [28]. T-DM1 is a milestone drug which is standard of care second line treatment for patients with breast cancer and was the first ADC for the treatment of solid tumors. However, T-DM1 has limitations including moderate clinical activity (ORR 43.6% EMILIA and 31% in TH3RESA) [29] and Phase 3 failures (MARIANNE and GATSBY trials) [30, 31] . In addition, only high and homogeneously expressing HER2 tumors respond to T-DM1 [7]. The clinical activity of T-DM1 is also limited by intrinsic and acquired resistance. The mechanisms of resistance of T-DM1 are not completely understood, and the pharmacological complexity of this agent has confounded efforts to establish the clinically important mechanisms [15]. However, most evidence points to altered trafficking/ metabolism of T-DM1 and impaired lysine-MCC-DM1 mediated cytotoxicity as the predominant mechanisms of T-DM1 resistance in the clinic [15]. Loss of HER2 expression could also contribute to resistance, as has been proven for trastuzumab [32]. Also, evidence for mechanisms related to internalization, abnormal transit, lysosomal catabolism and drug efflux have been observed in non-patient derived experimental models [16, 33]. To help circumvent resistance, use of an alternative linker-payload in PF-06804103 would impede the T-DM1 resistance mechanisms that are specific to lysine-MCC-DM1 including impaired lysosomal degradation or enhanced efflux [16]. For all the reasons discussed above, novel differentiated HER2 therapies are required for the treatment of cancer.

Modeling and simulation strategy

To quantitatively compare PF-06804103 and T-DM1 a translational PK/PD modeling and simulation strategy was implemented. This is a useful technique capable of integrating data generated from diverse test platforms in a mechanistic framework to describe exposure-response relationships [34]. The strategy described herein uses a mechanism-based tumor growth inhibition (TGI) model which integrates system parameters (tumor growth and initial tumor size) and drug effects (transduction rate, kill rate and potency). It is used to characterize TGI in mouse as a function of ADC concentration, making use of PK and PD data routinely generated for ADCs in the discovery phase. A population modeling approach was utilized to quantify variability in tumor cell growth across mouse tumor models. This is combined with a transduction model of tumor cell death driven by plasma ADC concentrations. The model can be translated to the clinic by incorporation of human PK and used to simulate dosing regimens required for tumor volume reduction in patients. It has been applied previously to study the clinical translation of T-DM1 and an anti-5T4 ADC (A1mcMMAF) [18]. This modeling approach

differs from the larger quantitative systems pharmacology models that have been applied to ADCs to answer more complex mechanistic questions [35-37]. The level of model parsimony required depends upon the quantitative question asked [38]. In our case, the modeling question required comparison of 2 ADCs and a 'fit-for-purpose' modeling approach was applied, with the benefit that this could be easily re-applied to other ADCs or oncology drugs with a similar mechanism of action, such as mAbs or small molecule chemotherapeutics.

Efficacy differentiation

To determine the preclinical efficacy of PF-06804103, studies were completed in a range of mouse tumor models, including models resistant to T-DM1. PDX and CLX were selected from different disease origins (breast, gastric and non-small cell lung cancer (NSCLC)). They also differed in HER2 expression levels. For example, N87 has 400,000 to 1 million HER2 receptors per cell, whereas JIMT-1 has 110,000 HER2 receptors per cell. To compare with T-DM1, some CLX/PDX were selected with susceptibility to both PF-06804103 and T-DM1. In addition, some 'tougher' models were selected such as JIMT-1, established from the pleural metastasis of a patient with breast carcinoma who had failed trastuzumab therapy, and PDX 144580, which was derived from a triple negative breast cancer patient.

TSC was used as a quantitative efficacy indicator to compare PF-06804103 and T-DM1 across models. It is defined as the concentration of the drug where the tumor is neither growing nor regressing and can be considered as the minimal concentration required for efficacy. TSC is a useful comparative metric as it combines information on the tumor growth pattern and the drug effect. TSC values for PF-06804103 were lower than for T-DM1 across the CLX/ PDX studied (Figure 2). PF-06804103 was concluded to be more potent than T-DM1 across the mouse tumor cell lines studied and was efficacious in T-DM1 resistant models. Mechanistically, this makes sense as PF-06804103 has a cleavable linker which enables efficient intracellular release of membrane permeable payload and subsequent bystander killing. It is unknown whether the mechanisms of resistance to T-DM1 in animal models, that are overcome by PF-06804103, would directly translate to the clinical setting. However, alterations in lysine-mcc-DM1 mediated cytotoxicity appears to be a predominant mechanism of T-DM1 resistance in the clinic [15], which suggests that alternative therapies with different linker payloads may help overcome acquired T-DM1 resistance.

Translation to human: PK

The first step in the clinical translation process was prediction of the clinical PK of PF-06804103. T-DM1 is known to exhibit non-linear PK in the clinic with increasing half-life and decreasing clearance values over the dose range studied in Phase 1 [24, 39]. For oncology drugs the size of the tumor is often not large enough to drive significant target mediated clearance. However, circulating soluble target can act as a sink for the drug and reduce the free levels of drug available to distribute to the tumor and bind to the target. The ECD of the HER2 receptor is shed from the cell surface and serum concentrations of HER2 have been shown to be higher in patients with

metastatic breast cancer compared with healthy females [25]. Extremely high concentrations of HER2 ECD (approximately 1000 ng/mL) were observed in some patients with metastatic disease. For trastuzumab, high levels of serum HER2 ECD are associated with rapid CL and decreased benefit from trastuzumab therapy [6, 25, 40]. A TMDD model was developed for T-DM1 accounting for serum HER2 shedding, binding of T-DM1 to HER2 ECD and elimination of the T-DM1-HER2 ECD complex, in addition to the standard linear catabolic CL process (Figure 3, Table 4). This model was shown to describe the non-linear CL observed for T-DM1 in Phase 1 studies (Figure 4a, [24]). To test the model, it was used to predict PK of trastuzumab in a Phase 2 clinical study, where it was reported that a patient with high serum HER2 ECD exhibited vastly different PK to a patient with low serum HER2 ECD. Following IV administration of trastuzumab (250mg loading dose, followed by 100mg QW dosing), the patient with high HER2 ECD (> 700 ng/mL) showed rapid CL of trastuzumab resulting in steady state trastuzumab concentrations of approximately 4 μg/mL. The patient with low HER2 ECD (< 8.5 ng/mL) had steady state trastuzumab concentrations of approx. 70 μg/mL. The model was able to recapitulate the PK profiles with addition of only the reported HER2 ECD values and linear trastuzumab clearance (see Supplementary Figure 2).

Since PF-06804103 is more potent than T-DM1 it may require lower doses for efficacy in the clinic. It was therefore considered important to predict the potential impact of non-linear clearance on the clinical PK of PF-06804103. The model developed for T-DM1 was applied to predict the PK of PF-06804103 in patients. The 2 -compartment linear PK parameters were scaled from the cynomolgus monkey PK parameters for PF-06804103. The K_D for PF-06804103 binding to HER2 was included in the model. All other parameters, including shedding and degradation of the HER2-ECD and clearance of the PF-06804103- HER2 ECD complex were kept the same (Table 4). PF-06804103 is predicted to have similar PK to T-DM1.

Translation to human: efficacy

Prior knowledge of the expected efficacy of an ADC in the clinic is desirable for optimal design of clinical trials and to ensure that an efficacious dose can be reached before the onset of dose limiting toxicities. In this analysis, preclinical PK/PD of PF-06804103 in mouse xenograft studies is translated to the clinic to compare predicted clinical efficacy with T-DM1. Prediction of clinical efficacy from mouse xenograft TGI is contentious and there is a long-held debate about their predictive capability [41-44]. Our thesis is that these studies contain rich information on the system and the effect of the drug. However, they are often not interpreted properly, and a systematic, rigorous quantitative method is required. To translate the preclinical PK/PD for PF-06804103 to human, the predicted human PK was incorporated, and it was assumed that mouse PD parameters translated directly to human. Since tumor doubling time is much slower in cancer patients (in the order of months) than in mouse experimental tumors (in the order of days), this represents a conservative approach and predictions that achieved stable disease (stasis) using mouse PK/PD parameters are assumed to be minimally efficacious in humans, achieving tumor regression. This method has been tested previously for T-DM1 and was shown to predict an

efficacious dose of 2.4- 4.8 mg/kg Q3W from modeling T-DM1 data from 3 mouse tumor models, which is consistent with the efficacious dose of 3.6 mg/kg Q3W [18]. An alternative approach would be to incorporate clinical tumor doubling times into the predicted clinical model, and this could be used for a more rigorous exploration of doses and regimens required for efficacy in specific patient populations. However, it is often difficult to obtain these rates, due to absence of placebo data. As such, a fit-for purpose approach was taken which is useful to compare between PF-06804103 and T-DM1, and has been shown to successfully predict clinical efficacious dose of T-DM1 [18].

Translation of PF-06804103 to the clinic predicts efficacy at lower doses than T-DM1 (Figure 5a and 5b). These figures illustrate the benefit of studying several mouse tumor models to characterize efficacy and translate to the clinic. Depending on their individual characteristics and susceptibilities, different CLX and PDX tumor models predict a range of effects from complete response to tumor regrowth. An alternative approach to determining efficacy in mouse models was reported for PF-06804103 and T-DM1 [8]. They evaluated in vivo efficacy in a panel of HER2+ gastric and NSCLC PDX and completed a waterfall analysis, using RECIST criteria to define overall response rate (ORR). The NSCLC PDX were designated $HER2^{1+}$ to $HER2^{2+}$ and the gastric PDX were designated $HER2^{1+}$ to $HER2^{3+}$ by immunohistochemistry. In the panel of gastric cancer PDX models, PF-06804103 and T-DM1 had an ORR of 3/3 (100%) and 0/3 (0%), respectively. In the panel of NSCLC cancer PDX models, PF-06804103 and T-DM1 had an ORR of 8/9 (89%) and 1/10 (10%), respectively.

In conclusion, modeling and simulation strategies were used to demonstrate that a new generation HER2 ADC (PF-06804103) is a potentially exciting new therapy which differentiates from T-DM1 in its preclinical efficacy profile. PF-06804103 had a lower *Ceff* (TSC) in mouse models using CLX/PDX with both high and low HER2 expression and was efficacious in T-DM1 resistant models. Clinical PK of PF-06804103 is predicted to be similar to T-DM1 and non-linear across doses. The mouse PK/PD models were translated to the clinic and predicted superior efficacy compared to T-DM1. As a result, PF-06804103 is projected to provide benefit in HER2+ indications in the clinic.

4.6 Acknowledgements

The authors would like to thank Laurie Tylaska, Sean Han, Cong Wei and Brain Rago who completed the bioanalytical analyses described in this manuscript. The authors would also like to thank members of the in vivo and drug safety team who completed the mouse and cynomolgus monkey experiments. The authors would like to thank Shengjia Wu (SUNY Buffalo) for QC of model equations and code.

References

1. Dawood, S., et al., *Prognosis of women with metastatic breast cancer by HER2 status and trastuzumab treatment: an institutional-based review.* J Clin Oncol, 2010. **28**(1): p. 92-8.
2. Slamon, D., et al., *Human breast cancer: correlation of relapse and survival with amplification of the HER-2/neu oncogene.* Science, 1987. **235**(4785): p. 177-182.
3. Colomer, R., et al., *Herceptin: From the Bench to the Clinic.* Cancer Investigation, 2001. **19**(1): p. 49-56.
4. Chari, R.V., M.L. Miller, and W.C. Widdison, *Antibody-drug conjugates: an emerging concept in cancer therapy.* Angew Chem Int Ed Engl, 2014. **53**(15): p. 3796-827.
5. Lambert, J.M. and R.V. Chari, *Ado-trastuzumab Emtansine (T-DM1): an antibody-drug conjugate (ADC) for HER2-positive breast cancer.* J Med Chem, 2014. **57**(16): p. 6949-64.
6. Baselga, J., *Phase I and II clinical trials of trastuzumab.* Ann Oncol, 2001. **12 Suppl 1**: p. S49-55.
7. III, H.A.B., et al., *Phase II Study of the Antibody Drug Conjugate Trastuzumab-DM1 for the Treatment of Human Epidermal Growth Factor Receptor 2 (HER2) –Positive Breast Cancer After Prior HER2-Directed Therapy.* Journal of Clinical Oncology, 2011. **29**(4): p. 398-405.
8. Graziani, E. et al., *Creating a superior, site-specific anti-HER2 antibody-drug conjuigate (PF-06804103) for the treatment of breast, gastric, and lung cancers.* Cancer Cell, 2019 (in press).
9. Maderna, A., et al., *Discovery of cytotoxic dolastatin 10 analogues with N-terminal modifications.* J Med Chem, 2014. **57**(24): p. 10527-43.
10. Lu, J., et al., *Linkers Having a Crucial Role in Antibody-Drug Conjugates.* International journal of molecular sciences, 2016. **17**(4): p. 561-561.
11. Erickson, H.K., et al., *Antibody-Maytansinoid Conjugates Are Activated in Targeted Cancer Cells by Lysosomal Degradation and Linker-Dependent Intracellular Processing.* Cancer Research, 2006. **66**(8): p. 4426.
12. Barok, M., H. Joensuu, and J. Isola, *Trastuzumab emtansine: mechanisms of action and drug resistance.* Breast cancer research : BCR, 2014. **16**(2): p. 209-209.
13. Hamblett, K.J., *HER2-Targeted ADCs: At the Forefront of ADC Technology Development.* 2018: p. 163-185.
14. Staudacher, A.H. and M.P. Brown, *Antibody drug conjugates and bystander killing: is antigen-dependent internalisation required?* British Journal of Cancer, 2017. **117**(12): p. 1736-1742.
15. Hunter, F.W., et al., *Mechanisms of resistance to trastuzumab emtansine (T-DM1) in HER2-positive breast cancer.* British Journal of Cancer, 2020. **122**(5): p. 603-612.
16. Loganzo, F., et al., *Tumor Cells Chronically Treated with a Trastuzumab–Maytansinoid Antibody–Drug Conjugate Develop Varied Resistance Mechanisms but Respond to Alternate Treatments.* Molecular Cancer Therapeutics, 2015. **14**(4): p. 952.
17. Jumbe, N.L., et al., *Modeling the efficacy of trastuzumab-DM1, an antibody drug conjugate, in mice.* Journal of Pharmacokinetics and Pharmacodynamics, 2010. **37**(3): p. 221-242.
18. Haddish-Berhane, N., et al., *On translation of antibody drug conjugates efficacy from mouse experimental tumors to the clinic: a PK/PD approach.* Journal of Pharmacokinetics and Pharmacodynamics, 2013. **40**(5): p. 557-571.

19. Simeoni, M., et al., *Predictive pharmacokinetic-pharmacodynamic modeling of tumor growth kinetics in xenograft models after administration of anticancer agents.* Cancer Res, 2004. **64**(3): p. 1094-101.
20. Nguyen, T.H.T., et al., *Model Evaluation of Continuous Data Pharmacometric Models: Metrics and Graphics.* CPT: Pharmacometrics & Systems Pharmacology, 2017. **6**(2): p. 87-109.
21. Gabrielsson J, W.D., *Pharmacokinetic and Pharmacodynamic Data Analysis, Concepts and Applications*. 5th ed. 2017, Sweden: Swedish Pharmaceutical Press.
22. Mager, D.E. and W.J. Jusko, *General Pharmacokinetic Model for Drugs Exhibiting Target-Mediated Drug Disposition.* Journal of Pharmacokinetics and Pharmacodynamics, 2001. **28**(6): p. 507-532.
23. Asgeirsson, K.S., et al., *Serum epidermal growth factor receptor and HER2 expression in primary and metastatic breast cancer patients.* Breast cancer research : BCR, 2007. **9**(6): p. R75-R75.
24. Girish, S., et al., *Clinical pharmacology of trastuzumab emtansine (T-DM1): an antibody-drug conjugate in development for the treatment of HER2-positive cancer.* Cancer Chemother Pharmacol, 2012. **69**(5): p. 1229-40.
25. Jensen, B.V., J.S. Johansen, and P.A. Price, *High Levels of Serum HER-2/neu and YKL-40 Independently Reflect Aggressiveness of Metastatic Breast Cancer.* Clinical Cancer Research, 2003. **9**(12): p. 4423-4434.
26. Bostrom, J., et al., *High affinity antigen recognition of the dual specific variants of herceptin is entropy-driven in spite of structural plasticity.* PloS one, 2011. **6**(4): p. e17887-e17887.
27. Betts, A., et al., *Linear pharmacokinetic parameters for monoclonal antibodies are similar within a species and across different pharmacological targets: A comparison between human, cynomolgus monkey and hFcRn Tg32 transgenic mouse using a population-modeling approach.* mAbs, 2018. **10**(5): p. 751-764.
28. Meric-Bernstam, F., et al., *Advances in HER2-Targeted Therapy: Novel Agents and Opportunities Beyond Breast and Gastric Cancer.* Clinical Cancer Research, 2019. **25**(7): p. 2033-2041.
29. Peddi, P.F. and S.A. Hurvitz, *Ado-trastuzumab emtansine (T-DM1) in human epidermal growth factor receptor 2 (HER2)-positive metastatic breast cancer: latest evidence and clinical potential.* Ther Adv Med Oncol, 2014. **6**(5): p. 202-9.
30. Perez, E.A., et al., *Trastuzumab Emtansine With or Without Pertuzumab Versus Trastuzumab Plus Taxane for Human Epidermal Growth Factor Receptor 2-Positive, Advanced Breast Cancer: Primary Results From the Phase III MARIANNE Study.* J Clin Oncol, 2017. **35**(2): p. 141-148.
31. Thuss-Patience, P.C., et al., *Trastuzumab emtansine versus taxane use for previously treated HER2-positive locally advanced or metastatic gastric or gastro-oesophageal junction adenocarcinoma (GATSBY): an international randomised, open-label, adaptive, phase 2/3 study.* Lancet Oncol, 2017. **18**(5): p. 640-653.
32. Mittendorf, E.A., et al., *Loss of HER2 Amplification Following Trastuzumab-Based Neoadjuvant Systemic Therapy and Survival Outcomes.* Clinical Cancer Research, 2009. **15**(23): p. 7381.

33. Li, G., et al., *Mechanisms of Acquired Resistance to Trastuzumab Emtansine in Breast Cancer Cells.* Molecular Cancer Therapeutics, 2018. **17**(7): p. 1441-1453.
34. Agoram, B., S. Martin, and P. H van der Graaf, *The role of mechanism-based pharmacokinetic-pharmacodynamic (PK-PD) modelling in translational research of biologics*. Vol. 12. 2008. 1018-24.
35. Bender, B., et al., *A mechanistic pharmacokinetic model elucidating the disposition of trastuzumab emtansine (T-DM1), an antibody-drug conjugate (ADC) for treatment of metastatic breast cancer.* The AAPS journal, 2014. **16**(5): p. 994-1008.
36. Betts, A.M., et al., *Preclinical to Clinical Translation of Antibody-Drug Conjugates Using PK/PD Modeling: a Retrospective Analysis of Inotuzumab Ozogamicin.* AAPS J, 2016. **18**(5): p. 1101-16.
37. Shah, D.K., N. Haddish-Berhane, and A. Betts, *Bench to bedside translation of antibody drug conjugates using a multiscale mechanistic PK/PD model: a case study with brentuximab-vedotin.* Journal of Pharmacokinetics and Pharmacodynamics, 2012. **39**(6): p. 643-659.
38. Vicini, P. and P.H. van der Graaf, *Systems Pharmacology for Drug Discovery and Development: Paradigm Shift or Flash in the Pan?* Clinical Pharmacology & Therapeutics, 2013. **93**(5): p. 379-381.
39. Krop, I., et al., *A phase I study of weekly dosing of trastuzumab-DM1 (T-DM1) in patients with advanced HER2+ breast cancer.* Cancer Research, 2009. **69**(2 Supplement): p. 3136.
40. Ali, S.M., et al., *Serum HER-2/neu and relative resistance to trastuzumab-based therapy in patients with metastatic breast cancer.* Cancer, 2008. **113**(6): p. 1294-301.
41. Kelland, L.R., *"Of mice and men": values and liabilities of the athymic nude mouse model in anticancer drug development.* European Journal of Cancer, 2004. **40**(6): p. 827-836.
42. Kerbel, R., *Human Tumor Xenografts as Predictive Preclinical Models for Anticancer Drug Activity in Humans: Better than Commonly Perceived—But They Can Be Improved*. Vol. 2. 2003. S134-9.
43. Khaled, W.T. and P. Liu, *Cancer mouse models: Past, present and future.* Seminars in Cell & Developmental Biology, 2014. **27**: p. 54-60.
44. Ruggeri, B.A., F. Camp, and S. Miknyoczki, *Animal models of disease: Pre-clinical animal models of cancer and their applications and utility in drug discovery.* Biochemical Pharmacology, 2014. **87**(1): p. 150-161.

Supplementary Materials

Supplementary Figure 1: Goodness of fit plots for PF-06804103 PK/PD modeling in 3 CLX and 4 PDX xenograft mouse models Plots shown include: (i) visual predictive checks of tumor volume (mm^3) data and model prediction versus time at each dose level. The magenta band represents the 95% prediction distribution and (ii) observations versus model predictions using the population and individual parameters compared to line of unity.

JIMT-1:

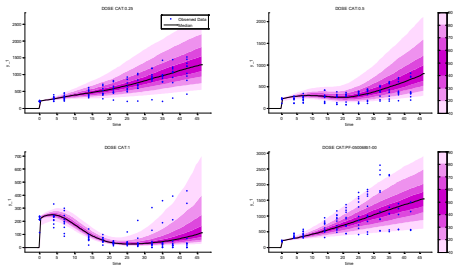

JIMT-1:

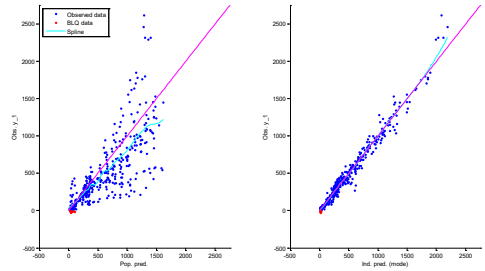

N87:

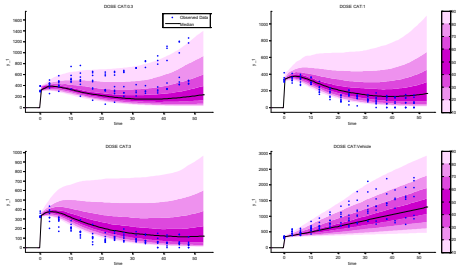

N87:

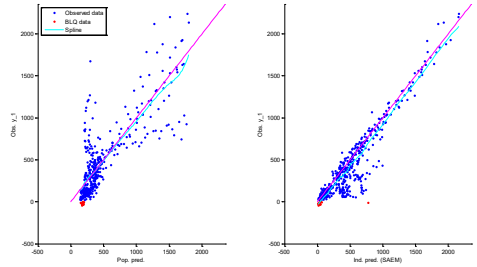

BT474:

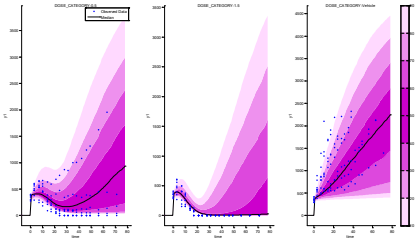

BT474:

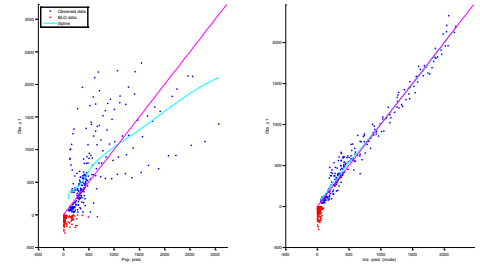

24312:

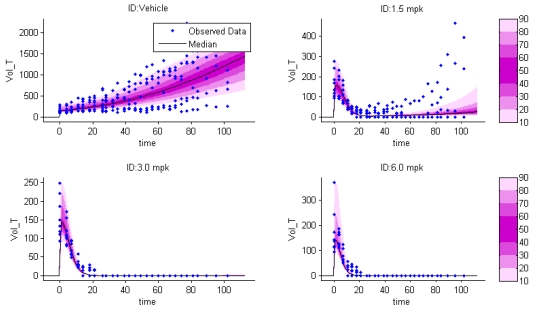

24312:

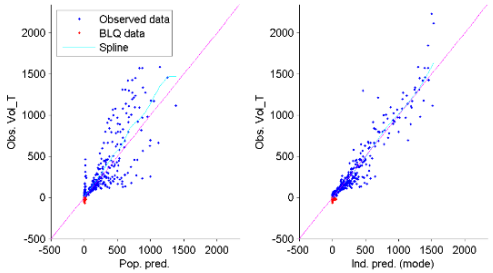

37622:

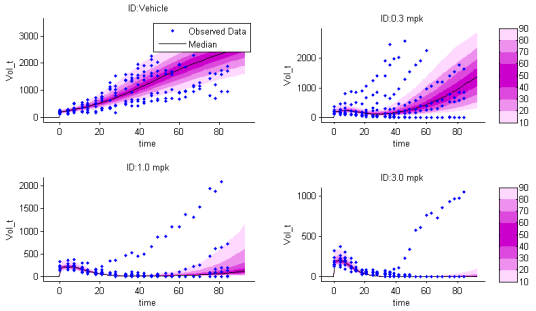

37622:

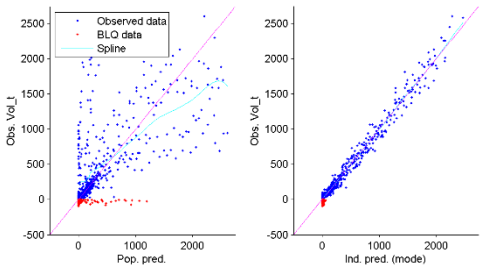

144580:

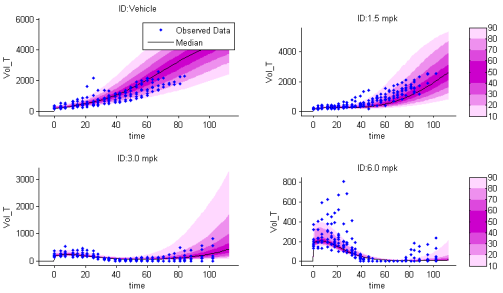

144580:

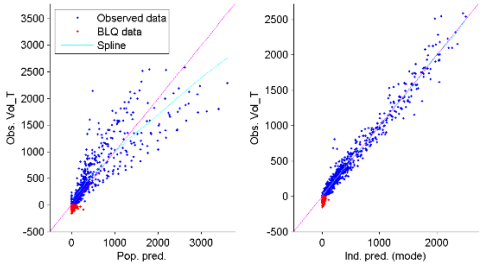

GA3109:

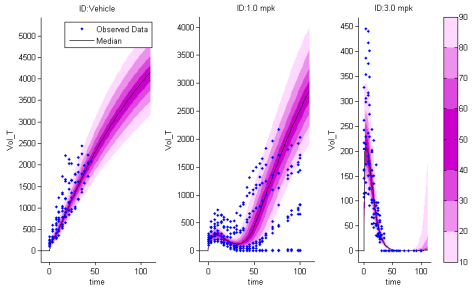

GA3109:

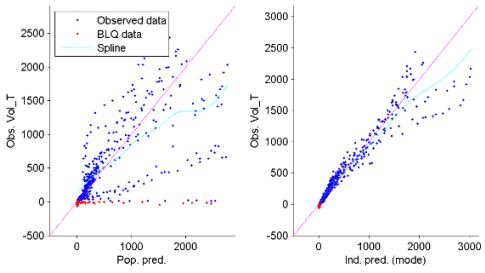

Supplementary Fig. 2 Validation of TMDD model by application to predict PK from a Phase II study [6] where discrepant PK was observed following trastuzumab administration to a patient with **(a)** low HER2 ECD (<8.5 ng/mL) and a patient with **(b)** high HER2 ECD concentration (>750 ng/ml). **Trastuzumab dose was 250mg IV loading dose, 100mg IV thereafter.** Symbols represent data digitized from [6]. Lines represent TMDD model predictions. A CL value of 0.23 mL/h/kg was used for trastuzumab. In (a) HER-2 ECD concentration was set to 2 ng/mL and in (b) HER2 ECD concentration was set to 750 ng/ml. All other parameters were kept the same.

(a)

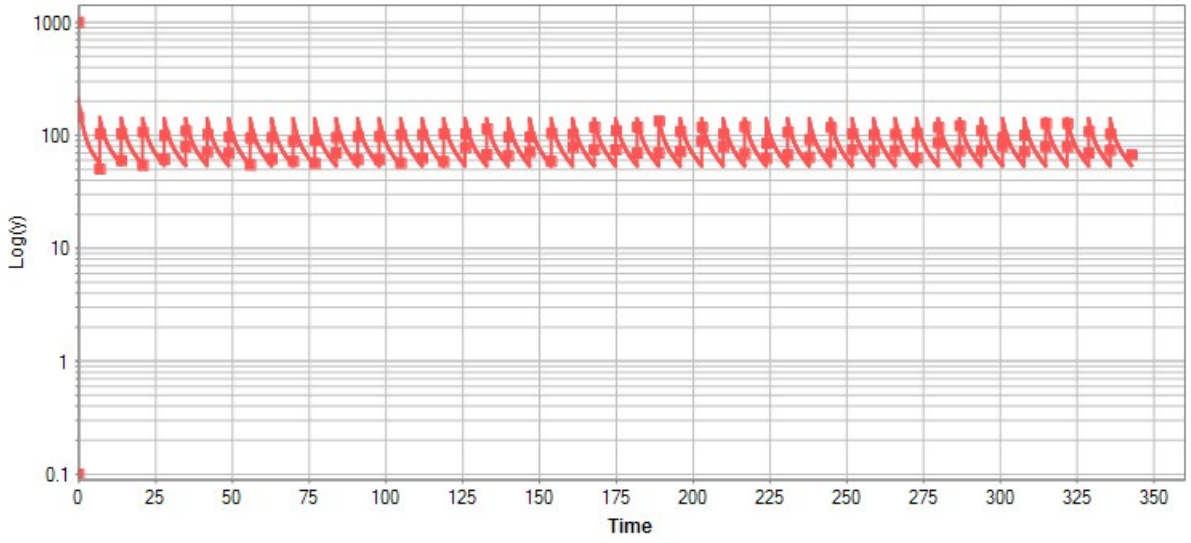

(b)

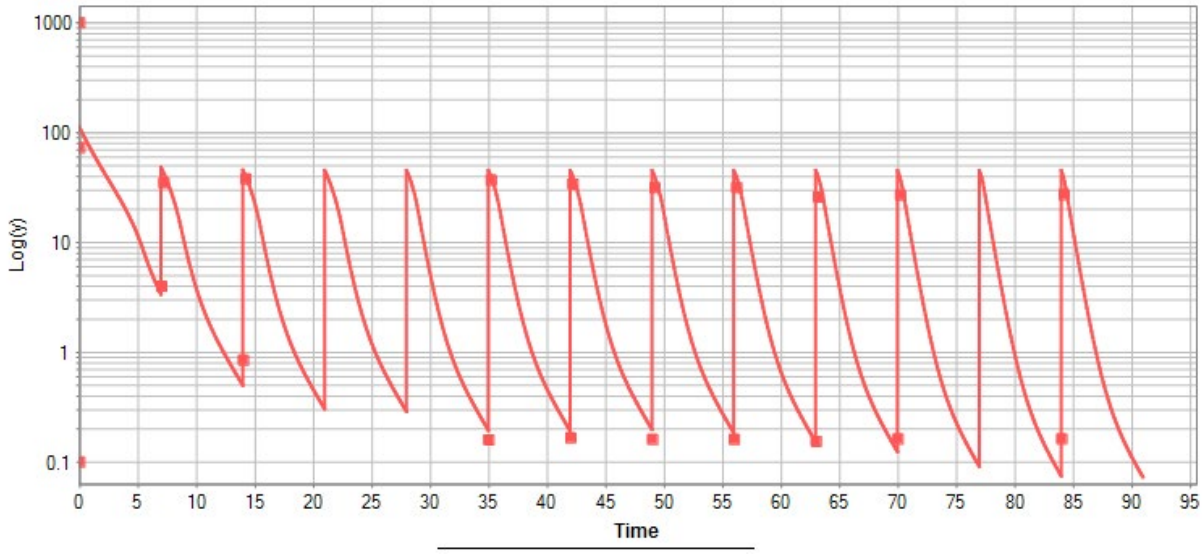

Model code for Clinical PK predictions (Berkeley Madonna v8.3.18)

```
METHOD Auto
STARTTIME = 0
STOPTIME = 100; days
DT = 0.02
Tolerance = 1e-12
Dose=210 ; mg or 3 mpk
Dose_nmole=Dose*1000000/150000 ; per human
;-----------------------------------------------
INFUSION=(INFrate*INFrepeat*INFend)/(Vc*70/1000) ; Infusion Rate nM/day

INFrepeat=IF TIME<(TINFstart) THEN 0 ELSE IF MOD(TIME+TINFstart,TINFrepeat)<=INFduration
THEN 1 ELSE 0

INFend=IF TIME>TINFend THEN 0 ELSE 1

TINFstart=0.0 ;START TIME OF FIRST INFUSION

TINFrepeat=21 ;TIME INTERVAL BETWEEN INFUSIONS

TINFend=4*21 ;TIME AFTER WHICH NO NEW INFUSIONS ARE GIVEN

INFduration=1/24 ;DURATION OF EACH INFUSION ;days

INFrate=Dose_nmole/INFduration ;RATE OF EACH INFUSION

;-----------------------------------------------
{INITIAL VALUES}
INIT Cadc         = 0 ; nM
INIT Cadc_per  = 0.0 ; nM
INIT Cecd         = T0 ; nM
INIT Cadc_ecd  = 0.0 ; nM

{DIFFERENTIAL EQUATIONS}
d/dt(Cadc)      =INFUSION -k12*Cadc + k21*Cadc_per*Vp/Vc - kon*Cadc*Cecd + koff*Cadc_ecd
-kel*Cadc

d/dt(Cadc_per)  =k12*Cadc*Vc/Vp - k21*Cadc_per

d/dt(Cecd)        =kshed - kdeg*Cecd - kon*Cadc*Cecd + koff*Cadc_ecd

d/dt(Cadc_ecd) =kon*Cadc*Cecd - koff*Cadc_ecd -kel2*Cadc_ecd


{PARAMETERS}
; PF-06804103 parameters
CL        = 5.52        ; mL/day/kg
Q         = 14.9        ; mL/day/kg
Vc        = 38.1        ; mL/kg
Vp        = 20.2        ; mL/kg
T0        = 0.2         ; nM
```

```
kdeg      = 33.3        ; 1/day
KD        = 0.1         ; nM
koff      = 6.13        ; 1/day
kel2      = 32.6        ; 1/day ;Cadc_ecd

; static secondary parameters
k12       = Q/Vc            ; 1/day
k21       = Q/Vp            ; 1/day
kel       = CL/Vc           ; 1/day
kon       = koff/KD     ; 1/nM/Day
kshed     = kdeg*T0     ;nM/Day

{OUTPUTS}
Free_Drug    = Cadc
Total_Drug   = Cadc + Cadc_ecd
Complex      = Cadc_ecd
Free_Target  = Cecd
Total_Target = Cecd  + Cadc_ecd
Cadc_ugmL = Cadc*150000/1e6
```

Chapter 5

Preclinical to Clinical Translation of Antibody-Drug Conjugates Using PK/PD Modeling:

A Retrospective Analysis of Inotuzumab Ozogamicin

Alison M. Betts, Nahor Haddish-Berhane, John Tolsma, Paul Jasper, Lindsay E. King, Yongliang Sun, Subramanyam Chakrapani, Boris Shor, Joseph Boni and Theodore R. Johnson

The AAPS Journal 18(5): 1101-1116 (2016)

5.1 Abstract

A mechanism-based pharmacokinetic/pharmacodynamic (PK/PD) model was used for preclinical to clinical translation of inotuzumab ozogamicin, a CD22-targeting antibody-drug conjugate (ADC) for B-cell malignancies including non-Hodgkin's lymphoma (NHL) and acute lymphocytic leukemia (ALL). Preclinical data was integrated in a PK/PD model which included: (1) a plasma PK model characterizing disposition and clearance of inotuzumab ozogamicin and its released payload N-Ac-γ-calicheamicin DMH, (2) a tumor disposition model describing ADC diffusion into the tumor extracellular environment, (3) a cellular model describing inotuzumab ozogamicin binding to CD22, internalization, intracellular N-Ac-γ-calicheamicin DMH release, binding to DNA or efflux from the tumor cell (4) tumor growth and inhibition in mouse xenograft models. The preclinical model was translated to the clinic by incorporating human PK for inotuzumab ozogamicin and clinically relevant tumor volumes, tumor growth rates and values for CD22 expression in the relevant patient populations. The resulting stochastic models predicted progression free survival (PFS) rates for inotuzumab ozogamicin in patients comparable to the observed clinical results. The model suggested that a fractionated dosing regimen is superior to a conventional dosing regimen for ALL, but not for NHL. Simulations indicated that tumor growth is a highly sensitive parameter and predictive of successful outcome. Inotuzumab ozogamicin PK and N-Ac-γ-calicheamicin DMH efflux are also sensitive parameters and would be considered more useful predictors of outcome than CD22 receptor expression. In summary, a multi-scale, mechanism-based model has been developed for inotuzumab ozogamicin, which can integrate preclinical biomeasures and PK/PD data to predict clinical response.

5.2 Introduction

Antibody-drug conjugates (ADCs) represent a promising therapeutic modality for clinical management of cancer (1, 2). There are more than 40 ADCs currently in different stages of clinical development for the treatment of various malignant diseases (3). In addition, brentuximab vedotin (Adcetris; Seattle Genetics) and ado-trastuzumab emtansine (T-DM1, Kadcyla; Roche-Genentech) are examples of recently approved ADCs on the market for oncology indications (2). ADCs currently in clinical development offer substantial improvements over first generation ADCs with more potent cytotoxins and superior conjugation stability (4). However, some ADCs are failing in the clinic due to insufficient efficacy (relative to standard of care) and off-target toxicity. For example, IMGN-901 is a CD-56-targeting ADC which failed to demonstrate sufficient improvement in efficacy over standard of care (etoposide/ carboplatin) in a Ph2 SCLC trial (5). Seattle Genetics discontinued the clinical development of vorsetuzumab mafodotin (SGN-75), an ADC for the treatment of solid tumors and hematological malignancies in favor of SGN-CD70A, an ADC against the same target but with a more potent payload (6). The timing is right to learn from these ADCs and to use the latest technology advancements to understand how they can be improved upon. Refinements in next generation ADCs are already being seen with advances in antibody engineering, improvements in linker-payload conjugation strategies (7) and the generation of novel highly potent payloads with different mechanisms of action (4, 8).

Mechanistic pharmacokinetic/pharmacodynamic (PK/PD) modeling is an example of an applied quantitative tool which can be used to provide understanding of the mechanistic processes of

drug action (9). The complex, non-linear processes involved in the physiological and cellular disposition of ADCs and their component parts make them ideal candidates for mechanistic modeling to enable integration and understanding of these multiple processes (10). The result is not only comprehension of the underlying system and mechanism of action, but also more tractable applications, including target feasibility, optimal ADC selection, preclinical to clinical translation and guidance on dose regimen optimization.

Quantitative modeling of ADCs in the literature to date has focused on empirical, data-driven PK/PD models (11, 12). These models are relatively easy to develop and apply and can be used for some level of extrapolation, e.g., across species (with some assumptions), to enable quantitative decision making. However, ADCs have intricate mechanisms of action, and the quantitative questions asked often require the use of more complex mechanistic models. For example, to optimize an ADC, properties of the target, including receptor expression, internalization rate and intracellular processing/recycling rate, need to be balanced (13). Properties of the ADC and its payload, including affinity for their targets and pharmacokinetics, also need to be included. While such models are an investment in terms of data requirements, they offer a high return of investment with respect to the granularity of the questions answered. Such a mechanistic PK/PD model for ADCs, capable of integrating preclinical biomeasures and PK/PD data to predict clinical response, was proposed by Shah, *et al.* (10). The authors used this model to quantitatively understand and characterize the disposition of brentuximab vedotin and its payload MMAE at the cellular and physiological level. A novel tumor penetration model was developed to predict intracellular tumor payload concentration, which was then linked to an optimized tumor growth inhibition model to characterize ADC efficacy in mouse xenograft models. The integrated mechanism-based PK/PD model was translated to the clinic and used to perform clinical trial simulation for brentuximab vedotin. The resulting multi-scale mechanistic modeling approach predicted progression free survival (PFS) rates and complete response rates for brentuximab vedotin in patients that were comparable to the observed clinical results. A different application of this model was described in a subsequent publication by Shah, *et al.* where it was used for a priori prediction of tumor concentrations of ADC and payload for an anti-5T4 ADC, A1mcMMAF (14). The model was also used to investigate sensitivity of model parameters. For example, payload dissociation from ADC and tumor size were found to be the most important determinants of plasma and tumor payload exposure.

In the analysis described herein, a mechanistic modeling approach was used to gain quantitative insight into the system dynamics of an anti-CD22 ADC in late stage clinical development for B-cell malignancies. Inotuzumab ozogamicin (CMC-544, PF-05208773) is an ADC composed of an IgG4 anti-CD22 monoclonal antibody conjugated to the enediyne DNA damaging agent N-Ac-γ-calicheamicin DMH via an acid-labile 4-(4'-acetylphenoxy)butanoic acid (Acbut) linker (15, 16). Inotuzumab ozogamicin is currently being evaluated in Phase 2/3 clinical trials for treatment of acute lymphoblastic leukemia (ALL). A Phase 3 study of inotuzumab ozogamicin in relapsed or refractory aggressive non-Hodgkin lymphoma (NHL) was discontinued due to lack of superiority relative to an active comparator arm (investigator's choice of bendamustine + rituximab or gemcitabine + rituximab) (17). Preclinically, inotuzumab ozogamicin inhibited the growth and establishment of B-cell lymphomas and induced the regression of disseminated B-cell lymphomas (Ramos, RL) and acute lymphoblastic leukemia (REH) in mouse xenograft models (15, 16). Mouse tumor growth inhibition data, along with inotuzumab ozogamicin plasma PK and target/system

parameters were used to perform mechanistic PK/PD modeling for inotuzumab ozogamicin and to predict intracellular tumor concentrations of N-Ac-γ-calicheamicin DMH. The model was translated to the clinic, and the results from simulated clinical trials were compared with observed clinical trial data to validate the translation process. The human model has subsequently been utilized for hypothesis generation and as a tool to answer mechanistic questions, including the effect of changes in antigen expression or efflux transporter capacity/status in patient tumors and the effect of changes in dose and/or regimen (in particular for ALL vs. NHL). This application of mechanistic PK/PD modeling demonstrates how preclinical data can be translated to the clinic to help scrutinize the mechanism of action of an ADC and predict outcome. Learnings can be applied to earlier stage programs as a quantitative tool to help guide their development.

5.3 Materials and Methods

CD22 Receptor Numbers

A quantitative flow cytometry method was developed to determine surface antibody binding capacity (ABC) per cell as a measure of receptor numbers using the parent antibody (G544) of inotuzumab ozogamicin conjugated 1:1 with phycoerythrin (PE) (18). Ramos and REH cell lines were cultured under standard culture conditions. A full binding curve was generated at 4°C under conditions that approached equilibrium to prevent internalization and samples were analyzed by FACS. The maximum specific binding fluorescent intensity derived from this data analysis was interpolated off a BD QuantiBRITE PE calibration curve to calculate the maximum ABC per cell as a measure of receptor numbers.

G544 Internalization

An imaging flow cytometry-based method was developed to measure internalization of G544, conjugated with PE or Alexa Fluor 647, under constant exposure condition. For each sample membrane and cytosolic intensity from CD22+ single cells were determined using area masks defined from the brightfield image of each cell. The extent of internalization at each time point was determined using IDEAS software internalization wizard which calculated an internalization score (IS) (19) based on the ratio of cytosolic intensity to total cell intensity using the upper quartile of pixel intensities. A plot of the IS vs. time was used to determine the initial half-life of internalization.

Binding Affinities

The binding of inotuzumab ozogamicin to CD22 receptors was evaluated using surface plasma resonance analysis, using the method of DiJoseph *et al.* (15), and the resulting K_d was determined to be 200 pM. The association rate constant (k_{on}) was assumed to be typical of monoclonal antibodies at approximately 5 x 10^5 $M^{-1}s^{-1}$ (20). The dissociation rate constant (k_{off}) was interpolated from the K_d and k_{on} using the relationship $K_d = k_{off} / k_{on}$ and was calculated to be 7.5 x 10^{-5} s^{-1}. As previously reported by Tianhu, *et al.*, N-Ac-γ-calicheamicin DMH binds to DNA with an estimated K_d of 135 nM (21).

Materials for Mouse Pharmacokinetic Study

Humanized IgG4 anti-CD22 antibody (G544) was provided by Celltech Chiroscience, plc, Wayne, PA. It was linked to calicheamicin with an acid labile AcBut (4-(4_acetylphenoxyl) butanoic acid) linker at Wyeth Research. Loading of calicheamicin onto the CD22 antibody was 50 μg of calicheamicin per mg of antibody and the average DAR was 3.5. The NHL B cell line RL (CRL-2261) was obtained from the American Type Culture Collection (ATCC, Manassas, VA). The cell line was determined to be mycoplasma free by a polymerase chain reaction mycoplasma detection assay. The cells were maintained as suspension cultures in RPMI medium plus 10% FCS, 10 mM HEPES, 1 mM sodium pyruvate, 0.2% glucose, Penicillin G sodium 100 U/mL, and streptomycin sulfate 100 μg/mL.

Mouse Pharmacokinetics

The PK of inotuzumab ozogamicin were determined following single intraperitoneal (IP) dose administration to non-tumor bearing female nude mice at 20 μg calicheamicin/kg (0.27 mg/kg inotuzumab) and 160 μg calicheamicin/kg (3.2 mg/kg inotuzumab), or to tumor (RL) bearing mice at 160 μg calicheamicin/kg (3.2 mg/kg inotuzumab) (Monolix software v3.2 (Lixoft, Antony, France)). Non-serial, terminal blood samples were collected by cardiac puncture under CO_2 anesthesia from 4 animals/group/time point at 0.1, 0.5, 1, 4, 8, 24, 48, 72, 96, 120, 168, 240 and 336 h post-dose. All blood samples were collected into tubes and stored on wet ice until the serum was separated by centrifugation at approximately 4°C for 15 min.

Assays to Quantify G544 (Total mAb) and Inotuzumab Ozogamicin (ADC)

Total mAb and ADC concentrations in mouse plasma were determined using a validated enzyme-linked immunosorbent assay (ELISA) with colorimetric detection. For the total mAb assay, the capture protein was a soluble form of recombinant CD22 protein (CD22:Fc fusion protein) and a monoclonal murine anti-human IgG4 conjugated to horseradish peroxidase (HRP) was used to detect bound G544, using 3,3',5,5'-tetramethylbenzidine (TMB) as the substrate for a colorimetric readout . For the ADC assay, CD22: Fc fusion protein was used to capture the G544 antibody portion of the ADC molecule. The calicheamicin portion of the molecule was then recognized with a rabbit anti-calicheamicin antibody. A goat anti-rabbit antibody conjugated to HRP was used to detect the bound rabbit antibody with TMB as the substrate for colorimetric readout.

Estimating Preclinical Pharmacokinetic Parameters for Total mAb, ADC and Payload Dissociation Rate

PK parameters for the mouse mAb were determined by fitting a 2-compartment PK model to the total mAb concentrations. It was assumed that the difference in clearance between the total mAb and ADC profiles was due to the dissociation of the calicheamicin payload (PL) from the mAb. The total mAb model with an additional clearance term describing dissociation of the PL was then fitted to the ADC concentration profile to estimate the dissociation rate constant, k_{dis}, *as* described previously (14).

Mouse Tumor Xenograft Studies

Tumor growth inhibition studies were completed in three different xenograft bearing mouse models: Ramos (Burkitt lymphoma), RL (non-Hodgkin's lymphoma) and REH (acute lymphoblastic leukemia), as reported in (15, 16). Briefly, female athymic nude mice were exposed to total body irradiation (400 rad) to suppress their residual immune system and facilitate the establishment of xenografts. Three days later, mice were injected subcutaneously with 5 x 10^6 REH ALL cells (6-8 mice/group) or 1 x 10^7 Ramos or RL cells (7-9 mice/group) suspended in Matrigel (Collaborative Biomedical Products, Belford, MA, USA, diluted 1:1 in RPMI-1640 medium) in the right flank for REH and left flank for RL and Ramos. Mice with staged tumors were administered normal saline (vehicle) or inotuzumab ozogamicin at Q4D x 3 regimen IP. Doses of inotuzumab ozogamicin were calculated based on quantity of N-Ac-γ-calicheamicin DMH AcBut and were 10, 40 and 160 µg calicheamicin/kg (0.14, 0.56, 2.22 mg/kg inotuzumab) for REH and Ramos or 20, 80 and 320 µg calicheamicin/kg (0.28, 1.11, 4.44 mg/kg inotuzumab) for RL. Tumors were measured at least once a week and their mass was defined as tumor volume (mm^3) = 0.5 × (tumor $width^2$) x (tumor length).

PK/PD Modeling

The mechanistic PK/PD model developed in this work and calibrated with the mouse xenograft data involved four major parts: 1) PK model describing time evolution of ADC and unconjugated payload in plasma, 2) tumor disposition model relating exposure between plasma and tumor, 3) cellular model describing intracellular payload at site of action, and 4) tumor growth and inhibition. This model is similar to the model developed and described previously (10), with main differences being a CD22 target in contrast to CD30 and calicheamicin payload (DNA toxin) in contrast to MMAE payload (tubulin inhibitor).

ADC and Unconjugated Payload PK

Plasma PK of inotuzumab ozogamicin and unconjugated payload (calicheamicin) after dose administration was modeled with a two-compartment IP model with additional terms characterizing the specific clearance into the tumor (JACOBIAN Modeling and Optimization Software, RES Group Inc., Needham, MA). The tumor disposition model is described in the subsequent section. The model equations are:

$$\frac{dA_0}{dt} = -k_a A_0$$

$$\frac{dA_1}{dt} = k_a A_0 + CLD\left(\frac{A_2}{V_2} - \frac{A_1}{V_1}\right) - CL\frac{A_1}{V_1} - \left(\frac{2P_{ADC}R_{cap}}{R_{krogh}^2} + \frac{6D_{ADC}}{R_{tumor}^2}\right)\left(\frac{A_1}{V_1} - \frac{Ab_f}{\epsilon}\right)\frac{w}{10^6}$$

$$\frac{dA_2}{dt} = CLD\left(\frac{A_1}{V_1} - \frac{A_2}{V_2}\right)$$

$$\frac{dPL_1}{dt} = k_{dis}DAR\frac{A_1}{V_{PL,1}} + CL\frac{A_1}{V_1}\frac{DAR}{V_{PL,1}} + CLD_{PL}\left(\frac{PL_2}{V_{PL,1}} - \frac{PL_1}{V_{PL,1}}\right) - CL_{PL}\frac{PL_1}{V_{PL,1}}$$
$$-\left(\frac{2P_{PL}R_{cap}}{R_{krogh}^2} + \frac{6D_{PL}}{R_{tumor}^2}\right)\left(PL_1 - \frac{PL_T}{\epsilon_{PL}}\right)\frac{w}{10^6}$$

$$\frac{dPL_2}{dt} = CLD_{PL}\left(\frac{PL_1}{V_{PL,2}} - \frac{PL_2}{V_{PL,2}}\right)$$

Parameter and variables for these equations are described in Tables 1 and 2.

Tumor Disposition Model

The tumor PK of ADC and unconjugated payload is described by a tumor disposition model (10, 22-24). Expressions describing transport into the tumor appear in the PK equations above and tumor compartment expression below as additional source and sink terms involving a number of additional parameters (e.g., $R_{cap}, R_{krogh}, P_{ADC}$, etc). Rather than estimating these parameters from the mouse xenograft data, values for permeability and diffusivity of the ADC and payload are determined from established correlations with molecular weight and known tumor size parameters (22-24). Values and references are provided in Table 2.

Tumor and Intracellular Concentrations and Dynamics

Concentrations of ADC and unconjugated payload in the tumor compartment and intracellular space are described by the equations below. The equations account for transport into the tumor compartment from plasma, binding and internalization into cell and binding of payload to the DNA target of calicheamicin.

$$\frac{dAb_f}{dt} = \left(\frac{2P_{ADC}R_{cap}}{R_{krogh}^2} + \frac{6D_{ADC}}{R_{tumor}^2}\right)\left(\frac{A_1}{V_1} - \frac{Ab_f}{\epsilon}\right) - k_{on}Ab_f\left(\frac{Ag - Ab_b}{\epsilon}\right) + k_{off}Ab_b$$

$$\frac{dAb_b}{dt} = k_{on}Ab_f\left(\frac{Ag - Ab_b}{\epsilon}\right) - k_{off}Ab_b - k_{int}Ab_b$$

$$\frac{dPL_T}{dt} = \left(\frac{2P_{PL}R_{cap}}{R_{krogh}^2} + \frac{6D_{PL}}{R_{tumor}^2}\right)\left(PL_1 - \frac{PL_T}{\epsilon_{PL}}\right) - k_{int}^{PL}PL_T + k_{out}^{PL}PL_{free}^{cell} + k_{dis}DAR\left(Ab_f + Ab_b\right)$$

$$\frac{dPL_{free}^{cell}}{dt} = k_{int}Ab_bDAR + k_{int}^{PL}PL_T - k_{out}^{PL}PL_{free}^{cell} - k_{on}^{PL}PL_{free}^{cell}\left(DNA - PL_b^{cell}\right) + k_{off}^{PL}PL_b^{cell}$$

$$\frac{dPL_b^{cell}}{dt} = k_{on}^{PL}PL_{free}^{cell}\left(DNA - PL_b^{cell}\right) - k_{off}^{PL}PL_b^{cell}$$

ADC and unconjugated payload enter the tumor compartment as described by the tumor disposition model. ADC binds with CD22 on the cell surface followed by internalization and

release of payload. Payload enters the cell via the ADC and also by non-specific internalization of unconjugated payload in the tumor compartment. Once inside the cell, payload can exit by exocytosis or remain in the cell and bind to the DNA target.

Tumor Growth and Inhibition

Tumor growth and inhibition is described using the Haddish-Berhane model (12), with equations shown below. Model variables are defined in Table 1.

$$\frac{dM_1}{dt} = \frac{k_{g0}\left(1-\frac{w}{M_{max}}\right)M_1}{\left(1+\left(\frac{k_{g0}}{k_g}w\right)^{\psi}\right)^{1/\psi}} - k_{max}\frac{PL_{total}^{\gamma}}{IC_{50}^{\gamma}+PL_{total}^{\gamma}}M_1$$

$$\frac{dM_2}{dt} = k_{max}\frac{PL_{total}^{\gamma}}{IC_{50}^{\gamma}+PL_{total}^{\gamma}}M_1 - \frac{M_2}{\tau}$$

$$\frac{dM_3}{dt} = \frac{M_2 - M_3}{\tau}$$

$$\frac{dM_4}{dt} = \frac{M_3 - M_4}{\tau}$$

The tumor growth portion of this model accounts for a preliminary exponential phase growth, followed by linear phase growth and a maximum tumor volume possible in the xenograft. Growth inhibition is modeled by a Hill equation as a function of intracellular payload concentration and several transduction compartments as cells are killed. The growth parameters are calibrated with data from the control arm of the mouse xenograft experiments and the drug-related death parameters are calibrated from the various dose arms.

Table 1: Model variables and terms used in equations

Variable	Definition	Unit
Ab_f, Ab_b	ADC concentration in tumor compartment, free and bound	nM
PL_T	Total free payload in cell	nM
$PL_{free}^{cell}, PL_b^{cell}$	Intracellular concentration of free and DNA-bound payload	nM
A_0, A_1, A_2	ADC dosed, central and peripheral compartments, respectively	nmol/kg
PL_1, PL_2	Concentration of free payload in central and peripheral compartments	nM
w	Tumor volume	mm^3
M_1, M_2, M_3, M_4	Tumor volume in growth and three transduction compartments	mm^3

Additional Equations

Several additional equations appear in the model, including tumor volume as a function of the transduction compartments, tumor mass radius (assuming spherical tumor), total intracellular payload and DAR as a function of dissociation rate.

$$w = M_1 + M_2 + M_3 + M_4$$

$$R_{tumor} = \left(\frac{3w}{4\pi}\right)^{1/3} \frac{1}{10}$$

$$PL_{total} = PL_T + PL_{free}^{cell} + PL_b^{cell}$$

$$\frac{dDAR}{dt} = -k_{dis} DAR$$

Calicheamicin Pharmacokinetics

Parameters for the plasma PK model of unconjugated calicheamicin are required for mouse to fit the xenograft tumor growth inhibition (TGI) data and for human for the subsequent clinical predictions. However, single dose IV data for calicheamicin was only available for rat and dog. A two compartment PK model was fit to this data to obtain values for $V_{PL,1}, V_{PL,2}, CL_{PL}$ and CLD_{PL} for both available species. PK parameter values for mouse and human were then obtained by allometric scaling the fitted rat and dog values. Note that the PK assay for unconjugated calicheamicin used a non-specific ELISA assay, which detects multiple forms of calicheamicin (i.e., N-Ac-γ-calicheamicin DMH + metabolites).

Clinical Pharmacokinetics of Inotuzumab ozogamicin

Clinical PK of inotuzumab ozogamicin is reported in two different Phase 1 studies in the literature (25, 26). Advani *et al.* describe a Phase 1 study of inotuzumab ozogamicin in an expanded MTD cohort of patients with relapsed or refractory CD22+ B-cell NHL (25). Ogura, *et al.* report a Phase 1 study of inotuzumab ozogamicin in Japanese patients with follicular lymphoma (FL) pre-treated with rituximab-based therapy (26). The PK was similar across both studies. For the modeling analysis herein, a simple 2-compartment model with linear elimination from the central compartment was used to characterize the PK of inotuzumab ozogamicin from Ogaru, *et al.* (26).

Preclinical to Clinical Translation

The integrated preclinical PK/PD model describing inotuzumab ozogamicin concentration-response relationship in REH, RL and Ramos xenograft bearing mice was translated to the clinic and used to perform clinical trial simulations. Three different types of CD22+ B-cell malignancies were considered in clinical trial simulations: follicular lymphoma (FL) and diffuse large B cell (DLBCL) subtypes of NHL and ALL. To enable preclinical to clinical translation the following changes were made to the model parameters: (a) relevant CD22 receptor expression levels for FL, DLBCL and ALL were included in the model (27), (b) initial tumor volumes and maximal

possible tumor volumes were changed to clinically observed/ plausible values (28, 29), and (c) growth rates for FL, DLBCL and ALL were set to clinically observed values (30-34). Clinical PK parameters for inotuzumab ozogamicin and calicheamicin were incorporated into the model as described above. The rest of the parameter values, including the inter-individual variability in PD parameters, were kept the same as the preclinical case. Preclinical PK/PD parameter estimates from RL/ Ramos cell lines were used to inform NHL clinical trial simulations, and REH cell line data was used for ALL clinical trial simulations. Please refer to Table 2 for the specific parameter values.

Clinical Trial Simulations

Clinical trial simulations for inotuzumab ozogamicin were performed using the parametric simulation method (JACOBIAN Modeling and Optimization Software, RES Group Inc., Needham, MA) (35). In each trial, 1,000 patients were simulated for each dose. For the NHL clinical trial simulations, the full PK/PD model was used including the parameters describing penetration of ADC into solid tumors (see Figure 1 and Table 2). Three different trials were simulated for NHL: patients with follicular lymphoma (FL), DLBCL patients (slow growth) and DLBCL patients (rapid growth). Two different tumor growth rates were considered for DLBCL to account for the large range in growth rates reported in the literature encompassing low-grade through to refractory aggressive B-cell NHL (30, 33)).

For the ALL clinical trial simulations the PK model was simplified by eliminating the parameters describing penetration into the solid tumor (Figure 1, red box). Instead rapid equilibrium between ADC in plasma and tumor interstitium was assumed, consistent with a liquid tumor. For both the NHL and ALL clinical trial simulations, two different dosing regimens were considered: 1.8 mg/m^2 (0.05mg/kg) Q4w x 3 and a fractionated regimen of 0.8, 0.5 and 0.5 mg/m^2 on day 1, 8 and 15 of a 28 day cycle, consistent with regimens explored in actual clinical trials for inotuzumab ozogamicin (25, 26, 36). In each case, the total dose administered was 1.8 mg/m^2.

For each simulated clinical trial, predicted tumor volumes were determined over time and PFS rates were calculated. For the NHL trials, these were compared to clinical trial data for inotuzumab ozogamicin (25). The criteria to categorize response rates for progressive disease, stable disease (SD), partial regression (PR), and complete regression (CR) for NHL were: more than 20% increase in tumor diameter, less than 30% reduction in tumor diameter, more than 30% decrease in tumor diameter but still detectable, and below the detection limit of 0.5 cm tumor diameter, respectively, according to the methods of Cheson, *et al.*(37). For hematological tumors like ALL, the criteria for SD, PR and CR were bone marrow blast cells >25%, 6-25% and < 5% respectively. CR with incomplete recovery (CRi) was defined as CR but without recovery of platelets to ≥ 100 × 10^9 / L or neutrophil counts to ≥ 10^9/L (36).

Table 2: Model parameters used in equations

	Parameter	Definition	Unit	Value (CV%)	Source
Preclinical Cellular Parameters	Ag	CD22 (antigen) concentration	nM	17.9$_{(Ramos)}$ 4.0$_{(RL)}$ 3.4$_{(REH)}$	Ramos/ REH: experimentally derived. RL from (27)
	k_{on}	Binding of antibody to CD22	1/nM/day,	43.2	Derived (20)
	k_{off}		1/day	6.48	(15)
	k_{int}	Internalization rate of bound antibody	1/day	199.6$_{(Ramos)}$ 199.6$_{(RL)}$ 199.6$_{(REH)}$	(38)
	k_{int}^{PL}	Internalization rate of free payload	1/day	9.66	Assumed same as MMAE
Preclinical Plasma PK Parameters	V_1	Volume of distribution in central compartment for ADC	L/kg	0.0478 (11)	Estimated from in-house mouse PK data
	V_2	Volume of distribution in peripheral compartment for ADC	L/kg	0.0214 (16)	
	CL	Plasma clearance of ADC	L/day/kg	0.039 (16)	
	CLD	Distribution clearance of ADC	L/day/kg	0.024 (-)	
	k_a	Absorption rate of ADC into central compartment	1/day	5.8 (37)	
	$V_{PL,1}$	Volume of distribution in central compartment for payload	L/kg	4.74	Extrapolated from in-house data
	$V_{PL,2}$	Volume of distribution in peripheral compartment for payload	L/kg	37.4	
	CL_{PL}	Plasma clearance of payload	L/day/kg	53.9	
	CLD_{PL}	Distribution clearance of payload	L/day/kg	31.8	
	k_{dis}	Dissociation rate of payload from ADC	1/day	0.24 (12)	Estimated from in-house data
	DAR	Drug-to-Antibody ratio	Unitless	3.5	Measured
Tumor Penetration Parameters	P_{ADC}, P_{PL}	Permeability of ADC and payload into tumor	µm/day	334, 18144	(22)
	D_{ADC}, D_{PL}	Diffusivity of ADC and payload into tumor	cm^2/day	0.022 0.125	(22)
	ϵ, ϵ_{PL}	Void fraction in tumor for ADC and payload	Unitless	0.24 0.44	(22)
	R_{cap}	Capillary radius	µm	8	(22)
	R_{krogh}	Average distance between 2 capillaries	µm	75	(22)
	R_{tumor}	Tumor radius	cm	Calculated	Assume spherical tumor

Preclinical PD Parameters	k_{g0}	Exponential tumor growth rate	1/day	0.08 (37)(REH) 0.122 (9)(RL) 0.211(16)(Ramos)	Estimated
	k_g	Linear tumor growth rate	mm^3/day	225 (43)(REH) 220 (-)(RL) 274 (27)(Ramos)	Estimated
	ψ	Switch between exponential and linear growth phases	Unitless	20	Fixed based on (39)
	M_{max}	Maximum tumor volume	mm^3	5000 (-)(REH), 6120 (82)(RL), 6160 (45)(Ramos)	Estimated
	k_{out}^{PL}	Exocytosis rate of intracellular payload	1/day	1.1 (57)	Estimated across models
	DNA	Concentration of DNA target in cell	nM	196 (60)	Estimated across models
	k_{max}	Maximum killing rate constant	1/day	17.6 (57)(REH), 14.0 (59)(RL), 15.6 (63)(Ramos)	Estimated
	IC_{50}	Concentration of payload corresponding to a killing rate constant of half maximum value	nM	399 (15)(REH), 237 (9)(RL), 227 (8)(Ramos)	Estimated
	γ	Hill coefficient of tumor killing function	Unitless	1	Fixed
	τ	Transduction time between tumor compartments	day	1.21 (14)(REH), 4.06 (52)(RL), 3.11 (75)(Ramos)	Estimated
Clinical PK Parameters	V_1	Volume of distribution in central compartment for ADC	L/kg	0.058 (11)	Derived from (26)
	V_2	Volume of distribution in peripheral compartment for ADC	L/kg	0.0124 (56)	
	CL	Plasma clearance of ADC	L/day/kg	0.029 (9)	
	$CLD,$	Distribution clearance of ADC	L/ day/kg	0.071 (135)	
	$V_{PL,1}$	Volume of distribution in central compartment for payload	L/kg	5.54	Extrapolated from in-house data
	$V_{PL,2}$	Volume of distribution in peripheral compartment for payload	L/kg	8.48	
	CL_{PL}	Plasma clearance of payload	L/day/kg	19.8	
	CLD_{PL}	Distribution clearance of payload	L/day/kg	114	
	k_{dis}	Dissociation rate of payload from ADC	1/day	0.47 (31)	Estimated from in-house data

	Ag	CD22 (antigen) concentration	nM	4.0(NHL:FL) 4.0(NHL:DLBCL) 0.09(ALL)	(27) Experimentally derived
	k_{g0}	Exponential tumor growth rate	1/day	0.012(FL) 0.02-0.05(DLBCL) 0.347(ALL, fast) 0.173(ALL,med) 0.120(ALL,slow)	(27-30)
Clinical PD Parameters	k_g	Linear tumor growth rate	mm^3/day	13,397	(34)
	$w0$	Initial tumor volume*	mm^3	>64cm^3 (76) >500cm^3 (30)(DLBCL) 1995 (1e9 cells) (ALL)	(32,33)

Sensitivity Analysis

A local sensitivity analysis was performed using the NHL clinical model to determine sensitivity of outcome (ORR) to variation in key model parameters. The parameters chosen were: exponential tumor growth rate (k_{g0}), CD22 receptor expression (Ag), calicheamicin efflux out of tumor cells ($k_{out,PL}$) and inotuzumab ozogamicin plasma clearance (CL). Nominal parameter values were k_{g0} = 0.012 day^{-1}, Ag = 8000 receptors/cell, $k_{out,PL}$ = 1.1 day^{-1}, CL = 29 mL/kg and initial tumor volume of 100 cm^3. Each parameter value was varied 10 fold in the sensitivity analysis, and model simulations used to calculate ORR according to the method of Cheson, *et al.* (37).

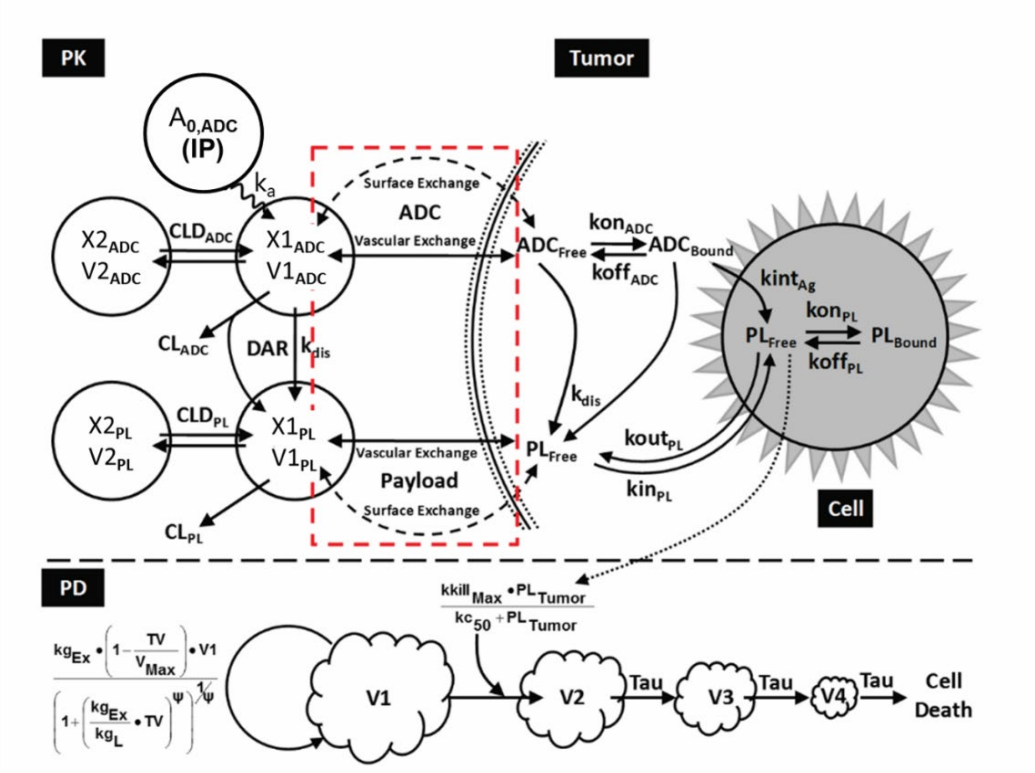

Figure 1: The PK/PD model for solid tumors (10). Note the model for liquid tumors (ALL) was approximated by eliminating transport to the solid tumor (shown in the red box). Please refer to the methods section and Tables 1 and 2 for detailed description of the symbols used in schematics.

5.4 Results

CD22 Receptor Expression and G544 Internalization

Anti-CD22 mAb (G544) binding capacity per cell was used as a measure of receptor number. G544 binding was saturable and minimal non-specific binding was observed for the cell lines tested. The receptor numbers for each cell line were determined from 3 separate independent experiments. On the Ramos NHL cell line there were 36,029 ± 5,004 CD22 receptors/cell, and on the ALL REH cells there were 5,037 ± 287 CD22 receptors/cell. These values were converted to nM for modeling purposes and are reported in Table 2. The internalization rate constant for G544 was found to be 199.6 day^{-1}, which corresponds to a half-life of internalization of 5 min (Table 2).

Mouse Pharmacokinetics

Determination of ADC PK Parameters

The plasma concentration-time profiles for inotuzumab ozogamicin obtained following single dose IP administration to non-tumor bearing mice at 20 μg calicheamicin/kg (0.27 mg/kg inotuzumab) and 160 μg calicheamicin/kg (3.2 mg/kg inotuzumab), or to tumor (RL) bearing mice at 160 μg calicheamicin/kg (3.2 mg /kg inotuzumab) are shown in Figure 2a. The data was dose proportional and concentrations were similar in both tumor bearing and non-tumor bearing mice. As a result, the data were pooled for parameter estimation. The estimated 2-compartment model parameters are provided in Table 2.

PK/PD Modeling of Mouse Xenograft Data

The characterization of mouse tumor growth inhibition data using the PK/PD model for Ramos, RL and REH bearing xenografts are shown in Figure 2b. The model was able to describe the observed data well and provided a set of PD parameters for preclinical to clinical translation of inotuzumab ozogamicin efficacy. Parameter estimates are provided in Table 2.

Determination of Calicheamicin PK Parameters

The pharmacokinetics of calicheamicin in mouse and human were obtained by allometric scaling of rat and dog data, available from in-house reports. The rat and dog PK parameters were estimated using a 2-compartment linear PK model. The calicheamicin mouse PK parameters were estimated by back extrapolation, and the human PK by forward extrapolation utilizing allometric principles (see Table 2 and Figure 3).

Clinical PK

A 2-compartmental linear PK model was used to characterize inotuzumab ozogamicin PK in clinical patients from Ogaru, *et al.* (26). The dissociation rate of calicheamicin in patients (k_{dis}) was determined by simultaneous fitting of the total Ab and ADC data, as described previously (*vide supra*). The estimated k_{dis} was 0.47 day^{-1} in patients. The estimated inotuzumab ozogamicin PK parameters utilized in the clinical trial simulations are presented in Table 2.

a.

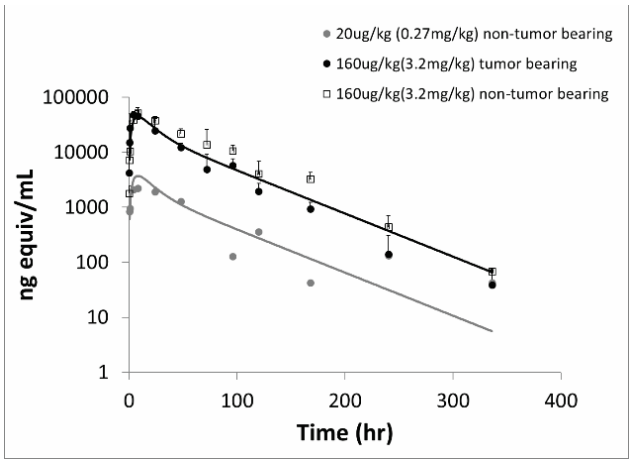

b.

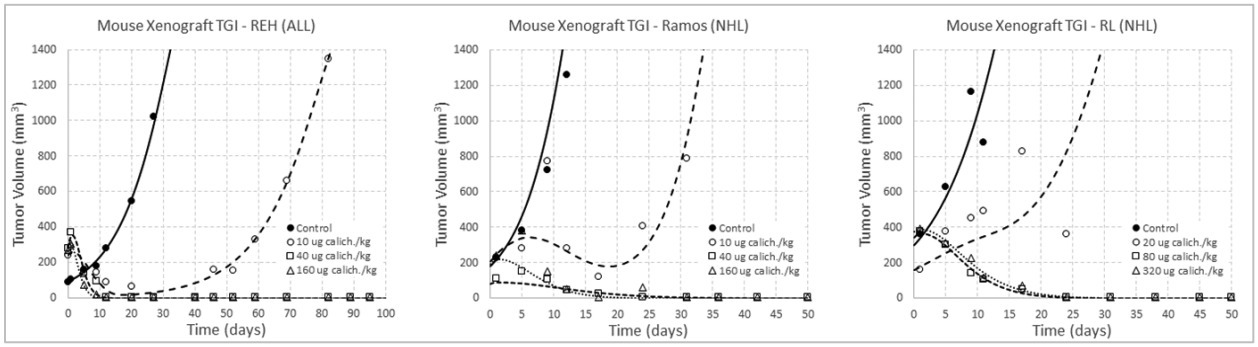

Figure 2a: Observed (*symbols*) and model fitted (*lines*) pharmacokinetics of inotuzumab ozogamicin in mouse plasma following single IP dose administration to non-tumor-bearing mice at 20 and 160 µg calicheamicin/kg (0.27 and 3.2 mg/kg inotuzumab, respectively) or to tumor (RL)-bearing mice at 160 µg calicheamicin/kg (3.2 mg/kg inotuzumab). **2b:** Observed (*symbols*) and model fitted (*lines*) tumor growth inhibition data in REH, Ramos and RL xenograft tumor-bearing mice following IP administration of inotuzumab Q4D × 3

Model Predictions of Tumor Calicheamicin Concentrations in NHL and ALL Cancer Patients

The model was used to simulate intracellular tumor calicheamicin concentrations in NHL (DLBCL) and ALL patient populations (see Figure 4). Following a single dose of inotuzumab ozogamicin at 1.8 mg/m^2, the concentrations of calicheamicin in the tumor were predicted to be significantly greater in ALL patients compared with NHL patients. This is consistent with greater diffusion/ accessibility of ADCs into liquid tumors (such as ALL) compared to solid tumors (such as NHL).

Use of the Model to Compare Tumor Volume Reductions in ALL Patients Following Different Dosing Regimens

The model was used to simulate reduction in tumor volume following different dosing regimens of inotuzumab ozogamicin. In Figure 5, four weekly administration of inotuzumab ozogamicin at 1.8 mg/m^2 and a weekly fractionated regimen of 0.8, 0.5 and 0.5 mg/m^2 are compared for ALL patients. The fractionated dosing regimen was predicted to be more efficacious than the Q4w regimen, sustaining tumor volume reduction for longer time periods.

Model Predictions of Clinical Outcome in NHL and ALL Cancer Patients

The model was used to simulate PFS times in NHL and ALL patient populations. The NHL clinical trial simulation was completed for FL and both slow and fast growing DLBCL patient populations using a regimen of inotuzumab ozogamicin given every 4 weeks, to mimic treatment in the Advani clinical trial (25). Figure 6 compares the model simulated and observed PFS data, which were found to correlate well. PFS rates were also predicted for ALL following a fractionated regimen (0.8, 0.5 and 0.5 mg/m^2 on days 1, 8 and 15 of a 28 day cycle), but could not be compared with clinical observations as studies are still under completion and PFS data is not available yet. However, the model predictions for complete response (CR) of 60-79% using two different growth rates for ALL, compare favorably with CR/CRi of 80.7% (72-88) demonstrated by inotuzumab ozogamicin in an ongoing phase 3 study in patients with ALL (40).

Sensitivity Analysis

Sensitivity of variation in exponential tumor growth rate (k_{g0}), CD22 receptor expression (Ag), calicheamicin efflux out of tumor cells ($k_{out,PL}$) and inotuzumab plasma clearance (CL) on inotuzumab ORR was examined in the NHL (FL) model. The plots in Figure 7 show how ORR varies over a dose range from 0 to 0.06mg/kg (2.16mg/m^2) with a 10- fold change in each parameter from its nominal value. The cross hairs on the plots represent the nominal case for Inotuzumab given at its recommended dose of 0.05mg/kg (1.8mg/m^2). The most sensitive parameter was tumor growth rate, followed by PL efflux and then Inotuzumab clearance. CD22 expression was the least sensitive parameter.

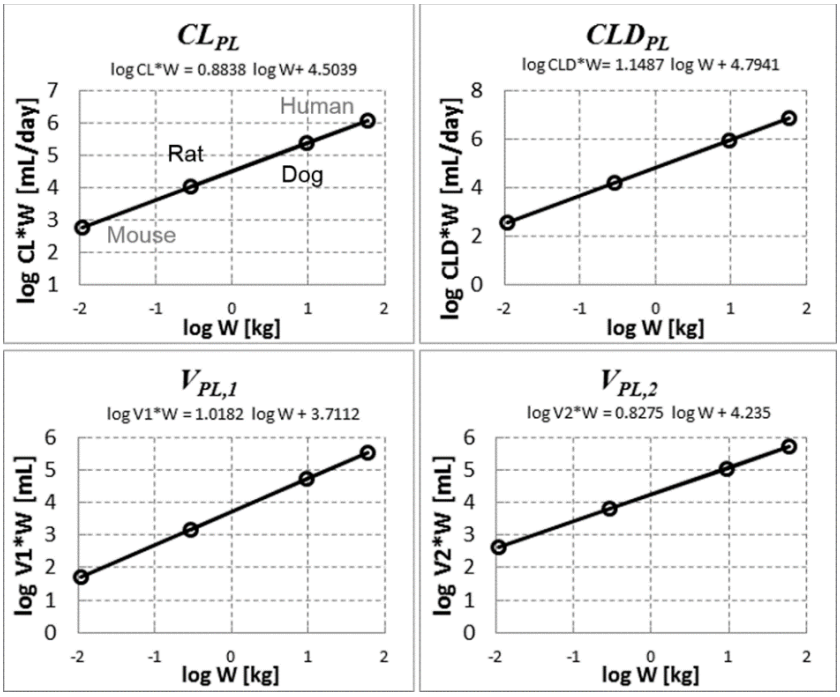

Figure 3: Allometric scaling of calicheamicin PK from rat and dog to human and mouse. In this context, *W* refers to body weight.

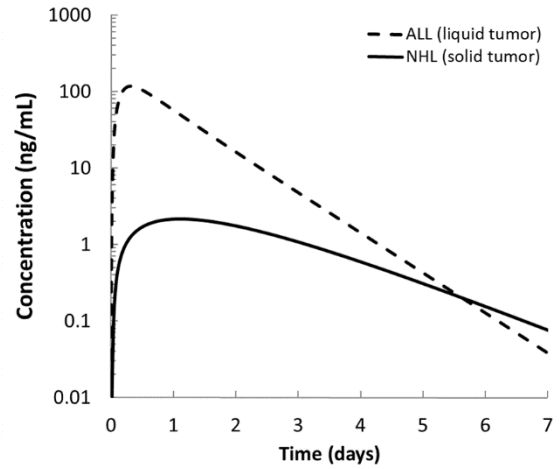

Figure 4: Model predicted intracellular calicheamicin PK for ALL (liquid tumor) and NHL (solid tumor).

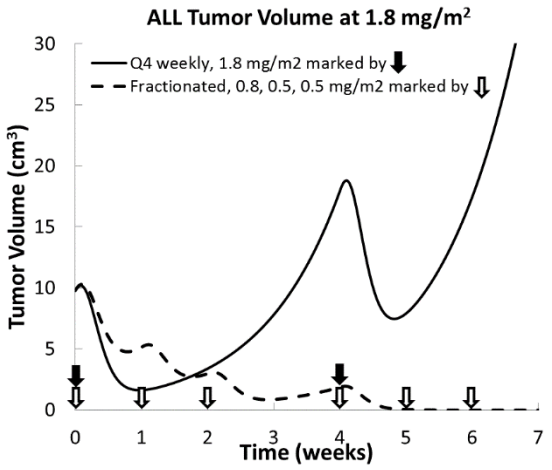

Figure 5: Simulated tumor volume profiles over time for a Q4 weekly dosing regimen and a fractionated Q1 weekly regimen for ALL patients receiving a total dose of inotuzumab ozogamicin of 1.8 mg/m^2

5.5 Discussion

Challenges in Predicting Clinical Efficacy of Anti-Cancer Agents from Preclinical Data

Prior knowledge of the expected efficacious dose of an oncology drug in the clinic is desirable for optimal design of clinical trials to ensure that an efficacious dose can be reached with acceptable toxicity profile. However, predicting efficacy of anti-cancer agents in the clinic remains a challenge. A problematic issue is that the preclinical tools used for identification of clinical drug candidates, such as mouse xenograft models, are thought to be poorly predictive of the clinical outcome (41-44). At a minimum, differences between preclinical and clinical drug exposures should be factored into clinical predictions. Indeed analyses by Rochetti *et al.* and Wong *et al.* showed that incorporation of human PK into xenograft data significantly improved quantitative prediction (43, 45).

ADCs offer an additional level of complexity, as they are composed of multiple entities including an antibody, linker, and payload, which could potentially be responsible for driving efficacy and toxicity (46). The accuracy of the exposure response characterization and translation to the clinic will depend upon the exposure endpoint chosen. Typically, the concentration of drug in the plasma or blood is the preferred exposure endpoint to correlate with efficacy, as it is both an easily accessible biological sample and for many small molecule drugs it correlates well with drug concentration at the site of action. However, for large molecules such as antibodies and ADCs, the concentration in the plasma does not represent concentration in the solid tumor due to a complex biodistribution mechanism. Optimal translation requires use of drug concentration in the tumor as the exposure endpoint to accurately determine the exposure response relationship. Measurement of drug in the tumor is a costly, labor intensive process which may not be feasible and presents another challenge. For ADCs, it is necessary to determine the concentration of the released payload following ADC administration, as this concentration is responsible for eliciting the pharmacological action.

Given the challenges of trying to predict efficacy using mouse xenografts, which are an imperfect representation of human tumors, and the complexity of determining the relevant exposure endpoint (tumor payload concentration), it is not surprising that predicting efficacy of ADCs in the clinic is problematic. When dealing with complex biological systems with multiple variables and pathways, it is advisable to build a mathematical model of the system, capable of integrating and interpreting preclinical data and providing a quantitative framework for translation to the clinic (9, 47).

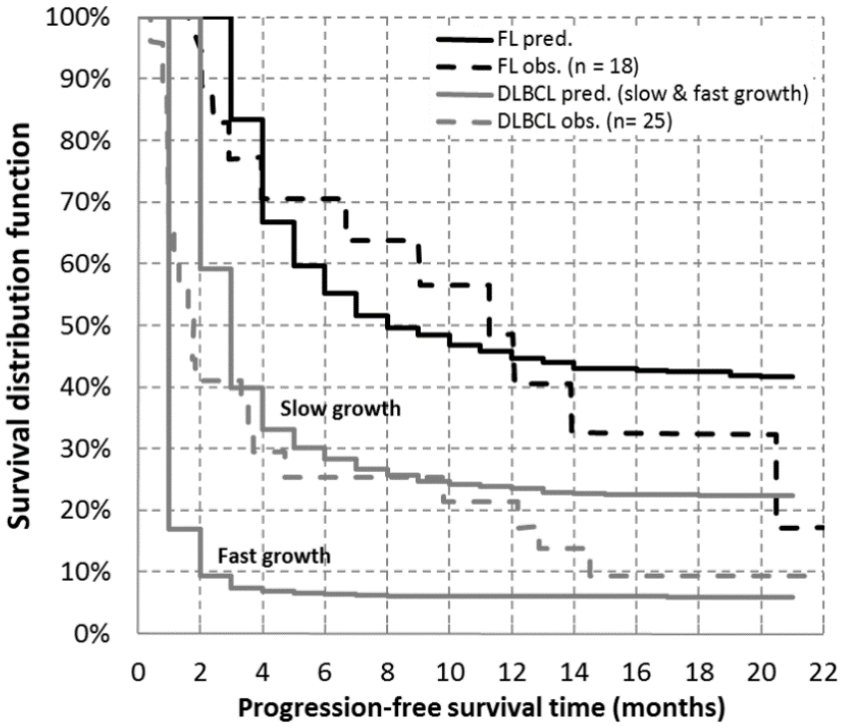

Figure 6: Model predicted PFS rates in NHL patients from Clinical Trial Simulations and Comparison with Clinical Trial Results. The solid lines represent model simulated PFS rates after dosing inotuzumab ozogamicin at 1.8 mg/m^2 every 4 weeks to NHL patients. The dashed lines represent observed PFS rates in patients administered the same dose and regimen in clinical trials. Note, clinical trial simulations were completed for FL and both slow and fast growing DLBCL patient populations, to be consistent with treatment in clinical trials.

Tumor Cell Processing of Inotuzumab ozogamicin

In this work, we have taken inotuzumab ozogamicin (CMC-544), which is an anti-CD22 ADC in the clinic for both solid tumor (NHL) and hematological malignancies (ALL) (48), and used a systems pharmacology modeling approach to investigate translation from pre-clinical data to the clinic. The model used was based on a mechanism-based, multiscale ADC PK/PD model proposed by Shah *et al.,* capable of integrating preclinical biomeasures and PK/PD data to predict clinical response (10). Shah and colleagues used this model for a 'bench to bedside' translation of brentuximab vedotin and demonstrated its ability to predict clinical responses for this ADC. In

the analysis herein, we applied the same type of approach for inotuzumab ozogamicin to gain quantitative insight into the mechanism of action of this ADC.

The modeling process starts with a rigorous understanding of the mechanism of action of inotuzumab ozogamicin at the cellular level to build a model which represents the disposition of the ADC and release of payload in the tumor cell. Once in the extracellular tumor environment, inotuzumab ozogamicin binds to its target CD22 on the surface of tumor cells and is rapidly internalized by receptor mediated endocytosis. The ADC is trafficked intracellularly from the endosomes to the lysosomes. The AcBut-hydrazone linker, which tethers the CD22 mAb to the payload calicheamicin, is acid labile and is cleaved in the lysosomes to release the payload. The liberated N-Ac-γ-calicheamicin DMH payload is subsequently released into the cytosol where it is reduced by glutathione to form the reactive diradical form. This activated form of calicheamicin distributes to the nucleus where it binds to the minor groove in DNA and causes double-strand breaks, resulting in cell death (48). Alternatively, the released payload form, N-Ac-γ-calicheamicin DMH, can also bind to P-glycoprotein (P-gp) prior to nuclear translocation and be effluxed from the cell (49).

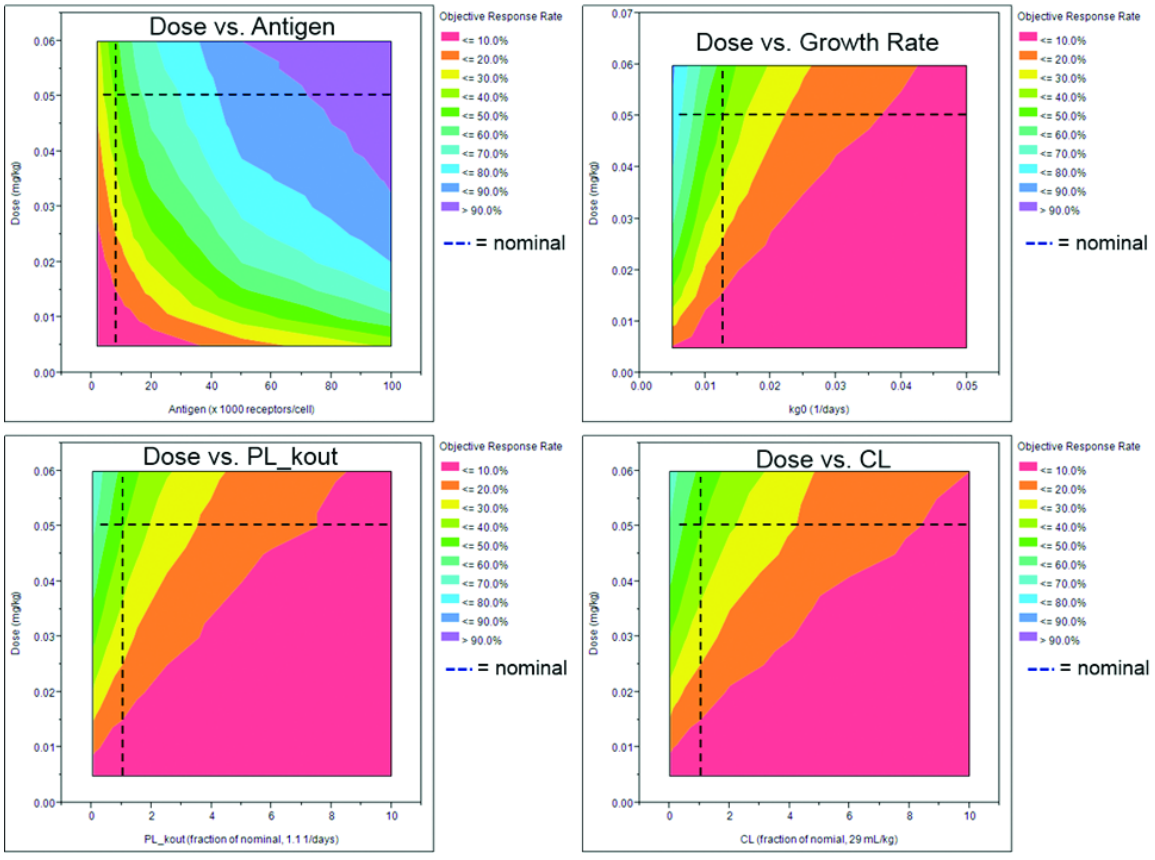

Figure 7: Local Parameter Sensitivity Analysis. Sensitivity of outcome (ORR) to variation in CD22 antigen concentration (*Ag*), exponential tumor growth rate (k_{g0}), calicheamicin efflux (*PL_kout*) and inotuzumab ozogamicin clearance (CL) was examined in the NHL (FL) model. Nominal parameter values were *Ag* = 8000 receptors/cell, k_{g0} = 0.012 day^{-1}, *PL_kout* = 1.1 day^{-1}, CL = 29 mL/kg and initial tumor volume of 100 cm^3. The cross hairs on the plots represent the nominal case for Inotuzumab given at its recommended dose of 0.05mg/kg (1.8mg/m^2).

In building the tumor cell component of the PK/PD model, the goal was to provide a quantitative description of the principal operative intracellular processes. The first step was to determine which parameters were available from the literature and which were considered important enough to warrant experimental work to inform the model. From previous analyses, key cellular parameters governing the success of an ADC include antibody affinity to its receptor, receptor expression levels and internalization rate into the tumor cell (13, 14, 50). Payload affinity for its target and efflux of payload out of the cell are also key parameters in establishing payload concentration and retention in the cell (10). For this analysis, binding affinity data for antibody to CD22 (15) and calicheamicin to DNA (21), were available from the literature and could be incorporated directly into the model. Internalization rates and CD22 receptor expression were not available for all relevant cell lines and were therefore determined in-house.

The parameter k_{out} describes the exocytosis rate of N-Ac-γ-calicheamicin DMH from the tumor cell, incorporating active processes such as efflux by P-glycoprotein (P-gp). This is important as **P-**gp is upregulated on many tumor cell types. Data to inform k_{out} was not available in the literature and a method was not available to determine this experimentally. Instead k_{out} was estimated within the model. The value of k_{out} estimated for calicheamicin in the model (1.1 day^{-1}; Table 2) was very similar to values used for monomethylauristatin E (MMAE; 0.68-1.1 day^{-1}) in a similar modeling application (10). This makes some sense, as calicheamicin and MMAE are ADC payloads which are both reported to be substrates for P-gp (49, 51). Experimental data would have been optimal to inform the k_{out} parameter for calicheamicin, but in absence of this data the estimated value is in line with a similar ADC payload.

Tumor Growth Inhibition in Mouse as a Function of Tumor Calicheamicin Concentrations

The next step was to combine the tumor cell component with a PK model describing the disposition/ elimination of ADC and payload in the plasma and distribution to the tumor cell. The plasma PK model structure describes distribution of inotuzumab ozogamicin into peripheral tissues, and ADC catabolism and de-conjugation to release payload into the systemic circulation. The entire payload released systemically from the hydrolysis of the acid-labile hydrazone linker was assumed to be N-Ac-γ-calicheamicin DMH. It is possible that metabolites are also formed which were not specified in the model. However, since the unconjugated calicheamicin PK assay used a non-specific ELISA method, it may well detect some of these calicheamicin metabolites. The model also accounts for distribution and clearance of the payload. Important data to characterize this part of the model included inotuzumab ozogamicin PK in mouse (total antibody and ADC) and calicheamicin PK. The plasma concentrations of ADC and payload were characterized using a simple two compartmental model. This step also enabled estimation of the rate of dissociation of payload from the ADC (k_{dis}), providing an estimate of the drug to antibody ratio (DAR) for ADCs that would internalize into cancer cells.

The solid tumor penetration part of the model was incorporated using drug exchange parameters from the literature (10, 22, 52, 53). The model assumes that diffusion is the predominant pathway of ADC passage into the tumor, as the high interstitial pressure within the tumor and absence of lymphatics means that convection is absent or minimal. The drug exchange parameters account for the size of the molecule being exchanged, the vascular permeability, tissue diffusion rates and accessible tissue volume corresponding to that size. The model includes diffusion from the

periphery of the tumor which is predominant when the tumors are small and avascular. As the tumor becomes larger, diffusion from the vasculature takes over as the dominant pathway (10, 22, 52, 53). Once the ADC is in the tumor interstitium, the cellular model is used to describe binding to the target and intracellular processing and binding.

The advantage of using a physiological relevant PK model for inotuzumab ozogamicin was that it enabled prediction of tumor calicheamicin concentrations, which are a more appropriate exposure endpoint to link to tumor regression/efficacy. The efficacy of inotuzumab ozogamicin was studied in 3 different xenograft bearing mouse models: Ramos (Burkitts lymphoma), RL (NHL) and REH (ALL) (15, 16). The mechanism-based tumor disposition model was combined with a pharmacodynamic model of tumor growth and cell kill (12), in which tumor payload concentrations were used to drive efficacy. The model features a dynamic interaction between tumor distribution parameters and tumor size, where changes in tumor volume are directly able to influence the concentration of payload in the tumor, which in turn is responsible for the size of the tumor. As shown in Fig. 2b, the PK/PD model was able to provide a good fit to the observed inotuzumab ozogamicin preclinical TGI data, providing estimates of the efficacy parameters and the inter-individual variability associated with them.

Translation to the Clinic

Once the preclinical PK/PD relationship describing tumor growth inhibition as a function of tumor calicheamicin concentration had been characterized, the next step was to translate this model to the clinic to predict inotuzumab ozogamicin efficacy in patients. The overall model structure was kept the same, with the exception that mouse system parameters such as initial tumor size, tumor growth rates and receptor expression were replaced with clinically relevant parameters, to make the model representative of the human system. In addition, inotuzumab ozogamicin and calicheamicin clinical PK were incorporated into the model. To accomplish this, a two compartment linear PK model was used to fit the Phase 1 clinical PK data for inotuzumab ozogamicin (26). Clinical PK for calicheamicin was allometrically scaled from rat and dog (Figure 3). The rate of dissociation of payload from the ADC (k_{dis}) was determined in clinical data by simultaneous fitting of the total mAb and ADC data. Since the parameters describing the tumor disposition are clinically translatable, they were kept the same (10). In addition, drug specific parameters including binding parameters for ADC and calicheamicin to their targets, internalization rate, exocytosis rate of intracellular payload (k_{outPL}), IC_{50}, kill rate (k_{max}) and transduction time between tumor compartments (τ) were not changed. Most importantly, systems parameters were changed to match literature estimates for NHL and ALL patients. For example, initial tumor volumes for NHL and ALL were taken from the literature (28, 29). Tumor growth rates and CD22 receptor expression for low grade NHL (FL), refractory aggressive NHL (DLBCL) and ALL were all used in clinical simulations (27, 30-34).

This 'switching' of systems parameters from murine values to relevant clinical values for the disease population gives this method for translating efficacy a greater level of relevance and fidelity compared to previous translational approaches which account for exposure differences only (43, 45). Following translation of the PK/PD model to the clinic, the model was used to perform clinical trial simulations.

Simulations of Tumor Calicheamicin Concentrations

In the first simulations, tumor concentrations of calicheamicin in NHL (DLBCL) and ALL patient populations were compared following equivalent doses of inotuzumab ozogamicin (1.8mg/m^2 Q4w) to each group. The PK model for NHL (DLBCL) differed from the ALL model in terms of the tumor penetration parameters. NHL is considered to be a malignant solid tumor of the immune system which can arise from undifferentiated lymphoid cells in virtually any part of the body. Drug exchange parameters for solid tumors are therefore required to describe penetration of inotuzumab ozogamicin into the NHL tumor types. In contrast, ALL is a hematopoietic or 'liquid' tumor which arises in the bone marrow. These tumors have less of a barrier to diffusion compared with solid tumors. As a result, the PK/PD model was simplified by elimination of the drug exchange tumor penetration parameters, and equilibrium was assumed between ADC concentration in plasma and tumor interstitium. The manifestation of the difference in the tumor model between a liquid tumor (such as ALL) and a solid tumor (such as DLBCL) is shown in Figure 4. Following the same dose of inotuzumab ozogamicin, the ALL tumor calicheamicin concentrations are predicted to be approximately 2 orders of magnitude higher than the DLBCL tumor calicheamicin concentrations. This simulation suggests that liquid tumors such as ALL will be easier to treat, requiring lower doses than solid tumors. This simulation agrees with the observation that solid tumors are often difficult for drugs to penetrate (54).

Simulations of Optimal Dosing Regimens for ALL

The model was also used to simulate different dosing regimens for treating ALL. The first regimen selected was 1.8mg/m^2 Q4w, which had been investigated in clinical trials for inotuzumab ozogamicin in the treatment of NHL (25). The second regimen was a fractionated schedule of 3 weekly doses over a 4-week treatment cycle, with doses of 0.8, 0.5, and 0.5mg/m^2 on days 1, 8 and 15 respectively. This regimen is under investigation in clinical trials for the treatment of ALL (40). Both regimens had the same total dose of 1.8mg/m^2 per monthly cycle. Individual subject tumor volume plots over time are shown in Figure 5 (with the subject chosen having median rate of clearance of inotuzumab ozogamicin). In the ALL simulations, the fractionated dosing regimen was predicted to be more tumor regressive than the Q4 weekly regimen. Although Q4 weekly dosing results in higher tumor suppression at each dose, this is offset by considerable tumor re-growth. In contrast, the fractionated dosing results in a more constant suppression over the dosing period. This analysis demonstrates that prediction of optimal dosing regimen is dependent on integration of all parameters and is therefore a worthy application of this type of mechanistic model.

Prediction of Progression Free Survival Rates

For each simulated clinical trial, PFS rates were calculated (Figure 6). For the NHL trial, PFS predictions could be compared with clinical trial data for inotuzumab ozogamicin (25). For both FL and DLBCL, the model predicted PFS and observed data from clinical trial compared well. Interestingly, large drops in PFS were observed at the longest survival times in the clinical trial, which may have been due to the small 'n' number by this stage of the analysis. In contrast, the model predicts a more logical flattening of PFS at the longer survival times.

Sensitivity Analysis

The final application of the model in this analysis was to perform a local sensitivity analysis to give insight into the most important parameters defining, or even limiting, efficacy of inotuzumab ozogamicin versus NHL. CD22 receptor expression, calicheamicin efflux rate, inotuzumab ozogamicin PK (clearance rate) and tumor growth rate were selected as interesting parameters to vary in the model. The impact of varying these parameters over orders of magnitude from their nominal values, at a range of inotuzumab ozogamicin doses, is shown in Figure 7. At the recommended dose of 1.8 mg/m^2 (0.05 mg/kg) the least sensitive parameter was CD22 receptor expression, indicating that for inotuzumab ozogamicin this is least limiting for efficacy and probably reflects the optimal characteristics of this receptor as an ADC target, due to its high expression across B-cell types and rapid internalization (and recycling rates). Calicheamicin efflux from the tumor cell was a more sensitive parameter, indicating the impact of this parameter on intracellular payload concentrations and resultant efficacy. This is important, as N-Ac-γ-calicheamicin DMH is known to be a substrate for P-glycoprotein (P-gp), an efflux transporter which is upregulated on many tumor cell types (49). A further development of the model would be to include P-gp expression across cell lines or patients to investigate its relationship with efflux. Data was not available to support this in the current version of the model; however, this refinement would enable assessment of MDR1 as a quantitative diagnostic of efficacy.

Clearance was also a sensitive parameter for inotuzumab ozogamicin. Compared to more recent ADCs, inotuzumab ozogamicin has a faster rate of clearance, likely due to the contribution of CD22 receptor-mediated clearance as an additional CL mechanism, supplemental to the usual mechanisms of ADC catabolism and de-conjugation. As can be seen from the sensitivity plots, high clearance values of inotuzumab ozogamicin have a substantial impact on efficacy. However, the most sensitive parameter was rate of tumor growth in the model, indicating that even at nominal clearance and efflux values, the most aggressive, refractory tumors require higher doses for treatment of NHL.

5.6 Conclusions

In summary, a mechanism-based PK/PD model has been used for preclinical to clinical translation of inotuzumab ozogamicin. The model was able to predict PFS responses for inotuzumab versus NHL that were comparable to observed clinical trial results, demonstrating its utility for predicting efficacy of ADCs. The model was also able to give useful mechanistic insight into optimal dosing regimens and sensitive parameters impacting outcome, including tumor growth rate, inotuzumab ozogamicin clearance and calicheamicin efflux. This knowledge could be applied to optimize the design of ADCs in the discovery phase of research, and/or for selection of predictive diagnostics in the clinic.

References

1. Webb, S. Pharma interest surges in antibody drug conjugates. *Nature biotechnology* **29**, 297-8 (2011).
2. Zolot, R.S., Basu, S. & Million, R.P. Antibody-drug conjugates. *Nature reviews Drug discovery* **12**, 259-60 (2013).

3. Sohayla Rostami, I.Q., Robert Sikorski. *The Clinical Landscape of Antibody-drug Conjugates*. (2014).
4. Mack, F., Ritchie, M. & Sapra, P. The next generation of antibody drug conjugates. *Seminars in oncology* **41**, 637-52 (2014).
5. *ImmunoGen, Inc. Announces Discontinuation of IMGN901 Study in Small-Cell Lung Cancer (SCLC)*. (2013).
6. Williams, R. Discontinued in 2013: oncology drugs. *Expert opinion on investigational drugs* **24**, 95-110 (2015).
7. Panowksi, S., Bhakta, S., Raab, H., Polakis, P. & Junutula, J.R. Site-specific antibody drug conjugates for cancer therapy. *mAbs* **6**, 34-45 (2014).
8. Maderna, A. *et al.* Discovery of cytotoxic dolastatin 10 analogues with N-terminal modifications. *Journal of medicinal chemistry* **57**, 10527-43 (2014).
9. Agoram, B.M., Martin, S.W. & van der Graaf, P.H. The role of mechanism-based pharmacokinetic-pharmacodynamic (PK-PD) modelling in translational research of biologics. *Drug Discov Today* **12**, 1018-24 (2007).
10. Shah, D.K., Haddish-Berhane, N. & Betts, A. Bench to bedside translation of antibody drug conjugates using a multiscale mechanistic PK/PD model: a case study with brentuximab-vedotin. *Journal of pharmacokinetics and pharmacodynamics* **39**, 643-59 (2012).
11. Jumbe, N.L. *et al.* Modeling the efficacy of trastuzumab-DM1, an antibody drug conjugate, in mice. *Journal of pharmacokinetics and pharmacodynamics* **37**, 221-42 (2010).
12. Haddish-Berhane, N. *et al.* On translation of antibody drug conjugates efficacy from mouse experimental tumors to the clinic: a PK/PD approach. *Journal of pharmacokinetics and pharmacodynamics* **40**, 557-71 (2013).
13. Sadekar, S., Figueroa, I. & Tabrizi, M. Antibody Drug Conjugates: Application of Quantitative Pharmacology in Modality Design and Target Selection. *The AAPS journal* **17**, 828-36 (2015).
14. Shah, D.K. *et al.* A priori prediction of tumor payload concentrations: preclinical case study with an auristatin-based anti-5T4 antibody-drug conjugate. *The AAPS journal* **16**, 452-63 (2014).
15. DiJoseph, J.F. *et al.* Antibody-targeted chemotherapy with CMC-544: a CD22-targeted immunoconjugate of calicheamicin for the treatment of B-lymphoid malignancies. *Blood* **103**, 1807-14 (2004).
16. Dijoseph, J.F., Dougher, M.M., Armellino, D.C., Evans, D.Y. & Damle, N.K. Therapeutic potential of CD22-specific antibody-targeted chemotherapy using inotuzumab ozogamicin (CMC-544) for the treatment of acute lymphoblastic leukemia. *Leukemia* **21**, 2240-5 (2007).
17. *Pfizer Discontinues Phase 3 Study of Inotuzumab Ozogamicin in Relapsed or Refractory Aggressive Non-Hodgkin Lymphoma (NHL) Due to Futility* (2013). Accessed May 20th 2013.
18. Wang, L., Abbasi, F., Gaigalas, A.K., Hoffman, R.A., Flagler, D. & Marti, G.E. Discrepancy in measuring CD4 expression on T-lymphocytes using fluorescein conjugates in comparison with unimolar CD4-phycoerythrin conjugates. *Cytometry Part B, Clinical cytometry* **72**, 442-9 (2007).
19. Sherree Friend, T.G., Brian Hall, Vidya Venkatachalam, Philip Morrissey. *Intracellular localization and trafficking using the ImageStream® imaging flow cytometer*.
20. Poulsen, T.R., Jensen, A., Haurum, J.S. & Andersen, P.S. Limits for antibody affinity maturation andrepertoire diversification in hypervaccinated humans. *Journal of immunology* **187**, 4229-35 (2011).
21. Tianhu Li, Z.Z., Virginia A. Estevez, Kai U. Baldenius, K. C. Nicolaou, and Gerald F. Joyce. Carbohydrate-Minor Groove Interactions in the Binding of Calicheamicin γ1 to Duplex DNA. *J Am Chem Soc* **116**, 3709-15 (1994).
22. Schmidt, M.M. & Wittrup, K.D. A modeling analysis of the effects of molecular size and binding affinity on tumor targeting. *Molecular cancer therapeutics* **8**, 2861-71 (2009).

23. Thurber, G.M., Schmidt, M.M. & Wittrup, K.D. Antibody tumor penetration: transport opposed by systemic and antigen-mediated clearance. *Adv Drug Deliv Rev* **60**, 1421-34 (2008).
24. Thurber, G.M., Schmidt, M.M. & Wittrup, K.D. Factors determining antibody distribution in tumors. *Trends in pharmacological sciences* **29**, 57-61 (2008).
25. Advani, A. *et al.* Safety, pharmacokinetics, and preliminary clinical activity of inotuzumab ozogamicin, a novel immunoconjugate for the treatment of B-cell non-Hodgkin's lymphoma: results of a phase I study. *Journal of clinical oncology : official journal of the American Society of Clinical Oncology* **28**, 2085-93 (2010).
26. Ogura, M. *et al.* Phase I study of inotuzumab ozogamicin (CMC-544) in Japanese patients with follicular lymphoma pretreated with rituximab-based therapy. *Cancer science* **101**, 1840-5 (2010).
27. Polson, A.G. *et al.* Anti-CD22-MCC-DM1: an antibody-drug conjugate with a stable linker for the treatment of non-Hodgkin's lymphoma. *Leukemia* **24**, 1566-73 (2010).
28. Armitage, J.O. & Weisenburger, D.D. New approach to classifying non-Hodgkin's lymphomas: clinical features of the major histologic subtypes. Non-Hodgkin's Lymphoma Classification Project. *Journal of clinical oncology : official journal of the American Society of Clinical Oncology* **16**, 2780-95 (1998).
29. Skipper, H.E. & Perry, S. Kinetics of normal and leukemic leukocyte populations and relevance to chemotherapy. *Cancer research* **30**, 1883-97 (1970).
30. Brons, P.P. *et al.* Cell cycle kinetics in malignant lymphoma studied with in vivo iododeoxyuridine administration, nuclear Ki-67 staining, and flow cytometry. *Blood* **80**, 2336-43 (1992).
31. Frei, E., 3rd & Freireich, E.J. Progress and perspectives in the chemotherapy of acute leukemia. *Advances in chemotherapy* **2**, 269-98 (1965).
32. 0Holland, J.F. Clinical Studies of Unmaintained Remissions in Acute Lymphocytic Leukemia. In: *The Proliferation and Spreadof Neoplastic Cells* pp. 453-62. (The Williams& WilkinsCo, Baltimore, TheUniversity of Texas M. D. Anderson Hospital and Tumor Institute at Houston, 1968).
33. Tolo Diebkile, A. *et al.* Characteristics and Results of the Management of Diffuse Large B-Cell Lymphomas: The Experience of Cote d'Ivoire. *Advances in hematology* **2012**, 945138 (2012).
34. Gregory, W.M., Richards, M.A., Slevin, M.L. & Souhami, R.L. A mathematical model relating response durations to amount of subclinical resistant disease. *Cancer research* **51**, 1210-6 (1991).
35. Zhao, Y., Kosorok, M.R. & Zeng, D. Reinforcement learning design for cancer clinical trials. *Statistics in medicine* **28**, 3294-315 (2009).
36. Kantarjian, H. *et al.* Results of inotuzumab ozogamicin, a CD22 monoclonal antibody, in refractory and relapsed acute lymphocytic leukemia. *Cancer* **119**, 2728-36 (2013).
37. Cheson, B.D. *et al.* Revised response criteria for malignant lymphoma. *Journal of clinical oncology : official journal of the American Society of Clinical Oncology* **25**, 579-86 (2007).
38. Carnahan, J. *et al.* Epratuzumab, a humanized monoclonal antibody targeting CD22: characterization of in vitro properties. *Clinical cancer research : an official journal of the American Association for Cancer Research* **9**, 3982S-90S (2003).
39. Simeoni, M. *et al.* Predictive pharmacokinetic-pharmacodynamic modeling of tumor growth kinetics in xenograft models after administration of anticancer agents. *Cancer research* **64**, 1094-101 (2004).
40. Daniel J. DeAngelo, M.S., Giovanni Martinelli, Hagop Kantarjian, Michaela Liedtke, Wendy Stock, & Nicola Goekbuget, K.W., Luisa Pacagnella, Barbara Sleight, Erik Vandendries, Anjali S. Advani. EFFICACY AND SAFETY OF INOTUZUMAB OZOGAMICIN (INO) VS STANDARD OF CARE (SOC) IN SALVAGE 1 OR 2 PATIENTS WITH ACUTE LYMPHOBLASTIC LEUKEMIA (ALL): AN ONGOING GLOBAL PHASE 3 STUDY. In European Hematology Association.
41. Peterson, J.K. & Houghton, P.J. Integrating pharmacology and in vivo cancer models in preclinical and clinical drug development. *European journal of cancer* **40**, 837-44 (2004).

42. Kelland, L.R. Of mice and men: values and liabilities of the athymic nude mouse model in anticancer drug development. *European journal of cancer* **40**, 827-36 (2004).
43. Wong, H. *et al.* Antitumor activity of targeted and cytotoxic agents in murine subcutaneous tumor models correlates with clinical response. *Clinical cancer research : an official journal of the American Association for Cancer Research* **18**, 3846-55 (2012).
44. Kamb, A. What's wrong with our cancer models? *Nature reviews Drug discovery* **4**, 161-5 (2005).
45. Rocchetti, M., Simeoni, M., Pesenti, E., De Nicolao, G. & Poggesi, I. Predicting the active doses in humans from animal studies: a novel approach in oncology. *European journal of cancer* **43**, 1862-8 (2007).
46. Ducry, L. & Stump, B. Antibody-drug conjugates: linking cytotoxic payloads to monoclonal antibodies. *Bioconjugate chemistry* **21**, 5-13 (2010).
47. Agoram, B.M. & Demin, O. Integration not isolation: arguing the case for quantitative and systems pharmacology in drug discovery and development. *Drug Discov Today* **16**, 1031-6 (2011).
48. Shor, B., Gerber, H.P. & Sapra, P. Preclinical and clinical development of inotuzumab-ozogamicin in hematological malignancies. *Molecular immunology* **67**, 107-16 (2015).
49. Takeshita, A. *et al.* CMC-544 (inotuzumab ozogamicin) shows less effect on multidrug resistant cells: analyses in cell lines and cells from patients with B-cell chronic lymphocytic leukaemia and lymphoma. *British journal of haematology* **146**, 34-43 (2009).
50. Shah, D.K., Barletta, F., Betts, A. & Hansel, S. Key bioanalytical measurements for antibody-drug conjugate development: PK/PD modelers' perspective. *Bioanalysis* **5**, 989-92 (2013).
51. Okeley, N.M. *et al.* Intracellular activation of SGN-35, a potent anti-CD30 antibody-drug conjugate. *Clinical cancer research : an official journal of the American Association for Cancer Research* **16**, 888-97 (2010).
52. Thurber, G.M. & Dane Wittrup, K. A mechanistic compartmental model for total antibody uptake in tumors. *Journal of theoretical biology* **314**, 57-68 (2012).
53. Thurber, G.M., Schmidt, M.M. & Wittrup, K.D. Antibody tumor penetration: Transport opposed by systemic and antigen-mediated clearance. *Advanced Drug Delivery Reviews* **60**, 1421-34 (2008).
54. Minchinton, A.I. & Tannock, I.F. Drug penetration in solid tumours. *Nature reviews Cancer* **6**, 583-92 (2006).

Section IV.
Modeling of bispecific antibodies

Chapter 6

A Translational Quantitative Systems Pharmacology Model for CD3 Bispecific Molecules: Application to Quantify T Cell-Mediated Tumor Cell Killing by P-Cadherin LP DART®

Alison Betts, Nahor Haddish-Berhane, Dhaval K. Shah, Piet H. van der Graaf, Frank Barletta, Lindsay King, Tracey Clark, Cris Kamperschroer, Adam Root, Andrea Hooper and Xiaoying Chen

The AAPS Journal 21(4):66 (2019)

6.1 Abstract

CD3 bispecific antibody constructs recruit cytolytic T-cells to kill tumor cells, offering a potent approach to treat cancer. T-cell activation is driven by the formation of a trimolecular complex (trimer) between drug, T-cells, and tumor cells, mimicking an immune synapse. A translational quantitative systems pharmacology (QSP) model is proposed for CD3 bispecific molecules capable of predicting trimer concentration and linking it to tumor cell killing. The model was used to quantify the pharmacokinetic (PK) /pharmacodynamic (PD) relationship of a CD3 bispecific targeting P-cadherin (PF-06671008). It describes disposition of PF-06671008 in the central compartment and tumor in mouse xenograft models, including binding to target and T-cells in the tumor to form the trimer. The model incorporates T-cell distribution to the tumor, proliferation, and contraction. PK/PD parameters were estimated for PF-06671008 and a tumor stasis concentration (TSC) was calculated as an estimate of minimum efficacious trimer concentration. TSC values ranged from 0.0092 to 0.064 pM across mouse tumor models. The model was translated to the clinic and used to predict the disposition of PF-06671008 in patients, including the impact of binding to soluble P-cadherin. The predicted terminal half-life of PF-06671008 in the clinic was approximately 1 day, and P-cadherin expression and number of T-cells in the tumor were shown to be sensitive parameters impacting clinical efficacy. A translational QSP model is presented for CD3 bispecific molecules, which integrates in silico, in vitro and in vivo data in a mechanistic framework, to quantify and predict efficacy across species.

6.2 Introduction

Immunotherapy, which recruits a patient's own immune system to kill cancer cells, has begun to revolutionize cancer treatment (1). Within the class of immune-oncology therapies are the bispecific immune cell re-targeting molecules (2). These are typically recombinant bispecific antibodies, or antibody fragments, with one binding domain targeting a specific tumor antigen of choice and the other domain targeting CD3 on T- cells. Because CD3 serves as the signaling component of the T-cell receptor (TCR) complex, these CD3 bispecific molecules enable T-cells to circumvent the need for the interaction between the TCR and antigen presented by major histocompatibility complex (MHC) class I molecules. This expands the repertoire of T-cells able to recognize the tumor and stimulate them to act as effector cells (3). Similar to the standard immune synapse formation, once a threshold of bispecific mediated molecular interactions has been reached, CD3 signals the T-cell to initiate a cytotoxic response toward the adjacent tumor cell expressing the specific antigen. Cytotoxicity is mediated by the release of cytotoxic granules containing perforin and granzymes by the T cell. Perforin is a pore-forming protein enabling entry of granzymes, and the granzymes trigger a caspase cascade that leads to apoptosis. Activation of T-cells leads to transient release of cytokines and T-cell proliferation, recruitment, and infiltration into the tumor environment, which drives serial killing of tumor cells.

In 2014, blinatumomab (CD3-CD19) was the first CD3 bispecific construct approved in the US for the treatment of resistant/ refractory B-cell acute lymphocytic leukemia (B-ALL) (4).

Blinatumomab is also being investigated in a Phase 2 clinical trial in patients with resistant/ refractory non-Hodgkin's lymphoma (NHL) (5). The first generation bispecific T-cell retargeting molecules such as blinatumomab are tandemly linked single-chain Fv (scFv) known as bi-specific T-cell engager (BiTE) molecules (2, 3). These molecules are around 50kDa and have a short circulating half-life (approx. 2 hour) requiring constant infusion through the use of a pump to achieve a stable therapeutic exposure of the molecule (6). New generation CD3 bispecifics with a variety of formats are being tested in clinical trials. These include PF-06671008 which is a P-cadherin-specific LP DART: a molecule based on the DART® platform, but containing a human IgG1 Fc domain to extend the half-life (7). This bispecific targets CD3 and P-cadherin expressed on solid tumors. P-cadherin is a member of a family of molecules that mediate calcium dependent cell-cell adhesion and has been reported to correlate with increased tumor cell motility and invasiveness when over-expressed (8-10). Upregulation of P-cadherin has been reported in breast, gastric, endometrial, colorectal and pancreatic carcinomas and correlates with poor survival of breast cancer patients (11-14). In contrast, P-cadherin has low expression in normal tissues, making it an attractive target for immunotherapy (12). In preclinical studies, in vitro and in vivo data indicate that PF-06671008 is a highly potent molecule eliciting P-cadherin expression dependent cytotoxic T-cell activity across a range of tumor indications (15). In addition, PF-06671008 is stable and has desirable biophysical and PK properties with a half-life of 3.7- 6 days in mouse (7, 15). PF-06671008 is currently being investigated in Phase 1 clinical trials in patients with advanced solid tumors with the potential to have P-cadherin expression (https://clinicaltrials.gov/ct2/show/NCT02659631).

In order to characterize the in vivo efficacy of PF-06671008 in tumor bearing mice, a quantitative systems pharmacology (QSP) model was established. This model integrates the PK of PF-06671008, its binding to shed P-cadherin and circulating T-cells in the systemic circulation, its biodisposition in the tumor and the formation of a trimolecular complex (trimer) with T-cells and P-cadherin expressing tumor cells in the tumor microenvironment (TME). The model incorporates T-cell kinetics in the tumor including T-cell proliferation and contraction. The concentration of the trimer in the tumor is used to drive efficacy in mouse using an optimized transduction model of tumor cell growth and killing. In this manuscript, we discuss the use of the model to characterize the underlying pharmacology in mouse, and translation of the preclinical efficacy data to the clinic by incorporation of predicted human PK and disease parameters. The quantitative translational framework for CD3 bispecific molecules presented here can aid in drug design, candidate selection and clinical dosing regimen projection.

6.3 Materials and Methods

In vivo studies

All procedures in animals were approved by the Pfizer Institutional Animal Care and Use Committees and studies were performed according to established guidelines.

PF-06671008 mouse PK study

PF-06671008 was administered as a single intravenous (IV) dose of 0.05 or 0.5 mg/kg to HCT-116 tumor-bearing female NOD-scid IL-2rg^{null} (NSG) mice, (n=3/ time point /dose) with or without human peripheral blood mononuclear cell (PBMC) engraftment. Mice were injected with 5x10^6 HCT-116 cells in matrigel subcutaneously in the dorsal left flank. When the tumors had grown to approximately 0.5 g in size (after 14 days), the mice were administered PF-06671008. Serum and tumor samples were collected at predetermined time points from 5 minutes (min) to 240 hours (h) post dose.

ELISA assay to quantify PF-06671008

PF-06671008 concentrations in mouse serum and tumor homogenate were determined using an enzyme-linked immunosorbant assay (96-well format) with colorimetric detection. Briefly, the capture protein was a polyclonal goat antibody recognizing the CD3 scFv domain and the detection antibody was a goat anti-human IgG-Biotin (Qualex), followed by HRP-Streptavidin conjugate (Jackson ImmunoResearch, West Grove, PA). Optical density was measured on a spectrophotometer (Molecular Devices). The lower limit of quantitation (LLOQ) of the assay was 12.5 ng/mL for serum samples, and 1.5 ng/mL for tumor samples. The minimal required dilution was 1:25 for serum and 1:6 for tumor.

Flow cytometric tumor infiltrating lymphocyte (TIL) analysis

HCT-116 tumor-bearing mice (n=3) engrafted with human PBMC and administered a single IV dose of 0.01, 0.05, or 0.5 mg/kg PF-06671008 were euthanized pre-dose and 24, 72 and 144 h following dosing to assess tumor infiltrating human CD3+ lymphocytes. Tumor samples were collected into gentleMACS C tubes containing human tumor cell dissociation buffer (Miltenyi Biotech) and processed to single cell suspensions using the manufacturer's suggested protocol for soft human tumors using the gentleMACS tissue dissociator (Miltenyi Biotech). After subsequent washing steps and live cell counting (using a hemocytometer and trypan blue exclusion), 1x10^6 live cells from each sample were collected and stained with CD3 FITC (BD Pharmingen) for 30 min on ice. Samples were analyzed using LSRII with FACS Diva software (BD Pharmingen). Absolute numbers of CD3+ T-cells per gram of tumor were then calculated using the number of CD3+ events and sample tumor weight.

PF-06671008 mouse xenograft studies

Mouse xenograft studies were completed in human T-cell engrafted (HCT-116) or adoptive transfer (HCT-116 or SUM-149) established tumor models. In the human T-cell engrafted model, tumor cells (5x10^6 HCT-116) were implanted subcutaneously (SC) into the right flank of 6-8 week old female NSG mice as a 0.2mL bolus mixed with 4 mg/mL Cultrex basement membrane extract (Trevigen) in PBS. Seven days prior to randomization, mice were inoculated with 5x10^6 or 2.5x10^6 freshly isolated human PBMC as an intraperitoneal injection of 0.2mL cell suspension in PBS. In addition to vehicle (PBS), dose levels of 0.01, 0.05, 0.1, 0.15, and 0.5 mg/kg PF-06671008 were

administered for HCT-116 studies (n= 10 /dose). The doses were administered IV as a q7d x 2 regimen.

For the T-cell adoptive transfer established tumor model, 8- to 10-week old NSG mice were inoculated with either $5x10^6$ HCT-116 cells in the flank or $5x10^6$ SUM-149 cells in the mammary fat pad in a total injection volume of 0.2mL, seven days prior to randomization. HCT-116 cells were suspended in PBS, while SUM-149 cells were suspended in growth media and mixed 1:1 with Matrigel Basement Membrane Matrix (BD Biosciences, San Jose, CA). T-cells, which had been isolated from PBMCs, were activated and expanded using Dynabeads Human T-Expander CD3/CD28 magnetic beads (Life Technologies) for 6-9 days, depending on the study, were harvested and re-suspended in PBS at $1x10^7$ cells/ ml for in vivo inoculation. An initial dose of PF-06671008 or vehicle was administered to mice on day 0 and on the following day mice were inoculated with 0.5, 1, 2, 2.5 or 5 $x10^6$ T-cells/ mice IV. In addition to vehicle, dose levels of 0.05, 0.15 and 0.5 mg/kg PF-06671008 were administered for HCT116 xenograft studies and 0.05, 0.15, and 0.5 mg/kg PF-06671008 for SUM149 xenograft studies (n= 10 /dose). The doses were administered IV as a q7d x 3 or q7d x 5 regimens.

Tumor volume was measured using a digital Vernier caliper (Mitutoyo America, Aurora, IL), and volumes were calculated by use of the modified ellipsoid formula ½ ($width^2$ × length). Tumor measurements were collected twice weekly, with continuous health monitoring, until the animals had to be euthanized due to tumor burden or health concerns out to a maximum of 16 days (HCT-116 in the human T-cell engrafted model), 42 days (SUM-149 adoptive transfer) or 65 days (HCT-116 adoptive transfer). For a full description of the mouse xenograft studies, please refer to (15).

PF-06671008 cynomolgus monkey PK study

The PK of PF-06671008 in cynomolgus monkey was evaluated following IV bolus and SC administration at weekly escalating doses for 1 month. The IV doses administered were 1.1/3.3, 3.3/10, or 10/20 µg/kg/week, and the SC dose administered was 10/30 µg/kg/week. This study has been described previously (16).

Measurement of soluble P-cadherin (sPcad)

Baseline sPcad levels were measured in cynomolgus monkey, healthy volunteer, and cancer patient serum samples (Bioreclamation). sPcad levels were also measured in cynomolgus monkey after treatment with PF-06671008 (in-house samples). A qualified Meso Scale Discovery (MSD) human P-cadherin kit was used to measure soluble P-cadherin levels, as described previously (16).

Modeling of mouse tumor growth inhibition (TGI) data: A QSP model was constructed to describe the disposition of PF-06671008 and T-cells in the central compartment and tumor of the xenograft mouse models (Figure 1A). The model accounts for the binding of PF-06671008 to tumor cells and T-cells in the extracellular space of the TME to form trimers. The trimers are

assumed to drive tumor cell killing. Description of all the symbols and parameters used in the mouse equations are shown in Tables I and II.

1. Modeling of PF-06671008 and T-cells in central / peripheral compartments and distribution to the tumor

Following systemic administration to mouse, PF-06671008 is assumed to be able to distribute to a peripheral compartment, distribute to the tumor, bind to circulating T-cells or be cleared from the central compartment. In the mouse model, PF-06671008 does not bind to sPcad. **Mouse PK:** The mouse serum concentration profiles in human PBMC engrafted mice, following IV administration of PF-06671008 at 0.05 and 0.5 mg/kg were described using a 2-compartment model with linear elimination from the central compartment (Equations 1 - 2). *C1, C2 and C3* are the concentrations of the drug, PF-06671008, in plasma, peripheral compartment and tumor, respectively. *kel* is the elimination rate of PF-06671008 from the central compartment. *k12* and *k21* are the inter-compartmental rate constants describing distribution of PF-06671008 between the central compartment and the peripheral compartment. These values were fixed in the subsequent TGI modeling. Distribution of free PF-06671008 to the extracellular environment of the tumor was characterized using tumor disposition equations (Equations 3 - 4) that have been described previously (17-19). Briefly, *P* is the rate of permeability and *D* is the diffusion of drug, across and around the tumor blood vessels. R_{cap} is the radius of the tumor blood capillary; R_{krogh} is the average distance between 2 capillaries, R_{tumor} is the radius of the tumor and ε is the tumor void volume for the drug.

Binding to T-cells: Binding of PF-06671008 to circulating T-cells was determined from CD3 binding (k_{onCD3} and k_{offCD3}), the number of CD3 receptors per T-cell (*CD3*) and number of T-cells in the central compartment, or plasma ($Tcells_p$). These values were used to calculate total CD3 in the central compartment ($TotCD3_p$) (Equation 5). Binding to CD3 (and P-cadherin) was determined using surface plasmon resonance (SPR) assays run on a Biacore instrument as described previously (7). The number of CD3 receptors per T-cell was taken from literature data (20, 21). The number of T-cells administered per mouse was used to inform the initial number of T-cells in the central compartment. See Equation 6 for binding of PF-06671008 to CD3 in the central compartment. *DCD3p and DCD3t* are the concentration of drug-CD3 dimers in plasma and tumor, respectively.

T-cell trafficking: Following administration of T-cells to mouse, T-cells were assumed to be able to distribute to the tumor (Equations 7 – 8), bind to PF-06671008 or be cleared from the central compartment. k_{12T} and k_{21T} are the rate constants describing distribution of T-cells between the central compartment and the tumor. k_{elT} is the elimination rate of the T-cells from the central compartment. These parameters were determined from modeling of in-house PBMC data in tumor bearing mice (not shown here). A lag time of 5 days was introduced to accommodate the disposition and start of proliferation of T-cells at the tumor site. This was informed from in-house immunohistochemistry data and was equivalent to time of T-cell observation in the tumor. $Tcells_{tm}$ are T-cells which have migrated from the central compartment to TME during the 5 days.

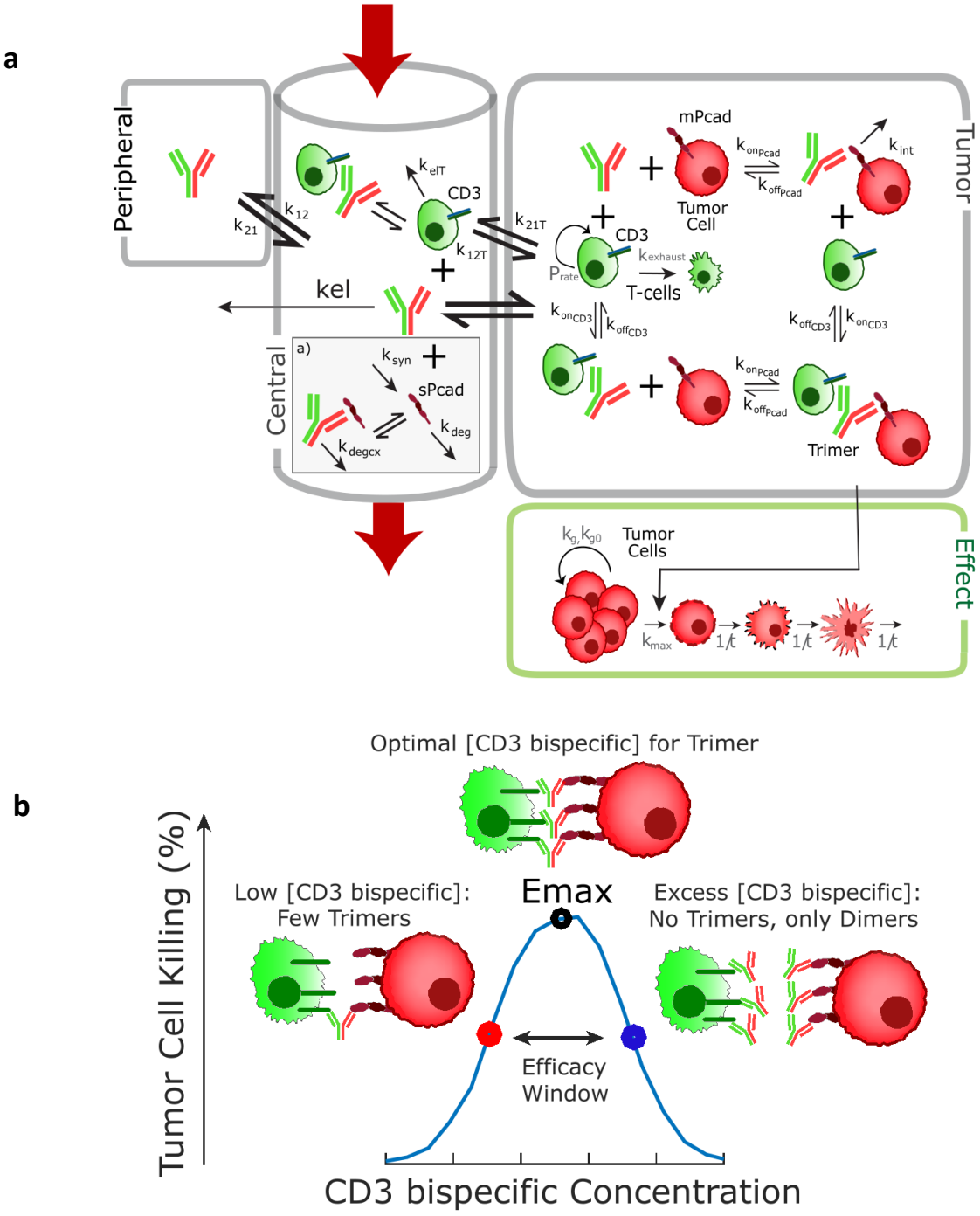

Figure 1a: Translational quantitative systems pharmacology model for CD3 bispecific molecules. Parameter descriptions and values are summarized in Tables I to III. The figure represents both mouse and human models, with the following exceptions: (a) binding to sPcad was only included in the human model (b) T-cell proliferation and exhaustion in the tumor was only included in the mouse model **1b:** Schematic of the bell-shaped concentration relationship which can be observed for CD3 bispecific molecules. Formation of trimers between drug, T-cells and tumor cells are required for efficacy. The QSP model predicts trimer concentration and links it to tumor cell killing.

2. Modeling of T-cell proliferation and trimer formation in the TME

T-cell kinetics in the tumor: CD3+ cells/ mg tumor was measured in HCT-116 tumor bearing mice, engrafted with human PBMCs, following administration of PF-06671008 at 0.01, 0.05 or 0.5mg/kg (described above). This data was used to determine the proliferation rate of T-cells in the tumor. The relationship between CD3+ cells/ mg tumor with time at each dose level was described using an exponential function. The slope of each line represents the rate of proliferation of CD3+ cells and was plotted versus PF-06671008 dose. An empirical model was then used to describe the CD3+ proliferation rates (*Prate*) as a function of dose (Equation 9). Please see supplementary material for additional information and plots. T-cells migrating into the TME during the 5-day lag time ($Tcells_{tm}$) undergo proliferation for 7 days (Equation 10).

Following proliferation, T-cells undergo contraction which was characterized using mono-exponential decline ($k\_{exhaust}$) (Equation 11). The time (7 days) and rate of decline (0.0412 1/h) was estimated from literature data (22). It was assumed that T-cell proliferation was only taking place in the tumor environment and that proliferation and contraction rates were the same in the human T-cell engraftment and adoptive transfer mouse tumor models.

Trimer formation: In the TME, PF-06671008 can bind to P-cadherin on tumor cells or to CD3 on T-cells to form dimers, or both tumor cells and T-cells to form the active trimers. The binding constants between drug and P-cadherin are: k_{onPcad} and $k_{offPcad}$ and the binding constants between drug and CD3 are: k_{onCD3} and k_{offCD3}. In addition to binding affinity values, trimer formation was a function of P-cadherin receptors per tumor cell (*mPcad*), number of tumor cells ($Tumor_{cellst}$), CD3 receptors per T-cell (*CD3*) and number of T-cells in the TME (*Tcellst*). These values were used to calculate total P-cad ($TotPcad_t$) and total CD3 ($TotCD3_t$) in the TME (Equations 12 – 13). P-cadherin receptor expression in HCT-116 and SUM-149 tumor cell lines was determined by phycoerythrin (PE) labelling of anti-P-cadherin mAb and flow cytometry to determine number of PE labeled antibodies bound per cell. This study has been described previously (15). Internalization rate of drug bound to P-cadherin (k_{int}) in the tumor was determined from the mouse PK study, completed in the presence of PBMCs. The number of tumor cells was determined from xenograft data. The number of CD3 receptors/ T-cell was taken from published data (20, 21). See Equations 14 – 16 for binding of PF-06671008 to P-cadherin and CD3 to form dimers and trimers

3. Tumor growth inhibition

The mouse xenograft PK/PD relationship was established by relating mouse PF-06671008 trimer concentration in the TME to measured xenograft tumor volume data using an optimized cell distribution transduction model (23). The presented model is a modified version of the model by *Simeoni et al.* (24). Briefly, the unperturbed tumor growth was fitted first using individual animal growth data from the vehicle control group, using a logistic model describing linear (k_g) and exponential (k_{g0}) growth. The measured initial tumor volume in each animal was used to inform the initial conditions (*M1*). *M1 -M4* are the tumor volumes in the growth compartment and three

transduction compartments, respectively. w is the total tumor volume (mm^3). The inter-individual variability of the growth parameters and the maximum tumor volume (M_{max}) obtained from the unperturbed growth model were then fixed in the simultaneous estimation of growth and drug effect parameters from the complete tumor volume data set. Tumor cell killing was driven by the concentration of the trimolecular complex (*Trimer*). τ is the transduction time, k_{max} is the maximum kill rate, kc_{50} is the concentration of the trimer in the tumor at half the maximal kill rate, and ψ is the constant for switching from exponential to linear growth patterns. Equations 17-22 describe the tumor growth inhibition modeling.

Table 1: Model variables and terms used in equations

Variable	Definition	Unit
$TotPcad_t$	Total Pcad in the tumor	nM
$TotCD3_p$	Total CD3 in the central compartment	nM
$TotCD3_t$	Total CD3 in the tumor	nM
$Tcells_p$	T-cells in the central compartment	cells/L
$Tcells_{tm}$	T-cells migrated from plasma to tumor, during 5-day lag time	cells/L
$Tcells_t$	T-cells in the tumor	cells/L
Dose	Dose of PF-06671008	nmols
C1	Concentration of PF-06671008 in central compartment	nM
C2	Concentration of PF-06671008 in the peripheral compartment	nM
C3	Concentration of PF-06671008 in the tumor	nM
$DCD3_p$	Dimer of PF-06671008-CD3 in the central compartment	nM
$DCD3_t$	Dimer of PF-06671008-CD3 in the tumor	nM
$DPcad_p$	Dimer of PF-06671008-Pcad in the central compartment	nM
$DPcad_t$	Dimer of PF-06671008-Pcad in the tumor	nM
Trimer	Trimer of PF-06771008-CD3-Pcad in the tumor	nM
w	Total tumor volume	mm^3
M_1, M_2, M_3, M_4	Tumor volume in growth and three transduction compartments	mm^3

Determination of tumor static concentration (TSC)

TSC is the concentration of trimers at which tumor growth and death rate are equal and is defined as the minimal efficacious concentration (C_{eff}). This PK/PD derived parameter combines growth information and drug effect, providing insight into the efficacy of PF-06671008 in mouse xenograft models. TSC was used as a translational factor for extrapolation of xenograft data to the clinic. See Equation 23 for TSC calculation. An 80% confidence interval on TSC was calculated using parametric bootstrap by resampling from the estimated parameters using a log-normal distribution.

$$\frac{dC1}{dt} = -kel \times C1 - k12 \times C1 + k21 \times C2 \times \frac{V2}{V1} - kon_{CD3} \times C1 \times \left(TotCD3_p - DCD3_p\right) + koff_{CD3} \times DCD3_p - Tumor\ Disposition \times \frac{TV}{V1} \quad (1)$$

C1(t=0) = Dose in nmols

$$\frac{dC2}{dt} = k12 \times C1 \times \frac{V1}{V2} - k21 \times C2 \quad (2)$$

C2(t=0) = 0

$$Tumor\ Disposition = \left(\frac{2 \times P \times R_{cap}}{R_{krogh}^2} + \frac{6 \times D}{R_{tumor}^2}\right) \times \left(C1 - \frac{C3}{\varepsilon}\right) \quad (3)$$

$$\frac{dC3}{dt} = Tumor\ disposition - k_{onPcad} \times C3 \times \left(\frac{(TotPcadt - DPcadt - Trimer)}{\varepsilon}\right) + k_{off_{Pcad}} \times DPcadt - k_{onCD3} \times C3 \times \left(\frac{(TotCD3t - DCD3t - Trimer)}{\varepsilon}\right) + k_{off_{CD3}} \times DCD3t \quad (4)$$

C3(t=0) = 0

$$TotCD3_p = \left(\frac{Tcells_p \times CD3}{6.023 \times 10^{23}}\right) \times (1 \times 10^9) \quad (5)$$

$$\frac{dDCD3_p}{dt} = kon_{CD3} \times C1 \times \left(TotCD3_p - DCD3_p\right) - koff_{CD3} \times DCD3_p \quad (6)$$

DCD3(t=0) = 0;

$$\frac{dTcells_p}{dt} = -kel_T \times Tcells_p - k12_T \times Tcells_p + k21_T \times Tcells_{tm} \times \frac{TV}{V1} \quad (7)$$

Tcellsp(t=0) = $Tcell_p0$

$$\frac{dTcells_{tm}}{dt} = k12_T \times Tcells_p \times \frac{V1}{TV} - k21_T \times Tcells_{tm} \quad (8)$$

$Tcells_{tm}$(t=0) = 0

$$P_{rate} = \left(\frac{0.014}{4 + dose} + 1.5e - 5\right) \times dose \quad (9)$$

$Tcell_t = Tcell_{tm} \times e^{P_{rate} \times t}$ for t ≤ 7 days, after 5-day lag time (10)

$Tcell_t = (Tcell_{tm} \times e^{P_{rate} \times 7}) \times e^{-0.0412 \times (t-7)}$ for t > 7 days, after 5-day lag time (11)

$$TotPcad_t = \left(\frac{Tumor_{cells_t} \times mPcad}{6.023 \times 10^{23}}\right) \times (1 \times 10^9) \quad (12)$$

$$TotCD3_t = \left(\frac{Tcells_t \times CD3}{6.023 \times 10^{23}}\right) \times (1 \times 10^9) \quad (13)$$

$$\frac{dDCD3t}{dt} = k_{onCD3} \times C3 \times \left(\frac{(TotCD3t - DCD3t - Trimer)}{\varepsilon}\right) - k_{off_{CD3}} \times DCD3t - k_{onPcad} \times DCD3t \times \left(\frac{(TotPcadt - DPcadt - Trimer)}{\varepsilon}\right) + k_{off_{Pcad}} \times Trimer \quad (14)$$

DCD3t(t=0) = 0

$$\frac{dDPcadt}{dt} = k_{onPcad} \times C3 \times \left(\frac{(TotPcadt - DPcadt - Trimer)}{\varepsilon}\right) - k_{off_{Pcad}} \times DPcadt - k_{onCD3} \times DPcadt \times \left(\frac{(TotCD3t - DCD3t - Trimer)}{\varepsilon}\right) + k_{off_{CD3}} \times Trimer - kint \times DPcadt \quad (15)$$

DPcadt(t=0) = 0

$$\frac{dTrimer}{dt} = k_{onCD3} \times DPcadt \times \left(\frac{(TotCD3t - DCD3t - Trimer)}{\varepsilon}\right) - k_{off_{CD3}} \times Trimer + k_{onPcad} \times DCD3t \times \left(\frac{(TotPcadt - DPcadt - Trimer)}{\varepsilon}\right) - k_{off_{Pcad}} \times Trimer \quad (16)$$

Trimer(t=0) = 0

$$k_{kill} = \frac{k_{max} \times Trimer}{kc_{50} + Trimer} \quad (17)$$

$$\frac{dM_1}{dt} = \frac{k_{g0} \times \left(1 - \frac{w}{M_{max}}\right) \times M_1}{\left(1 + \left(\frac{k_{g0}}{k_g} \times w\right)^{\psi}\right)^{\frac{1}{\psi}}} - k_{kill} \times M_1 \quad (18)$$

M1(t = 0) = TV

$$\frac{dM_2}{dt} = k_{kill} \times M_1 - \frac{M_2}{\tau} \quad (19)$$

M2(t=0)=0

$$\frac{dM_3}{dt} = \frac{M_2 - M_3}{\tau} \quad (20)$$

M3(t=0) = 0

$$\frac{dM_4}{dt} = \frac{M_3 - M_4}{\tau} \quad (21)$$

M4(t=0) = 0

$$w = M_1 + M_2 + M_3 + M_4 \quad (22)$$

$$TSC = \frac{k_{g0} \times k_{C50}}{k_{max} - k_{g0}} \quad (23)$$

Table 2: Mouse model parameters

	Parameter	Definition	Unit	Value (CV%)	Source
Binding	k_{onCD3}, k_{offCD3}, K_{d_CD3}	Binding of PF-06671008 to CD3	1/nM/h, 1/h	1.72, 19.66 11.4	(7)
	k_{onPcad}, $k_{offPcad}$, K_{d_Pcad}	Binding of PF-06671008 to P-cadherin	nM	1.57, 0.74 0.47	
Central / Peripheral Compartment	V_1	Volume of distribution in the central compartment	mL/kg	49.6 (9)	Estimated from mouse PK data. *kel*= CL/V_1 *k12*= CL_d/V_1 *k21*= Cl_d/V_2
	V_2	Volume of distribution in the peripheral compartment	mL/kg	60.7 (16)	
	CL	Clearance	mL/h/kg	0.45 (12)	
	CL_d	Inter-compartmental clearance	mL/h/kg	4.95 (28)	
	Omega CL	Inter-individual variability in clearance	-	0.064 (41)	
	a	Additive error	-	0.067 (32)	
	b	Proportional error	-	0.207 (15)	
	$Tcells_p0$	Number of T-cells administered/mouse	cells/L	0, 2.5e8, 5e8, 1e9, 1.25e9, 2.5e9	See methods section
	CD3	CD3 expression on T-cells	receptors/cell	100,000	(20, 21)
Tumor Disposition of PF-06671008/ T-cells	*P*	Permeability of drug into tumor	µm/day	334	(18)
	D	Diffusivity of drug into tumor	cm2/day	0.022	
	ε	Void fraction in tumor for drug	-	0.24	
	Rcap	Capillary radius	µm	8	
	Rkrogh	Average distance between 2 capillaries	µm	75	
	Tlag	Lag time for T-cell disposition/ onset of T-cell proliferation in the tumor	day	5	Set empirically, using in-house data
	k_{elT}, k_{12T}, k_{21T}	T-cell re-distribution from the central compartment to the tumor	1/day	2.51, 0.002, 0.0005	

Tumor Compartment	*Prate*	T-cell proliferation rate	1/h	Function of dose. Equation (9)			See methods
	kexhaust[c]	Slope of T-cell decline	1/h	0.0412			Interpolated from (22)
	$Tumor_{cellst}$	Number of tumor cells	cells/ gram of tumor	1e8			(26)
	mPcad	P-cadherin expression on tumor cells	receptors/ cell	28,706 (HCT-116) 17,500 (SUM-149)			(15)
	Rtumor	Tumor radius	cm	Calculated from w			Measured
	k_{int}	P-cadherin internalization rate	day^{-1}	0.1728 (-)			Estimated from mouse tumor PK data. 96h half-life of internalization.
Tumor Growth Inhibition		Mouse tumor models		HCT116[a]	HCT116[b]	SUM149[b]	
	k_{g0}	Exponential tumor growth rate	1/day	0.30 (-)	0.19 (3)	0.12 (3)	Estimated in mouse models from unperturbed tumor growth data
	k_g	Linear tumor growth rate	mm3/day	105 (4)	123 (2)	74.3 (5)	
	M_{max}	Maximum tumor volume	mm3	$3.8x10^3$ (-)	$6.0 x10^3$ (-)	$5.8 x10^3$ (-)	
	ψ	Switch between exponential and linear growth phases	-		20 (-)		Fixed based on (24)
	k_{max}	Maximum killing rate	1/day	0.74 (7)	1.32 (7)	2.71 (14)	Estimated in mouse models
	kC_{50}	Concentration at half maximum kill rate	nM	$1.0x10^{-4}$ (6)	$6.9x10^{-5}$ (7)	$2.0x10^{-4}$ (15)	
	τ	Transduction time between tumor compartments	day	4.78 (10)	3.99 (1)	2.25 (3)	
	Omega k_{g0}	Inter-individual variability in exponential growth rate		0.46 (14)	0.34 (11)	0.12 (25)	
	Omega k_g	Inter-individual variability in linear growth rate		0.35 (13)	0.16 (13)	0.16 (28)	
	a	Additive error		5 (-)	60 (-)	60 (-)	
	b	Proportional error		0.26 (3)	0.06 (6)	0.01(50)	
	TSC (pM) [80% confidence interval]	Tumor static concentration of the trimer		**0.064** [0.044, 0.096]	**0.011** [0.0096, 0.013]	**0.0092** [0.0071, 0.012]	

[a]Tcell engrafted tumor model, [b]T cell adoptive transfer tumor model, [c]onset of exhaustion of T-cells set to 7d after disposition in the tumor

Modeling: All modeling was performed using Monolix software v4.3.3 (Paris, France). The quality of the model fitting was assessed using:

Diagnostic plots: (a) plots of observations versus population/ individual predictions and comparison with line of unity, (b) plots of weighted residuals versus time/concentration and check for systematic deviation from zero, (c) visual predictive checks of observations and predictions for all individuals at each dose level to check for goodness of fit.

Diagnostic criteria: (a) reasonable precision of the parameter estimates (RSE/ CV%) (b) lack of correlation between model predicted parameters (<0.95) (c) lack of shrinkage (η-) as a check for model over-parameterization (<40%) (d) reduction in objective function values and/or Aikake and Schwarz criterion for model comparison.

Translation of the model to human

Prediction of human PK: Human PK parameters were predicted from cynomolgus monkey PK parameters using a two-compartmental PK model which incorporates binding to sPcad (Table III and Figure 1A). PK parameters were scaled from monkey to human using allometric exponents of 0.9 for clearance, 1 for volume of distribution and -0.25 for absorption rate. These exponents were selected as they have been previously identified as optimal for monoclonal antibodies (25). The degradation rate of sPcad (k_{deg}) was scaled from monkey to human using an exponent of -0.25. The degradation rate of the PF-06671008-sPcad complex (k_{degcx}) was assumed to be the same as PF-06671008 elimination rate.

Prediction of clinical PK/PD: The QSP model used to describe the PK/PD relationship in mouse was translated to human using the physiological parameters and assumptions described in Table III. An important difference from the mouse model is that PF-06671008 binds to circulating target (*sPcad*) to form drug-P-cadherin (*DPcadp*) dimers in the central compartment in the human model. The additional model equations are shown in Equations 24 – 26. In addition, T-cell proliferation/ contraction kinetics were not included in the human model. Instead, a 'steady state' number of T-cells in tumor are assumed (T_{cellst}). All model simulations were completed using Berkeley-Madonna v8.3.18.

$$\frac{dC1}{dt} = -kel \times C1 - k12 \times C1 + k21 \times C2 \times \frac{V2}{V1} - kon_{CD3} \times C1 \times \left(TotCD3_p - DCD3_p\right) + koff_{CD3} \times DCD3_p - kon_{Pcad} \times C1 \times sPcad + koff_{Pcad} \times DPcad_p - Tumor\ Disposition \times \frac{TV}{V1} \quad (24)$$

$C1(t=0) = \text{Dose in nmols}$

$$\frac{dsPcad}{dT} = ksyn - kdeg \times sPcad - kon_{Pcad} \times C1 \times sPcad + koff_{Pcad} \times DPcad_p \quad (25)$$

$sPcad\ (t=0) = \text{sPcad in nM}$

$$\frac{dDPcad_p}{dT} = \left(kon_{Pcad} \times C1 \times sPcad - koff_{Pcad} \times DPcad_p\right) - k_{degcx} \times DPcad_p \quad (26)$$

$$DPcadp(t=0)=0$$

Sensitivity analyses: Local sensitivity analyses were performed to assess the sensitivity of the QSP model to P-cadherin receptor expression on tumor cells, and to tumor T-cell (effector) to tumor cell ratio (E:T), as these are potentially variable parameters in patients. P-cadherin receptor numbers of 1,000, 3,000, 10,000 and 28,706 were used for simulations with the human model. These values represented the range of P-cadherin expression measured across human tumor cell lines (15). The nominal value of E:T used in the model was 1:150, which is thought to be representative of a solid tumor (26, 27). In the sensitivity analysis, E:T ratios of 10-fold lower (1:15) and 10-fold higher (1:1500) than the nominal value were investigated in the human model. For quantitative comparison, sensitivity was represented as predicted tumor trimer concentration at each expression level, or E:T ratio, following an IV dose of 0.1µg/kg PF-06671008 QW to cancer patients.

6.4 Results

Serum and tumor PK of PF-06671008 in mouse: PK profiles of PF-06671008 in PBMC engrafted and non-PBMC engrafted HCT-116 tumor-bearing mice following single dose IV administration at 0.05 and 0.5 mg/kg are shown in Figure 2A. Area under the curve (AUC) of PF-06671008 in serum was dose proportional between 0.05 and 0.5 mg/kg and similar between PBMC engrafted and non-PBMC engrafted mice (Figure 2). In contrast, the tumor AUC from the study with PBMC engraftment was more than 5-fold higher than the study without PBMCs (Figure 2B). This was attributed to a reduction in the internalization of PF-06671008 bound to P-cadherin on tumor cells in the presence of PBMCs.

The serum PK in the PBMC engrafted mice was used for PK modeling. The estimated serum PK parameter estimates for PF-06671008 are shown in Table 2, and the goodness of fit plots are shown in Supplemental Figure 1. The tumor internalization rate in the presence of PBMCs was used in the TGI PK/PD modeling (Table 2).

Tumor T-cell kinetics: HCT-116 tumor bearing mice engrafted with PBMCs and administered PF-06671008, showed dose dependent increases of tumor infiltrating/proliferating CD3+ lymphocytes (TILs) over time (Figure 3). The relationship with time was transformed to calculate a proliferation rate of CD3+ cells as a function of dose which was used to describe tumor T-cell kinetics in the QSP model (Supplementary Figure 2).

PK/PD relationship of PF-06671008 in mouse xenograft models: The QSP model (Figure 1A) was used to fit the tumor growth inhibition data obtained from the HCT-116 and SUM-149 mouse xenograft studies. The tumor trimer concentration was used as a driver of tumor cell killing.

A

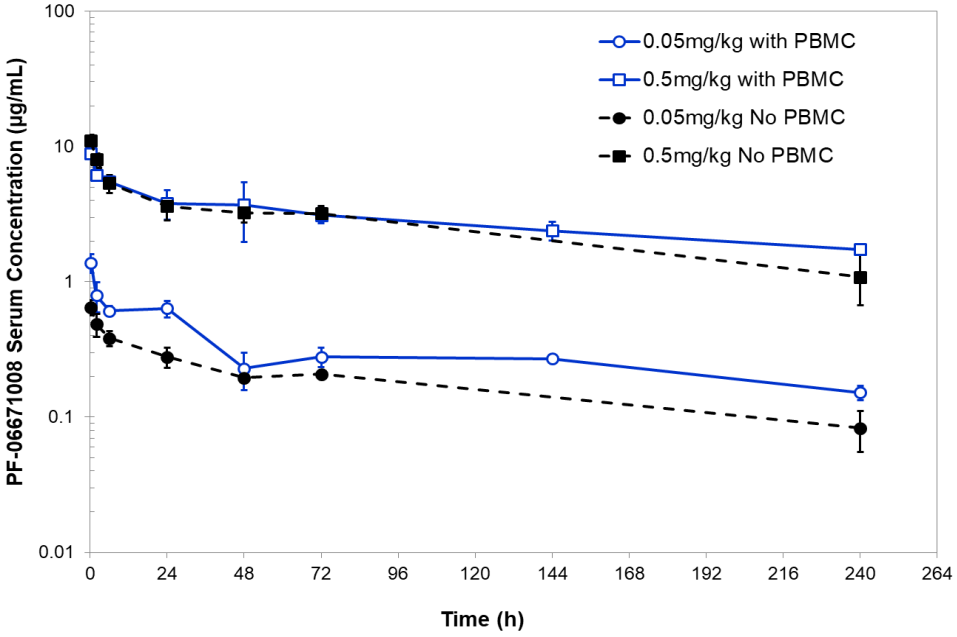

B

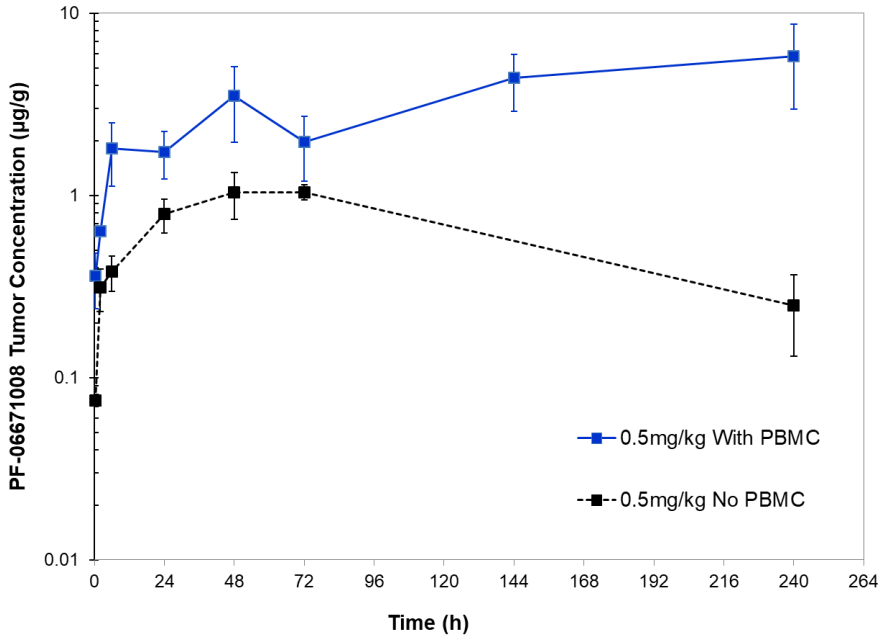

Figure 2: (A) Serum and **(B)** Tumor PK profiles of PF-06671008 in PBMC engrafted and non-PBMC engrafted HCT-116 tumor bearing mice following single dose intravenous administration at 0.05 and 0.5mg/kg.

Estimated model parameters with percent co-efficient of variation (CV) and calculated tumor trimer TSCs with 80% confidence intervals are shown in Table II. Parameters were estimated with good precision as assessed by the % CV for all cell lines. The goodness of fit and model performance were assessed using goodness of fit plots (population prediction, individual prediction and visual predictive check) that are shown in Supplemental Figure 3 for HCT-116 in the T-cell engrafted model, and for HCT-116 and SUM-149 in T-cell adoptive transfer experimental model. Overall, the median response and variability of all cell lines were described well by the mechanistic model. The calculated population median TSCs were 0.064, 0.011 and 0.0092 pM for HCT-116 in T-cell engrafted model, and for HCT-116 and SUM-149 in T-cell adoptive transfer experimental models, respectively. The Ceff for tumor stasis is defined as the geometric mean of the TSCs in three mouse xenograft models and was calculated to be 0.028 pM trimer concentration in the tumor.

Serum P-cadherin concentrations across species: The concentrations of sPcad in serum samples from cynomolgus monkey, healthy humans and cancer patients are shown in Table IV. There was no difference in sPcad levels in serum of healthy human volunteers and cancer patients. Higher variability was observed in lung and colorectal cancer samples compared to samples from breast cancer patients or healthy humans. Levels of sPcad in cynomolgus monkeys were similar to those in human.

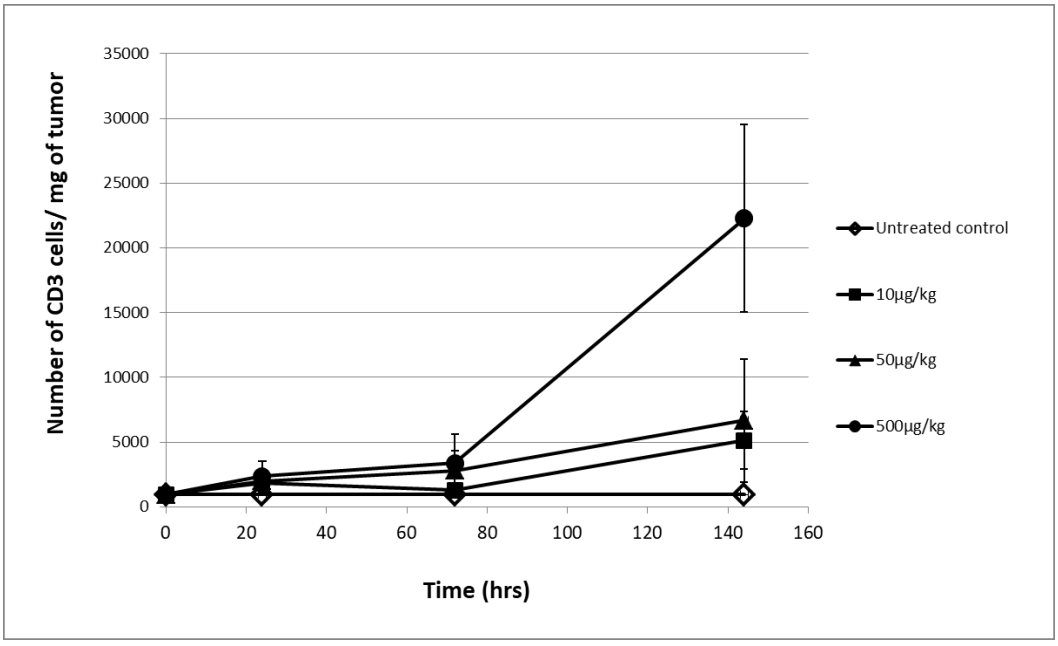

Figure 3: PF-06671008 induced tumor T-cell proliferation in mice bearing HCT-116 tumors with human PBMC engraftment. Number of CD3+ cells/ mg of tumor (with standard deviations) are plotted against time following IV administration of control and PF-06671008 at 10 µg/kg, 50 µg/kg and 500 µg/kg.

Clinical PK predictions for PF-06671008: The predicted human PK parameters for PF-06671008 are shown in Table 3. The predicted human CL and Vss were 4.6 mL/h/kg and 251 mL/kg, respectively, and the terminal half-life was predicted to be approximately 1 day.

Clinical PK/PD predictions for PF-06671008 and sensitivity to P-cadherin expression on tumor cells and T-cell number: To translate the QSP model from mouse to human, the predicted human PK was incorporated along with assumptions and parameters describing the human physiology (Table 3). Model simulated serum PK and tumor trimer concentrations following IV infusion of PF-06671008 at 0.01, 0.1, and 1µg/kg QW to cancer patients are shown in Figures 4A and 4B, respectively. Expression levels of P-cadherin on tumor cells are expected to vary across patients. To investigate the potential impact on tumor trimer concentrations, a sensitivity analysis was performed varying P-cadherin receptor numbers from 1,000 -28,706 (HCT-116). Predicted tumor trimer concentration increases with increasing receptor expression (Figure 5A) suggesting that P-cadherin expression is a sensitive parameter. Tumor immune status is also likely to vary across patients. The nominal E:T ratio in the model is assumed to be low (1:150) in a solid tumor (26, 27). To investigate potential impact of tumor T-cell number on tumor trimer concentrations, a sensitivity analysis was performed varying E:T ratio from 1:15 to 1:1500 and assuming a constant number of tumor cells. Predicted tumor trimer concentration correlates with E:T ratio (Figure 5B), suggesting T-cells in the tumor are a sensitive parameter.

6.5 Discussion

Complex exposure response relationships for CD3 bispecific molecules

Bispecific antibodies are emerging as a leading class of biotherapeutic drugs in oncology, with potential to enhance efficacy, increase tumor targeting and reduce systemic toxicity compared to their monospecific counterparts. These formats can vary in their molecular weight, PK, and ability to support immune effector functions. Perhaps more significantly, they can also vary in geometry, number of antigen binding sites, and the intrinsic affinity of individual arms (28). As a result of this complexity, dose response relationships for bispecific antibodies can be non-intuitive and difficult to rationalize.

An additional complexity emerges for the CD3 bispecific T-cell retargeting modality, where efficacy is driven by the formation of a trimer between the drug, T-cell, and tumor cell. A bell-shaped concentration response relationship can be observed (Figure 1B), which is a well described phenomenon for ternary complexes (29-32). When concentrations of antibodies are low, conditions favor the formation of trimers, with an optimal antibody concentration needed for trimer formation. However, as concentrations increase further, antibodies will be in excess and the equilibrium will shift to formation of dimers between antibodies and T-cell, or antibodies and tumor cell. This results in a decrease of response as dimers cannot trigger cytotoxicity. Since trimer concentration is a function of drug Kd values, tumor antigen expression, CD3 expression and E:T ratio, a single drug concentration could potentially result in different trimer concentrations. Therefore, interpretation of response by drug exposure alone can be misleading. For the CD3 bispecific molecule discussed in this manuscript (PF-06671008), a bell-shaped dose response relationship was not observed in mouse xenograft studies. This is probably because there was high P-cadherin expression on the tumor cell lines studied and good infiltration of T-

Table 3: Predicted human parameters used in simulations

	Parameter	Definition	Unit	Value (CV%)	Source
Binding	k_{onCD3}	Binding of PF-06671008 to CD3	1/nM/h	1.72	(7)
	k_{offCD3}		1/h	19.66	
	K_{d_CD3}		nM	11.4	
	k_{onPca}	Binding of PF-06671008 to P-cadherin	1/nM/h	1.57	
	$k_{offPcad}$		1/h	0.74	
	K_{d_Pcad}		nM	0.47	
Central / Peripheral Compartment	V_1	Volume of distribution in central compartment	mL/kg	40.2	Allometrically scaled from cynomolgus monkey PK analysis (16) *kel*= CL/V1 *k12*= CL_d/V1 *k21*= Cl_d/V2
	V_2	Volume of distribution in peripheral compartment	mL/kg	211	
	CL	Clearance	mL/h/kg	4.61	
	CL_D	Inter-compartmental clearance	mL/h/kg	25.2	
	sPcad	sPcadherin concentration in central compartment	nM	1.1 (0.4- 4.1)	Measured in-house (= 92.7ng/mL) Median value of healthy subjects and patient data
	k_{deg}	sPcad degradation rate	1/h	0.15	Allometrically scaled from cynomolgus monkey PK analysis (0.31 1/h in cyno) (16)
	k_{degcx}	sPcad-PF-06671008 complex degradation rate	1/h	0.115	Assumed to equal PF-06671008 elimination rate (CL/V1)
	$Tcells_p$	T-cell concentration in central compartment	cells/ µL	5000	(42)
	CD3	CD3 expression on T-cells	receptors/cell	100,000	(20, 21)
Tumor Disposition of PF-06671008/ T-cells	*P*	Permeability of drug into tumor	µm/d	334	(18)
	D	Diffusivity of drug into tumor	cm^2/d	0.022	
	ε	Void fraction in tumor for drug	-	0.24	
	Rcap	Capillary radius	µm	8	
	Rkrogh	Average distance between 2 capillaries	µm	75	
	$Tcells_t$ [a]	Number of T-cells in tumor	cells/gram of tumor	6.49e5	(27)
	$Tumor_{cellst}$	Number of Tumor cells	cells/ gram of tumor	1e8	(26)
	mPcad	P-cadherin expression on tumor cells	receptors/cell	28,706	(15)
	Rtumor	Tumor radius	cm	1	Assumed
	k_{int}	Internalization rate with PBMCs	day^{-1}	0.1728 (-)	Estimated from mouse tumor PK data. Represents 96h half-life of internalization.

[a] *Assume no proliferation in tumor; ksyn = kdeg*sPcad MWt of PF-06671008= 105kDa, MWt of sPcad=85kDa*

cells. In addition, PF-06671008 is a potent drug with low Kd values for P-cadherin and CD3. As a result, sufficient trimer concentrations were achieved at each dose for efficacy. The bell-shaped relationship has been confirmed for other CD3 bispecific molecules in-house, where target expression is lower and/ or affinity weaker. It has also been observed in the literature from modeling of in vitro and in vivo experimental data (33, 34).

Translational QSP model for CD3 bispecific molecules

QSP models, which map out the causal path between drug administration and effect in a mechanistic framework, can be a useful tool to deconvolute complex mechanisms (35). Some examples of the use of mechanistic PK/PD models to quantify and understand system dynamics of CD3 bispecific molecules are emerging in the literature. For example, Jiang *et al.* (33) proposed a cell killing model based on target cell-biologic-effector cell complex formation and used it to describe and predict in vitro cytotoxicity data for multiple T-cell redirecting bispecific antibodies under different experimental conditions. Campagne *et al.* (36), developed a PK/PD model for a bispecific CD123/CD3 DART molecule in non-human primates. The model describes DART molecule binding to peripheral CD3 expressing cells and CD123+ cells, T-cell trafficking, activation, and expansion, and resulting peripheral depletion of CD123 cells.

In this manuscript, a translational QSP model is proposed for CD3 bispecific T-cell retargeting molecules, capable of predicting trimer formation and linking it to tumor cell killing in in vivo efficacy models. In addition, the mechanistic nature of the model enables integration of patient data/ parameters and subsequent clinical predictions. The model consists of 3 parts describing the central, tumor and effect compartments (Figure 1A). The first part includes the bispecific antibody PK, binding to circulating T-cells, and binding to soluble target (when applicable) in the central compartment. The second part describes distribution of the antibodies to the tumor compartment using mechanistic tumor penetration equations, and parameters calculated based on the drug's molecular weight and tumor size (18, 19, 37). If the model is being used for a liquid tumor these drug exchange tumor penetration parameters can simply be removed, as liquid tumors are assumed to provide less of a diffusion barrier than solid tumors, and equilibrium can be assumed between drug concentration in the central compartment and tumor interstitium. In the tumor compartment, the model incorporates binding of the drug to CD3 on T-cells and the specific antigen on tumor cells to form inactive dimers and ultimately the active trimers. In the mouse model a simple description of T-cell expansion and contraction is included, constructed using mouse TIL data and published information. For translation of this model to human, data on T-cell kinetics was not available and instead a baseline concentration of T-cells was assumed with no proliferation.

In the third part of the model the trimer concentration is used as the basis for quantifying tumor volume reduction using a tumor growth inhibition model. The model used is a transduction model describing tumor cell growth and tumor cell killing (as a function of the tumor trimer concentration). The model parameters from each mouse study can be used to calculate a secondary parameter called the TSC. This is the concentration of trimer where the tumor is

neither growing nor regressing and can be considered as the minimum concentration of tumor trimer required for efficacy. The TSC is a useful parameter which can be used as a pharmacodynamic index to rank compounds, or to understand the difference in compound potency across mouse xenograft models, or as the denominator in therapeutic index calculations.

Application of the QSP model to quantify PK/PD relationship for PF-06671008 in mouse xenograft models

The model was used to quantify the preclinical PK/PD relationship of a CD3 bispecific molecule targeting P-cadherin (PF-06671008). To implement the model, the first step was to collect drug and system parameters describing the mechanism of action in mouse. To calculate trimer concentration in the tumor, receptor expression of P-cadherin was determined for the HCT-116 and SUM-149 human tumor cell lines used in the mouse xenograft experiments. P-cadherin receptor expression in both cell lines (28,706 for HCT-116 and 17,500 for SUM-149) was lower than the expression of CD3 on T-cells (100,000 (20, 21)). This is typical for CD3 bispecific molecules as expression of most tumor targets is less than 100,000, and as a result tumor antigen receptor expression can be limiting and a key driver of efficacy. This was exemplified for a carcinoembryonic antigen T-cell bispecific (CEA-TCB) for the treatment of solid tumors. CEA-TCB activity was found to be strongly correlated with CEA expression, with a higher potency observed in highly CEA expressing tumor cells, with a threshold of 10,000 CEA binding sites/ cell (38). Target affinity data was also required to calculate trimer concentration. PF-06671008 binds to P-cadherin with a Kd of 0.47 nM and CD3 with a Kd of 11.4 nM (7). Binding to the tumor target antigen is often more potent than binding to CD3 on T-cells in order to target the CD3 bispecific toward the tumor and away from peripheral tissues (34). In addition, strong binding to CD3 has been shown to drive more rapid clearance of an anti-CD3/anti-CLL1 bispecific in preclinical in vivo models (39).

The QSP model was used to integrate the mouse PK for PF-06671008 with the TGI data and to calculate TSCs in T-cell engrafted (HCT-116) and T-cell adoptive transfer (HCT-116 and SUM-149) established mouse tumor models. TSC values were very similar in the adoptive transfer model for both the SUM-149 and HCT-116 tumor cell lines (0.0092 and 0.011 pM respectively, with overlapping 80% confidence intervals). In contrast, a 6-fold higher TSC value was obtained in the T-cell engrafted versus T-cell adoptive transfer model with the same cell line (HCT116, 0.064pM), and the respective 80% confidence intervals do not overlap. This is probably due to differences in T-cell engraftment between the two mouse tumor models. In the T-cell engrafted model the T-cells are administered as freshly isolated human PBMCs, 7 days prior to drug administration. In contrast, in the adoptive transfer model, activated T-cells are given 1-day post drug treatment. There are also other factors which can result in different TSCs including initial tumor size, and differences in tumor growth rates.

Table 4: Concentration of soluble P-cadherin in cynomolgus monkey and human serum

Species	Disease state	n	Soluble P-cadherin concentration	
			Median (ng/mL)	Range (ng/mL)
Cynomolgus monkey[a]	Healthy	32	47	29-273
Cynomolgus monkey[b]	Healthy	4	68	57-74
Human[a]	Healthy	40	90	45-150
Human[a]	Breast cancer patients	23	78	32-190
Human[a]	Colon cancer patients	31	102	36-328
Human[a]	Lung cancer patients	25	102	65-320

[a]Samples from Bioreclamation (Westbury, NY), [b]Samples from in-house studies

MWt of PF-06671008= 105kDa, MWt of sPcad=85kDa

Translation of the model to the clinic

The first step in translation to human was prediction of the clinical PK parameters. For PF-06671008, circulating soluble target can act as a sink for the drug and reduce free drug exposure by forming complexes with PF-06671008. The reduction of free sPcad concentrations in cynomolgus monkey following dosing of PF-06671008 has been reported previously (16). The human PK of PF-06671008 was predicted from cynomolgus monkey PK using a two-compartmental PK model which incorporates binding to sPcad. Levels of sPcad were measured in healthy volunteers and in breast, colon and lung cancer patients and the median concentration in cancer patients was used in the human model.

The next step in the clinical translation process was incorporation of human systems parameters into the QSP model. These parameters are summarized in Table III and include T-cell concentration in the circulation and tumors, tumor cell concentration and typical tumor volumes in cancer patients. Values for all these parameters were obtained from the literature. CD3 receptor expression was kept the same as the mouse model (which used human T-cells or PBMCs). P-cadherin expression of 28,706 was used in the clinical simulations. This was the value from the HCT-116 cell line, and represents a medium-high level expression of P-cadherin measured across human tumor cell lines used in in vitro cytotoxicity experiments (874- 37,582 (15)).

Model simulated serum PK and tumor trimer concentrations following IV infusion of PF-06671008 at 0.01, 0.1 and 1µg/kg QW to cancer patients are shown in Figures 4A and 4B,

respectively. In human, the terminal half-life of PF-06671008 was predicted to be approximately 1 day. Concentration of trimer in the tumor, which is the more relevant concentration for efficacy, accumulates slowly (Cmax approx. 2 days post first dose) and persists for longer (Figure 4B). This is due to slow diffusion of the drug into the tumor and formation of a more stable trimer which is retained within the TME. Since receptor expression of tumor target was known to be a key parameter, a sensitivity analysis was completed using the human model with P-cadherin expression varying from 1,000-28,706 receptors/cell. This analysis confirmed that P-cadherin receptor expression was a sensitive parameter and that concentration of trimer formed in the tumor correlates with expression level (Figure 5A). This has an impact on predicted clinical efficacy with a higher dose required for efficacy in patients with lower P-cadherin expression. In addition, the T-cell number in the tumor was found to be a sensitive parameter (Figure 5B), with higher predicted concentration of trimer in the tumor with increasing E:T ratio. High doses of PF-06671008 were also simulated, to check to see where the bell-shaped relationship might be observed. At doses of >1.8mg/kg, a reduction in tumor trimer concentration is predicted with increasing dose levels (Supplementary Figure 4). However, at these doses the predicted trimer concentrations in the tumor are high enough that good responses would be expected (assuming the doses would be tolerated). A translational flow diagram describing the steps taken to translate CD3 bispecific drugs from preclinical TGI data in mouse to human is shown in Figure 6.

The translational QSP model described for CD3 bispecific compounds can be used to drive decision making at different stages of the drug discovery and development continuum. At early stages the model can be used to provide guidance on compound selection, by predicting optimal Kd values for CD3 and the tumor antigen. This can be achieved by modeling of in vitro data, using a reduced version of the model without the PK (central and peripheral) compartments. For example, the model was previously used to describe the in vitro exposure response of PF-06671008 in cytotoxicity assays and was able to simultaneously describe the kinetics of tumor and T-cells at various E:T ratios (16). Once a lead compound has been selected the model can be used to predict clinical doses and regimens and to optimize efficient clinical study design (40). A precision medicine approach could be adopted, whereby parameters in the model such as immune cell numbers, or tumor target expression levels, are tailored to individual characteristics of patients. This could result in recommendation of different doses for different patients. The model has also been used to predict clinical starting dose for PF-06671008 using a minimal biological effect level approach (MABEL), which is recommended for CD3 bispecific constructs due to their immune agonistic activity following target engagement (16, 41). A recent analysis by the FDA concluded that receptor occupancy-based methods were not advised for CD3 bispecifics. The QSP modeling approach is more suitable to determine MABEL as efficacy is driven by drug bound to both T-cells and tumor cell, rather receptor occupancy of either target singly. It is also independent of E:T ratio or other experimental specificities.

A

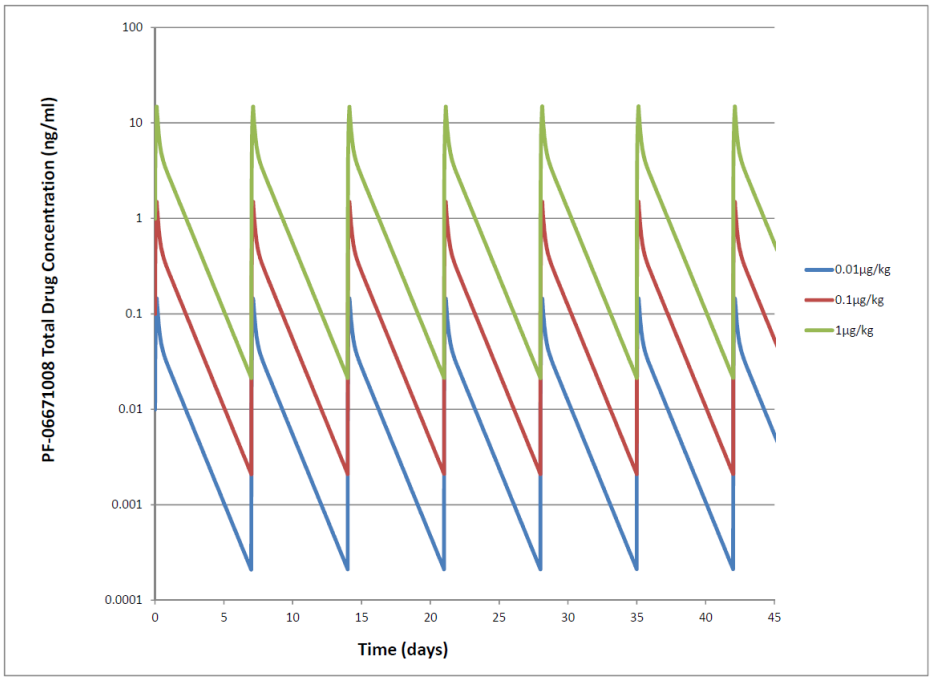

B

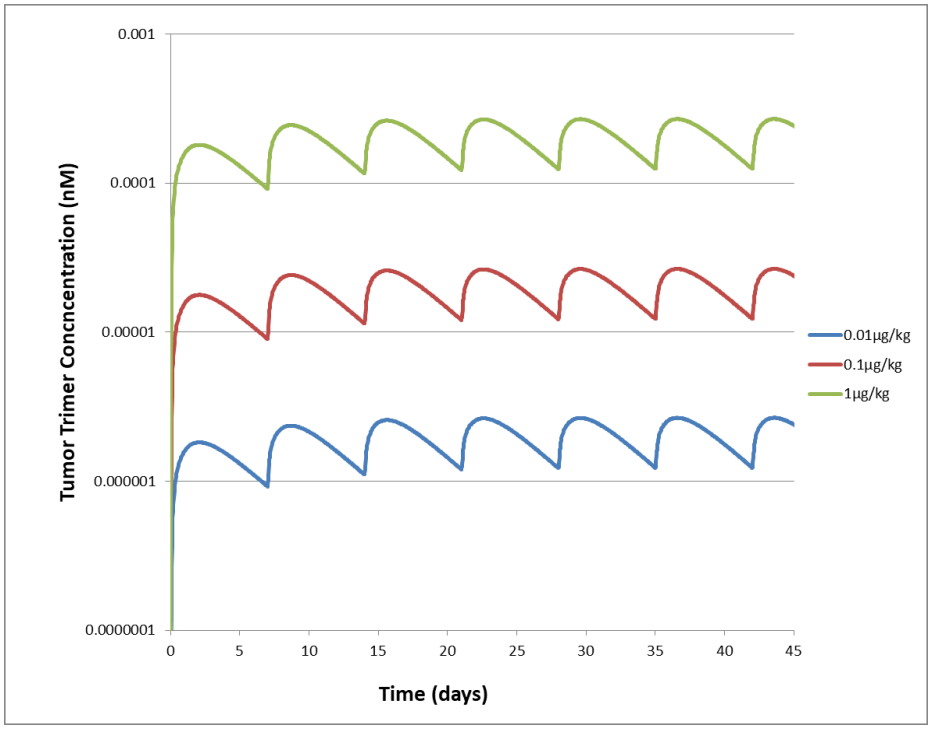

Figure 4: Model simulated **(A)** serum PK and **(B)** tumor trimer concentrations following IV infusion of PF-06671008 at 0.01, 0.1, and 1µg/kg QW to cancer patients

A

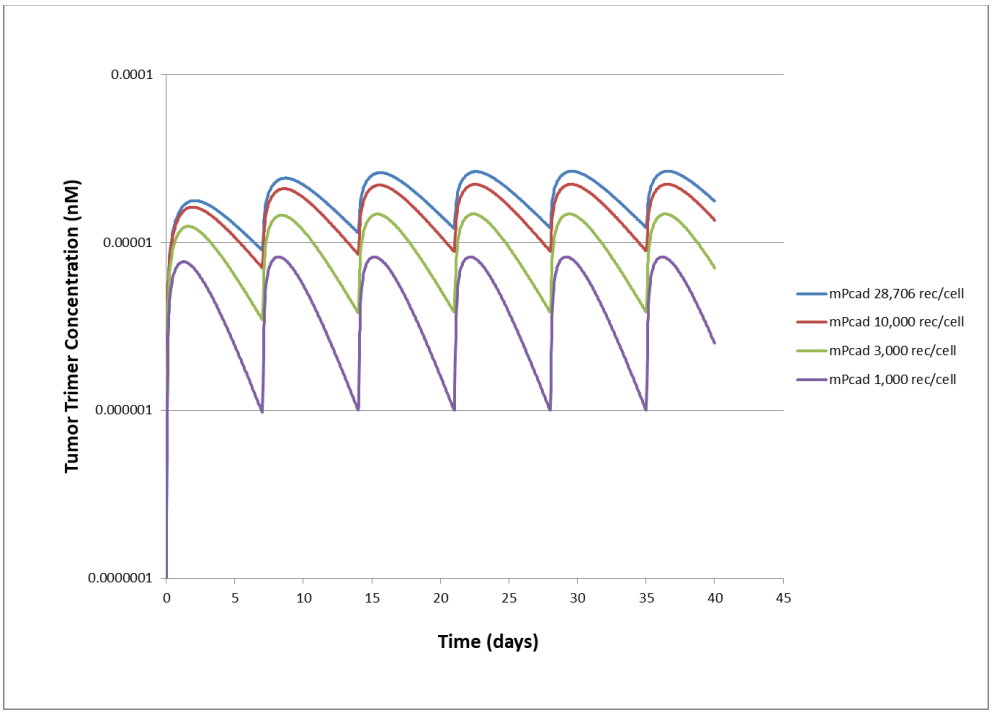

B

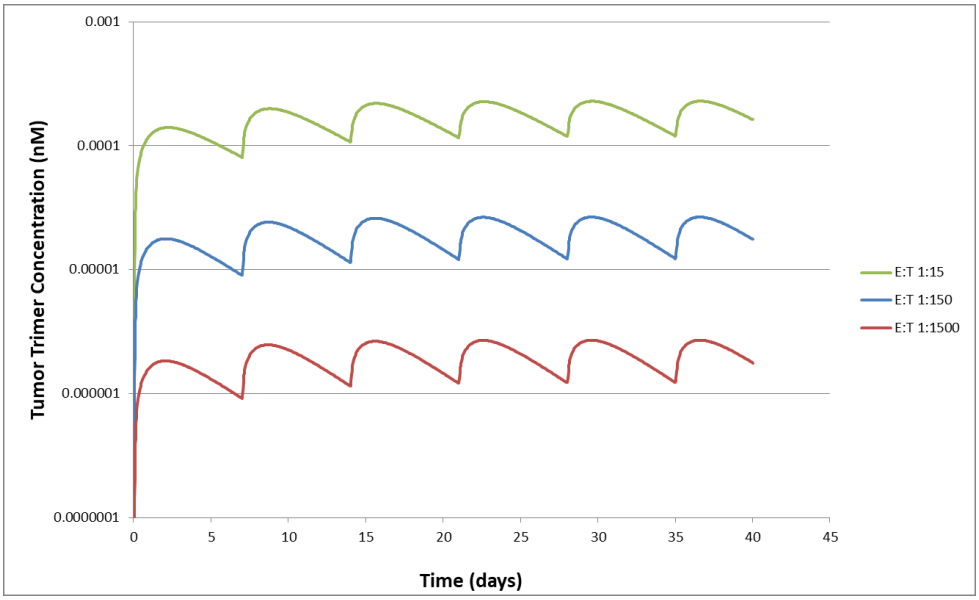

Figure 5: Model simulated tumor trimer concentrations at **(A)** different P-cadherin receptor expression values (1,000- 28,706 receptors/ cell) and **(B)** different E:T ratios (1:1500- 1:15) following IV infusion of PF-06671008 at 0.1µg/kg QW to cancer patients

The model in its current state is very useful for a range of tasks from optimization of drug design to clinical dose predictions. However, opportunities exist to improve the model. For example, the current model includes an empirical description of T-cell activation/ proliferation in mouse, constructed based on TIL analysis across dose and time. A more mechanistic model could be developed by collection and characterization of more tumor lymphocyte kinetic data across species. In addition, the model is based upon a 'well-mixed' hypothesis in which tumor target

and T-cells are assumed to be homogeneously distributed throughout the tumor environment with equal opportunity for trimer formation. However, tumors are known to be a complex environment with heterogeneous distribution of T-cells and tumor cells expressing target. Future versions of the model will take this into account.

6.6 Conclusion

The mechanistic PK/PD model and translational framework described for CD3 bispecific molecules, provides a holistic solution for quantitative decision making throughout the drug discovery and development process. In this manuscript, use of the model to characterize the in vivo PK/PD relationship of a P-cadherin/ CD3 bispecific construct (PF-06671008) across mouse efficacy models is described. The model can also be translated to the clinic for human PK/PD predictions and sensitivity analysis to determine important parameters driving efficacy. The model can be applied at early stages to aid in the design of CD3 bispecific constructs and to select molecules with optimal properties.

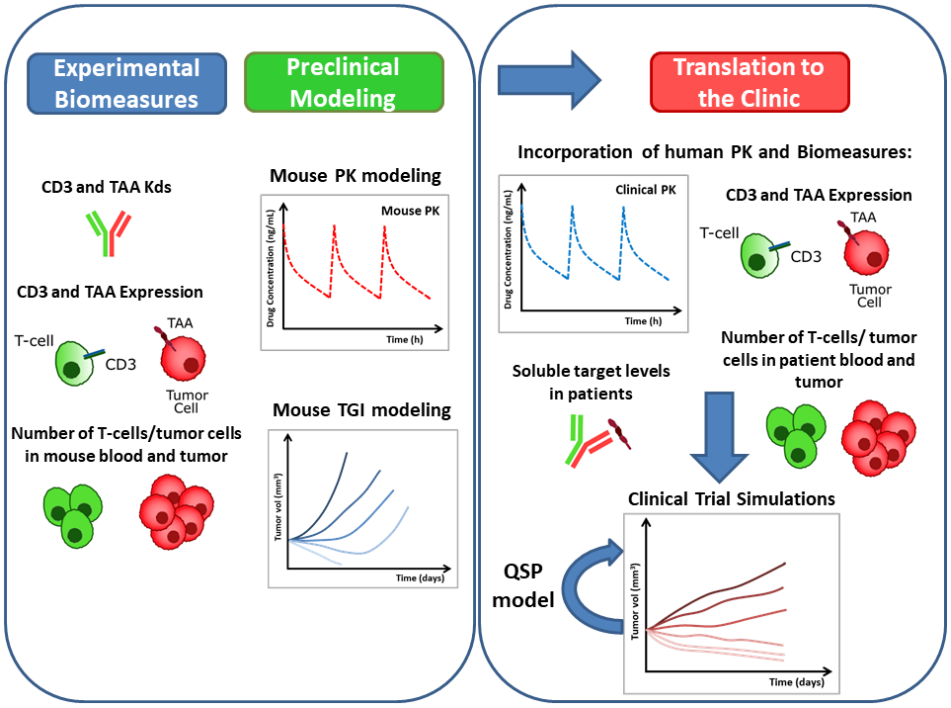

Figure 6: QSP model-based strategy for translating preclinical data for CD3 bispecific compounds to the clinic. 'Biomeasures' can be defined as system dependent parameters. TAA is tumor associated antigen.

6.7 Acknowledgements:

The author would like to thank Brian Peano, Mike Cinque, Ed Rosfjord, Tim Fisher, Konstantinos Tsaparikos and Hui Wang for generation of the mouse xenograft data for PF-06671008. In addition, many thanks to Hannah Jones, Wenlian Qiao and Jatin Narula for useful discussions and their critical review of this manuscript. PF-06671008 was discovered as part of a collaboration between Pfizer and Macrogenics, Inc.

References

1. Farkona S, Diamandis EP, Blasutig IM. Cancer immunotherapy: the beginning of the end of cancer? BMC Med. 2016;14:73.
2. Lameris R, de Bruin RC, Schneiders FL, van Bergen en Henegouwen PM, Verheul HM, de Gruijl TD, et al. Bispecific antibody platforms for cancer immunotherapy. Crit Rev Oncol Hematol. 2014;92(3):153-65.
3. Baeuerle PA, Reinhardt C. Bispecific T-cell engaging antibodies for cancer therapy. Cancer Res. 2009;69(12):4941-4.
4. Zimmerman Z, Maniar T, Nagorsen D. Unleashing the clinical power of T cells: CD19/CD3 bi-specific T cell engager (BiTE(R)) antibody construct blinatumomab as a potential therapy. Int Immunol. 2015;27(1):31-7.
5. Oak E, Bartlett NL. Blinatumomab for the treatment of B-cell lymphoma. Expert Opin Investig Drugs. 2015;24(5):715-24.
6. Zhu M, Wu B, Brandl C, Johnson J, Wolf A, Chow A, et al. Blinatumomab, a Bispecific T-cell Engager (BiTE((R))) for CD-19 Targeted Cancer Immunotherapy: Clinical Pharmacology and Its Implications. Clin Pharmacokinet. 2016;55(10):1271-88.
7. Root A, Cao W, Li B, LaPan P, Meade C, Sanford J, et al. Development of PF-06671008, a Highly Potent Anti-P-cadherin/Anti-CD3 Bispecific DART Molecule with Extended Half-Life for the Treatment of Cancer. Antibodies. 2016;5(1):6.
8. Cheung LW, Leung PC, Wong AS. Cadherin switching and activation of p120 catenin signaling are mediators of gonadotropin-releasing hormone to promote tumor cell migration and invasion in ovarian cancer. Oncogene. 2010;29(16):2427-40.
9. Paredes J, Stove C, Stove V, Milanezi F, Van Marck V, Derycke L, et al. P-cadherin is up-regulated by the antiestrogen ICI 182,780 and promotes invasion of human breast cancer cells. Cancer Res. 2004;64(22):8309-17.
10. Taniuchi K, Nakagawa H, Hosokawa M, Nakamura T, Eguchi H, Ohigashi H, et al. Overexpressed P-cadherin/CDH3 promotes motility of pancreatic cancer cells by interacting with p120ctn and activating rho-family GTPases. Cancer Res. 2005;65(8):3092-9.
11. Hardy RG, Tselepis C, Hoyland J, Wallis Y, Pretlow TP, Talbot I, et al. Aberrant P-cadherin expression is an early event in hyperplastic and dysplastic transformation in the colon. Gut. 2002;50(4):513-9.
12. Imai K, Hirata S, Irie A, Senju S, Ikuta Y, Yokomine K, et al. Identification of a novel tumor-associated antigen, cadherin 3/P-cadherin, as a possible target for immunotherapy of pancreatic, gastric, and colorectal cancers. Clin Cancer Res. 2008;14(20):6487-95.
13. Paredes J, Albergaria A, Oliveira JT, Jeronimo C, Milanezi F, Schmitt FC. P-cadherin overexpression is an indicator of clinical outcome in invasive breast carcinomas and is associated with CDH3 promoter hypomethylation. Clin Cancer Res. 2005;11(16):5869-77.
14. Stefansson IM, Salvesen HB, Akslen LA. Prognostic impact of alterations in P-cadherin expression and related cell adhesion markers in endometrial cancer. J Clin Oncol. 2004;22(7):1242-52.

15. Fisher TS, Hooper AT, Lucas J, Clark TH, Rohner AK, Peano B, et al. A CD3-bispecific molecule targeting P-cadherin demonstrates T cell-mediated regression of established solid tumors in mice. Cancer Immunol Immunother. 2018;67(2):247-59.
16. Chen X, Haddish-Berhane N, Moore P, Clark T, Yang Y, Li H, et al. Mechanistic Projection of First-in-Human Dose for Bispecific Immunomodulatory P-Cadherin LP-DART: An Integrated PK/PD Modeling Approach. Clin Pharmacol Ther. 2016;100(3):232-41.
17. Thurber GM, Dane Wittrup K. A mechanistic compartmental model for total antibody uptake in tumors. J Theor Biol. 2012;314:57-68.
18. Schmidt MM, Wittrup KD. A modeling analysis of the effects of molecular size and binding affinity on tumor targeting. Mol Cancer Ther. 2009;8(10):2861-71.
19. Thurber GM, Schmidt MM, Wittrup KD. Antibody tumor penetration: transport opposed by systemic and antigen-mediated clearance. Adv Drug Deliv Rev. 2008;60(12):1421-34.
20. Carpentier B, Pierobon P, Hivroz C, Henry N. T-cell artificial focal triggering tools: linking surface interactions with cell response. PLoS One. 2009;4(3):e4784.
21. Nicolas L, Monneret G, Debard AL, Blesius A, Gutowski MC, Salles G, et al. Human gammadelta T cells express a higher TCR/CD3 complex density than alphabeta T cells. Clin Immunol. 2001;98(3):358-63.
22. Klein L, Trautman L, Psarras S, Schnell S, Siermann A, Liblau R, et al. Visualizing the course of antigen-specific CD8 and CD4 T cell responses to a growing tumor. Eur J Immunol. 2003;33(3):806-14.
23. Haddish-Berhane N, Shah DK, Ma D, Leal M, Gerber HP, Sapra P, et al. On translation of antibody drug conjugates efficacy from mouse experimental tumors to the clinic: a PK/PD approach. J Pharmacokinet Pharmacodyn. 2013;40(5):557-71.
24. Simeoni M, Magni P, Cammia C, De Nicolao G, Croci V, Pesenti E, et al. Predictive pharmacokinetic-pharmacodynamic modeling of tumor growth kinetics in xenograft models after administration of anticancer agents. Cancer Res. 2004;64(3):1094-101.
25. Betts A, Keunecke A, van Steeg TJ, van der Graaf PH, Avery LB, Jones H, et al. Linear pharmacokinetic parameters for monoclonal antibodies are similar within a species and across different pharmacological targets: A comparison between human, cynomolgus monkey and hFcRn Tg32 transgenic mouse using a population-modeling approach. MAbs. 2018;10(5):751-64.
26. Del Monte U. Does the cell number 10(9) still really fit one gram of tumor tissue? Cell Cycle. 2009;8(3):505-6.
27. Kovacsovics-Bankowski M, Chisholm L, Vercellini J, Tucker CG, Montler R, Haley D, et al. Detailed characterization of tumor infiltrating lymphocytes in two distinct human solid malignancies show phenotypic similarities. J Immunother Cancer. 2014;2(1):38.
28. Mazor Y, Hansen A, Yang C, Chowdhury PS, Wang J, Stephens G, et al. Insights into the molecular basis of a bispecific antibody's target selectivity. MAbs. 2015;7(3):461-9.
29. Douglass EF, Jr., Miller CJ, Sparer G, Shapiro H, Spiegel DA. A comprehensive mathematical model for three-body binding equilibria. J Am Chem Soc. 2013;135(16):6092-9.
30. Verhamme IM. Fluorescent reporters of thrombin, heparin cofactor II, and heparin binding in a ternary complex. Anal Biochem. 2012;421(2):489-98.

31. Lever M, Lim HS, Kruger P, Nguyen J, Trendel N, Abu-Shah E, et al. Architecture of a minimal signaling pathway explains the T-cell response to a 1 million-fold variation in antigen affinity and dose. Proc Natl Acad Sci U S A. 2016;113(43):E6630-E8.
32. Duensing TD, Putten JP. Vitronectin binds to the gonococcal adhesin OpaA through a glycosaminoglycan molecular bridge. Biochem J. 1998;334 (Pt 1):133-9.
33. Jiang X, Chen X, Carpenter TJ, Wang J, Zhou R, Davis HM, et al. Development of a Target cell-Biologics-Effector cell (TBE) complex-based cell killing model to characterize target cell depletion by T cell redirecting bispecific agents. MAbs. 2018.
34. Mandikian D, Takahashi N, Lo AA, Li J, Eastham-Anderson J, Slaga D, et al. Relative Target Affinities of T-Cell-Dependent Bispecific Antibodies Determine Biodistribution in a Solid Tumor Mouse Model. Mol Cancer Ther. 2018;17(4):776-85.
35. Agoram BM, Martin SW, van der Graaf PH. The role of mechanism-based pharmacokinetic-pharmacodynamic (PK-PD) modelling in translational research of biologics. Drug Discov Today. 2007;12(23-24):1018-24.
36. Campagne O, Delmas A, Fouliard S, Chenel M, Chichili GR, Li H, et al. Integrated Pharmacokinetic/Pharmacodynamic Model of a Bispecific CD3xCD123 DART Molecule in Nonhuman Primates: Evaluation of Activity and Impact of Immunogenicity. Clin Cancer Res. 2018;24(11):2631-41.
37. Thurber GM, Schmidt MM, Wittrup KD. Factors determining antibody distribution in tumors. Trends Pharmacol Sci. 2008;29(2):57-61.
38. Bacac M, Fauti T, Sam J, Colombetti S, Weinzierl T, Ouaret D, et al. A Novel Carcinoembryonic Antigen T-Cell Bispecific Antibody (CEA TCB) for the Treatment of Solid Tumors. Clin Cancer Res. 2016;22(13):3286-97.
39. Leong SR, Sukumaran S, Hristopoulos M, Totpal K, Stainton S, Lu E, et al. An anti-CD3/anti-CLL-1 bispecific antibody for the treatment of acute myeloid leukemia. Blood. 2017;129(5):609-18.
40. Schropp J, Khot A, Shah DK, Koch G. Target-Mediated Drug Disposition Model for Bispecific Antibodies: Properties, Approximation and Optimal Dosing Strategy. CPT Pharmacometrics Syst Pharmacol. 2018.
41. Saber H, Del Valle P, Ricks TK, Leighton JK. An FDA oncology analysis of CD3 bispecific constructs and first-in-human dose selection. Regul Toxicol Pharmacol. 2017;90:144-52.
42. Yarbro CH, Frogge, Margaret Hansen, Goodman, Michelle , . Cancer Nursing: Principles and Practice. 6 ed: Jones & Bartlett Learning; 2005.

Supplemental Files:

Supplemental Figure 1: Goodness of fit plot for PF-06671008 PK model fitting in PBMC engrafted HCT-116 tumor bearing mice following IV administration at 0.05mg/kg and 0.5mg/kg. The cyan band represents the 95% prediction distribution.

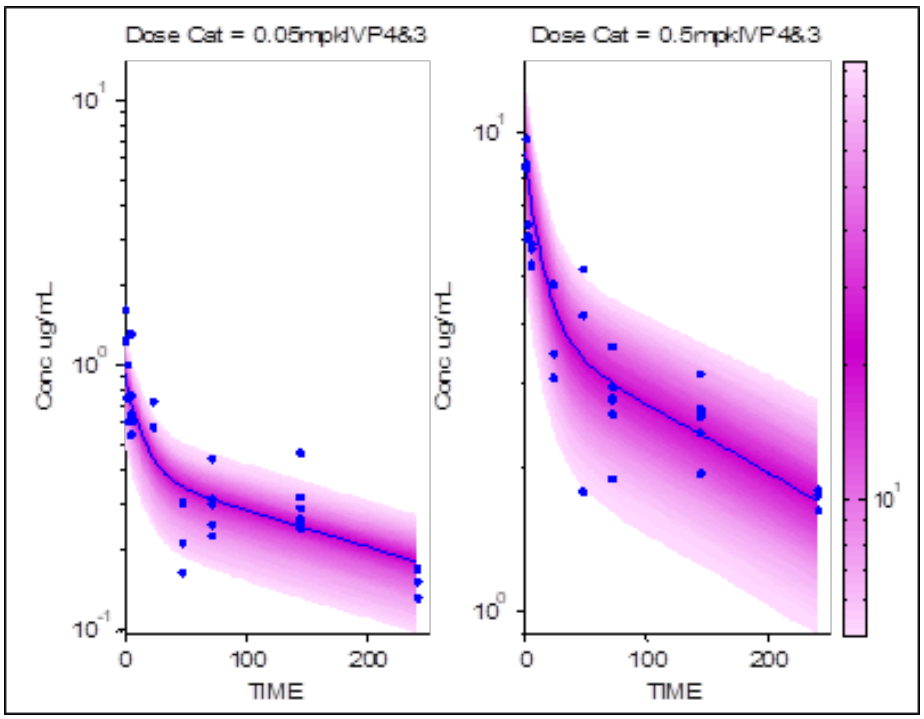

Supplemental Figure 2: CD3+ cells/ mg tumor versus time relationship following IV administration of PF-06671008 at **(A)** 10µg/kg, **(B)** 50µg/kg and **(C)** 500µg/kg. An exponential function was fitted to the data and the equations are shown on each plot. In **(D)** the slope of each line is plotted versus dose, and an empirical model is fitted to the data.

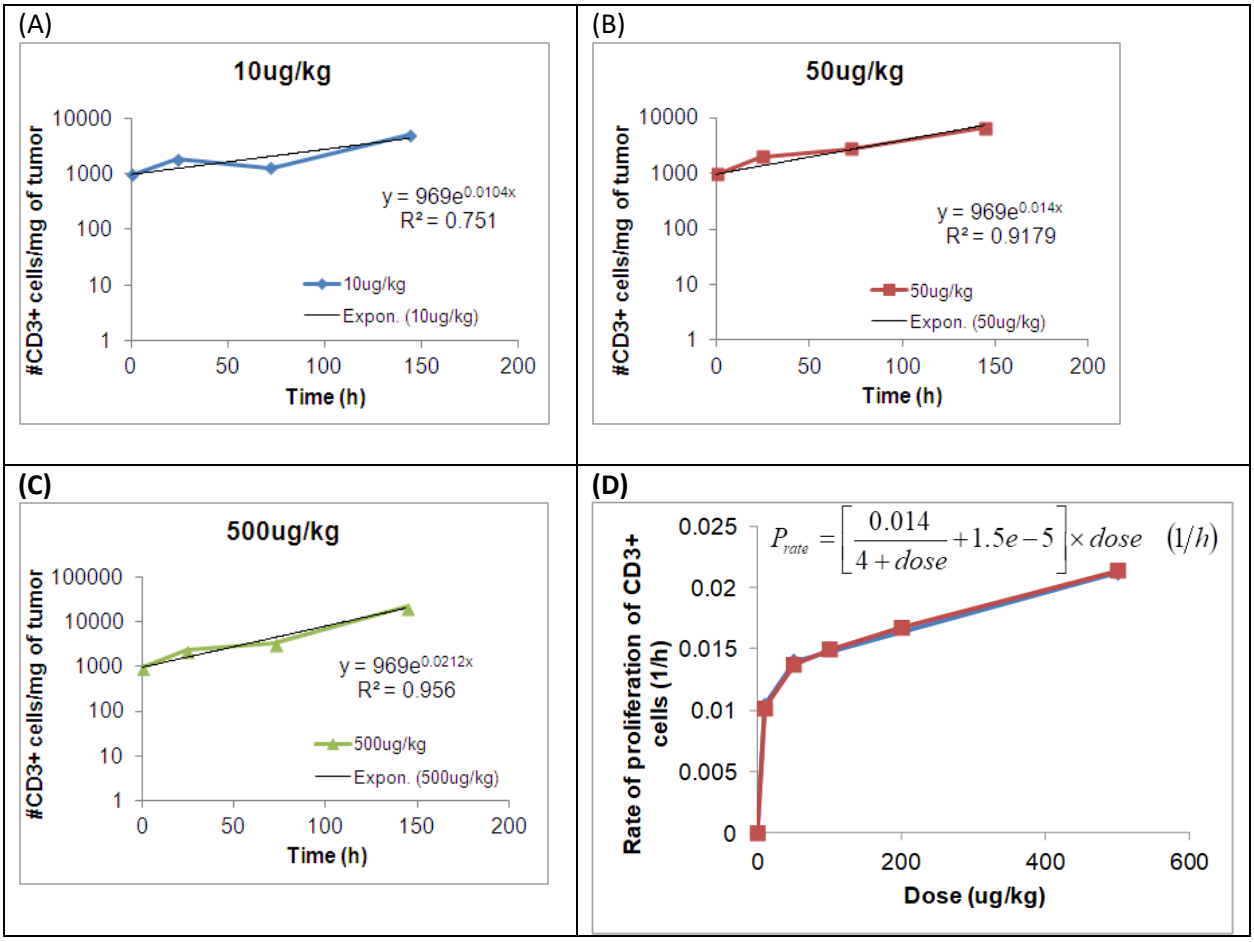

Supplemental Figure 3: Goodness of fit plots for (A) HCT-116 in T-cell engrafted model, (B) HCT-116 in T-cell adoptive transfer model, and (C) SUM-149 in T-cell adoptive transfer model.

Plots shown include: (i) observations versus model predictions using the population and individual parameters compared to line of unity and (ii) visual predictive checks of tumor volume (mm3) data and model prediction versus time at each dose level. The cyan band represents the 95% prediction distribution.

(A)

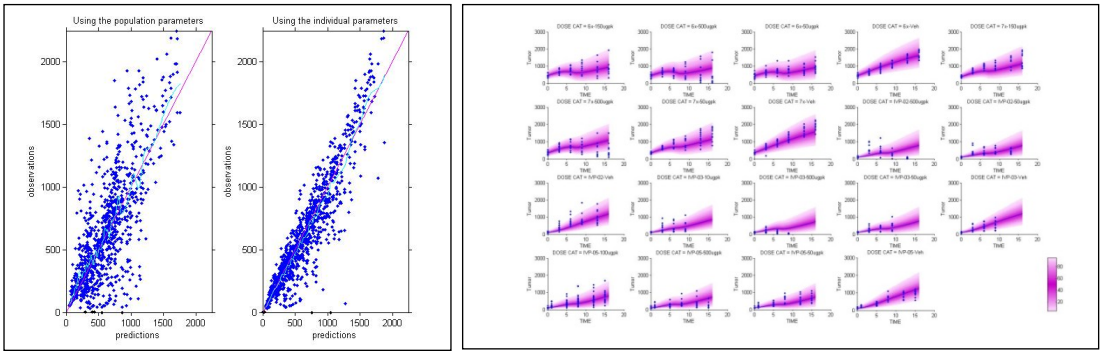

(B)

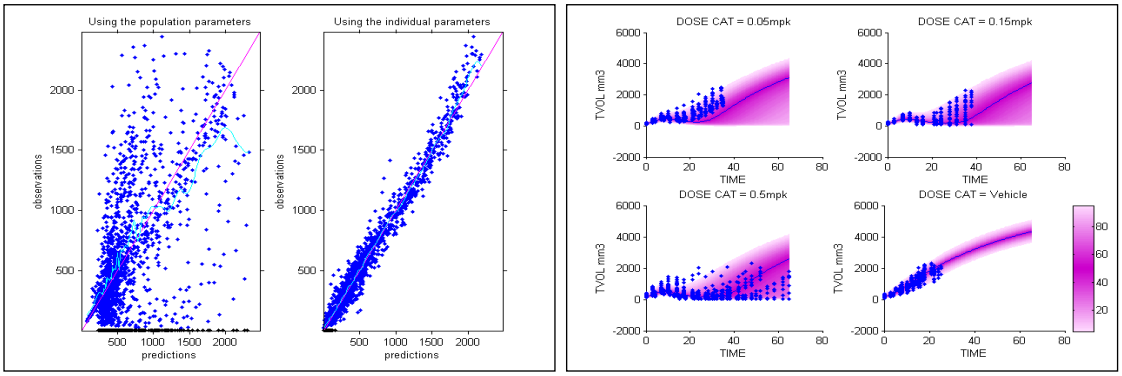

(C)

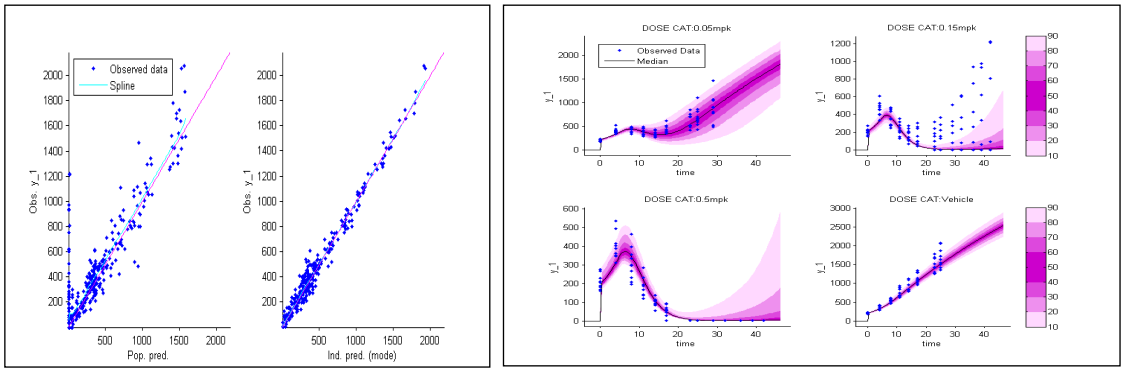

Supplemental Figure 4: Model simulated tumor trimer concentrations following IV infusion of PF-06671008 at 0.01, 0.06, 0.3, 1.8 and 10mg/kg QW to cancer patients. At doses of >1.8mg/kg predicted tumor trimer concentrations start to decrease with increasing dose, representing the bell-shaped relationship.

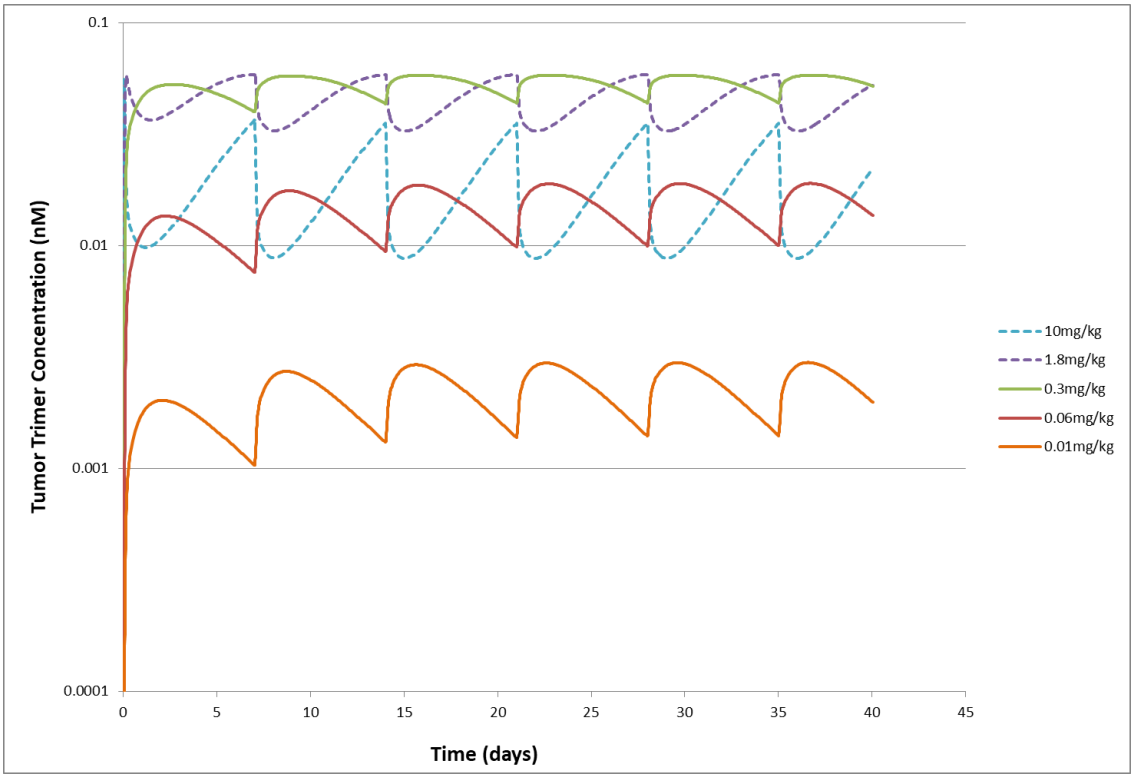

Chapter 7

Mechanistic quantitative pharmacology strategies for the early clinical development of bispecific antibodies in oncology

Alison Betts and Piet H. van der Graaf

Clinical Pharmacology & Therapeutics 108(3):528-541 (2020).

7.1 Abstract

Bispecific antibodies (bsAbs) have become an integral component of the therapeutic research strategy to treat cancer. In addition to clinically validated immune cell re-targeting, bsAbs are being designed for tumor targeting and as dual immune modulators. Explorative preclinical and emerging clinical data indicate potential for enhanced efficacy and reduced systemic toxicity. However, bsAbs are a complex modality with challenges to overcome in early clinical trials including selection of relevant starting doses using a minimal anticipated biological effect level (MABEL) approach and predicting efficacious dose despite non-intuitive dose response relationships. Multiple factors can contribute to variability in the clinic including differences in functional affinity due to avidity, receptor expression, effector to target cell ratio and presence of soluble target. Mechanistic modeling approaches are a powerful integrative tool to understand the complexities and aid in clinical translation, trial design and prediction of regimens and strategies to reduce dose limiting toxicities of bsAbs. In this tutorial the use of mechanistic modeling to impact decision making for bsAbs is presented and illustrated using case study examples.

7.2 Introduction

Cancer is a complex, multifactorial disease. Crosstalk between signaling cascades and multiple mediators of tumor survival and immune evasion exist. Genetic alterations lead to heterogeneity in tumor cell antigen expression within and between patients. Acquisition of resistance to therapy is associated with upregulation of alternative receptors as well as pathway switching between receptors. Overall, this means that specific targeting of a single receptor is often insufficient for efficacy and standard of care consists of combinations of therapies to kill tumor cells (1). However, development of individual drugs for a combination therapy can be a costly and time-consuming process requiring separate manufacturing processes and filing of the safety of each antibody component separately (2, 3).

During the past decade, advances in protein engineering have resulted in the ability to robustly and cost effectively synthesize bispecific antibodies (bsAbs) as an alternative to combination therapy or use of mixtures (4). This has led to an explosion of bispecific antibodies in drug development- currently there are 57 bsAbs in clinical trials in cancer patients (5), with a large diversity in formats (6). Thus far, blinatumomab (Blincyto, Amgen Inc.) is the only bsAb approved in oncology (7). Blinatumomab is a CD19/CD3 bispecific T cell engager (BiTE®) which was initially approved in 2014 for Philadelphia chromosome (Ph)-negative relapsed or refractory (r/r) B-cell precursor acute lymphoblastic leukemia (ALL) in adults (8). Since then it has gained approval for treatment in pediatric patients with ALL and for minimal residual disease positive B-cell precursor ALL, where it is the first FDA approved treatment for this specific patient population. Despite the success of blinatumomab, there remains many opportunities to improve this modality in new generation bsAbs. For example, blinatumomab has a boxed warning due to cytokine release syndrome (CRS) and neurological toxicities experienced by patients (8). In addition, the small structure of blinatumomab and lack of an Fc domain leads to accelerated clearance and short half-life in patients, such that a continuous infusion regimen is required (9). This has opened the door to an evolution of approximately 100 different bispecific formats varying in size,

arrangement, valency, flexibility and geometry of their binding modules, as well as in their distribution and pharmacokinetic (PK) properties (6). In addition to immune cell re-targeting, bsAbs have the capacity to simultaneously target multiple disease pathways, releasing the potential for attractive new therapies with enhanced efficacy and tumor selectivity leading to reduced systemic toxicity and improved therapeutic index (TI). To this end, bsAbs are being utilized for several different applications in oncology, which are summarized below and illustrated in **Figure 1**.

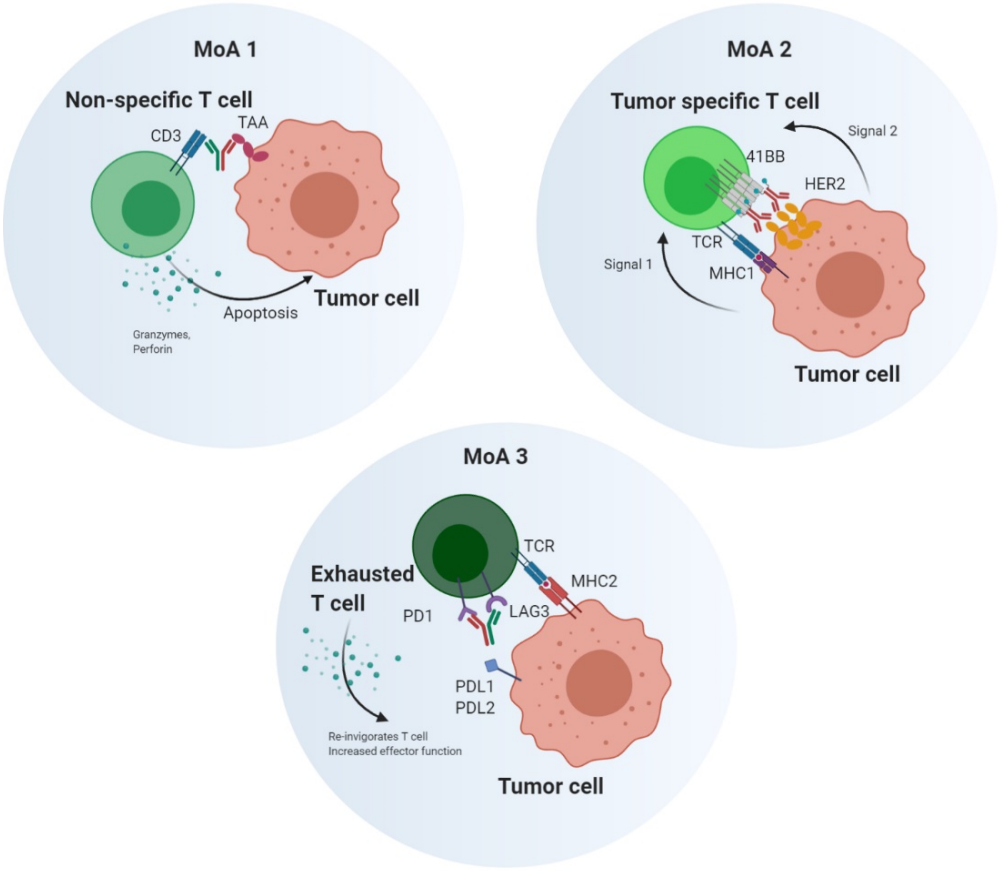

Figure 1: Mechanism of action (MoA) of bsAbs. MoA 1- CD3 T cell engagers. These bsAbs bind to CD3 expressed by the T cell and a specific antigen expressed by the tumor cell, resulting in the formation of an immune synapse. This stimulates the T cell and 're-directs' cytotoxicity against the tumor cell. MoA 2- Tumor targeting. These bsAbs direct binding towards the tumor by binding to a specific antigen on the tumor cell and to an immune receptor expressed on tumor infiltrating T cells (or other immune cells). For example, a bsAb binding to HER2 on tumor cells and 4-1BB on T cells is shown, which can result in a potent anti-tumor immune response. MoA 3- Targeting multiple immune modulatory receptors. These bsAbs can bind to different targets modulating immune responses, thus allowing combined biological effects and synergies. For example, a bsAb targeting PD-1 and LAG-3 expressed on exhausted T cells and/or TILs is shown which inhibits the immunosuppressive mechanisms associated with these targets.

Although bsAbs have great potential, their clinical development is complex with many inherent challenges. To start with, it is difficult to translate from preclinical efficacy studies, which may be

conducted in immunodeficient mice engrafted with human cancer cells and immune cells, or with immune competent syngeneic mice engrafted with human cancer cells using surrogate murine antibodies, or in transgenic mice to predict clinical efficacy. Many bsAbs in oncology have immune agonistic properties and a MABEL approach is required for selection of clinical starting doses. Selection of clinical starting dose is highly dependent upon the type of in vitro assay chosen to determine MABEL and can result in selection of overly conservative doses and many rounds of dose escalation before reaching efficacious doses in the clinic. In addition, the efficacious dosing regimen of the two targets cannot be independently controlled for a bsAb, as it would for a combination therapy of two monospecific antibodies. As a result, it may be challenging to optimize target engagement for two targets. For example, combination of a binding domain for an immune agonist with an immune antagonist would require different levels of target engagement necessitating different PK profiles from pulsatile to complete exposure. There are many factors impacting variability in the clinic including affinity of the individual arms, potential for avidity, target expression, presence of soluble target and PK, to name a few (**Table 1**). In addition, key safety concerns such as CRS require to be minimized and managed in the clinical setting.

The inherent complexity of bsAbs lends itself well to the use of mathematical modeling and simulation, in order to map out the mechanistic pathways and consider the impact of multiple variables. Mechanistic approaches, such as quantitative systems pharmacology (QSP) models, combine computational modeling and experimental data to examine the relationships between a drug, the biological system, and the disease process (10, 11). These models describe the biophysics of binding of bsAbs to their membrane receptors and soluble target in different compartments (e.g. blood, periphery, tumor, immune tissues) using a system of ordinary differential equations. The receptor binding interactions can then be linked to downstream pharmacodynamics of response and efficacy or toxicity. To do this, QSP models integrate data from diverse sources and assays, including drug assays (e.g. K_ds or EC_{50}s), system parameters (receptor expression, internalization rates), in vitro experimental data, preclinical in vivo studies, and clinical data. A quantitative framework is assembled which can provide mechanistic understanding of bsAb function, enabling optimal experimental design and faster data interpretation. The model framework can be used at early stages to aid in the identification of optimal drug properties for next generation molecules, including optimal target, epitopes and drug format. Once a lead compound has been selected, the QSP model can be used to translate from preclinical in vitro and in vivo studies to the clinic, to inform clinical study design including prediction of clinical starting dose, efficacious dose and regimen.

In this tutorial, the mechanism of action of bsAbs in oncology drug development will be discussed, and specific clinical pharmacology challenges in early stage clinical development will be considered and reviewed. The use of mechanistic modeling and simulation strategies to address these challenges will be presented, supported by case studies which exemplify the application and impact of mechanistic modeling in the drug development process. Note that challenges and modeling strategies for bsAbs in later stage clinical development are out of the scope of this tutorial and will not be discussed.

Table 1: Variables impacting efficacy and toxicity of bispecific antibodies

Variable (Unit)	Quantitative method of analysis	Potential range	Examples		Considerations
Drug properties of bsAbs					
Affinity for each target (Kd; nM)	Surface plasmon resonance (SPR) (e.g. Biacore, Kinexa)	pM- nM	Blinatumomab: CD19 1.49nM/ CD3 260nM (9) Solitomab: Epcam 16nM /CD3 77nM (74) AMG330: CD33 8.0nM/ CD3 5.1nM (75) PCad-LP-DART: Pcad 0.47nM/ CD3 11.4nM (13) PRS-343: HER-2 0.3nM/ 41BB 5nM (19) MGD-013: PD1 1.0/ LAG3 0.1 nM (76)		For CD3 bsAbs, a relatively higher affinity for the TAA compared to CD3 may improve tumor localized T-cell activation and reduce systemic CD3 targeting and toxicity.
Avidity (cross linking chi-factor)	On cell binding by ELISA and/or flow cytometry & QSP model	1e2- 1e6 (46)			May be a requirement for tumor targeting to prevent on target/ off tumor toxicity.
PK: elimination half-life (hours- days)	Ligand binding assay. Occasional mass spectrometry.	hours-days	Typical mAb: 16-21 days (77) Blinatumomab (BiTE): 2 hr (9) Pcad-LP-DART: 1 day (13) Solitomab (BiTE): 4.5 hr (70) AFM-13: 8.7-19.2 hr (15) PRS-343: 5 days (20)		Dictated by presence of an Fc domain. Soluble target may act as a peripheral sink. Potential for target mediated drug disposition.
System properties of bsAb targets					
			Tumor cells[1]	**Immune cells[2]**	
Receptor expression (receptors/cell)	Flow cytometry: Phycoerythrin (PE) conjugated antibodies (1:1) and calibration beads (QuantiBRITE or Bangs®) to determine antigen binding capacity	100: limit of detection 1e3: low 1e4: medium 1e5–1e6: high	PDL1: 1e4 (78) HER2 (different cancers): 2e4 - 1e6 (79, 80) BCMA (Multiple Myeloma): 1479 (42-1.4e4) (81) Pcad: 2.8e4 (13) Epcam: 1.1e5 (74) CD19 (B cell leukemias): 1-3.8e4	CD3 (T cells): 5e4-1e5 (82) CD16 (NK cells): 7.9e4 ± 3.0 (82) 3.64e5 (median) (83) 41BB (monocytes and other immune cell types) ~1e3 (84) PD1 (TILs): 5e4 (1e4 – 1e5) (78)	Is the receptor constitutively expressed or inducible? What % of cells express the receptor (heterogeneity of expression)? Quantify across tissues, species and in disease.

Soluble target in the central compartment **(nM)**	Mass spectrometry or ELISA	<1nM-100nM	HER2: 0.15nM (upper limit of normal)-22µM (MW = 100kDa) (49) BCMA: 16nM- 94nM (MW = 5.3kDa) (53) Pcad: 1.1 nM (0.4- 4.1) (13) PDL1: 0.05 – 0.139nM (MW = 25kDa) (Durvalumab BLA) PD1 (pancreatic and NSCLC patients): 0.00143- 1.85 nM (MW=14kDa) (85, 86)	Variable across species. May be higher in patients expressing high levels of target. For HER2 and BCMA correlates with efficacy.
Internalization/ turnover rate	Amnis FACS	mins-hours	Pcad: 0.1728 1/d (13)	

1- Expression on human tumor cells (where possible). 2- Expression on human whole blood lymphocytes

7.3 Mechanism of action of bispecific antibodies in oncology

1. Engagement of immune cells (adaptive immune response)

The majority of bsAbs in clinical trials are CD3 T cell engager (TCE) molecules. These bsAbs bind to CD3 in the T cell receptor/ CD3 protein complex expressed on the surface of T cells and to a tumor associated antigen (TAA) on the tumor cell surface. When both CD3 and TAA are engaged, the proximity of the T cell and the tumor cell result in the formation of an immune synapse, stimulation of the T cell and 're-direction' of cytotoxicity against the tumor cell (**Figure 1, MoA 1**). CD3 bsAbs have minimal tumor cell killing on their own (12), and efficacy and on-target toxicity are driven by the formation of a trimolecular complex (hereafter trimer) between the bsAb, T cell and tumor cell (13).

CD3 bsAbs have exhibited clinical validation for hematological malignancies through blinatumomab, and several other TCEs in clinical trials. These include BiTE®s, half-life extended diabodies/ antibody fragments and full length heterodimeric IgGs targeting TAAs including CD20, BCMA, CD33, CD19, CD123 and others. There are a smaller number of CD3 bsAbs in clinical development for solid tumors, targeting for example HER2, DLL3, gpA33 and CEA for metastatic breast, small cell lung, colorectal and other solid tumor indications, respectively. Blinatumomab and other CD3 bsAbs are reviewed extensively in the work by Yuraszeck *et al.* (14).

2. Engagement of immune cells (innate immune response)

In addition to T cells, other effector cells or immune cell subsets can also be recruited to tumor cells. For example, bsAbs have been developed to target natural killer (NK) cells which are potent cytotoxic lymphocytes of the innate immune system. An example of an NK cell re-director is AFM13, a tandem diabody construct targeting CD16 on NK cells and CD30 on tumor cells (15). In a phase 1 trial in patients with r/r Hodgkin's lymphoma, treatment with AFM-13 resulted in activation of NK cells and a decrease in soluble CD30 in peripheral blood, and 3 out of 26 patients had a partial response (15). AFM-13 is now in a phase 2 trial for patients with Hodgkin's lymphoma.

3. Tumor targeting

These bsAbs focus their immune-activating pharmacologic effects to the tumor environment, thereby achieving improved efficacy as well as reduced systemic immune-related adverse effects (**Figure 1, MoA 2**). They are an emerging class of bsAbs which are mainly in the preclinical phase. However, explorative preclinical and emerging clinical data suggest great potential (16).

4-1BB is a potent co-stimulatory receptor which is upregulated on effector T cells, and upon stimulation promotes cytotoxic function as well as induction of immunological memory (17). It is a good candidate for tumor targeting as systemic activation can result in severe toxicity. For example, the initial clinical development of the agonistic 4-1BB monospecific antibody urelumab was terminated due to fatal hepatotoxicity, with a maximum tolerated dose of 0.1 mg/kg Q3w (18). A 4-1BB/ HER2 bispecific molecule PRS-343 is designed to facilitate T-cell co-stimulation by tumor-localized, HER2-dependent 4-1BB clustering and activation (**Figure 1**) (19). In a phase 1 study in HER2+ cancer patients, PRS-343 demonstrated single-agent anti-tumor activity, including partial responses, and was well tolerated at doses up to 8mg/kg Q2w (20).

Another popular target for tumor focused bsAbs is CD47, an innate checkpoint receptor which is widely expressed on many tumor types. Interaction with its receptor SIRPα on macrophages and dendritic cells (DCs) acts as a 'don't eat me signal' enabling tumor cells to evade phagocytosis and clearance. Blockade of CD47 in preclinical studies using monospecific antibodies has resulted in encouraging efficacy. However, CD47 is expressed on the membranes of all cells in mice and humans, including red blood cells, which can act as a substantial 'antigen sink', resulting in limited systemic use of CD47 inhibitors due to side-effects. BsAbs which target tumor specific receptors with high binding affinity on one arm, and CD47 with weaker affinity on the other arm are a popular strategy for increasing tumor cell targeting and enhancing therapeutic index. A bispecific antibody targeting PD-L1 and CD47 (21), showed significantly enhanced tumor targeting and therapeutic efficacy versus monotherapy. In addition, as critical innate and adaptive checkpoints on tumor cells, CD47 and PD-L1 coordinate to suppress immune sensing.

4. Combining checkpoint inhibition and immune modulating receptors

BsAbs are also being used to combine checkpoint inhibitors (CPIs) or for dual targeting of CPIs and co-stimulators of the immune response, or inhibitors of exhaustion markers (**Figure 1, MoA 3**). These compounds may combine the activity of the original drugs, but also allow for additional synergies and unexpected novel biological effects that could not be achieved by combining the corresponding monospecific antibodies. A potential disadvantage of such compounds may be the risk of toxicity due to strong immune activation. Most of these bsAbs block two inhibitory checkpoint pathways, such as PD-1 or PD-L1 combined with other immunosuppressive targets such as TGF-β, LAG-3 and TIM-3. For example, MGD-013 is a bsAb based on the dual affinity re-targeting (DART®) platform which targets PD-1 and LAG-3, which are both expressed on exhausted T cells and tumor infiltrating lymphocytes (TILs) (**Figure 1**). Inhibition of these targets has been shown to exert a synergistic effect on tumor immunity in mice (22). MGD-013 is currently in phase 1 clinical trials. There are many other dual immunomodulator bsAbs in preclinical development including MCLA-134 which targets PD-1/ TIM-3 and XmAb-20717 which

targets CTLA-4/ PD-1 (16). The mechanism of action of T cell engagers, tumor targeting bsAbs and bsAbs targeting multiple immune modulating receptors are shown pictorially in **Figure 1**.

7.4 Early clinical pharmacology challenges for bispecific antibodies

1. Selection of clinical starting dose: how to define MABEL

To ensure maximum clinical benefit of phase 1 dose escalation clinical trials, particularly for patients in early dose cohorts, it is important to select a safe starting dose and then rapidly escalate to the efficacious dose. To select starting dose of bsAbs, including CD3 bsAbs, a MABEL approach is recommended due to their immune agonistic properties (14). The principal of MABEL is that it is better to start with the lowest dose believed to be active, rather than the highest dose thought to be safe. However, MABEL can be difficult to interpret, and this can result in selection of a starting dose that is far below doses required for efficacy in patients and consequently dose escalation trials can take several years (23). For example, Amgen's BCMA BiTE (AMG-420) entered clinical trials in 2015 with a starting dose of 0.2 μg/ day. The first positive clinical results were reported 3 years later in patient cohorts that were dosed several logs higher than the initial cohort, with a dose of 400 μg/ day finally selected as the efficacious dose for further investigations (24). Another example is Roche's CEA-TCB, a novel T-cell-bispecific (TCB) antibody targeting CEA, which started Phase 1 clinical trials in 2014, at a starting dose of 52 μg (25). In the dose expansion cohort doses up to 600 mg have been evaluated over a period of 5 years (26).

An important issue is the approach used for determining MABEL of CD3 bsAbs. Traditionally MABEL is based upon doses which achieve receptor occupancy (RO) of approximately 10 – 20%, however this approach is not recommended for CD3 bsAbs as they are immune agonists with low and variable RO required for efficacy (27). The most popular method is to use a PK driven approach, where the recommended clinical starting dose is calculated by setting the predicted drug exposure below the EC_{20}, which is selected as a threshold from in vitro assays (27, 28). This method is easy to accomplish, and regulatory agencies typically accept proposed starting doses corresponding to 10- 30%, or even in some cases 50% pharmacological activity (27), depending the target biology and other factors including the proposed application, available data and impact of the model based decision. However, this approach can be misleading as it is calculated using bsAb concentration rather than trimer concentration which is required to drive efficacy and toxicity (13). It is highly dependent upon the experimental conditions of the in vitro assay used to determine EC20, which can result in substantially different MABEL doses. These assays include cytokine release, cytotoxicity and T-cell activation/ proliferation assays which are commonly used to determine bsAb activity. In order to observe activity in vitro in short time frames, the assays are generally completed under non-physiological conditions, including effector: target (E:T) cell ratios of > 5:1 which are significantly higher than those observed in patient tumors and use cell lines which over-express target. In addition, often the most sensitive assay is selected for MABEL determination. Depending on the in vitro experimental conditions, an overly conservative in vitro threshold can be selected, which may result in a starting dose which results in many rounds of sub-efficacious dose escalation, or a starting dose could be selected which is too close to the

efficacious dose such that it gives safety concerns. A better method is to use a mathematical modeling approach for selection of clinical starting doses for bsAbs, which can integrate in vitro data generated under different experimental conditions to estimate a single EC_{20} based on trimer concentrations, rather than bsAb concentrations. The mathematical model can be translated to the clinic and the in vitro trimer EC_{20} can be used as a threshold to predict a relevant clinical starting dose, which is independent of experimental conditions. A QSP modeling approach to MABEL is discussed in detail below.

2. Determining clinical efficacious dose: non-intuitive dose-response relationships of bsAbs in early clinical trials

Historically, in oncology drug development, efficacy has been assumed to be dose related and cancer drugs are escalated to the maximum tolerated dose (MTD) in phase 1 clinical trials, which is subsequently defined as the efficacious dose (29). However, bsAbs have a complex mechanism of action, which can make dose response relationships non-intuitive and difficult to rationalize. For example, a specific complexity of CD3 bsAbs is efficacy and on-target toxicity are driven by trimer formation between the bsAb, T cell and tumor cell (13). A bell-shaped concentration versus response relationship can be observed which is a well described phenomenon for ternary complexes (30-32). When bsAb concentrations are low, conditions favor bivalent binding and the formation of trimers. As bsAb concentration is increased, an optimal concentration is reached for trimer formation. If additional bsAb is added, it will be in excess and favor monovalent binding to form dimers between bsAb and T cells or bsAb and tumor cells. This results in decrease in response as dimers cannot trigger cytotoxicity (**Figure 2**). The width of the bell shape, or efficacy window of the bsAb (**Figure 2**), will depend upon variables impacting trimer formation, such as receptor expression, E: T ratio and the binding affinity of the bsAb for CD3 and its specific tumor antigen (33). As a result, the bell-shaped relationship will be different for every bsAb and could be different for every patient treated with a given bsAb. This could potentially impede interpretation of phase 1a dose escalation trials and impact selection of doses for phase 1b expansion cohorts, or even recommended phase 2 doses. For example, it may be difficult to determine whether a dose close to projected efficacious dose is ineffective due to being on the right-hand side of the bell-shaped response and when to stop dose escalation. The bell-shaped relationship has been confirmed preclinically for CD3 bsAbs (34, 35) and mechanistic modeling can be used to predict it and to optimize variables to minimize its impact on efficacy and toxicity. For example, Schropp *et al.* developed an equilibrium binding model for bsAbs and investigated how changes in receptor and bsAb concentration impacted the formation of the trimolecular complex and the efficacy window of the bell-shaped curve (33).

In addition to CD3 bsAbs, the bell-shaped relationship could affect other bsAbs that form ternary complexes by binding *in trans* to link effector and target cells, including NK cell engagers, tumor targeting agents and dual immunomodulators. To optimize drug dosing and scheduling in the clinic, a rational dose selection approach using mathematical modeling is recommended, which will account for the variables discussed above. This mathematical framework could be updated with emerging clinical data (such as PK, or receptor expression data) to refine dosing protocols in real time and to help in the interpretation of complex data.

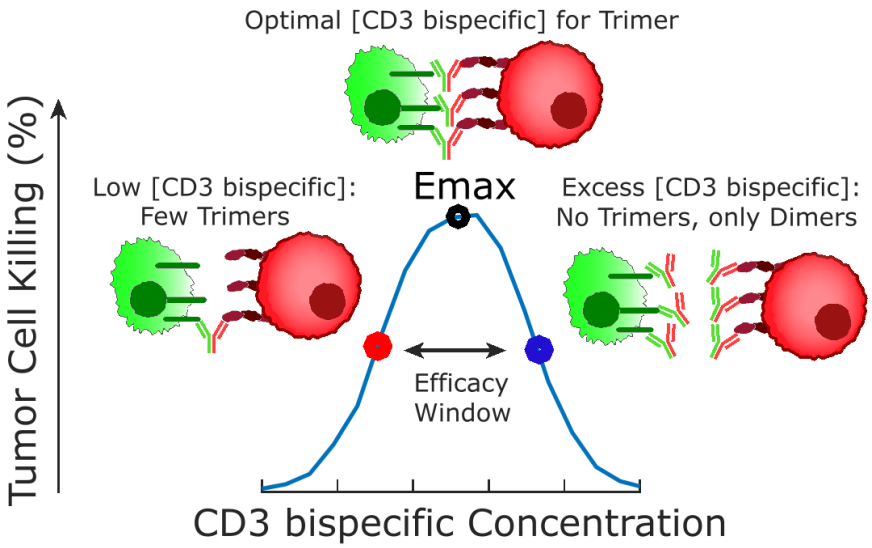

Figure 2: Bell-shaped concentration response relationship observed for CD3 bispecific antibodies.

3. Specific features of bsAbs impacting variability in clinical response

A major challenge in oncology drug development is interindividual variability in drug response, which affects both efficacy and toxicity. BsAbs are a complex drug modality, binding to two distinct targets, often with two separate mechanisms of action. As a result, many different variables can impact the concentration versus response and toxicity relationship for bsAbs in individual patients. These variables can be categorized as 'drug specific' and 'system specific' parameters (36). Drug specific parameters typically include pharmacologic parameters such as affinity and avidity, and PK parameters including clearance, volume of distribution and elimination half-life. System specific parameters include receptor expression, concentrations of soluble target, receptor internalization/ turnover rates and E:T ratio. In **Table 1** some of these variables are listed along with quantitative methods of analysis and ranges of values possible for bsAbs and their targets. The PK of bsAbs has already been reviewed and will not be covered here (37). Also, variability due to co-morbidities, comedications and disease severity are other important factors influencing variability in clinical responses, especially at later stages of clinical development, which are out of scope in this tutorial. Further discussion on some of the unique features of bsAbs which may impact response across patients are reviewed below.

Impact of avidity: A key variable of bsAbs, especially those with multi-valency, is their ability to have enhanced functional affinity due to avidity (16, 38). Affinity is defined as the strength, expressed in thermodynamic terms, of the binding interaction between a single antigen and a single region of the mAb (38). Avidity, however, is the accumulated strength of multiple affinities summed up from multiple binding interactions and is commonly referred to as a functional affinity (38). The strength of avidity is likely a function of tethering producing an increased local

concentration of the antibody due to restriction of diffusion to the cell membrane, and epitope- and format-specific steric variability (39).

Avidity arising from binding of a bsAb to two receptors on a target cell may lead to greater efficacy than a combination with two antibody molecules, each binding only a single receptor (40). Avidity often correlates with receptor expression (39-41), and it is therefore believed that the avidity effect could, in some circumstances, be exploited to reduce systemic toxicity, due to the higher density of receptors on tumor cells leading to enhanced avidity of bsAbs compared with normal cells expressing a lower concentration of receptors (42). To benefit from the potential advantages of avidity, protein engineers are modulating bsAbs to have weaker affinity for their receptors in order to minimize normal tissue binding, without impairing the potency for target cells (43). This is seen in nature, where T cells can distinguish between high and low antigen expressing cells by means of relatively low affinity T cell receptors that can still achieve high affinity binding to target cells expressing high levels of target antigen (44). However, these are complex interactions and the interplay of factors such as affinity, avidity and format valence in relation to the ability of a bsAb to promote target selectivity is not yet well understood (42). Since avidity can vary with receptor expression, it is likely to result in different observed functional affinities/ potencies of bsAbs across patients. To understand avidity and predict its variability and impact on tumor targeting, efficacy and potential to reduce systemic toxicity, it is important that it can be quantified. First of all, the intrinsic affinity of the monovalent interaction in equilibrium binding experiments should be determined (41). The avidity could then be predicted using a mathematical model of the bivalent interaction and related to receptor expression, ratios of targets and affinity under different conditions relevant to the clinic (39-41, 45, 46)

Impact of soluble target: Another factor which can impact the PK/PD of bsAbs and lead to patient variability in the clinic is the presence of soluble target, or the shed ectodomain (ECD) of a membrane bound target, which can act as a significant sink for bsAbs restricting the amount of drug free to distribute to the tumor (47) and potentially impacting efficacy (48). This is especially prevalent for bsAbs in immune oncology which are often potent activators of the immune system requiring low doses for efficacy (27). As a result, circulating concentrations of soluble target/ ECD are not saturated at dose levels administered in clinical trials. Levels of soluble target/ ECD can also vary significantly across species, complicating preclinical to clinical translation. They are often higher in patients who over-express tumor target and are variable across patients, impacting doses driving efficacy and toxicity. For example, high levels of shed HER2 ECD have been detected in cancer patients (2.21 μg/mL) compared with those in healthy subjects (< 15 ng/mL) (49). For the anti-HER2 antibody trastuzumab, high levels of serum HER2 ECD are associated with rapid clearance and decreased benefit from trastuzumab therapy (49-51). BCMA was found to be shed and is elevated in multiple myeloma (MM) patients, correlating with disease status and survival (52). Ghermezi *et al.* showed that serum BCMA (sBCMA) was significantly lower in 43 aged matched healthy donors (median 36.8 ng/mL), than 46 patients with smoldering MM (median 88.9 ng/mL) and 44 patients with active MM prior to treatment (median 505.9 ng/mL) (53). There was significant variability in each group; for example, the active untreated group had sBCMA levels ranging from undetectable to approximately 5,500 ng/mL (53). sBCMA levels were found to directly correlate with response to treatment and clinical

status. Specifically, patients with complete response had significantly lower sBCMA levels (median 38.6 ng/mL) than those with partial response (median 99.7 ng/mL) or non-responsive disease (median 195.3 ng/mL) (53). There are several bsAbs targeting HER2 and BCMA in clinical development and levels of shed target are likely to impact patient variability to drug treatment and resulting efficacy. For targets less well understood, measurement of soluble target levels is also recommended to de-risk impact on efficacy and toxicity. For the CD3 bsAbs, binding to circulating T cells expressing CD3 can also act as significant sink for the drug. Leong *et al.* showed that high affinity CLL1/CD3 TCEs were more potent in vitro but had comparable potency to lower affinity variants in vivo (54). This was due to differences in PK, with higher affinity variants showing higher clearance in vivo due to binding to CD3 on circulating T cells. Given the ability to impact the therapeutic efficacy of bsAbs, binding to soluble target needs to be accounted for in all experimental systems and species in order to provide meaningful PK and dose predictions. QSP modeling is an ideal way to do this and will be discussed later in this tutorial.

Impact of target burden: Target burden is an important factor which can vary substantially across patients and correlate with doses driving efficacy/ toxicity and the likelihood of clinical success of bsAbs. Target burden is a function of the number of receptors expressed per cell and the number of cells. For bsAbs, targets can be expressed on both tumor cells and immune cells, and can vary substantially depending on tumor burden, E:T ratio, disease status and patient specific factors such as prior treatment. Immune targets can also be inducible with potential to vary during treatment in response to therapy. In addition, tumor targets can display significant intratumoral heterogeneity resulting in bsAbs only targeting a sub-population of cells where receptor is expressed (55). An analysis of the CEA/CD3 TCB showed that activity strongly correlated with CEA expression, with higher potency observed in high CEA expressing tumor cells with a threshold of approximately 10,000 CEA binding sites per cell required for efficient tumor cell killing (44). In line with this, the CEA TCB was unable to induce T cell mediated killing of primary epithelial cells expressing less than 2000 CEA binding sites per cell in vitro (44). The measurement of target burden is therefore recommended as an important factor impacting the success of bsAb clinical trials and may require adaptation of clinical trial design to include comprehensive longitudinal tissue collection protocols. Incorporation of target burden into predictions of efficacious doses using QSP modeling are exemplified in the case studies presented below.

7.5 Use of modeling & simulation in decision making for bispecific antibodies

Model-based approaches are increasingly being used to support decisions spanning the entire drug development process, from preclinical development through to post marketing (56). In early clinical trials, mechanistic modeling can be used to select a clinical starting dose so that patients in early cohorts can benefit from clinical trials. Modeling approaches can also be used to select optimal regimens and step-dosing protocols to avoid cytokine release syndrome, and other toxicities. Mechanistic modeling can be used to predict efficacious dose so that phase 1 first-in-patient trials can be designed to escalate efficiently to doses where most benefit to patients is predicted (57). Quantitative modeling approaches can be used to determine which biomarkers are predicted to best correlate with efficacy or toxicity (10). In the face of significant variability, modeling can be used to deconvolve efficacy from variability to predict a robust dose and

regimen for phase 1b expansion trials, or recommended phase 2 dose. Mechanistic modeling can be used to optimize predictions in specific patient populations or for different indications and for defining patient selection criteria so that the trials have greater chance of success. Simulation based on mechanistic models could be used as a basis for selecting combination therapies, which is generally more empirically derived, and unfeasible to determine experimentally via a 'trial and error' process (10, 58).

In this section, the utility of mechanistic models to drive decision making and enable success for bsAbs in early clinical trials will be discussed including preclinical to clinical translation, determining clinical starting and efficacious doses, considerations for early clinical trial design and predicting toxicities. In addition, consideration of good QSP practice including model verification, validation and uncertainty quantification will be reviewed.

1. Translational strategies

Preclinical to clinical translation of bsAbs is required to predict efficacious doses in patients and is a key determinant of clinical success (23). It is particularly challenging for bsAbs as they have (at least) 2 targets and mechanisms of action to translate, with multiple inter-related factors impacting efficacy. In oncology, mouse xenograft models have become the mainstay of clinical translation, as efficacy (tumor growth inhibition) in response to drug can be measured dynamically over time (59). However, for bsAbs in immune oncology in vivo models are not ideal and often contrived, with very different conditions to those observed in patients. Two classes of in vivo models are currently most widely used: 1) immunocompromised mice with engraftment of human cancer cells and immune cells 2) immunocompetent syngeneic mice engrafted with human cancer cells (59). The latter are perhaps more translationally relevant as they possess fully intact immune systems, however they require mouse surrogate bsAbs to be used instead of human bsAbs to avoid immunogenicity (60). Non-human primates serve as good toxicology species; however, they lack tumor tissue and are therefore not relevant for understanding efficacy. The complex mechanism of action of bsAbs and the distinct conditions of preclinical in vivo models demands an integrated analysis to translate to the clinic. QSP modeling and simulation approaches can incorporate and systematically analyze in vitro, preclinical, and clinical data to simultaneously assess the individual effect of, as well as the dynamic interactions among, various factors (34). Some examples of the use of QSP models to translate preclinical data to the clinic are emerging in the literature for the CD3 bsAbs. For example, Campagne *et al.* (61) developed a PK/PD model for a bispecific CD123/ CD3 DART molecule in non-human primates. The model describes DART molecule binding to peripheral CD3 expressing cells and CD123+ cells, T-cell trafficking, activation and expansion, and resulting peripheral depletion of CD123 cells. By integrating primary PK and pharmacology, the model represents an efficient translational framework to provide quantitative predictions of drug disposition and potency in humans, and to predict dosing strategies to inform ongoing clinical trials. A translational QSP model is presented for CD3 bispecific molecules by Betts *et al.* (13), which integrates in silico, in vitro and in vivo data in a mechanistic framework to quantify and predict efficacy across species. This is discussed in more detail in **Case Study 1**.

Jiang *et al.* (34) proposed a mechanism-based PK/PD model based on target cell-biologic effector cell complex formation and used it to describe and predict in vitro cytotoxicity. The model was also used to translate from in vitro data to the clinic, validated using blinatumomab data. The model reasonably projected the exposure-response relationship of blinatumomab in ALL patients by incorporating drug-specific parameters identified from in vitro cytotoxicity data and system-specific parameters based on human physiology and pathology data for multiple T cell redirecting bispecific antibodies under different experimental conditions. A similar approach was taken by Hua *et al.* (62) who developed in vitro and human QSP models for an Epcam/ CD3 bsAb, solitomab, and used the model to show that number of trimers/ T cell required to drive cytotoxicity in vitro could be used as a target engagement metric to translate to human and predict clinical efficacious dose. The inherent complexities of bsAbs mean that clinical translation will be challenging to determine empirically, but may be aided by mechanistic models that capture the pathophysiology of the disease and the mechanisms of action of each agent (14).

2. Optimizing design of clinical trials

A holistic, mechanistic methodology to select MABEL based clinical starting doses of bsAbs is to use a QSP modeling approach (28). For CD3 bsAbs, an in vitro QSP model can be used to estimate the trimer concentration that results in 20% tumor cell killing (trimer EC_{20}). The model describes bsAb binding to CD3 on T cells and TAA on tumor cells to form dimers and then trimers, which are linked to cytotoxicity and/or T cell proliferation. The model accounts for the specific conditions of the in vitro assay including the number of cells, E:T ratio, and receptor expression on tumor cell lines used in the experiment. It can then be translated to human by incorporation of a PK model, and updating parameters (including E:T ratio, and receptor expression) to reflect patient tumors, in order to determine the dose required to achieve trimer concentrations approximating trimer EC_{20} in the clinic. This approach accounts for tumor trimer concentrations driving efficacy/ toxicity and normalizes for differences between in vitro experimental conditions and the clinic. This method was used to predict clinical starting dose of a P-cadherin/ CD3 bsAb using the MABEL approach and is described in **Case Study 2**. Another advantage of using a QSP model is that it provides a translational framework where the same model can be used for determining the starting and efficacious doses. Clinical trials can subsequently be designed for rapid escalation from the predicted starting dose to the efficacious dose, to reduce patients receiving subtherapeutic doses and reducing overall time in phase 1 (63). The QSP approach to MABEL can be integrated with other clinical trial design strategies such as use of single patient cohorts early in the early stages of dose escalation and even intrapatient dose escalation. The model can also be used for a sensitivity analysis to determine key parameters driving efficacy and toxicity. Such a QSP modeling approach was described in **Case Study 1**. The mathematical model can be updated with emerging clinical data and used to refine drug dosing and scheduling as well as guiding go/ no-go decisions.

3. Predicting toxicities associated with bsAbs

The key safety concerns with bsAbs, mainly from clinical data on CD3 bsAbs, are excessive release of cytokines, which may translate to potentially life threatening CRS and target organ toxicity due to redirection of T cells to normal tissues expressing the TAA (off-tumor/ on-target cytotoxicity)

(63). These toxicities can prevent efficacious doses of bsAbs being reached in the clinic before the onset of adverse events (AEs) and consequently limit the clinical utility of bsAbs.

Since the development of the first CD3 bsAb, clinical trials have shown that they can cause rapid and uncontrolled T cell mediated CRS, even at very low doses (64, 65). Mechanisms for mitigating CRS in the clinic have been implemented including a 'priming' dose strategy (i.e. a lower initial dose followed by a higher maintenance dose), timely supportive care, corticosteroids administered prophylactically or upon onset of symptoms, and IL6/ IL6R mAbs (e.g. tocilizumab) upon onset of CRS (66, 67). New generation CD3 bsAbs are being designed with reduced CD3 affinity, or with novel CD3 epitopes that limit cytokine release but maintain cytotoxic activity, or with different mAb formats to reduce potential for CRS (68). However, predicting the incidence and severity of CRS from preclinical experiments remains a challenge and selection of dose priming regimens in the clinic is mostly based on an empirical trial and error approach. These challenges could be addressed through mathematical modeling, and an example of a 'fit-for-purpose' PK/PD approach is discussed in **Case Study 3.**

Due to the small number of TAA required on target cells, off-tumor/ on-target toxicities can become an issue with CD3 bsAbs (69) and result in dose-limiting toxicities, limiting TI in some cases (70). For example, in a phase 1 clinical study with solitomab, an EpCAM/ CD3 BiTE® construct, treatment of r/r EpCAM+ solid tumors was associated with AEs including severe diarrhea and increase in liver enzymes which precluded dose escalation to potential therapeutic levels (70). EpCAM was subsequently shown to be expressed in the gastrointestinal tract epithelia and liver bile duct of patients (70). The AEs associated with solitomab treatment therefore likely represent off-tumor/ on-target toxicity due to T cell activation and killing of non-malignant cells. A QSP model developed for solitomab demonstrated that trimers/ T cell required for in vitro cell killing (approx. 200- 400) were similar to the number predicted at the maximum tolerated dose observed in the clinical study. The TI for solitomab was predicted to be close to 1 based on the trimers/ T cell formed in tumor and in normal tissue. Multiple ways to mitigate potential off-tumor/ on-target toxicities are currently being investigated in preclinical development. If the TAA is overexpressed in tumors, relying on avidity is one potential way to selectively target the tumor (43). An alternative mechanism, shown in non-human primate studies, is the use of masked antibodies, where the mask is only cleaved in the tumor microenvironment (71).

4. Good QSP practice

QSP models are complex, with a variety of data used in model development, often from disparate sources. Many calculations require propagation between models. In addition, models often span multiple time scales from binding to disease modification. As such QSP models need to be rigorously evaluated and conform to a set of best practices before enabling clinical decisions. A process of good QSP practice is recommended based on model verification, validation, and uncertainty quantification paradigm. A white paper has been published which presents a minimum set of recommendations to guide QSP practitioners (72). Some critical considerations are also discussed below.

First, a 'right sized' model should be used which is suitable for the question asked and has reasonable assumptions. A model verification step should be included to determine that the computational model and analysis accurately represent the underlying mathematical model and its solution. The model should be validated to determine if it is an accurate representation of the real world from the perspective of intended use. Finally, to quantify the accuracy of the prediction and the data, an uncertainty quantification step should be undertaken. These steps are a requirement to evaluate QSP models, to increase understandability to enable model reuse and to enable routine and unbiased calculation of prediction uncertainty to better understand the consequence of parameter error and patient variability.

7.6 Case studies

The following case studies were selected as useful representative examples where QSP or other mechanistic modeling approaches have impacted early clinical development strategies for particular bsAbs, with the ability to be re-purposed for other bsAbs. Case study 1 exemplifies the impact of a QSP modeling approach to translate from preclinical in vivo studies to the clinic to predict efficacious dose of a CD3 bsAb (13). Case study 2 uses the same modeling framework to predict clinical starting dose and demonstrates in vitro to clinical translation (28). Case study 3 demonstrates a QSP approach to predict and therefore minimize CRS toxicities upon bsAb dosing (73). In each case, the focus is on the strategic applications of the mechanistic modeling and its impact. Technical details including specific models structures, equations and parameter values are not included, and can be found in the published manuscripts (13, 28, 73). The case studies all describe a generalized CD3 bsAb model based on CD3 engaged through trimer formation, as the important variable driving efficacy and on-target/off-tumor toxicity. As such, this model is a useful platform for all CD3 bsAbs and bsAbs which bind in trans configuration (described as MoA 1 and 2 in **Figure 1**). The CRS model has further applicability to immune modulators resulting in cytokine release. These models could play an important role in design and interpretation of early clinical trials.

Case study 1: Preclinical to clinical translation of a P-cadherin/CD3 DART® molecule using QSP modeling

A QSP model was developed for a P-cadherin/CD3 DART® bsAb (Pcad-LP-DART), capable of predicting trimer formation and linking it to tumor cell killing **(13)**. The model was used to quantify the PK/PD relationship of Pcad-LP-DART in mouse xenograft models. The model, which had the general structure presented in **Figure 3**, integrated the PK of Pcad-LP-DART, its binding to soluble P-cadherin and circulating T cells in the systemic circulation, its biodisposition in the tumor and the formation of a trimolecular complex with T cells and P-cadherin expressing tumor cells in the tumor microenvironment. The model incorporated T cell kinetics in the tumor including T cell proliferation and contraction. The concentration of the trimer in the tumor was used to drive efficacy in mouse using a model of tumor cell growth and killing. A hybrid approach was used in the modeling where known parameters were fixed in the model up-front (binding

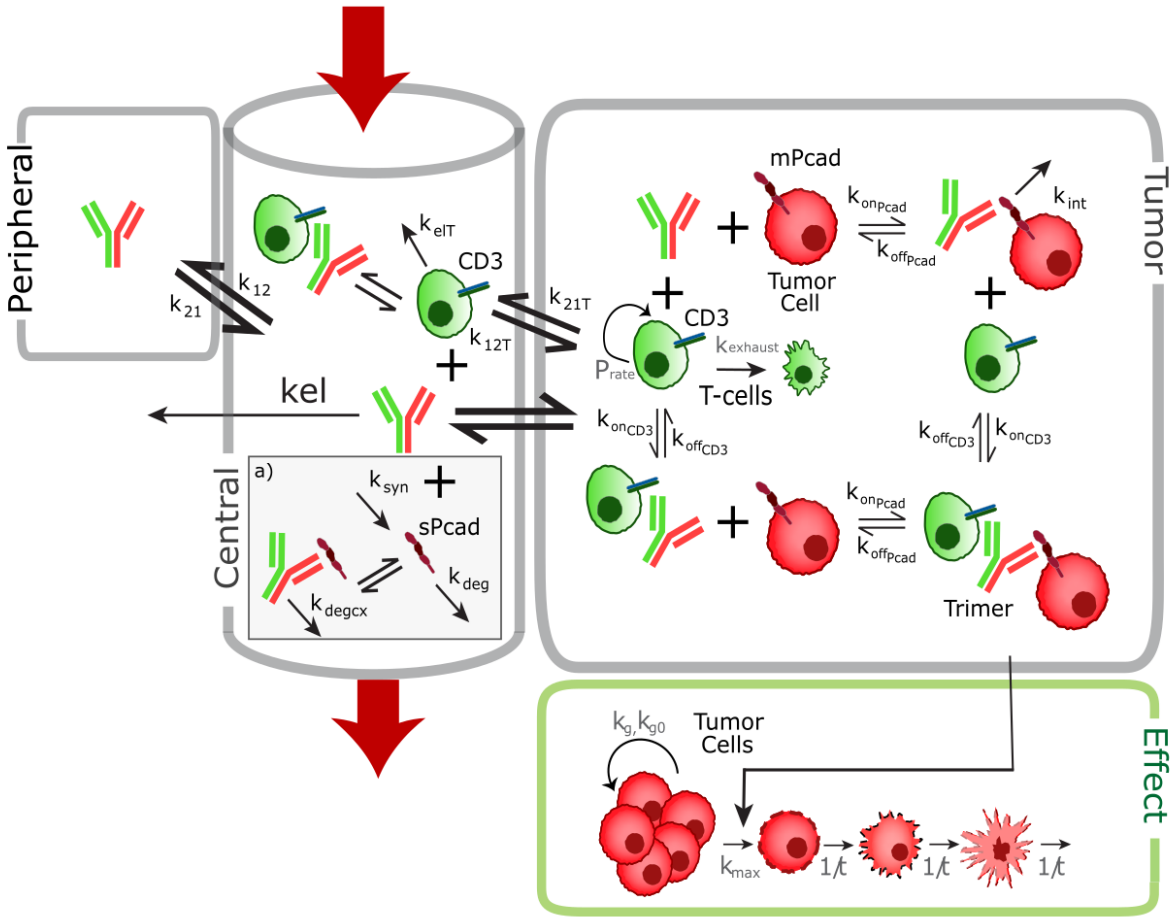

Figure 3: Model framework for trimer formation and tumor growth inhibition of CD3 bispecific antibodies. Formation of trimers between drugs, T cells, and tumor cells, is required for efficacy. The QSP model predicts trimer concentration and links it to tumor cell killing**.** The model shown here is for P-cadherin-LP-DART, which is a bispecific antibody molecule which binds to P-cadherin (Pcad) on tumor cells and CD3 on T cells. Drug can also bind to soluble P-cadherin (sPcad) in the central compartment.

kinetics, receptor expression, number of T cells and tumor cells) and unknown parameters were estimated using the model to fit the data (tumor cell growth and killing parameters). A tumor static concentration (TSC) was calculated and used as an estimate of minimum efficacious trimer concentration across mouse tumor models. The TSC values were in the picomolar range, demonstrating the inherent potency of this mechanism.

The model was translated to the clinic by incorporating predicted human PK and clinically relevant measures such as T cell concentration (circulating and tumor), tumor volumes, soluble P-cadherin levels, CD3 and P-cadherin expression. The model was subsequently applied to predict clinical PK, including impact of binding to soluble P-cadherin and prediction of clinical efficacious dose. The model was also used for sensitivity analysis and showed that P-cadherin expression and number of T cells in the tumor were sensitive parameters impacting clinical efficacy. The resulting QSP model and strategy offer a translational framework for CD3 bsAbs which could be

used for decision making at different stages of the drug discovery and development process from drug design through to candidate selection and clinical dose predictions (13).

Case study 2: Predicting clinical starting dose of a P-cadherin/CD3 DART® bsAb using a QSP model/ MABEL based approach

A QSP modeling approach was used to project clinical starting dose based on MABEL principles for a P-cadherin/ CD3 DART bsAb (Pcad-LP-DART; described in **Case Study 1**) (28). The QSP approach was based on the principle that trimer formation between drug, T cell and tumor cell is driving efficacy and not drug concentration alone. Orthogonal approaches including PK based methods and receptor occupancy were also investigated. In the QSP modeling approach, a mechanistic in vitro model was constructed describing binding of P-cad-LP-DART to T cells and tumor cells in a dish, to form inactive dimers and the active trimer species. Predicted trimer concentration was linked to in vitro T cell kinetic and cytotoxicity experiments to determine EC_{20} of trimer driving T cell proliferation and tumor cell killing. The model was able to capture in vitro data at various E:T ratios using the same EC_{20} value, which was considered to be the in vitro MABEL. The in vitro MABEL was then translated to the in vivo MABEL in order to predict human MABEL dose, by incorporation of predicted human PK (which included binding to soluble P-cadherin) and physiological parameters (described previously in **Case Study 1**). The MABEL human dose was determined as the predicted average tumor trimer concentration at steady state equal to the in vitro MABEL (EC_{20}, trimer). The predicted clinical MABEL dose using the QSP approach was 1.9 ng/kg/dose.

To build confidence in projecting the MABEL dose, additional approaches were explored including a PK driven and receptor occupancy approach (**Table 2**). For the PK driven approach, MABEL was defined as the lowest EC_{20} (based on drug concentration) across a panel of in vitro assays including cytotoxicity and cytokine release. The MABEL based human starting dose was calculated by simulating the predicted human PK and identifying the dose to keep drug concentrations below the EC_{20} values defined from cytotoxicity and cytokine release assays. The resulting MABEL was 1.5ng/kg dose, which was similar to the PK/PD approach. Finally, MABEL was estimated by determining drug concentration required for 10% RO, using equilibrium drug-receptor interaction theory and predicted human PK. This method resulted in MABEL doses of 360 and 8300 ng/kg/week for 10% P-cadherin and 10% CD3 occupancy respectively, which were much higher than the QSP model or PK driven approaches. The RO based approach is not considered to be appropriate for immune agonists (27). The MABEL doses using the PK, QSP and RO approaches are summarized in Table 2. Collectively, a dose of 1.5 ng/kg/week was suggested as the FIH starting dose consistently supported by the QSP- and PK-driven approaches (28). In this example, the QSP- and PK- based approaches gave similar starting dose predictions, which increased confidence in the suitability of the proposed starting dose to ensure the safety of patients given the potency of Pcad-LP-DART. The same model was used to predict efficacious dose (Case Study 1) and therefore the clinical trial could be designed to escalate efficiently to the projected efficacious dose. The prediction using the PK method, assumes drug concentration **Table 2:** Projection of Minimal Anticipated Biological Effect Level for P-cadherin LP-DART, reviewed in **Case Study 2**. Reproduced with permissions from (28).

Table 2: Projection of Minimal Anticipated Biological Effect Level for P-cadherin LP-DART, reviewed in **Case Study 2**. Reproduced with permissions from (28).

	In vitro Assay	Efficacy Variable	MABEL	Starting Dose[a] (ng/kg/wk)
PK/PD-driven approach	In vitro kinetic cytotoxicity assay	**Cytotoxicity** EC20, syn=1.2×10^{-6} nM	Maximum tumor synapse conc. < EC20, syn	1.9
PK-driven approach	In vitro cytokine release assay	**Cytokine release** EC20, CRA= 0.025 ng/mL	Cmax < EC20, CRA	1.5
	In vitro cytotoxicity assay	**Cytotoxicity** EC20, CTL= 0.01 ng/mL	Cave < EC20, CTL	
Receptor Occupancy (RO)	In vitro binding	**RO** EC10, RO = 6 (P-cad) and 134 (CD3) ng/mL	Cmax < EC10, RO	360 (P-cad) 8300 (CD3)

[a] – 1 hour infusion

alone is driving efficacy and is very sensitive to conditions used in the in vitro assay (including E:T ratio, incubation times and cell lines). For example, the predicted PK driven MABEL dose ranged from 1.5 ng/kg/week to 79.5 ng/kg with only a small difference in E:T ratios (5:1 and 3:1) and incubation times (24, 48, or 72 h). If this in vitro experiment had been used to inform MABEL using the PK- driven approach the clinical starting dose would have been much closer to the projected efficacious dose and potentially an inappropriate choice. The advantage of the QSP method is that it uses trimer concentration for driving efficacy and the predicted dose is independent of experimental conditions.

Case study 3: A model framework to characterize cytokine release upon CD3 bsAb therapy

In the work by Chen *et al.* 2019 (73), a quantitative modeling framework was developed for characterizing cytokine profiles upon CD3 bsAb treatment, with the goal to facilitate the design of priming dose strategies to minimize CRS toxicities (**Figure 4**). The model describes cytokine release stimulated by CD3 bsAbs forming trimers by binding to CD3 on T cells and TAA on tumor cells. Tumor kinetics are accounted for in the model to determine the impact of tumor burden on the active trimer concentration. The release of cytokines is controlled by a time variant negative feedback loop which prevents over activation of the immune system and accounts for the priming effect, where negative inhibition increases with increasing number of doses. The model was able to describe cytokine release data for blinatumomab in patients and for P-cadherin LP DART in cynomolgus monkeys, across a wide range of dose levels and regimens. The model could be used to design optimal dosing regimens to be tested in clinical trials, and with

more development could be used to translate from cynomolgus monkey to human. In addition, based on similarities in underlying mechanisms, the current model could be used for other immune agonistic bsAb therapeutics.

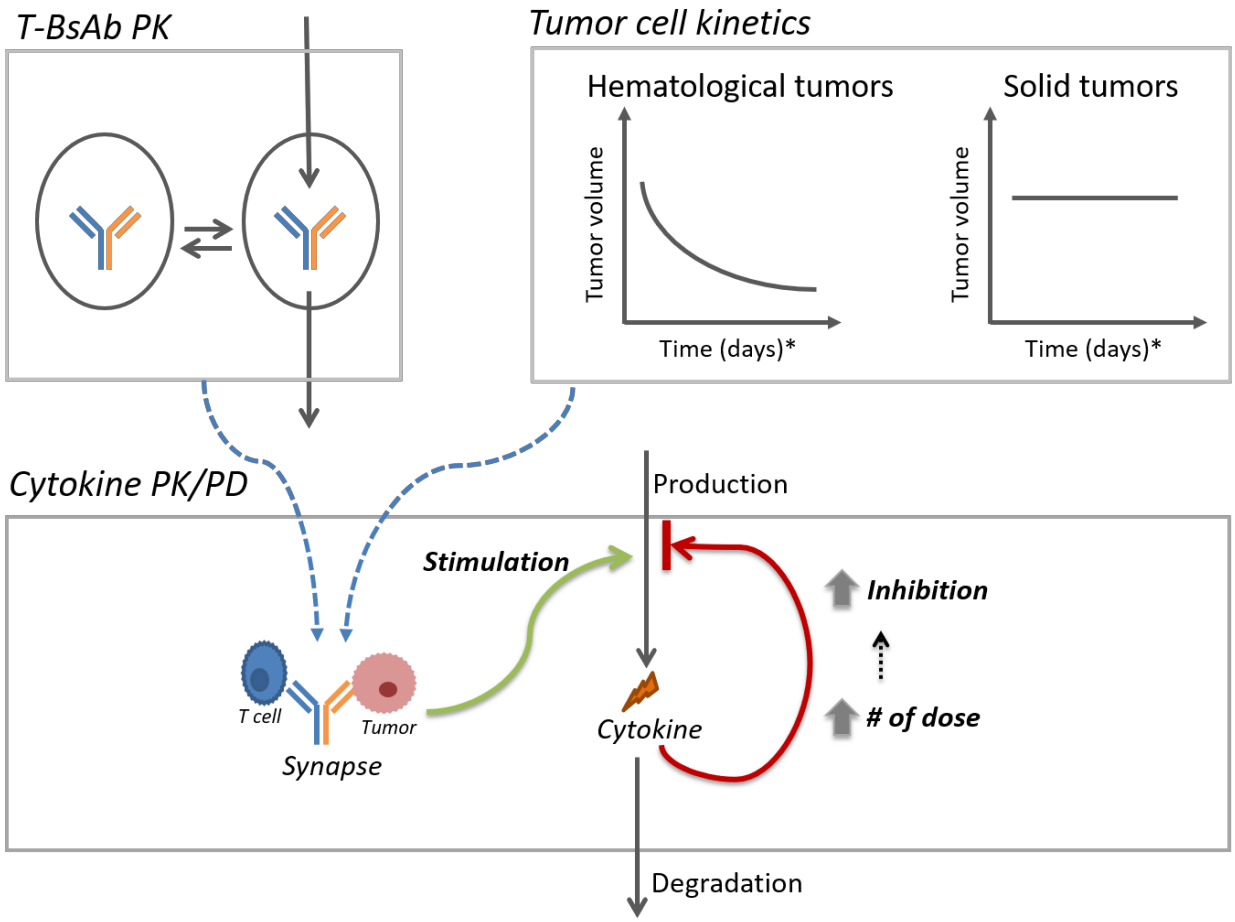

Figure 4: Cytokine release PK/PD model for CD3 bsAbs, reviewed in **Case Study 3**. Reproduced with permissions from (73). Briefly, an appropriate PK model accounts for the drug exposure. Depending on the tumor type (hematological or solid), the tumor kinetics are accounted for in the model to account for the impact of tumor burden on the active synapse concentration. For the cytokine PD model, the synapse exposure then stimulates cytokine release. A time-variant negative feedback loop accounts for the priming effect, where the negative inhibition increases with the increasing number of doses. T-bsAb, T cell-engaging bispecific antibody.

7.7 Conclusion

In conclusion, bsAbs are an exciting immunotherapeutic modality with potential to further improve clinical efficacy and safety in the treatment of cancer. Their inherent complexity leads to significant clinical pharmacology challenges in a disease area which is already difficult to treat and characterized by heterogeneity and development of resistance. Mathematical modeling and simulation is a powerful tool which can be used to integrate diverse knowledge and data to predict/ refine clinical dosing regimens and design trials to optimize efficacy and TI. Modeling can

be used to guide rational decision making, to inform precision medicine strategies and to increase overall efficiency and effectiveness of the oncology clinical development process. In the future, combination of QSP modeling with data science methods including machine learning will further strengthen the role of modeling as an essential quantitative tool in oncology.

7.8 Acknowledgements

The authors would like to acknowledge John Burke and Joshua Apgar for critical review of this manuscript. The authors would also like to thank Marc Presler, David Bassen, Diana Marcantonio and Emily Pace for biology discussions and for help populating Table 1. Thanks to Xiaoying Chen for modeling discussions and permissions to reprint Table 2 and Figure 4.

REFERENCES

1. Kontermann, R.E. Dual targeting strategies with bispecific antibodies. *MAbs* **4**, 182-97 (2012).
2. FDA guidance on co-developing investigational drugs. *Nature Reviews Drug Discovery* **10**, 86- (2011).
3 Rasmussen, S.K., Næsted, H., Müller, C., Tolstrup, A.B. & Frandsen, T.P. Recombinant antibody mixtures: Production strategies and cost considerations. *Archives of Biochemistry and Biophysics* **526**, 139-45 (2012).
4. Husain, B. & Ellerman, D. Expanding the Boundaries of Biotherapeutics with Bispecific Antibodies. *BioDrugs* **32**, 441-64 (2018).
5. Suurs, F.V., Lub-de Hooge, M.N., de Vries, E.G.E. & de Groot, D.J.A. A review of bispecific antibodies and antibody constructs in oncology and clinical challenges. *Pharmacol Ther* **201**, 103-19 (2019).
6. Brinkmann, U. & Kontermann, R.E. The making of bispecific antibodies. *MAbs* **9**, 182-212 (2017).
7. Amgen. *Blincyto (blinatumomab) prescribing information*. <https://www.pi.amgen.com/~/media/amgen/repositorysites/pi-amgen-com/blincyto/blincyto_pi_hcp_english.pdf> (2014). Accessed March 2020.
8. Przepiorka, D. *et al.* FDA Approval: Blinatumomab. *Clinical Cancer Research* **21**, 4035 (2015).
9. Nagorsen, D., Kufer, P., Baeuerle, P.A. & Bargou, R. Blinatumomab: A historical perspective. *Pharmacology & Therapeutics* **136**, 334-42 (2012).
10. Helmlinger, G. *et al.* Quantitative Systems Pharmacology: An Exemplar Model-Building Workflow With Applications in Cardiovascular, Metabolic, and Oncology Drug Development. *CPT: Pharmacometrics & Systems Pharmacology* **8**, 380-95 (2019).
11. Sorger, P.K.e.a. Quantitative and Systems Pharmacology in the Post-genomic Era: New Approaches to Discovering Drugs and Understanding Therapeutic Mechanisms 2011.
12. Sun, L.L. *et al.* Anti-CD20/CD3 T cell–dependent bispecific antibody for the treatment of B cell malignancies. *Science Translational Medicine* **7**, 287ra70 (2015).
13. Betts, A. *et al.* A Translational Quantitative Systems Pharmacology Model for CD3 Bispecific Molecules: Application to Quantify T Cell-Mediated Tumor Cell Killing by P-Cadherin LP DART((R)). *AAPS J* **21**, 66 (2019).
14. Yuraszeck, T., Kasichayanula, S. & Benjamin, J.E. Translation and Clinical Development of Bispecific T-cell Engaging Antibodies for Cancer Treatment. *Clinical pharmacology and therapeutics* **101**, 634-45 (2017).
15. Rothe, A. *et al.* A phase 1 study of the bispecific anti-CD30/CD16A antibody construct AFM13 in patients with relapsed or refractory Hodgkin lymphoma. *Blood* **125**, 4024-31 (2015).
16. Dahlen, E., Veitonmaki, N. & Norlen, P. Bispecific antibodies in cancer immunotherapy. *Ther Adv Vaccines Immunother* **6**, 3-17 (2018).
17. Lee, H.-W., Park, S.-J., Choi, B.K., Kim, H.H., Nam, K.-O. & Kwon, B.S. 4-1BB Promotes the Survival of CD8+ T Lymphocytes by Increasing Expression of Bcl-xL and Bfl-1. *The Journal of Immunology* **169**, 4882 (2002).

18. Segal, N.H. *et al.* Results from an Integrated Safety Analysis of Urelumab, an Agonist Anti-CD137 Monoclonal Antibody. *Clinical Cancer Research* **23**, 1929 (2017).
19. Hinner, M.J. *et al.* Tumor-Localized Costimulatory T-Cell Engagement by the 4-1BB/HER2 Bispecific Antibody-Anticalin Fusion PRS-343. *Clin Cancer Res* **25**, 5878-89 (2019).
20. Piha-Paul, S.e.a. Phase 1 Dose Escalation Study of PRS-343, a HER2/4-1BB Bispecific Molecule, in Patients with HER2+ Malignancies. In Society for Immunotherapy of Cancer.
21. Liu, X. *et al.* Dual Targeting of Innate and Adaptive Checkpoints on Tumor Cells Limits Immune Evasion. *Cell Rep* **24**, 2101-11 (2018).
22. Woo, S.R. *et al.* Immune inhibitory molecules LAG-3 and PD-1 synergistically regulate T-cell function to promote tumoral immune escape. *Cancer Res* **72**, 917-27 (2012).
23. Duell, J. *et al.* Bispecific Antibodies in the Treatment of Hematologic Malignancies. *Clin Pharmacol Ther* **106**, 781-91 (2019).
24. Topp, M.S. *et al.* Evaluation of AMG 420, an anti-BCMA bispecific T-cell engager (BiTE) immunotherapy, in R/R multiple myeloma (MM) patients: Updated results of a first-in-human (FIH) phase I dose escalation study. *Journal of Clinical Oncology* **37**, 8007- (2019).
25. Dudal, S. *et al.* Application of a MABEL Approach for a T-Cell-Bispecific Monoclonal Antibody: CEA TCB. *Journal of Immunotherapy* **39**, 279-89 (2016).
26. Tabernero, J. *et al.* Phase Ia and Ib studies of the novel carcinoembryonic antigen (CEA) T-cell bispecific (CEA CD3 TCB) antibody as a single agent and in combination with atezolizumab: Preliminary efficacy and safety in patients with metastatic colorectal cancer (mCRC). *Journal of Clinical Oncology* **35**, 3002- (2017).
27. Saber, H., Del Valle, P., Ricks, T.K. & Leighton, J.K. An FDA oncology analysis of CD3 bispecific constructs and first-in-human dose selection. *Regul Toxicol Pharmacol* **90**, 144-52 (2017).
28. Chen, X. *et al.* Mechanistic Projection of First-in-Human Dose for Bispecific Immunomodulatory P-Cadherin LP-DART: An Integrated PK/PD Modeling Approach. *Clin Pharmacol Ther* **100**, 232-41 (2016).
29. Zhu, A.Z. Quantitative translational modeling to facilitate preclinical to clinical efficacy & toxicity translation in oncology. *Future Sci OA* **4**, FSO306-FSO (2018).
30. Douglass, E.F., Jr., Miller, C.J., Sparer, G., Shapiro, H. & Spiegel, D.A. A comprehensive mathematical model for three-body binding equilibria. *J Am Chem Soc* **135**, 6092-9 (2013).
31. Lever, M. *et al.* Architecture of a minimal signaling pathway explains the T-cell response to a 1 million-fold variation in antigen affinity and dose. *Proceedings of the National Academy of Sciences* **113**, E6630 (2016).
32. Verhamme, I.M. Fluorescent reporters of thrombin, heparin cofactor II, and heparin binding in a ternary complex. *Anal Biochem* **421**, 489-98 (2012).
33. Schropp, J., Khot, A., Shah, D.K. & Koch, G. Target-Mediated Drug Disposition Model for Bispecific Antibodies: Properties, Approximation, and Optimal Dosing Strategy. *CPT Pharmacometrics Syst Pharmacol* **8**, 177-87 (2019).
34. Jiang, X. *et al.* Development of a Target cell-Biologics-Effector cell (TBE) complex-based cell killing model to characterize target cell depletion by T cell redirecting bispecific agents. *MAbs* **10**, 876-89 (2018).

35. Mandikian, D. *et al.* Relative Target Affinities of T-Cell-Dependent Bispecific Antibodies Determine Biodistribution in a Solid Tumor Mouse Model. *Mol Cancer Ther* **17**, 776-85 (2018).
36. Agoram, B.M., Martin, S.W. & van der Graaf, P.H. The role of mechanism-based pharmacokinetic–pharmacodynamic (PK–PD) modelling in translational research of biologics. *Drug Discovery Today* **12**, 1018-24 (2007).
37. Chen, Y. & Xu, Y. Pharmacokinetics of Bispecific Antibody. *Current Pharmacology Reports* **3**, 126-37 (2017).
38. Rudnick, S.I. & Adams, G.P. Affinity and avidity in antibody-based tumor targeting. *Cancer Biother Radiopharm* **24**, 155-61 (2009).
39. Harms, B.D., Kearns, J.D., Iadevaia, S. & Lugovskoy, A.A. Understanding the role of cross-arm binding efficiency in the activity of monoclonal and multispecific therapeutic antibodies. *Methods* **65**, 95-104 (2014).
40. van Steeg, T.J., Bergmann, K.R., Dimasi, N., Sachsenmeier, K.F. & Agoram, B. The application of mathematical modelling to the design of bispecific monoclonal antibodies. *MAbs* **8**, 585-92 (2016).
41. Kaufman, E.N. & Jain, R.K. Effect of bivalent interaction upon apparent antibody affinity: experimental confirmation of theory using fluorescence photobleaching and implications for antibody binding assays. *Cancer Res* **52**, 4157-67 (1992).
42. Mazor, Y. *et al.* Enhanced tumor-targeting selectivity by modulating bispecific antibody binding affinity and format valence. *Sci Rep* **7**, 40098 (2017).
43. Slaga, D. *et al.* Avidity-based binding to HER2 results in selective killing of HER2-overexpressing cells by anti-HER2/CD3. *Science Translational Medicine* **10**, eaat5775 (2018).
44. Bacac, M. *et al.* A Novel Carcinoembryonic Antigen T-Cell Bispecific Antibody (CEA TCB) for the Treatment of Solid Tumors. *Clin Cancer Res* **22**, 3286-97 (2016).
45. Doldán-Martelli, V., Guantes, R. & Míguez, D.G. A Mathematical Model for the Rational Design of Chimeric Ligands in Selective Drug Therapies. *CPT: Pharmacometrics & Systems Pharmacology* **2**, 26 (2013).
46. Harms, B.D., Kearns, J.D., Su, S.V., Kohli, N., Nielsen, U.B. & Schoeberl, B. Optimizing properties of antireceptor antibodies using kinetic computational models and experiments. *Methods Enzymol* **502**, 67-87 (2012).
47. Samineni, D., Girish, S. & Li, C. Impact of Shed/Soluble targets on the PK/PD of approved therapeutic monoclonal antibodies. *Expert Review of Clinical Pharmacology* **9**, 1557-69 (2016).
48. Li, L., Gardner, I., Rose, R. & Jamei, M. Incorporating Target Shedding Into a Minimal PBPK-TMDD Model for Monoclonal Antibodies. *CPT: pharmacometrics & systems pharmacology* **3**, e96-e (2014).
49. Jensen, B.V., Johansen, J.S. & Price, P.A. High Levels of Serum HER-2/neu and YKL-40 Independently Reflect Aggressiveness of Metastatic Breast Cancer. *Clinical Cancer Research* **9**, 4423-34 (2003).
50. Ali, S.M. *et al.* Serum HER-2/neu and relative resistance to trastuzumab-based therapy in patients with metastatic breast cancer. *Cancer* **113**, 1294-301 (2008).

51. Baselga, J. Phase I and II clinical trials of trastuzumab. *Annals of Oncology* **12**, S49-S55 (2001).
52. Sanchez, E. *et al.* Serum B-cell maturation antigen is elevated in multiple myeloma and correlates with disease status and survival. *British Journal of Haematology* **158**, 727-38 (2012).
53. Ghermezi, M. *et al.* Serum B-cell maturation antigen: a novel biomarker to predict outcomes for multiple myeloma patients. *Haematologica* **102**, 785-95 (2017).
54. Leong, S.R. *et al.* An anti-CD3/anti-CLL-1 bispecific antibody for the treatment of acute myeloid leukemia. *Blood* **129**, 609-18 (2017).
55. Fisher, R., Pusztai, L. & Swanton, C. Cancer heterogeneity: implications for targeted therapeutics. *Br J Cancer* **108**, 479-85 (2013).
56. Trivedi, A. *et al.* Clinical Pharmacology and Translational Aspects of Bispecific Antibodies. *Clinical and Translational Science* **10**, 147-62 (2017).
57. van der Graaf, P.H. & Benson, N. The Role of Quantitative Systems Pharmacology in the Design of First-in-Human Trials. *Clin Pharmacol Ther* **104**, 797 (2018).
58. Sheng, J. *et al.* Clinical Pharmacology Considerations for the Development of Immune Checkpoint Inhibitors. *J Clin Pharmacol* **57 Suppl 10**, S26-s42 (2017).
59. Murphy, J.F. Pre-Clinical Murine Models: Syngeneic Models for Immuno-Oncology. *MOJ Immunology* **2**, (2015).
60. Lechner, M.G. *et al.* Immunogenicity of murine solid tumor models as a defining feature of in vivo behavior and response to immunotherapy. *J Immunother* **36**, 477-89 (2013).
61. Campagne, O. *et al.* Integrated Pharmacokinetic/Pharmacodynamic Model of a Bispecific CD3xCD123 DART Molecule in Nonhuman Primates: Evaluation of Activity and Impact of Immunogenicity. *Clinical Cancer Research* **24**, 2631 (2018).
62. Hua, F., Lin, L., Betts, A.M., Wille, L., Burke, J., Apgar, J. *Bridging Non-clinical Studies to Clinical Design Using Quantitative Systems Pharmacology Model of T Cell Engaging Bispecifics*. <https://www.eventscribe.com/2019/PharmSci360/fsPopup.asp?efp=SUlFUEhHSFQ4MDkx&PosterID=240309&rnd=0.4667056&mode=posterinfo> (2019).
63. Kamperschroer, C., Shenton, J., Lebrec, H., Leighton, J.K., Moore, P.A. & Thomas, O. Summary of a workshop on preclinical and translational safety assessment of CD3 bispecifics. *Journal of Immunotoxicology* **17**, 67-85 (2020).
64. De Gast, G.C. *et al.* Clinical Experience with CD3 X CD19 Bispecific Antibodies in Patients with B Cell Malignancies. *Journal of Hematotherapy* **4**, 433-7 (1995).
65. Tibben, J.G., Boerman, O.C., Massuger, L.F.A.G., Schijf, C.P.T., Claessens, R.A.M.J. & Corstens, F.H.M. Pharmacokinetics, biodistribution and biological effects of intravenously administered bispecific monoclonal antibody OC/TR F(ab')2 in ovarian carcinoma patients. *International Journal of Cancer* **66**, 477-83 (1996).
66. Frey, N. Cytokine release syndrome: Who is at risk and how to treat. *Best Practice & Research Clinical Haematology* **30**, 336-40 (2017).
67. Lee, D.W. *et al.* Current concepts in the diagnosis and management of cytokine release syndrome. *Blood* **124**, 188-95 (2014).
68. Trinklein, N.D. *et al.* Efficient tumor killing and minimal cytokine release with novel T-cell agonist bispecific antibodies. *MAbs* **11**, 639-52 (2019).

69. Lutterbuese, R. *et al.* T cell-engaging BiTE antibodies specific for EGFR potently eliminate KRAS- and BRAF-mutated colorectal cancer cells. *Proceedings of the National Academy of Sciences* **107**, 12605 (2010).
70. Kebenko, M. *et al.* A multicenter phase 1 study of solitomab (MT110, AMG 110), a bispecific EpCAM/CD3 T-cell engager (BiTE®) antibody construct, in patients with refractory solid tumors. *OncoImmunology* **7**, e1450710 (2018).
71. Autio, K.A., Boni, V., Humphrey, R.W. & Naing, A. Probody Therapeutics: An Emerging Class of Therapies Designed to Enhance On-target Effects with Reduced Off-tumor Toxicity for Use in Immuno-Oncology. *Clinical Cancer Research*, clincanres.1457.2019 (2019).
72. Cucurull-Sanchez, L. *et al.* Best Practices to Maximize the Use and Reuse of Quantitative and Systems Pharmacology Models: Recommendations From the United Kingdom Quantitative and Systems Pharmacology Network. *CPT: Pharmacometrics & Systems Pharmacology* **8**, 259-72 (2019).
73. Chen, X., Kamperschroer, C., Wong, G. & Xuan, D. A Modeling Framework to Characterize Cytokine Release upon T-Cell-Engaging Bispecific Antibody Treatment: Methodology and Opportunities. *Clin Transl Sci* **12**, 600-8 (2019).
74. Brischwein, K. *et al.* MT110: A novel bispecific single-chain antibody construct with high efficacy in eradicating established tumors. *Molecular Immunology* **43**, 1129-43 (2006).
75. Friedrich, M. *et al.* Preclinical Characterization of AMG 330, a CD3/CD33-Bispecific T-Cell–Engaging Antibody with Potential for Treatment of Acute Myelogenous Leukemia. *Molecular Cancer Therapeutics* **13**, 1549 (2014).
76. Motte-Mohs, R.L., et al. MGD013, a Bispecific PD-1 x LAG-3 Dual-Affinity Re-Targeting (DART®) Protein with T-cell Immunomodulatory Activity for Cancer Treatment. In American Association for Cancer Research Annual Meeting.
77. Betts, A. *et al.* Linear pharmacokinetic parameters for monoclonal antibodies are similar within a species and across different pharmacological targets: A comparison between human, cynomolgus monkey and hFcRn Tg32 transgenic mouse using a population-modeling approach. *mAbs* **10**, 751-64 (2018).
78. Zhao, Y., Harrison, D.L., Song, Y., Ji, J., Huang, J. & Hui, E. Antigen-Presenting Cell-Intrinsic PD-1 Neutralizes PD-L1 in cis to Attenuate PD-1 Signaling in T Cells. *Cell Reports* **24**, 379-90.e6 (2018).
79. Maass, K.F., Kulkarni, C., Betts, A.M. & Wittrup, K.D. Determination of Cellular Processing Rates for a Trastuzumab-Maytansinoid Antibody-Drug Conjugate (ADC) Highlights Key Parameters for ADC Design. *The AAPS journal* **18**, 635-46 (2016).
80. van der Lee, M.M. *et al.* The Preclinical Profile of the Duocarmycin-Based HER2-Targeting ADC SYD985 Predicts for Clinical Benefit in Low HER2-Expressing Breast Cancers. *Mol Cancer Ther* **14**, 692-703 (2015).
81. Seckinger, A. *et al.* Target Expression, Generation, Preclinical Activity, and Pharmacokinetics of the BCMA-T Cell Bispecific Antibody EM801 for Multiple Myeloma Treatment. *Cancer Cell* **31**, 396-410 (2017).
82. Bikoue, A., George, F., Poncelet, P., Mutin, M., Janossy, G. & Sampol, J. Quantitative analysis of leukocyte membrane antigen expression: Normal adult values. *Cytometry* **26**, 137-47 (1996).

83. Chen, G. *et al.* Combining expression of GPC3 in tumors and CD16 on NK cells from peripheral blood to identify patients responding to codrituzumab. *Oncotarget* **9**, 10436-44 (2018).
84. Kienzle, G. & von Kempis, J. CD137 (ILA/4-1BB), expressed by primary human monocytes, induces monocyte activation and apoptosis of B lymphocytes. *International Immunology* **12**, 73-82 (2000).
85. Sorensen, S.F., Demuth, C., Weber, B., Sorensen, B.S. & Meldgaard, P. Increase in soluble PD-1 is associated with prolonged survival in patients with advanced EGFR-mutated non-small cell lung cancer treated with erlotinib. *Lung Cancer* **100**, 77-84 (2016).
86. Kruger, S. *et al.* Serum levels of soluble programmed death protein 1 (sPD-1) and soluble programmed death ligand 1 (sPD-L1) in advanced pancreatic cancer. *Oncoimmunology* **6**, e1310358-e (2017).

Section V.
Summary, discussion, and conclusion

Chapter 8

Summary, discussion, and conclusion

8.1 Mechanistic modeling in oncology research

The high cost and attrition of the drug development process is a fundamental challenge in biomedical research and requires novel approaches to improve efficiency and effectiveness [1]. This is particularly true in oncology drug development, which has the lowest success rate of all therapeutic areas [2]. Cancer treatment has been revolutionized with the advent of immune-oncology therapies; however, the biology is complex and difficult to translate and currently only a minority of patients are benefiting. Simultaneously, there has been rapid innovation in the field of protein engineering which has led to an explosion in the number of biological modalities being explored [3], including an increasing number of cell therapies [4]. Combination approaches are actively being pursued as a means of treating the heterogeneity of the disease across and within patients and reducing the risk of relapse to therapy. However, combination therapy is being approached as a 'trial and error process' in patients. A recent report showed that there were approximately 4000 immune-oncology drugs in development, and greater than 5000 clinical trials [5]. A more systematic process is required to enable more patients to benefit and to reduce clinical failures.

Mathematical modeling-based approaches have been shown to improve productivity in drug development and enhance decision making. Indeed, a recent publication by the FDA states that quantitative pharmacology modeling and simulation are seen as critical to accelerating drug development and assisting in regulatory decisions [1]. In the last two decades modeling and simulation has evolved from a tool primarily used in later stage clinical drug development, to playing a significant role in early clinical development (Phase 1 studies) and most recently in preclinical drug discovery and development [6]. As a result, the types of modeling and simulation approaches have evolved to support translational predictions across systems and species. Empirical PK/PD models have proved very useful in preclinical and clinical development to maximize information obtained from in vivo experiments, while minimizing resource utilization. These models are easy to develop and use, portable and good at extrapolating within a limited field of vision, across different doses and sub-populations [7]. However, they are limited in their ability to predict efficacy and safety across different targets and biomarkers. As a result, more mechanistic modeling and simulation is now being used to understand specifics of the pharmacology and mechanism of action of drugs to translate from in vitro experiments, to preclinical species and ultimately to human. These models are more data integrative, linking the exposure of drugs (or combination of drugs) and the modulation of pharmacological targets, physiological pathways and disease systems and can be used to develop a unified understanding of the data collected at different stages of drug discovery and development, and as such can provide a quantitative framework for drug research [6]. These mechanistic models have been termed 'quantitative systems pharmacology' or QSP models [7]. A key feature of these models is their explicit distinction between 'drug' and 'system' parameters. System specific parameters typically include organ/tissue blood flow rates, receptor expression, internalization rates and turnover rates, cell lifespans, and homoeostatic feedback mechanisms. Ideally, these parameters should be available from the literature or from prior experiments. Drug-specific parameters typically include PK parameters, such as intrinsic clearance and volume of distribution and pharmacologic parameters, such as in vivo target affinity and intrinsic efficacy of compounds and

are usually estimated from PK/PD data gathered for the drug [6]. A QSP modeling approach is particularly useful to answer more mechanistic questions for complex biotherapeutic modalities in oncology, which have intricate mechanisms of action and can require multiscale predictions.

In this thesis, the use of modeling and simulation, spanning the continuum from PK/PD to QSP modeling, was explored to help with quantitative decision making in oncology drug discovery and development. The type of model used in each case was dependent upon on the question asked (introduced in **Chapter 1)**. For example, a more statistical population-pharmacokinetic (pop-PK) modeling approach was used for analysis of a large mAb PK dataset with quantitation of variability (**Chapter 2**). Pharmacokinetic/ pharmacodynamic (PK/PD) modeling was used for data driven interpolation of in vitro and in vivo datasets with limited extrapolation (**Chapters 3 & 4**). Quantitative systems pharmacology (QSP) modeling was used to answer more complex mechanistic questions, involving integration of data from disparate sources (literature, in vitro, in vivo and the clinic), linkage of drug pharmacology to biological systems and disease, and multi-scale predictions (**Chapters 4, 5, 6 & 7**). Several key observations and learnings were made, which are discussed further in the sections below.

8.2 Use of mechanistic modeling to reduce animal use

An important finding was that use of modeling and simulation can reduce animal experimentation. In **Chapter 2**, a population PK analysis was completed on 27 mAbs in humans, cynomolgus monkey and in hFcRn transgenic (Tg32) mice and showed that a single set of typical linear PK parameters could be estimated across species with values similar to endogenous IgG [8]. These parameters could be used to inform initial parameters for PK/PD modeling and for simulations to optimize in vivo and first-in-human study designs. Importantly, knowledge of these parameters across species could be used to avoid unnecessary in vivo PK studies. Different translational strategies were also investigated for prediction of human linear PK of mAbs. Use of 'typical' human PK parameters gave good prediction accuracy for the majority of the mAbs in this study and for a test set of different mAbs with linear PK in the clinic. Allometric exponents were estimated within the pop-PK model and also gave good predictions, from both Tg32 mouse and cynomolgus monkey to human. Outliers with higher than typical clearance were found to have non-specific interactions in an affinity-capture self-interaction nanoparticle spectroscopy assay, offering a potential tool to screen out these mAbs at an early stage. The strategies presented call into question the value of completing extensive in vivo preclinical PK for mAbs with linear CL and encourage refinement of PK strategies consistent with the '3Rs', i.e., the reduction, refinement and replacement of animal use in research, testing and teaching [9]. This analysis provides alternatives to the use of cynomolgus monkey for PK prediction, including allometric scaling from Tg32 mouse, or use of human pop-PK parameters as a replacement to animal-based methods [8]. As such, it has the potential to reduce the numbers of cynomolgus monkey PK studies completed.

In **Chapter 3**, a PK/PD modeling approach was used to establish in vitro to in vivo correlations (IVIVC) for antibody drug conjugates (ADCs) [10]. In vitro cytotoxicity assays and mouse tumor xenograft models are the most widely used experimental systems in the preclinical development of oncology drugs. These experiments are very informative to determine drug potency and

efficacy, but no subsequent attempt has been made to integrate the information from these two systems to establish IVIVC for chemotherapeutic drugs. This is exacerbated by the fact that the in vitro and in vivo experiments are completed under different conditions, with different endpoints measured. To establish IVIVC, we determined in vitro efficacy of 19 ADCs using a kinetic cell cytotoxicity assay and determined the viability of cancer cells at multiple timepoints after incubation with various concentrations of ADCs. The data was fitted using a semi-mechanistic PK/PD model, and a secondary parameter called the in vitro tumor static concentration was estimated ($TSC_{in\ vitro}$), representing the concentration of ADC which would result in the cancer cells neither proliferating or decreasing, but held in stasis. The in vivo efficacy of ADCs was evaluated using tumor growth inhibition (TGI) studies performed on human tumor xenograft bearing mice. The TGI and PK data obtained from in vivo studies were characterized using a PK/PD model, parameter estimates from which were used to derive the in vivo TSC ($TSC_{in\ vivo}$), which was the concentration of ADC which would result in the tumor in the mouse neither growing nor regressing. The $TSC_{in\ vitro}$ and $TSC_{in\ vivo}$ values were found to correlate with a Spearman's rank correlation co-efficient of 0.82. On average TSC in vivo was found to be approximately 27 times higher than TSC in vitro, which roughly accounts for tumor penetration. The reasonable IVIVC for ADCs suggests that in vitro efficacy data was correctly able to differentiate ADCs for their in vivo efficacy. Thus, IVIVC can be used as a tool to triage ADC molecules in the discovery stage, thereby preventing unnecessary in vivo testing of ADCs. An ability to predict the concentration of ADC that is efficacious in vivo using the in vitro data can also help in optimizing the experimental design of preclinical efficacy studies. As such, the novel PK/PD modeling method presented here to establish IVIVC for ADCs holds promise for anticancer agents.

Key Learnings:

1. *Think before doing the in vivo experiment!*
2. *Modeling can be a useful tool to reduce animal experimentation, by enabling in vitro to in vivo correlations or use of simulation to replace experimental methodologies.*

8.3 Use of mechanistic modeling for preclinical to clinical translation

One of the key themes explored in this thesis was the use of modeling to translate from preclinical studies to the clinic. One reason to translate to human is to ensure that the best drug, in terms of predicted efficacy and safety, is being progressed to clinical trials. Another important reason is to ensure the most efficient design of clinical dose escalation studies, with the objective of minimizing risk to trial participants while acknowledging the need to quickly escalate to pharmacologically active doses.

The workhorse preclinical model in oncology is the mouse xenograft model, which comprises subcutaneous implantation of a human cell line or tumor into immune compromised host mice [11]. The xenograft model represents extreme simplification of human cancer, as it does not account for complexities of tumor metastasis, host immunity, tumor heterogeneity, and the development of treatment resistance that is routinely observed in cancer patients [12]. However, the drug exposure response relationship derived from these models is useful for understanding efficacy and if accompanied by rigorous quantitative analysis such as mathematical modeling,

can be used to translate from mouse to human to predict clinical anti-tumor response [13, 14]. A rigorous unifying preclinical to clinical translational framework could facilitate oncology clinical development by better identifying translational strategies, patient selection criteria and appropriate biomarkers to measure [15].

In **Chapter 4**, a PK/PD modeling and simulation approach was used for quantitative comparison of a new generation HER2 antibody drug conjugate (ADC, PF-06804103) with the clinical-standard-of-care trastuzumab-DM1 (T-DM1), to ensure that PF-06804103 would provide benefit if progressed to the clinic [16]. To compare preclinical efficacy, the PK/PD relationship of PF-06804103 and T-DM1 was determined across a range of mouse tumor xenograft models, using a tumor growth inhibition model. A secondary parameter, tumor static concentration (TSC), was calculated from the model parameters and defined as the minimal efficacious concentration. From comparison of TSCs, PF-06804103 was concluded to be more potent than T-DM1 across the cell lines studied, with TSCs ranging from 1.0 to 9.8 μg/mL (n = 7) for PF-06804103 and from 4.7 to 29 μg/mL (n = 5) for T-DM1. In addition, two experimental models which were resistant to T-DM1, responded to PF-06804103 treatment.
To translate to the clinic, first a mechanism-based target mediated drug disposition (TMDD) model was used to predict the human PK of PF-06804103. This model was constructed and validated based on T-DM1 which has non-linear PK at doses administered in the clinic, driven by binding to shed HER2. The predicted PK was incorporated into the mouse model and used to perform simulations of tumor regression at different dose levels for PF-06804103 and T-DM1. The model simulations accurately predicted the efficacious dose of T-DM1 and predicted efficacy at lower doses for PF-06804103 in the clinic. In this case, a fit-for-purpose translational strategy was deemed applicable to predict efficacy of two drugs with the same target and mechanism of action, which had been studied in the same experimental models. In addition, the availability of clinical data for T-DM1 was used to validate the modeling and to de-risk translation of PF-06804103 [16].

In **Chapters 5 and 6** more mechanistic QSP strategies are applied for translating from preclinical studies to the clinic, for ADCs and CD3 bispecific antibodies, respectively. In **Chapter 5**, a mechanistic QSP model was developed and used for preclinical to clinical translation of inotuzumab, a CD22 targeting ADC for B cell malignancies including non-Hodgkin's lymphoma (NHL) and acute lymphocytic leukemia (ALL) [17]. The model incorporates more of the mechanistic steps in the causal pathway between drug administration and efficacy compared to the model described in **Chapter 4**. These included (1) a plasma PK model characterizing disposition and clearance of inotuzumab and its released payload N-Ac-γ-calicheamicin DMH, (2) a tumor disposition model describing ADC diffusion into the tumor extracellular environment, (3) a cellular model describing inotuzumab binding to CD22, internalization, intracellular payload release, binding to DNA, or efflux from the tumor cell, and (4) tumor growth and regression driven by payload concentration. Preclinical data in mouse xenograft models for NHL and ALL, were modeled first and then translated to the clinic by incorporating human PK for inotuzumab and clinically relevant tumor volumes, tumor growth rates, and values for CD22 expression in the relevant patient populations. Clinical trial simulations were performed with 1000 patients simulated per dose level, incorporating variability in model parameters representing different

drug, patient, and disease characteristics. The resulting stochastic models predicted progression-free survival (PFS) rates for inotuzumab in patients comparable to the observed clinical results. The more mechanistic nature of the model meant that it could be used for specific quantitative questions, including optimization of dosing regimens for NHL and ALL, and to examine sensitive parameters impacting efficacy in the clinic which could be used to inform clinical diagnostics or potential biomarkers [17].

In **Chapter 6**, a translational QSP model was presented for CD3 bispecific molecules, which integrates in silico, in vitro and in vivo data in a mechanistic framework, to quantify and predict efficacy across species [18]. CD3 bispecific antibodies bind to CD3 on the surface of T cells and a tumor associated antigen on the surface of tumor cells to form a trimolecular complex (hereafter trimer), which mimics an immune synapse. Trimer formation triggers T cell activation, release of perforin and granzyme B which results in cytotoxicity. The proposed QSP model was capable of predicting trimer formation and linking it to tumor cell killing. The model was used to quantify the PK/PD relationship of a CD3 bispecific antibody targeting P-cadherin (PF-06671008). It describes the disposition of PF-06671008 in the central compartment and tumor in mouse xenograft models, including binding to target and T cells in the tumor to form the trimer. The model incorporates T cell distribution to the tumor, proliferation, and contraction. PK/PD parameters were estimated for PF-06671008 and a tumor stasis concentration (TSC) was calculated as an estimate of minimum efficacious trimer concentration. The model was translated to the clinic by incorporating predicted PF-06671008 human PK, including binding to soluble P-cadherin, and clinically relevant system parameters such as CD3 and P cadherin receptor expressions, numbers of T cells and tumor cells. The model was used to predict clinical PK and efficacy, and to determine sensitive parameters affecting clinical efficacious doses[18].

Key Learnings:

1. *When dealing with complex biological systems with multiple variables and pathways, it is advisable to build a mathematical model of the system, capable of integrating and interpreting preclinical data and providing a quantitative framework for translation to the clinic.*
2. *Choose the appropriately sized model and level of translational strategy for the question asked.*
3. *It is possible to translate from mouse xenograft studies to the clinic, if accompanied by rigorous, systematic quantitative analysis, which accounts for differences between the mouse experimental system and the clinic, as afforded by mathematical modeling.*
4. *Mechanistic QSP types of models are an investment in terms of data requirements and development time; however, they offer a high return of investment with respect to the granularity of the questions answered.*
5. *Deterministic models can be combined with stochastic simulations (e.g. virtual patient simulations) to predict efficacy endpoints such as RECIST criteria.*

8.4 Use of mechanistic modeling to optimize clinical dosing regimens

An important topic explored in this thesis was the use of mechanistic modeling and simulation to optimize the design of clinical dosing regimens. This included selection of clinical starting dose using a minimal anticipated biological effect level (MABEL) approach, prediction of clinical efficacious dose and regimen and identification of factors impacting variability in efficacious dose. As discussed above, in **Chapters 5 and 6**, mechanistic QSP models were developed and used to predict efficacious doses for an ADC (inotuzumab) and a CD3 bispecific molecule (P-cad LP-DART), respectively. For inotuzumab, different versions of the model were developed for treating hematological tumors such as ALL and solid tumors such as NHL, differing in their description of tumor disposition, and also in the typical tumor characteristics such as tumor growth rates and initial tumor volumes. The model was ultimately used to recommend a fractionated dosing regimen for ALL, which was predicted to be more tumor regressive compared to the standard Q4w regimen that was used to treat NHL [17].

In **Chapter 7**, a QSP modeling approach to select minimal anticipated biological effect level (MABEL)-based clinical starting dose of bispecific antibodies (bsAbs) was introduced. The approach is based on tumor trimer concentrations driving efficacy and normalizes for differences between in vitro experimental conditions and the clinic. The method was used to predict clinical starting doses of a P-cadherin/ CD3 bsAb. First, a mechanistic in vitro model was constructed which linked predicted trimer concentration and in vitro T cell kinetic and cytotoxicity experiments to determine EC_{20} of trimer driving T cell proliferation and tumor cell killing. The model was able to capture in vitro data at various E:T ratios using the same EC_{20} value. This in vitro MABEL was then translated to the in vivo MABEL to predict human MABEL dose, by incorporation of predicted human PK (including binding to soluble P-cadherin) and physiological parameters (described above). The MABEL human dose was determined as the predicted average tumor trimer concentration at steady-state equal to the in vitro MABEL (EC_{20}, trimer). This method was compared to orthogonal approaches, including PK based methods and receptor occupancy. The QSP-based approach was concluded to give the most appropriate starting dose to balance safety and efficacy, which was independent of experimental conditions [19].

Key Learnings:

1. *QSP modeling can be used to predict optimal dose and regimens for different oncology indications such as hematological versus solid tumors.*
2. *QSP modeling provides an alternative method to predict MABEL-based clinical starting doses which is less dependent on experimental conditions.*

8.5 Use of mechanistic modeling to address precision medicine questions

Another theme explored in this work, was the use of QSP modeling to investigate factors which may impact drug dosing and scheduling in oncology and to identify patients who may best respond to a therapy. Consistent with a precision medicine-based approach this information could be fundamental in the selection of suitable diagnostics and biomarkers to explore in the clinic to optimize therapeutic strategies in oncology [20].
In **Chapter 5**, a QSP model was developed for inotuzumab, a CD22-targetting ADC for B-cell malignancies [17]. The model was used for preclinical to clinical translation and to optimize doses

and regimens for a new indication being explored (ALL) versus the original indication (NHL). Development of inotuzumab for r/r NHL had recently been terminated due to lack of superiority versus standard of care. A sensitivity analysis was performed to give insight into the parameters defining, or even limiting, efficacy of inotuzumab versus NHL. CD22 receptor expression, calicheamicin efflux rate, inotuzumab PK (clearance rate), and tumor growth rate were selected as relevant parameters to vary in the model. Tumor growth rate was found to be the most sensitive parameter and suggested that for the more aggressive NHL sub-types like diffuse large B cell lymphoma (DLBCL) patients would require significantly higher doses for efficacy, compared with slower growing NHL sub-types such as follicular lymphoma. Calicheamicin efflux from the tumor cell was a sensitive parameter, which is important as N-Ac-γ-calicheamicin DMH is known to be a substrate for MDR1, an efflux transporter which is upregulated on many tumor-cell types. The least sensitive parameter was CD22 receptor expression which indicated the suitability of this receptor as an ADC target due to its high expression across B cells and rapid internalization rate. These findings suggest that MDR1 status in patients would be a more useful diagnostic of efficacy than CD22 receptor expression.

A similar approach was taken in **Chapter 6**, where a sensitivity analysis was used to determine key parameters impacting predicted clinical efficacious dose for P-cad LP-DART, a CD3 bispecific antibody [18]. The analysis showed that P-cad expression was a sensitive parameter with a higher dose required for patients exhibiting low P-cadherin expression. T cell number in the tumor was also a sensitive parameter with a higher predicted dose required for efficacy at low effector: target cell ratios. In conclusion, use of mathematical modeling and the strategies discussed above, can facilitate decisions on the most appropriate drugs for a given patient, help optimize dosing and combination regimens, and propose alternative and improved schedules of administration.

Key Learnings:

1. *QSP modeling can be used, via sensitivity analysis and simulations, to identify key parameters impacting outcome in the clinic.*

8.6 Platforms models for biotherapeutic modalities

Two models described in this thesis: the ADC QSP model (**Chapter 5**) and the CD3 bispecific model (**Chapter 6**) are potential platform models for specific biotherapeutic modalities in oncology. These are QSP models which provide a common integrated quantitative knowledge repository for continued preclinical and clinical evaluation [21]. They are not specific to a particular drug and therefore can be re-applied, providing a mechanistic framework for predicting efficacy distinct from other pharmacometrics strategies [21]. They are often multiscale and modular, and can be used to characterize in vitro, preclinical in vivo and clinical data. As such, they can be used to support program decision from exploratory research through to late-stage clinical trials. Platform models can be an investment in terms of data requirements, but they offer a high return of investment with respect to the granularity of the questions answered.

The ADC QSP model describes the intricate mechanism of action of ADCs including characterization of ADC and payload disposition at the cellular and physiological level to predict the clinical outcome of ADCs [17]. The model describes (1) plasma PK including disposition and clearance of ADC and released payload, (2) a tumor disposition model describing ADC and payload diffusion into the tumor extracellular environment, (3) a cellular model describing ADC binding to its target on tumor cells, internalization, intracellular payload release, payload binding to its target, payload efflux from the tumor cell, and (4) tumor growth and inhibition in mouse xenograft models as a function of tumor payload concentration.
The CD3 bispecific antibody (bsAb) model is a potential platform model for immune cell engaging bsAbs which act to cross-link a tumor cell with an immune effector cell to redirect cytotoxicity against the tumor cell [18]. The current model was used to characterize a bispecific molecule binding to CD3 on T cells and P-cadherin on tumor cells (Pcad-LP-DART) [18]. The model describes (1) plasma PK, including bsAb binding to soluble target and circulating T cells in the systemic circulation (2) a tumor disposition model describing bsAb diffusion into the tumor (3) binding of the bsAb to T cells and tumor cells to form dimers and trimers (4) T cell distribution to the tumor, proliferation, and contraction and (5) tumor growth and inhibition in mouse xenograft models as a function of tumor trimer concentration.

These platform models can be used for diverse purposes such as:

1. Optimizing design of ADCs or CD3 bsAbs at early stages to enable maximal chances of success.
2. Design and interpretation of preclinical in vitro and in vivo experiments for efficient and effective lead selection.
3. Translation of preclinical data to the clinic to predict clinical efficacious dose and regimen.
4. Prediction of drug response (e.g. tumor growth inhibition, RECIST criteria) and optimization of dose and regimen for different oncology indications.
5. Understanding variability to drug response in the clinic and use of this information for selection of suitable diagnostics to inform patient selection and clinical biomarkers to monitor for earlier signs of efficacy.
6. Comparison against clinical standard of care.

In addition, the current model structures have the potential to be expanded to predict toxicities associated with the mechanism of action. For example, the ADC model could be expanded to describe ADC uptake and release of payload in megakaryocytes and platelets to quantify typically observed ADC toxicities such as neutropenia and thrombocytopenia. The CD3 bsAb model could be expanded to relate trimer formation to cytokine release to predict cytokine release syndrome. Finally, both models could be extended to predict combination therapy treatments. For example, this could include addition of an immunotherapy model to predict combination with checkpoint inhibitors such as anti-PD1 mAbs.

Key Learnings:

1. *Platform QSP models are amenable to reuse and repurposing to support diverse decisions from early drug discovery through to clinical studies.*

8.7 Conclusions and future perspectives

In this thesis, mathematical modeling and simulation was applied as a tool to inform quantitative decision making in oncology drug discovery and development. Modeling based approaches were shown to be useful to understand the mechanism of action and deconvolve the complexities of novel biotherapeutic modalities being used to treat cancer, including monospecific and bispecific monoclonal antibodies and antibody drug conjugates. Several key observations and learnings were made. For example, modeling was shown to be a useful method to reduce animal experimentation, by enabling in vitro to in vivo correlations or use of simulation to replace experimental methodologies. Mechanism based modeling and simulation was found to be a useful means to translate from preclinical studies to the clinic to ensure progression of the best drug to clinical trials. These models could then be used to optimize design of clinical studies from selection of starting doses to recommended efficacious doses for pivotal trials. Modeling was shown to be beneficial to understand variability in the clinic and to identify factors impacting drug response in individual patients, paving the way for precision medicine strategies, informing clinical diagnostics, biomarkers, and doses for different oncology indications. Finally, the ADC QSP and CD3 bsAb models were identified as potential platform models amenable to reuse and repurposing to support diverse decisions across the drug discovery and development continuum.

Oncology drug discovery and development will get more complex, as we continue to unveil more of the intricate aspects of tumor biology and the pleiotropic role of the immune system. In parallel, the complexity of biological therapies will continue to evolve, with the introduction of multi-specific antibodies targeting several receptors and modulating different pathways, novel cell therapies, and multiple drug combinations leading to novel biological effects and synergies. As a result, mechanistic modeling and simulation will become an essential cornerstone of oncology drug discovery and development, to understand the often-non-intuitive processes and to aid in rational decision making. To facilitate this process, it will be imperative to apply modeling and simulation earlier in the drug discovery process to facilitate success and ensure reduced attrition rates later in clinical studies. There will be increasing opportunities to combine QSP modeling with emerging technologies. Undoubtedly integration of big data technology and data science (including crowd sourcing and machine learning) with QSP modeling will play an important role in the application of mathematical modeling for decision making within oncology drug research. Thus, the wealth of emerging genomics and biomarker data will be applied to maximize the power of QSP modeling to help ensure patients get the best possible treatment.

8.8 References

1. Zhu, H., et al., *Model-Informed Drug Development: A Regulatory Perspective on Progress.* Clinical Pharmacology & Therapeutics, 2019. **106**(1): p. 91-93.
2. Wong, C.H., K.W. Siah, and A.W. Lo, *Estimation of clinical trial success rates and related parameters.* Biostatistics (Oxford, England), 2019. **20**(2): p. 273-286.
3. Brinkmann, U. and R.E. Kontermann, *The making of bispecific antibodies.* mAbs, 2017. **9**(2): p. 182-212.
4. Yu, J.X., et al., *Cancer cell therapies: the clinical trial landscape.* Nat Rev Drug Discov, 2020.

5. Xin Yu, J., V.M. Hubbard-Lucey, and J. Tang, *Immuno-oncology drug development goes global.* Nat Rev Drug Discov, 2019. **18**(12): p. 899-900.
6. Agoram, B.M., S.W. Martin, and P.H. van der Graaf, *The role of mechanism-based pharmacokinetic-pharmacodynamic (PK-PD) modelling in translational research of biologics.* Drug Discov Today, 2007. **12**(23-24): p. 1018-24.
7. Agoram, B.M. and O. Demin, *Integration not isolation: arguing the case for quantitative and systems pharmacology in drug discovery and development.* Drug Discov Today, 2011. **16**(23-24): p. 1031-6.
8. Betts, A., et al., *Linear pharmacokinetic parameters for monoclonal antibodies are similar within a species and across different pharmacological targets: A comparison between human, cynomolgus monkey and hFcRn Tg32 transgenic mouse using a population-modeling approach.* MAbs, 2018. **10**(5): p. 751-764.
9. *The Principles of Humane Experimental Technique.* Medical Journal of Australia, 1960. **1**(13): p. 500-500.
10. Shah, D.K., et al., *Establishing in vitro–in vivo correlation for antibody drug conjugate efficacy: a PK/PD modeling approach.* Journal of Pharmacokinetics and Pharmacodynamics, 2018. **45**(2): p. 339-349.
11. Jung, J., *Human tumor xenograft models for preclinical assessment of anticancer drug development.* Toxicological research, 2014. **30**(1): p. 1-5.
12. Sausville, E.A. and A.M. Burger, *Contributions of Human Tumor Xenografts to Anticancer Drug Development.* Cancer Research, 2006. **66**(7): p. 3351.
13. Rocchetti, M., et al., *Predicting the active doses in humans from animal studies: A novel approach in oncology.* European Journal of Cancer, 2007. **43**(12): p. 1862-1868.
14. Wong, H., et al., *Antitumor Activity of Targeted and Cytotoxic Agents in Murine Subcutaneous Tumor Models Correlates with Clinical Response.* Clinical Cancer Research, 2012. **18**(14): p. 3846.
15. Zhu, A.Z., *Quantitative translational modeling to facilitate preclinical to clinical efficacy & toxicity translation in oncology.* Future science OA, 2018. **4**(5): p. FSO306-FSO306.
16. Betts, A., et al., *Use of translational modeling and simulation for quantitative comparison of PF-06804103, a new generation HER2 ADC, with Trastuzumab-DM1.* J Pharmacokinet Pharmacodyn, 2020.
17. Betts, A.M., et al., *Preclinical to Clinical Translation of Antibody-Drug Conjugates Using PK/PD Modeling: a Retrospective Analysis of Inotuzumab Ozogamicin.* Aaps j, 2016. **18**(5): p. 1101-1116.
18. Betts, A., et al., *A Translational Quantitative Systems Pharmacology Model for CD3 Bispecific Molecules: Application to Quantify T Cell-Mediated Tumor Cell Killing by P-Cadherin LP DART((R)).* AAPS J, 2019. **21**(4): p. 66.
19. Betts, A. and P.H. van der Graaf, *Mechanistic quantitative pharmacology strategies for the early clinical development of bispecific antibodies in oncology.* Clin Pharmacol Ther, 2020.
20. Barbolosi, D., et al., *Computational oncology — mathematical modelling of drug regimens for precision medicine.* Nature Reviews Clinical Oncology, 2016. **13**(4): p. 242-254.
21. Musante, C.J., et al., *Quantitative Systems Pharmacology: A Case for Disease Models.* Clinical pharmacology and therapeutics, 2017. **101**(1): p. 24-27.

Hoofdstuk 9

Nederlandse samenvatting

9.1 Het gebruik van mechanistische modellen in oncologieonderzoek

Aangezien in het biomedisch onderzoek de hoge ontwikkelkosten van nieuwe geneesmiddelen en lage succespercentages een grote uitdaging vormen, zijn nieuwe benaderingen nodig om tot een efficiënter en effectiever proces te komen [1]. Dit geldt met name voor de ontwikkeling van oncologiegeneesmiddelen, het therapeutische gebied dat het allerlaagste succespercentage kent [2]. De behandeling van kanker heeft met de komst van immuuntherapieën een revolutie doorgemaakt; de biologie erachter is echter zeer complex en laat zich moeilijk vertalen, waardoor momenteel slechts een minderheid van de patiënten ervan profiteert. Tegelijkertijd gaan de ontwikkelingen op het gebied van eiwitengineering razendsnel, wat heeft geleid tot een explosieve toename van het aantal te onderzoeken biologische modaliteiten [3], waaronder een groeiend aantal celtherapieën [4]. Er wordt momenteel actief onderzoek gedaan naar combinatietherapie als middel om de heterogeniteit van de ziekte aan te pakken tussen zowel verschillende patiënten als in een individuele patiënt, en om het risico op terugval tijdens de therapie te verlagen. Combinatietherapie wordt echter bij patiënten gezien als een 'trial-and-error'-proces. Uit een recent rapport blijkt dat er momenteel ongeveer 4.000 immuno-oncologische geneesmiddelen in ontwikkeling zijn, en dat er ruim 5.000 klinische studies lopen [5]. Er is een systematischere aanpak nodig om meer patiënten te laten profiteren en het aantal klinische successen te vergroten.

Het is aangetoond dat een wiskundig-modelmatige aanpak zowel de productiviteit op het gebied van geneesmiddelenontwikkeling als de besluitvorming ten goede komt. In een recente publicatie van de Amerikaanse Food and Drug Administration (FDA) staat dat het gebruik van kwantitatieve farmacologiemodellen en simulatie van cruciaal belang is om de geneesmiddelenontwikkeling te versnellen en te helpen bij het nemen van regulatoire beslissingen [1]. In de laatste 20 jaar is het gebruik van modellen en simulatie veranderd. Waar het eerst een instrument was dat voornamelijk werd ingezet in de latere fase van klinisch onderzoek, speelt het nu ook in de vroege klinische ontwikkeling (fase-I-studies) een belangrijke rol, en wordt het sinds kort zelfs gebruikt in preklinisch onderzoek naar nieuwe geneesmiddelen [6]. Als gevolg daarvan zijn de verschillende modellering- en simulatiebenaderingen doorontwikkeld om translationele voorspellingen over systemen en soorten heen te ondersteunen. Empirische farmacokinetische-farmacodynamische (pharmacokinetic-pharmacodynamic, hierna PKPD) modellen zijn in het preklinische en klinische onderzoek erg bruikbaar gebleken om zoveel mogelijk informatie uit *in vivo* experimenten te benutten met zo weinig mogelijk middelen. Deze modellen zijn eenvoudig te ontwikkelen en te gebruiken. Bovendien is hun portabiliteit goed, en zijn ze zeer geschikt voor extrapolatie binnen een beperkt gegevensgebied, voor verschillende doseringen en subpopulaties [7]. De modellen zijn echter minder geschikt om de werkzaamheid en veiligheid voor de verschillende targets en biomarkers te voorspellen. Als gevolg daarvan wordt nu vaker mechanistische modellering en simulatie ingezet om de bijzonderheden van de farmacologie en het werkingsmechanisme van een geneesmiddel te begrijpen in de translatie van *in vitro* experimenten naar het laboratorium en uiteindelijk naar de mens. In deze modellen kunnen meer data worden geïntegreerd, waardoor de blootstelling aan een medicijn (of aan een combinatie van medicijnen) gekoppeld kan worden aan de modulatie van farmacologische targets, fysiologische netwerken en

ziektesystemen. De modellen kunnen ingezet worden om een eenduidig begrip te ontwikkelen van de data die zijn verzameld in de verschillende fasen van geneesmiddelenontwikkeling, en ze bieden als zodanig een kwantitatief kader voor geneesmiddelenonderzoek [6]. Deze mechanistische modellen worden 'kwantitatieve systeemfarmacologie-modellen' genoemd (quantitative systems pharmacology, hierna QSP) [7]. Een belangrijk kenmerk van deze QSP-modellen is dat er expliciet onderscheid wordt gemaakt tussen *systeem-* en *geneesmiddel*parameters. Onder systeemspecifieke parameters vallen doorgaans de bloedstroomsnelheid in organen en weefsels, receptor expressie, internalisatie- en omloopsnelheden, de levensduur van cellen, en homeostatische terugkoppelingsmechanismen. Idealiter worden deze parameters uit de literatuur of uit eerdere experimenten verkregen. Geneesmiddelspecifieke parameters omvatten doorgaans zowel PK-parameters (bijvoorbeeld klaring en distributievolume), als farmacologische parameters (bijvoorbeeld *in vivo* targetaffiniteit en intrinsieke werkzaamheid van verbindingen). Deze parameters worden gewoonlijk geschat op basis van bestaande PKPD-data voor het geneesmiddel [6]. Het gebruik van QSP-modellen is vooral nuttig voor het beantwoorden van meer mechanistische vragen op het gebied van complexe biotherapeutische modaliteiten in de oncologie. Deze modaliteiten hebben ingewikkelde werkingsmechanismen en kunnen multischaalvoorspellingen vereisen.

In dit proefschrift zijn de mogelijkheden van modellering en simulatie – van PKPD tot QSP – verkend om de kwantitatieve besluitvorming op het gebied van onderzoek en ontwikkeling van oncologiegeneesmiddelen te ondersteunen. Welk model werd gebruikt, was afhankelijk van de gestelde vraag (geïntroduceerd in **hoofdstuk 1**). Zo is bijvoorbeeld de meer statistische populatie-farmacokinetiek (pop-PK) modelbenadering gebruikt voor de analyse van een grote mAb-PK dataset waarin de variabiliteit gekwantificeerd werd (**hoofdstuk 2**). PKPD-modellering werd ingezet voor datagestuurde interpolatie van *in vitro* en *in vivo* datasets met beperkte extrapolatie (**hoofdstuk 3 & 4**). QSP-modellering werd gebruikt om complexere mechanistische vragen te beantwoorden, waarbij data uit verschillende bronnen werden samengevoegd (literatuur, *in vitro*, *in vivo* en de kliniek), farmacologie aan biologische systemen en ziekten werd gekoppeld, en multischaalvoorspellingen werden gedaan (**hoofdstuk 4, 5, 6 & 7**). De voornaamste bevindingen en lessen worden in de volgende paragrafen worden besproken.

9.2 Het gebruik van mechanistische modellering om het aantal dierproeven te verminderen

Een belangrijke bevinding was dat door het gebruik van modellering en simulatie het aantal dierproeven kan worden verminderd. In **hoofdstuk 2** werd een pop-PK-analyse uitgevoerd op 27 mAbs in mensen, Java-apen en hFcRn transgene (Tg32) muizen. Deze analyse wees uit dat een enkele set van typisch lineaire PK-parameters kon worden geschat voor alle soorten met waarden die vergelijkbaar zijn met endogene gamma-immunoglobuline (IgG) [8]. Deze parameters kunnen worden gebruikt als basis voor de initiële parameters voor PKPD-modellering. In simulaties konden ze worden gebruikt om *in vivo* en 'first-in-human'-studies te verbeteren. Een belangrijk punt is dat kennis van deze parameters over de verschillende soorten heen gebruikt kan worden om onnodige *in vivo* PK-studies te vermijden. Ook zijn verschillende translationele strategieën onderzocht voor

de voorspelling van een humaan lineair PK-profiel van mAbs. De 'typisch' humane PK-parameters voorspelden nauwkeurig de meerderheid van de mAbs in deze studie, en een testset van verschillende mAbs met lineaire PK in de kliniek. Allometrische exponenten werden geschat binnen het pop-PK-model, en deze gaven ook goede voorspellingen, uit zowel Tg32-muizen, Java-apen als mensen. Uitschieters met een hogere klaring dan normaal bleken niet-specifieke interacties te hebben in een *affinity-capture self-interaction nanoparticle spectroscopy assay.* Hierdoor is het mogelijk om deze mAbs er in een vroeg stadium uit te filteren. De hier gepresenteerde strategieën stellen het nut van uitgebreide *in vivo* preklinische PK voor mAbs met lineaire klaring (CL) ter discussie, en stimuleren de verfijning van PK-strategieën in overeenstemming met de '3V's': vervanging, vermindering en verfijning van het gebruik van dieren in onderzoek, bij testen en in het onderwijs [9]. Deze analyse biedt alternatieven voor het gebruik van Java-apen voor het doen van PK-voorspellingen – waaronder de allometrische schaling vanuit Tg32-muizen – of het gebruik van humane pop-PK-parameters ter vervanging van dierproeven [8]. Hierdoor kan het aantal PK-studies met Java-apen worden verminderd.

In **hoofdstuk 3** werd PKPD-modellering gebruikt om *in vitro* naar *in vivo* correlaties (IVIVC) vast te stellen voor antilichaam-geneesmiddelconjugaten (ADC's) [10]. In de preklinische ontwikkeling van oncologische geneesmiddelen zijn de *in vitro* cytotoxiciteitstests en muismodellen met getransplanteerde tumorcellen (xenograft) de meest gebruikte experimentele systemen. Deze experimenten leveren zeer veel informatie voor het bepalen van de potentie en werkzaamheid van een medicijn, maar er is nooit geprobeerd om de informatie uit deze twee systemen te integreren om IVIVC voor chemotherapeutische medicijnen vast te stellen. Dit wordt bemoeilijkt door het feit dat de *in vitro* en *in vivo* experimenten onder verschillende omstandigheden worden uitgevoerd, waarbij verschillende eindpunten worden gemeten. Om IVIVC vast te stellen hebben we de *in vitro* werkzaamheid van 19 ADC's bepaald met behulp van een kinetische celcytotoxiciteitstest. Daarnaast bepaalden we de levensvatbaarheid van kankercellen op meerdere tijdstippen na incubatie met verschillende concentraties ADC's. Met behulp van een semi-mechanistisch PKPD-model hebben we de data geanalyseerd, en een secundaire parameter geschat – de *in vitro* tumor statische concentratie ($TSC_{in\ vitro}$). Dit is de concentratie ADC die tot gevolg heeft dat de kankercellen tot stilstand komen, en niet toe- of afnemen. De *in vivo* werkzaamheid van ADC's is geëvalueerd met behulp van tumorgroeiremmingsstudies (TGI) uitgevoerd op muizen met getransplanteerde menselijke tumorcellen (xenograft muismodellen). De TGI en PK-data verkregen uit *in vivo* studies werden in kaart gebracht met behulp van een PKPD-model, waarvan parameterschattingen werden gebruikt om de *in vivo* TSC ($TSC_{in\ vivo}$) af te leiden – de concentratie ADC die tot gevolg zou hebben dat de tumor in de muis niet groeit of afneemt. De $TSC_{in\ vitro}$ and $TSC_{in\ vivo}$ -waarden bleken te correleren met een Spearman's rangcorrelatiecoëfficiënt van 0,82. Gemiddeld bleek de $TSC_{in\ vivo}$ ongeveer 27 keer hoger dan de $TSC_{in\ vitro}$, wat de verminderde tumorpenetratie *in vivo* grofweg verklaart. Door de redelijk aanvaardbare IVIVC voor ADC's mag worden aangenomen dat de *in vitro* effectiviteitsdata in staat waren om ADC's in te delen naar *in vivo* werkzaamheid. IVIVC kan dus worden ingezet als hulpmiddel om ADC-moleculen in de onderzoeksfase te beoordelen, waardoor onnodige *in vivo* tests van ADC's voorkomen kunnen worden. Het vermogen om de effectieve *in vivo* concentratie ADC te voorspellen met behulp van de *in vitro* data kan ook helpen bij het verbeteren van de experimentele opzet van preklinische effectiviteitsstudies. De nieuwe PKPD-

modelleringsmethode die hier wordt voorgesteld om IVIVC voor ADC's vast te stellen, is dus veelbelovend voor antikankermiddelen.

Belangrijkste lessen:

1. *Denk na voordat je het in vivo experiment start!*
2. *Modellering kan dierproeven verminderen doordat het in vitro naar in vivo correlaties en simulaties mogelijk maakt om experimentele methoden te vervangen.*

9.3 Het gebruik van mechanistische modellering voor preklinische naar klinische translatie

Een hoofdthema in dit proefschrift is het gebruik van modellering voor de translatie van preklinische studies naar de kliniek. Een van de redenen hiervoor is te garanderen dat het beste medicijn wat betreft voorspelde werkzaamheid en veiligheid op mensen getest gaat worden. Een andere belangrijke reden is dat klinische dosis-escalatiestudies zo efficiënt mogelijk ontworpen moeten worden, om het risico voor de proefpersonen zo klein mogelijk te houden, maar tegelijkertijd een snelle escalatie naar farmacologisch actieve doses mogelijk te maken.
Het meest beproefde preklinische model in de oncologie is het 'xenograft' muismodel: het onderhuids implanteren van een menselijke cellijn of tumor in immuungecompromitteerde muizen [11]. Het xenograftmodel is een extreme vereenvoudiging van kanker in het menselijk lichaam, omdat het geen rekening houdt met de complexiteit van tumormetastases, gastheerimmuniteit, tumorheterogeniteit en het ontstaan van resistentie tegen de behandeling, iets wat regelmatig wordt waargenomen bij kankerpatiënten [12]. De blootstelling-responsrelatie die uit deze modellen kan worden afgeleid, helpt echter om de werkzaamheid te begrijpen en kan, mits vergezeld van een nauwgezette kwantitatieve analyse zoals wiskundige modellering, worden gebruikt om de klinische anti-tumorrespons van muis naar mens te voorspellen [13, 14]. Het klinische oncologieonderzoek zou gebaat zijn bij een strikt, overkoepelend preklinisch naar klinisch kader, waarmee translationele strategieën, criteria voor patiëntenselectie en geschikte meetbare biomarkers beter bepaald kunnen worden [15].

In **hoofdstuk 4** werd PKPD-modellering en simulatie gebruikt voor een kwantitatieve vergelijking van een nieuwe generatie HER2 antilichaam-geneesmiddelconjugaat (ADC, PF-06804103) met de standaardbehandeling trastuzumab-DM1 (T-DM1), om er zeker van te zijn dat PF-06804103 voordeel zou opleveren in de kliniek [16]. Om het preklinische effect te vergelijken werd de PKPD-relatie van PF-06804103 en T-DM1 bepaald over een reeks xenograft muismodellen, met behulp van een tumorgroeiremmermodel. We hebben een secundaire parameter, de *tumor static concentration* (TSC), berekend uit de modelparameters en gedefinieerd als de minimale effectieve concentratie. Uit de vergelijking van TSC's werd geconcludeerd dat PF-06804103 krachtiger is dan T-DM1 over de onderzochte cellijnen, met TSC's variërend van 1,0 tot 9,8 µg/mL (n = 7) voor PF-06804103, en van 4,7 tot 29 µg/mL (n = 5) voor T-DM1. Bovendien reageerden twee experimentele modellen die resistent waren tegen T-DM1, op de behandeling met PF-06804103.

Voor de translatie naar de kliniek werd eerst een op mechanisme gebaseerd *target mediated drug disposition* (TMDD) model gebruikt om de humane PK van PF-06804103 te voorspellen. Dit model werd samengesteld en gevalideerd op basis van T-DM1, waarbij sprake was van niet-lineaire PK bij doseringen die klinisch toegepast worden door binding aan afgescheiden HER2. De voorspelde PK werd toegevoegd aan het muismodel en gebruikt om tumorregressie te simuleren bij verschillende dosisniveaus voor PF-06804103 en T-DM1. De modelsimulaties voorspelden nauwkeurig de effectieve dosis T-DM1, en voorspelden het effect bij lagere doses voor PF-06804103 in de kliniek. In dit geval werd een *fit-for-purpose* translationele strategie van toepassing geacht om de werkzaamheid te voorspellen van twee geneesmiddelen die hetzelfde target en werkingsmechanisme hebben, en die in dezelfde experimentele modellen waren bestudeerd. Daarnaast werden de beschikbare klinische data voor T-DM1 gebruikt om de modellering te valideren en het risico van translatie van PF-06804103 te verlagen [16].

In **hoofdstuk 5 en 6** zijn meer mechanistische QSP-strategieën toegepast voor de translatie van preklinische studies naar de kliniek, voor respectievelijk ADC's en CD3-bispecifieke antilichamen. In **hoofdstuk 5** werd een mechanistisch QSP-model ontwikkeld en toegepast voor de preklinische naar klinische translatie van inotuzumab. Dat is een ADC dat CD22 aanvalt op B-celmaligniteiten, zoals non-hodgkinlymfoom (NHL) en acute lymfatische leukemie (ALL) [17]. Dit model omvat meer mechanistische stappen op het causale pad tussen toediening en effect van het medicijn, in vergelijking met het model dat in **hoofdstuk 4** is beschreven. Deze stappen omvatten:

1. een plasma-PK-model waarmee de dispositie en klaring van inotuzumab en de afgifte van N-Ac-γ-calicheamicine DMH in kaart wordt gebracht;
2. een tumordispositiemodel dat ADC-diffusie in het extracellulaire milieu van de tumor beschrijft;
3. een celmodel dat beschrijft hoe inotuzumab zich bindt aan CD22, internalisatie, intracellulaire vrijgave van N-Ac-γ-calicheamicine DMH, binding aan DNA, en efflux uit de tumorcel;
4. tumorgroei en -regressie afhankelijk van de concentratie N-Ac-γ-calicheamicine DMH.

Preklinische data in xenograft muismodellen voor NHL en ALL werden eerst gemodelleerd, waarna de translatie naar de kliniek volgde door gebruik te maken van humane PK voor inotuzumab en klinisch relevante tumorvolumes, tumorgroeisnelheden, en CD22-expressiewaarden in de relevante patiëntenpopulaties. Klinische studiesimulaties werden uitgevoerd met 1000 gesimuleerde patiënten per dosisniveau, waarbij in de modelparameters gevarieerd werd met verschillende geneesmiddel-, patiënt- en ziektekenmerken. De resulterende stochastische modellen voorspelden voor inotuzumab bij patiënten progressievrije overlevingspercentages (progression-free survival, PFS) die vergelijkbaar waren met de waargenomen klinische resultaten. Door de meer mechanistische aard kan het model worden gebruikt voor specifieke kwantitatieve vragen, zoals de optimalisatie van de doseringsschema's voor NHL en ALL. Ook kan het gebruikt worden om sensitieve parameters te onderzoeken die mogelijk van invloed zijn op de werkzaamheid in de kliniek en die gebruikt kunnen worden voor klinische diagnostiek en potentiële biomarkers [17].

In **hoofdstuk 6** werd een translationeel QSP-model gepresenteerd voor CD3-bispecifieke moleculen, dat *in silico*, *in vitro* en *in vivo* data samenvoegt in een mechanistisch kader, om het effect voor de verschillende soorten te kwantificeren en te voorspellen [18]. CD3-bispecifieke antilichamen binden zich aan CD3 op het oppervlak van T-cellen en een tumorgeassocieerd antigeen op het oppervlak van tumorcellen, om een trimeer te vormen (een molecuul dat is opgebouwd uit drie dezelfde eenheden), waarmee een immunologische synaps wordt nagebootst. De vorming van trimeren zet aan tot activatie van T-cellen en het vrijkomen van perforine en granzyme B, wat leidt tot cytotoxiciteit. Het voorgestelde QSP-model kon de vorming van trimeren voorspellen en deze koppelen aan het doden van tumorcellen. Het model werd gebruikt om de PKPD-relatie van een CD3-bispecifiek antilichaam te kwantificeren dat zich richt op P-cadherine (PF-06671008). Het beschrijft de dispositie van PF-06671008 in het centrale compartiment en de tumor in xenograft muismodellen, inclusief binding aan het target en aan T-cellen in de tumor om het trimeer te vormen. Het model omvat T-celdistributie naar de tumor, proliferatie en krimp. PKPD-parameters werden geschat voor PF-06671008 en een tumorstasisconcentratie (TSC) werd berekend als een schatting van de minimale effectieve trimeerconcentratie. De translatie naar de kliniek werd gemaakt door het opnemen van de voorspelde PF-06671008 humane PK, met inbegrip van binding aan oplosbare P-cadherine, en klinisch relevante systeemparameters zoals CD3 en P-cadherine receptor expressie, en het aantal T-cellen en tumorcellen. Het model werd gebruikt om de klinische PK en de werkzaamheid te voorspellen en om sensitieve parameters te bepalen die van invloed zijn op klinisch effectieve doses [18].

Belangrijkste lessen:

1. *In het geval van complexe biologische systemen met meerdere variabelen en netwerken is het raadzaam om een wiskundig systeemmodel te bouwen dat in staat is om preklinische data te integreren en te interpreteren, en dat een kwantitatief kader biedt voor de translatie naar de kliniek.*
2. *Kies het juiste formaat model en het juiste translationele strategieniveau in relatie tot de gestelde vraag.*
3. *De translatie van xenograft muisstudies naar de kliniek is mogelijk, mits vergezeld van een nauwgezette, systematische kwantitatieve analyse waarin rekening wordt gehouden met de verschillen tussen het muisexperimentele systeem en de kliniek, zoals door de wiskundige modellering mogelijk wordt gemaakt.*
4. *Mechanistische QSP-modellen vergen een investering op het gebied van datavereisten en ontwikkeltijd, maar leveren veel gedetailleerde antwoorden op.*
5. *Deterministische modellen kunnen worden gecombineerd met stochastische simulaties (bijvoorbeeld virtuele patiëntensimulaties) om werkzaamheidseindpunten zoals RECIST-criteria te voorspellen.*

9.4 Het gebruik van mechanistische modellering voor de optimalisatie van klinische doseringsschema's

Een belangrijk onderwerp in dit proefschrift was het gebruik van mechanistische modellering en simulatie om de opzet van klinische doseringsschema's te optimaliseren. Dit omvatte

achtereenvolgens de selectie van de klinische startdosis met behulp van een minimaal te verwachten biologisch effectniveau (minimal anticipated biological effect level, hierna MABEL), de voorspelling van de klinisch effectieve dosis en het doseringsschema, en het identificeren van factoren die van invloed kunnen zijn op variaties in de effectieve dosis. Zoals hiervoor besproken, werden in **hoofdstuk 5 en 6** mechanistische QSP-modellen ontwikkeld en ingezet om effectieve doses te voorspellen voor respectievelijk een ADC (inotuzumab) en een CD3-bispecifiek molecuul (P-cad LP-DART). Voor inotuzumab werden verschillende versies van het model ontwikkeld voor de behandeling van hematologische tumoren (bijvoorbeeld ALL) en vaste tumoren (bijvoorbeeld NHL). Deze versies verschillen in de beschrijving van tumordispositie en in typische tumorkenmerken zoals tumorgroeisnelheid en initiële tumorvolumes. Het model werd uiteindelijk gebruikt voor de aanbeveling van een gefractioneerd doseringsschema voor ALL, dat tumorregressiever zou zijn dan het standaard Q4W-schema voor de behandeling van NHL [17].

In **hoofdstuk 7** werd een QSP-modelleringsaanpak geïntroduceerd om een MABEL-gebaseerde klinische startdosis van bispecifieke antilichamen (bsAbs) te selecteren. Deze aanpak is gebaseerd op tumor-trimeerconcentraties die de werkzaamheid bevorderen, en corrigeert verschillen tussen *in vitro* experimentele condities en de kliniek. De methode werd gebruikt om de klinische startdosis van een P-cadherine/CD3-bsAb te voorspellen. Eerst werd een mechanistisch *in vitro* model gemaakt dat de voorspelde trimeerconcentratie koppelde aan de *in vitro* T-celkinetische en cytotoxiciteitsexperimenten, om de EC_{20} van het trimeer te bepalen die zorgt voor de T-celproliferatie en het doden van de tumorcellen. Het model was in staat om *in vitro* data te verzamelen bij verschillende E:T-verhoudingen met dezelfde EC_{20}-waarde. Dit *in vitro* MABEL werd vervolgens vertaald naar het *in vivo* MABEL om de humane MABEL-dosis te voorspellen, door de voorspelde humane PK (en binding aan oplosbaar P-cadherine) en de hiervoor beschreven fysiologische parameters hierin mee te nemen. De humane MABEL-dosis werd gesteld als de voorspelde gemiddelde tumor-trimeerconcentratie in evenwichtstoestand gelijk aan het *in vitro* MABEL (EC_{20}, trimeer). Deze methode werd vergeleken met benaderingen vanuit andere invalshoeken, zoals PK-gebaseerde methoden en receptorbezetting. De QSP-benadering leverde de meest geschikte startdosis, die onafhankelijk van de experimentele omstandigheden veiligheid en effect combineerde [19].

Belangrijkste lessen:

1. *QSP-modellering kan worden gebruikt om de optimale dosis en doseringsschema's voor verschillende indicaties te voorspellen, zoals hematologische versus vaste tumoren.*
2. *QSP-modellering biedt een alternatieve methode voor het voorspellen van MABEL-gebaseerde klinische startdoses die minder afhankelijk is van experimentele omstandigheden.*

9.5 Het gebruik van mechanistische modellering voor precisiemedicijnkwesties

Een ander thema in dit proefschrift was het gebruik van QSP-modellering om uit te vinden welke factoren de dosering en planning van oncologiegeneesmiddelen kunnen beïnvloeden, en om te bepalen welke patiënten het beste reageren op een bepaalde therapie. In overeenstemming met

een precisiemedicijnbenadering zou deze informatie van groot belang kunnen zijn bij de selectie van geschikte diagnostica en biomarkers die in de kliniek onderzocht kunnen worden, om zo de therapeutische strategieën in de oncologie te optimaliseren [20].

In **hoofdstuk 5** werd een QSP-model ontwikkeld voor inotuzumab, een ADC dat CD22 aanvalt op B-cel maligniteiten [17]. Het model werd gebruikt voor preklinische naar klinische translatie, en om doses en doseringsschema's te optimaliseren voor een nieuw te onderzoeken indicatie (ALL) versus de oorspronkelijke indicatie (NHL). De ontwikkeling van inotuzumab voor r/r NHL is onlangs beëindigd omdat het niet superieur was ten opzichte van de zorgstandaard. Een uitgevoerde sensitiviteitsanalyse gaf inzicht in de parameters die het effect van inotuzumab versus NHL definiëren of zelfs beperken. Relevante parameters waarmee in het model werd gevarieerd waren: CD22 receptor expressie, mate van calicheamicine efflux, inotuzumab PK (klaringssnelheid) en tumorgroeisnelheid. De tumorgroeisnelheid bleek de meest sensitieve parameter. Hieruit komt naar voren dat patiënten voor de agressievere NHL-subtypes zoals diffuus grootcellig B-cellymfoom (DLBCL) significant hogere doses zouden moeten krijgen om effect te hebben, in vergelijking met langzamer groeiende NHL-subtypes zoals folliculair lymfoom. Calicheamicine efflux uit de tumorcel was ook een sensitieve parameter. Dat is van belang omdat N-Ac-γ-calicheamicine DMH een substraat is voor MDR1, een effluxtransporter die op veel tumorceltypes is opgereguleerd. De minst sensitieve parameter was CD22 receptor expressie. Hieruit bleek de geschiktheid van deze receptor als een ADC-target, vanwege de hoge expressie in B-cellen en de hoge internalisatiesnelheid. Deze bevindingen suggereren dat de MDR1-status bij patiënten een betere indicatie van de werkzaamheid is dan de CD22 receptor expressie.

In **hoofdstuk 6** werd een soortgelijke benadering gevolgd. Hierin werden met behulp van een sensitiviteitsanalyse de belangrijkste parameters bepaald die van invloed zijn op de voorspelde klinisch effectieve dosis voor P-cad LP-DART, een CD3-bispecifiek antilichaam [18]. Uit de analyse kwam naar voren dat P-cad expressie een sensitieve parameter was, waaruit bleek dat er een hogere dosis nodig is voor patiënten met een lage P-cadherine expressie. Het aantal T-cellen in de tumor was ook een sensitieve parameter, die aangaf dat een hogere voorspelde dosis nodig is voor de werkzaamheid bij lage verhoudingen effector : doelcel. Concluderend kunnen wiskundige modellen en de hiervoor besproken strategieën helpen bij het bepalen welke geneesmiddelen het meest geschikt zijn voor een patiënt. Daarnaast kunnen ze gebruikt worden om doserings- en combinatieschema's te optimaliseren en om alternatieve en verbeterde toedieningsschema's voor te stellen.

Belangrijkste les:

> *Met behulp van sensitiviteitsanalyse en simulaties kan QSP-modellering worden gebruikt om essentiële parameters te identificeren die het resultaat van klinische studies kunnen beïnvloeden.*

9.6 Platformmodellen voor biotherapeutische modaliteiten

Het ADC QSP-model (**hoofdstuk 5**) en het CD3-bispecifieke model (**hoofdstuk 6**) zijn mogelijke platformmodellen voor specifieke biotherapeutische modaliteiten in de oncologie. Deze QSP-modellen vormen een geïntegreerde kwantitatieve gemeenschappelijke kennisbank voor

verdere preklinische en klinische evaluatie [21]. Ze zijn niet specifiek voor een bepaald geneesmiddel en kunnen daarom breed worden toegepast. Ze bieden een mechanistisch kader voor het voorspellen van de werkzaamheid, waardoor ze zich onderscheiden van andere farmacometrische strategieën [21]. Het zijn vaak zowel multischaalmodellen als modulaire modellen, die kunnen worden gebruikt om *in vitro*, preklinische *in vivo* en klinische data in kaart te brengen. Als zodanig kunnen ze worden gebruikt om beslissingen tijdens onderzoeksprogramma's te ondersteunen, van verkennend onderzoek tot de laatste klinische testfasen. Platformmodellen vergen een investering op het gebied van datavereisten, maar leveren veel gedetailleerde antwoorden op.

Het ADC QSP-model beschrijft het complexe werkingsmechanisme van ADC's, zoals de beschrijving van ADC en payloaddispositie op zowel celniveau als fysiologisch niveau, om de klinische resultaten van ADC's te voorspellen [17]. Het model beschrijft:

a. plasma PK inclusief dispositie en klaring van ADC en vrijgekomen payload;
b. een tumordispositiemodel voor ADC en payloaddiffusie in de extracellulaire omgeving van de tumor;
c. een celmodel dat beschrijft hoe ADC zich bindt aan zijn target op tumorcellen, internalisatie, intracellulaire payloadvrijgave, hoe de payload zich bindt aan zijn target, en de payload-efflux uit de tumorcel;
d. tumorgroei en -remming in xenograft muismodellen als functie van de tumor-payloadconcentratie.

Het CD3-bsAb-model is een mogelijk platformmodel voor bsAbs die immuuncellen binden, waarbij tumorcellen worden gekoppeld aan een immuuneffectorcel, zodat cytotoxiciteit wordt gericht tegen de tumorcel [18]. Het huidige model werd gebruikt om een bispecifiek molecuul te omschrijven dat zich bindt aan CD3 op T-cellen en P-cadherine op tumorcellen (P-cad LP-DART) [18]. Het model beschrijft:

1. plasma PK, waaronder bsAb-binding aan oplosbare targetcellen en circulerende T-cellen in de systemische circulatie;
2. een tumordispositiemodel dat de bsAb-diffusie in de tumor beschrijft;
3. binding van het bsAb aan T-cellen en tumorcellen om dimeren en trimeren te vormen;
4. T-celdistributie naar de tumor, proliferatie en krimp;
5. tumorgroei en -remming in xenograft muismodellen gerelateerd aan de tumor-trimeerconcentratie.

Deze platformmodellen kunnen voor een aantal doeleinden worden gebruikt:

7. optimalisatie van het ontwerp van ADC's of CD3-bsAbs in het vroege onderzoek, voor een maximale kans op succes;
8. ontwerp en interpretatie van preklinische *in vitro* en *in vivo* experimenten voor de efficiënte en effectieve selectie van veelbelovende verbindingen (lead compounds);
9. translatie van preklinische data naar de kliniek om de klinisch effectieve dosis en dosering te voorspellen;

10. voorspelling van de werking van een geneesmiddel (bijvoorbeeld tumorgroeiremming, RECIST-criteria) en optimalisatie van dosis en dosering voor oncologische indicaties;
11. inzicht in de verschillen in respons op een medicijn in de kliniek, en het gebruik van deze informatie voor de bepaling van geschikte diagnostische criteria voor patiëntenselectie en klinische biomarkers, om zo een vroeg beeld te krijgen van de werkzaamheid;
12. vergelijking met de klinische zorgstandaard.

Bovendien kunnen de huidige modelstructuren worden uitgebreid om toxiciteiten te voorspellen die in verband worden gebracht met het werkingsmechanisme. Zo kan het ADC-model worden uitgebreid met de beschrijving van de ADC-opname en -afgifte in megakaryocyten en bloedplaatjes, om ADC-toxiciteit die doorgaans wordt waargenomen te kwantificeren, zoals neutropenie en trombocytopenie. Het CD3-bsAb-model kan worden uitgebreid om de vorming van trimeren in verband te brengen met cytokineafgifte om het cytokine release syndroom te voorspellen. Verder zouden beide modellen kunnen worden uitgebreid om het effect van combinatietherapieën te voorspellen. Zo zou bijvoorbeeld een immuuntherapiemodel kunnen worden toegevoegd om de combinatie met checkpointremmers zoals anti-PD1 mAbs te voorspellen.

Belangrijkste les:

> *De QSP-platformmodellen kunnen in aangepaste vorm opnieuw worden gebruikt om beslissingen tijdens onderzoeksprogramma's te ondersteunen, van verkennend onderzoek tot de laatste klinische testfasen.*

9.7 Conclusies en perspectieven

In dit proefschrift is wiskundige modellering en simulatie toegepast als een instrument om weloverwogen kwantitatieve beslissingen te nemen in het onderzoek naar en de ontwikkeling van oncologiegeneesmiddelen. Modelmatige benaderingen blijken nuttig te zijn om het werkingsmechanisme te begrijpen en de complexiteit van nieuwe biotherapeutische modaliteiten voor de behandeling van kanker te ontrafelen, zoals monospecifieke en bispecifieke monoklonale antilichamen en antilichaam-geneesmiddelconjugaten. Er zijn een aantal conclusies getrokken. Zo is bijvoorbeeld aangetoond dat modellering een nuttige methode is om dierproeven te verminderen, door correlaties van *in vitro* naar *in vivo* mogelijk te maken, en door gebruik te maken van simulatie ter vervanging van experimentele methodes. Modellering en simulatie op basis van mechanismen blijkt nuttig voor de translatie van preklinische studies naar de kliniek, om zo te garanderen dat het beste geneesmiddel doorgaat naar klinische studies. Deze modellen kunnen vervolgens worden gebruikt om het ontwerp van klinische studies te optimaliseren, van de selectie van startdoses tot de aanbevolen effectieve doses voor fase-III-studies. De modellen kunnen helpen om de variabiliteit in de kliniek beter te begrijpen, en om factoren te identificeren die van invloed zijn op de respons bij individuele patiënten. Hierdoor wordt de weg vrijgemaakt voor precisiemedicijnstrategieën, en de bepaling van de klinische diagnostiek, biomarkers en doses voor de verschillende oncologische indicaties. Tot slot blijken de ADC QSP-en CD3-bsAb-modellen potentiële platformmodellen die in aangepaste vorm verder

kunnen worden gebruikt ter ondersteuning van uiteenlopende beslissingen in het hele spectrum van geneesmiddelenonderzoek en -ontwikkeling.

Het onderzoek en de ontwikkeling van oncologiegeneesmiddelen zal complexer worden naarmate we meer te weten komen over de details van de tumorbiologie en de pleiotrope rol van het immuunsysteem. Tegelijkertijd zullen biologische therapieën steeds complexer worden, door de multispecifieke antilichamen die zich kunnen richten op verschillende receptoren en die verschillende netwerken kunnen beïnvloeden, en door nieuwe celtherapieën en geneesmiddelencombinaties die leiden tot nieuwe biologische effecten en synergie. Mechanistische modellering en simulatie zullen hierdoor een essentiële methode worden in het onderzoek naar en de ontwikkeling van oncologische geneesmiddelen, om de vaak niet-intuïtieve processen te begrijpen en het nemen van rationele beslissingen te ondersteunen.
Om dit proces mogelijk te maken is het noodzakelijk om modellering en simulatie eerder in het geneesmiddelenonderzoek toe te passen, teneinde in latere klinische studies het succespercentage te verhogen. Er zullen steeds meer mogelijkheden komen om QSP-modellering te combineren met nieuwe technologieën. Ongetwijfeld zal de integratie van big data en datawetenschap (onder andere crowdsourcing en machinaal leren) met QSP-modellering een belangrijke rol gaan spelen bij de toepassing van wiskundige modellering voor de besluitvorming binnen het oncologiegeneesmiddelenonderzoek. Op deze manier kan de schat aan gegevens uit biomarkers en de genomica worden toegepast om de voordelen van QSP-modellering ten volle te benutten, zodat patiënten uiteindelijk de optimale behandeling zullen krijgen.

9.8 Referenties

1. Zhu, H., et al., *Model-Informed Drug Development: A Regulatory Perspective on Progress.* Clinical Pharmacology & Therapeutics, 2019. **106**(1): p. 91-93.
2. Wong, C.H., K.W. Siah, and A.W. Lo, *Estimation of clinical trial success rates and related parameters.* Biostatistics (Oxford, England), 2019. **20**(2): p. 273-286.
3. Brinkmann, U. and R.E. Kontermann, *The making of bispecific antibodies.* mAbs, 2017. **9**(2): p. 182-212.
4. Yu, J.X., et al., *Cancer cell therapies: the clinical trial landscape.* Nat Rev Drug Discov, 2020.
5. Xin Yu, J., V.M. Hubbard-Lucey, and J. Tang, *Immuno-oncology drug development goes global.* Nat Rev Drug Discov, 2019. **18**(12): p. 899-900.
6. Agoram, B.M., S.W. Martin, and P.H. van der Graaf, *The role of mechanism-based pharmacokinetic-pharmacodynamic (PK-PD) modelling in translational research of biologics.* Drug Discov Today, 2007. **12**(23-24): p. 1018-24.
7. Agoram, B.M. and O. Demin, *Integration not isolation: arguing the case for quantitative and systems pharmacology in drug discovery and development.* Drug Discov Today, 2011. **16**(23-24): p. 1031-6.
8. Betts, A., et al., *Linear pharmacokinetic parameters for monoclonal antibodies are similar within a species and across different pharmacological targets: A comparison between human, cynomolgus monkey and hFcRn Tg32 transgenic mouse using a population-modeling approach.* MAbs, 2018. **10**(5): p. 751-764.

9. *The Principles of Humane Experimental Technique.* Medical Journal of Australia, 1960. **1**(13): p. 500-500.
10. Shah, D.K., et al., *Establishing in vitro–in vivo correlation for antibody drug conjugate efficacy: a PK/PD modeling approach.* Journal of Pharmacokinetics and Pharmacodynamics, 2018. **45**(2): p. 339-349.
11. Jung, J., *Human tumor xenograft models for preclinical assessment of anticancer drug development.* Toxicological research, 2014. **30**(1): p. 1-5.
12. Sausville, E.A. and A.M. Burger, *Contributions of Human Tumor Xenografts to Anticancer Drug Development.* Cancer Research, 2006. **66**(7): p. 3351.
13. Rocchetti, M., et al., *Predicting the active doses in humans from animal studies: A novel approach in oncology.* European Journal of Cancer, 2007. **43**(12): p. 1862-1868.
14. Wong, H., et al., *Antitumor Activity of Targeted and Cytotoxic Agents in Murine Subcutaneous Tumor Models Correlates with Clinical Response.* Clinical Cancer Research, 2012. **18**(14): p. 3846.
15. Zhu, A.Z., *Quantitative translational modeling to facilitate preclinical to clinical efficacy & toxicity translation in oncology.* Future science OA, 2018. **4**(5): p. FSO306-FSO306.
16. Betts, A., et al., *Use of translational modeling and simulation for quantitative comparison of PF-06804103, a new generation HER2 ADC, with Trastuzumab-DM1.* J Pharmacokinet Pharmacodyn, 2020.
17. Betts, A.M., et al., *Preclinical to Clinical Translation of Antibody-Drug Conjugates Using PK/PD Modeling: a Retrospective Analysis of Inotuzumab Ozogamicin.* Aaps j, 2016. **18**(5): p. 1101-1116.
18. Betts, A., et al., *A Translational Quantitative Systems Pharmacology Model for CD3 Bispecific Molecules: Application to Quantify T Cell-Mediated Tumor Cell Killing by P-Cadherin LP DART((R)).* AAPS J, 2019. **21**(4): p. 66.
19. Betts, A. and P.H. van der Graaf, *Mechanistic quantitative pharmacology strategies for the early clinical development of bispecific antibodies in oncology.* Clin Pharmacol Ther, 2020.
20. Barbolosi, D., et al., *Computational oncology — mathematical modelling of drug regimens for precision medicine.* Nature Reviews Clinical Oncology, 2016. **13**(4): p. 242-254.
21. Musante, C.J., et al., *Quantitative Systems Pharmacology: A Case for Disease Models.* Clinical pharmacology and therapeutics, 2017. **101**(1): p. 24-27.

Section VI.
Appendices

Curriculum vitae

Alison Betts (1972, Edinburgh, Scotland) began her scientific career in 1990 at the University of St. Andrews in Scotland. She graduated in 1994 with a first-class honors degree in Biochemistry (BSc.) and was recipient of the class prize in Biochemistry. This course included an internship in an immunology research group at St. Andrews. In 1994, Alison moved from Scotland to the south of England to start her career at Pfizer in the department of Drug Metabolism. Here she gained extensive hands on experience of drug metabolism and pharmacokinetics and supported many small molecule drug discovery projects across diverse therapeutic areas.

From 2002-2004, Alison completed a secondment in the clinical pharmacometrics group at Pfizer. Here she learned the art and science of modeling, providing PK/PD support to the Pain research unit. In 2005, Alison joined the newly formed preclinical PK/PD group under the leadership of Dr. Piet van der Graaf. In this role she supported the Genitourinary and Obesity research units, using PK/PD modeling in the design and interpretation of experiments for small molecule drugs and performing PK and PK/PD predictions to human.

In September 2007, Alison moved to the USA with her family, to take up a new opportunity working in the Translational Modeling and Simulation (TMS) group in the department of Pharmacokinetics, Dynamics, and Metabolism (PDM) in Groton, CT. In this role, Alison had a diverse and extensive modeling career, supporting small and large molecule mathematical modeling across many research areas. Highlights included her role as TMS team leader supporting the antibacterial research group. In this role she was responsible for the successful execution of PK/PD modeling and translational strategy across the antibacterial portfolio including projects from exploratory stage through to Phase 1 clinical development. Here, Alison implemented mechanism-based PK/PD, PBPK and QSP models to predict efficacy and emergence of resistance and used these to develop novel strategies for clinical dose predictions of antibacterial drugs. In this work, Alison's team was awarded a Pfizer Leadership Team Excellence Award 2009. A particular focus was the establishment of *in vitro*: *in vivo* correlations so that *in vitro* models could be used to replace *in vivo* experiments. This work resulted in a reduction in *in vivo* animal spend by 40% and was awarded Pfizer Animal Care and Welfare Board 'Reduce, Re-use and Refine' award in 2010.

In 2010, Alison assumed responsibility as TMS team leader supporting the biotherapeutics division of the Oncology research unit at Pfizer. Alison's team supported a diversity of novel biotherapeutic modalities including proteins, peptides, antibodies, antibody drug conjugates (ADCs), bispecific antibodies, T cell engagers, cytokine conjugates and nanoparticles. Highlights of this work included providing modeling and simulation support to progress two ADCs to the market (Mylotarg® and Besponsa®) and many others to clinical studies. In this time, Alison was leader of the ADC working group at Pfizer, defining the quantitative analytical and predictive strategy for ADCs at Pfizer from preclinical stage through to clinical studies and she completed a

successful external partnership with Prof. Dane Wittrup's lab at the Koch Institute for Integrative Cancer Research, MIT to model intracellular trafficking of ADCs.

During this time, Alison became leader of the preclinical modeling and simulation discipline for the biotherapeutics division of PDM, including TMS teams in Cambridge MA, Groton CT and La Jolla CA. This included overseeing TMS support to Immunology & Inflammation, Oncology, Rare Diseases, Cardiovascular metabolic diseases, Neuroscience, and the Center for Therapeutic Innovation. Here she was responsible for leading scientific vision, defining strategy and for day-to-day process management of the group, including technical, infrastructure, resourcing (internal and outsourcing) and budgetary requirements. In this time, Alison's role and team transitioned from Groton, CT to Cambridge, MA.

In 2017, during her time at Pfizer, Alison started her PhD research on quantitative systems pharmacology modeling of biotherapeutic drugs in oncology at the Leiden Academic Centre for Drug Research (LACDR), under the supervision of Prof. dr. Piet H. van der Graaf. This gave Alison the opportunity to further explore her passions for using mechanistic modeling to enable quantitative decision making in oncology drug discovery, for preclinical to clinical translation, to optimize clinical dosing regimens and address precision medicine questions.

After 25 years at Pfizer, Alison started a new career path with Applied Biomath in 2019. Alison is Senior Director of Scientific Collaborations and Fellow of Modeling and Simulation at ABM, where she collaborates with partners to introduce mechanistic system pharmacology modeling approaches at preclinical and clinical stages to de-risk drug programs within the pharmaceutical and biotechnology industry. She maintains a hands-on approach as project leader for several modeling collaborations across therapeutic modalities. She is also recipient and Principal Investigator of an NIH SBIR Grant to build a platform QSP model for ADCs (ADC Workbench) capable of predicting efficacy and toxicity with the aim of reducing TI.

In her diverse and extensive modeling and simulation career, Alison has published 31 manuscripts and has given 40 invited presentations at conferences.

List of Publications

1. Spinosa, P., Musial-Siwek, M., Presler, M., **Betts, A.,** Rosentrater, E., Villali, J., Wille, L., Zhao, Y., McCaughtry, T., Subramanian, K., & Liu, H. (2021). Quantitative modeling predicts competitive advantages of a next generation anti-NKG2A monoclonal antibody over monalizumab for the treatment of cancer. *CPT: pharmacometrics & systems pharmacology*, *10*(3), 220–229. https://doi.org/10.1002/psp4.12592
2. Root, A.R., **Betts, A.,** *et al.* (2021). Discovery and optimization of a novel anti-GUCY2c x CD3 bispecific antibody for the treatment of solid tumors. *MAbs*, 13(1):1850395. doi:10.1080/19420862.2020.1850395
3. **Betts, A.,** Clark, T., Jasper, P., Tolsma, J., van der Graaf, P. H., Graziani, E. I., Rosfjord, E., Sung, M., Ma, D., & Barletta, F. (2020). Use of translational modeling and simulation for quantitative comparison of PF-06804103, a new generation HER2 ADC, with Trastuzumab-DM1. *Journal of pharmacokinetics and pharmacodynamics*, *47*(5), 513–526. https://doi.org/10.1007/s10928-020-09702-3
4. **Betts, A.,** & van der Graaf, P. H. (2020). Mechanistic Quantitative Pharmacology Strategies for the Early Clinical Development of Bispecific Antibodies in Oncology. *Clinical pharmacology and therapeutics*, *108*(3), 528–541. https://doi.org/10.1002/cpt.1961
5. **Betts, A.,** Haddish-Berhane, N., Shah, D. K., van der Graaf, P. H., Barletta, F., King, L., Clark, T., Kamperschroer, C., Root, A., Hooper, A., & Chen, X. (2019). A Translational Quantitative Systems Pharmacology Model for CD3 Bispecific Molecules: Application to Quantify T Cell-Mediated Tumor Cell Killing by P-Cadherin LP DART®. *The AAPS journal*, *21*(4), 66. https://doi.org/10.1208/s12248-019-0332-z
6. Jones, H. M., Zhang, Z., Jasper, P., Luo, H., Avery, L. B., King, L. E., Neubert, H., Barton, H. A., **Betts, A. M.,** & Webster, R. (2019). A Physiologically-Based Pharmacokinetic Model for the Prediction of Monoclonal Antibody Pharmacokinetics From In Vitro Data. *CPT: pharmacometrics & systems pharmacology*, *8*(10), 738–747. https://doi.org/10.1002/psp4.12461
7. **Betts, A.,** Keunecke, A., van Steeg, T.J., van der Graaf, P.H., Avery, L.B., Jones, H., Berkhout, J. (2018) Linear pharmacokinetic parameters for monoclonal antibodies are similar within a species and across different pharmacological targets: A comparison between human, cynomolgus monkey and hFcRn Tg32 transgenic mouse using a population-modeling approach. *MAbs,* 10(5):751-764. doi: 10.1080/19420862.2018.1462429.
8. Shah, D.K., Loganzo, F., Haddish-Berhane, N., Musto, S., Wald, H.S., Barletta, F., Lucas, J., Clark, T., Hansel, S., **Betts, A.,** (2018) Establishing in vitro-in vivo correlation for antibody drug conjugate efficacy: a PK/PD modeling approach. *J Pharmacokinet Pharmacodyn*, 45(2):339-349 (ISSN: 1573-8744)
9. Damelin, M., **Betts, A.**, *et al.* (2017) A PTK7-targeted antibody-drug conjugate reduces tumor-initiating cells and induces sustained tumor regressions. *Sci Transl Med,* 9(372). doi: 10.1126/scitranslmed.aag2611.
10. **Betts, A.M.,** Haddish-Berhane, N., Tolsma, J., Jasper, P., King, L.E., Sun, Y., Chakrapani, S., Shor, B., Boni, J., Johnson, T.R. (2016) Preclinical to Clinical Translation of Antibody-Drug Conjugates Using PK/PD Modeling: a Retrospective Analysis of Inotuzumab Ozogamicin. *AAPS J.*, 18(5):1101-1116. doi: 10.1208/s12248-016-9929-7.
11. Chen, X., Haddish-Berhane, N., Moore, P., Clark, T., Yang, Y., Li, H., Xuan, D., Barton, H. A., **Betts, A. M.,** & Barletta, F. (2016) Mechanistic Projection of First-in-Human Dose for Bispecific Immunomodulatory P-Cadherin LP-DART: An Integrated PK/PD Modeling Approach. *Clinical pharmacology and therapeutics,* 100(3), 232–241. https://doi.org/10.1002/cpt.393

12. Maass, K. F., Kulkarni, C., **Betts, A. M.,** & Wittrup, K. D. (2016) Determination of Cellular Processing Rates for a Trastuzumab-Maytansinoid Antibody-Drug Conjugate (ADC) Highlights Key Parameters for ADC Design. *The AAPS journal*, 18(3), 635–646. https://doi.org/10.1208/s12248-016-9892-3
13. Singh, A. P., Maass, K. F., **Betts, A. M.,** Wittrup, K. D., Kulkarni, C., King, L. E., Khot, A., & Shah, D. K. (2016) Evolution of Antibody-Drug Conjugate Tumor Disposition Model to Predict Preclinical Tumor Pharmacokinetics of Trastuzumab-Emtansine (T-DM1). *The AAPS journal*, 18(4), 861–875. https://doi.org/10.1208/s12248-016-9904-3
14. Maass, K. F., Kulkarni, C., Quadir, M. A., Hammond, P. T., **Betts, A. M.,** & Wittrup, K. D. (2015) A Flow Cytometric Clonogenic Assay Reveals the Single-Cell Potency of Doxorubicin. *Journal of pharmaceutical sciences*, 104(12), 4409–4416. https://doi.org/10.1002/jps.24631
15. Singh, A. P., Krzyzanski, W., Martin, S. W., Weber, G., **Betts, A.,** Ahmad, A., Abraham, A., Zutshi, A., Lin, J., & Singh, P. (2015) Quantitative prediction of human pharmacokinetics for mAbs exhibiting target-mediated disposition. *The AAPS journal*, 17(2), 389–399. https://doi.org/10.1208/s12248-014-9690-8
16. **Alison M. Betts**, Oliver Ackaert, Kristin Bergmann, Nahor Haddish- Berhane, Jian Lin, Sharon Ripp, John O'Donnell, and Deb Hanna. 'Use of a PK/PD Modeling and Simulation Approach to Predict Clinical Efficacy of Macrolide Antibiotics Telithromycin and PF-04287881 versus Streptococcus pneumonia'. In preparation.
17. Shah, D. K., King, L. E., Han, X., Wentland, J. A., Zhang, Y., Lucas, J., Haddish-Berhane, N., **Betts, A.,** & Leal, M. (2014). A priori prediction of tumor payload concentrations: preclinical case study with an auristatin-based anti-5T4 antibody-drug conjugate. *The AAPS journal*, *16*(3), 452–463. https://doi.org/10.1208/s12248-014-9576-9
18. Sapra, P., **Betts, A.,** & Boni, J. (2013). Preclinical and clinical pharmacokinetic/pharmacodynamic considerations for antibody-drug conjugates. *Expert review of clinical pharmacology*, *6*(5), 541–555. https://doi.org/10.1586/17512433.2013.827405
19. Shah, D. K., Barletta, F., **Betts, A.,** & Hansel, S. (2013). Key bioanalytical measurements for antibody-drug conjugate development: PK/PD modelers' perspective. *Bioanalysis*, *5*(9), 989–992. https://doi.org/10.4155/bio.13.78
20. Haddish-Berhane, N., Shah, D. K., Ma, D., Leal, M., Gerber, H. P., Sapra, P., Barton, H. A., & **Betts, A. M.** (2013). On translation of antibody drug conjugates efficacy from mouse experimental tumors to the clinic: a PK/PD approach. *Journal of pharmacokinetics and pharmacodynamics*, *40*(5), 557–571. https://doi.org/10.1007/s10928-013-9329- Experimental Tumors to the Clinic: a PK/PD Approach'.
21. Shah, D. K., & **Betts, A. M.** (2013). Antibody biodistribution coefficients: inferring tissue concentrations of monoclonal antibodies based on the plasma concentrations in several preclinical species and human. *mAbs*, *5*(2), 297–305. https://doi.org/10.4161/mabs.23684
22. Shah, D. K., Haddish-Berhane, N., & **Betts, A.** (2012). Bench to bedside translation of antibody drug conjugates using a multiscale mechanistic PK/PD model: a case study with brentuximab-vedotin. *Journal of pharmacokinetics and pharmacodynamics*, *39*(6), 643–659. https://doi.org/10.1007/s10928-012-9276-y
23. Shah, D. K., & **Betts, A. M.** (2012). Towards a platform PBPK model to characterize the plasma and tissue disposition of monoclonal antibodies in preclinical species and human. *Journal of pharmacokinetics and pharmacodynamics*, *39*(1), 67–86. https://doi.org/10.1007/s10928-011-9232-2
24. Attkins, N., **Betts, A.,** Hepworth, D., & Heatherington, A. C. (2010). Pharmacokinetics and elucidation of the rates and routes of N-glucuronidation of PF-592379, an oral dopamine 3 agonist in rat, dog, and human. *Xenobiotica; the fate of foreign compounds in biological systems*, *40*(11), 730–742. https://doi.org/10.3109/00498254.2010.514961

25. **Betts, A. M.,** Clark, T. H., Yang, J., Treadway, J. L., Li, M., Giovanelli, M. A., Abdiche, Y., Stone, D. M., & Paralkar, V. M. (2010). The application of target information and preclinical pharmacokinetic/pharmacodynamic modeling in predicting clinical doses of a Dickkopf-1 antibody for osteoporosis. *The Journal of pharmacology and experimental therapeutics*, *333*(1), 2–13. https://doi.org/10.1124/jpet.109.164129
26. Blasi, E., Bamberger, M., Knight, D., Engwall, M., Wolk, R., Winter, S., **Betts, A.,** John-Baptiste, A., & Keiser, J. (2009). Effects of CP-532,623 and torcetrapib, cholesteryl ester transfer protein inhibitors, on arterial blood pressure. *Journal of cardiovascular pharmacology*, *53*(6), 507–516. https://doi.org/10.1097/FJC.0b013e3181a8184c
27. Mantell, S. J., Gibson, K. R., Osborne, S. A., Maw, G. N., Rees, H., Dodd, P. G., Greener, B., Harbottle, G. W., Million, W. A., Poinsard, C., England, S., Carnell, P., **Betts, A. M.,** Monhemius, R., & Prime, R. L. (2009). In vitro and in vivo SAR of pyrido[3,4-d]pyramid-4-ylamine based mGluR1 antagonists. *Bioorganic & medicinal chemistry letters*, *19*(8), 2190–2194. https://doi.org/10.1016/j.bmcl.2009.02.106
28. **Betts, A.,** Atkinson, F., Gardner, I., Fox, D., Webster, R., Beaumont, K., & Morgan, P. (2007). Impact of physicochemical and structural properties on the pharmacokinetics of a series of alpha1L-adrenoceptor antagonists. *Drug metabolism and disposition: the biological fate of chemicals*, *35*(8), 1435–1445. https://doi.org/10.1124/dmd.107.015180
29. Harrison, A., **Betts, A.,** Fenner, K., Beaumont, K., Edgington, A., Roffey, S., Davis, J., Comby, P., & Morgan, P. (2004). Nonlinear oral pharmacokinetics of the alpha-antagonist 4-amino-5-(4-fluorophenyl)-6,7-dimethoxy-2-[4-(morpholinocarbonyl)-perhydro-1,4-diazepin-1-yl]quinoline in humans: use of preclinical data to rationalize clinical observations. *Drug metabolism and disposition: the biological fate of chemicals*, *32*(2), 197–204. https://doi.org/10.1124/dmd.32.2.197
30. Beaumont, K., **Harper, A.,** Smith, D. A., & Abel, S. (2000). Pharmacokinetics and metabolism of a sulphamide NK2 antagonist in rat, dog and human. *Xenobiotica; the fate of foreign compounds in biological systems*, *30*(6), 627–642. https://doi.org/10.1080/004982500406453
31. Beaumont, K., **Harper, A.,** Smith, D. A., & Bennett, J. (2000). The role of P-glycoprotein in determining the oral absorption and clearance of the NK2 antagonist, UK-224,671. *European journal of pharmaceutical sciences : official journal of the European Federation for Pharmaceutical Sciences*, *12*(1), 41–50. https://doi.org/10.1016/s0928-0987(00)00144-5

Affiliations of Authors

Lindsay B. Avery	*Department of Biomedicine Design, Pfizer Inc., 1 Burtt Road, Andover, MA*
Frank Barletta	*Oncology Research & Development, Pfizer Inc, 401 N Middletown Rd, Pearl River, NY 10965*
Jan Berkhout	*LAP&P, Archimedesweg 31, 2333 CM Leiden, The Netherlands*
Joseph Boni	*Department of Clinical Pharmacology, Pfizer Global Research and Development, Collegeville, PA*
Subramanyam Chakrapani	*Department of Worldwide Medicinal Chemistry, Pfizer Global Research and Development, Groton, CT 06340*
Xiaoying Chen	*Department of Clinical Pharmacology, 10555 Science Center Dr, San Diego CA 92121*
Tracey Clark	*Established Med Business, Pfizer Inc., Eastern Point Rd, Groton CT 06340*
Piet H. van der Graaf	*Division of Systems Biomedicine and Pharmacology, Leiden Academic Centre for Drug Research, 2300 RA Leiden, The Netherlands*
Edmund I. Graziani	*Apertor Labs Inc., 828 Contra Costa Ave., Berkeley, CA 94707*
Nahor Haddish-Berhane	*Clinical Pharmacology and Pharmacometrics, Quantitative Sciences, Janssen Pharmaceuticals, Spring House, PA 19002*
Steve Hansel	*Translational Research Group, Department of Pharmacokinetics Dynamics and Metabolism, Pfizer Global Research and Development, Groton, CT 06340*
Andrea Hooper	*Oncology Research & Development, Pfizer Inc, 401 N Middletown Rd, Pearl River, NY 10965*
Paul Jasper	*RES Group, Inc., 75 Second Avenue, Needham, MA 02494*
Theodore R. Johnson	*Department of Pharmacokinetics Dynamics and Metabolism, Pfizer Global Research and Development, La Jolla, CA*
Hannah Jones	*Department of Biomedicine Design, Pfizer Inc., 610 Main Street, Cambridge, MA*
Cris Kamperschroer	*Department of Immunotoxicology, Pfizer Inc, 558 Eastern Point Road, Groton CT 06340*
Anne Keunecke	*LAP&P, Archimedesweg 31, 2333 CM Leiden, The Netherlands*
Lindsay E. King	*Department of Biomedicine Design, Pfizer Inc., 1 Burtt Road, Andover, MA*
Frank Loganzo	*Oncology Research Unit, Pfizer Global Research and Development, Pearl River, NY 10965*
Judy Lucas	*Oncology Research & Development, Pfizer Inc, 401 N Middletown Rd, Pearl River, NY 10965*
Dangshe Ma	*Oncology Research & Development, Pfizer Inc, 401 N Middletown Rd, Pearl River, NY 10965*
Sylvia Musto	*Oncology Research & Development, Pfizer Inc, 401 N Middletown Rd, Pearl River, NY 10965*
Adam Root	*Department of Biomedicine Design, Pfizer Inc, 610 Main Street, Cambridge, MA 02139*
Edward Rosfjord	*Oncology Research & Development, Pfizer Inc, 401 N Middletown Rd, Pearl River, NY 10965*
Dhaval K. Shah	*Department of Pharmaceutical Sciences, 455 Kapoor Hall, University at Buffalo, The State University of New York, Buffalo, New York 14214-8033*

Boris Shor	*Immune Pharmaceuticals Inc., 430 East 29th Street, Suite 940, New York, NY 10016*
Tamara J. van Steeg	*LAP&P, Archimedesweg 31, 2333 CM Leiden, The Netherlands*
Matthew Sung	*Oncology Research & Development, Pfizer Inc, 401 N Middletown Rd, Pearl River, NY 10965*
John Tolsma	*RES Group, Inc., 75 Second Avenue, Needham, MA 02494*
Hallie S. Wald	*Oncology Research & Development, Pfizer Inc, 401 N Middletown Rd, Pearl River, NY 10965*

Acknowledgements

Completion of this thesis has been a tremendous experience for me, in particular because I decided to do this at a later stage in my scientific career when I had learned what I was truly passionate about. There are many people I would like to thank for their support, contribution, and motivation.

Foremost, I would like to thank my promotor Prof. dr. Piet Hein van der Graaf, for being a continued inspiration and mentor in the field of PK/PD and mechanistic modeling, over the period of many years. I will miss our modeling conversations and your great advice. I would also like to thank Prof. dr. J. Burggraaf for being my co-promotor and your time spent reviewing my thesis.

I would like to thank Pfizer and Applied Biomath for supporting this work and for enabling to me to complete this thesis whilst continuing with my day job. Special thanks to Hannah Jones for planting the idea in my head and providing the encouragement to put it into action! Thanks to John Burke, Lou Latino and Josh Apgar at Applied Biomath for your constant support to complete this thesis.

I thank all the co-authors on the publications and collaborators in this work, who stretch across many different disciplinary groups. Research is a team effort, and this thesis would not have been possible without you. In particular, I would like to thank my best modeling buddies Nahor Haddish-Berhane and Dhaval Shah, who were major collaborators in all parts of this work. Together, we kicked the tires on many of the ideas and concepts discussed in this thesis and had a lot of fun along the way. I have learned and grown from working with you both.

To my children, Hannah, and Daniel, for reminding me what is important in life and for making me smile every day. Follow your dreams and take every opportunity in life! To my husband Nic, for always being my biggest supporter. There were moments when I didn't believe in me, but you did and always have.

Finally, this thesis is dedicated to and inspired by my mother, Susan Harper, who died of metastatic breast cancer at the age of just 50. In her abbreviated time on this earth, she achieved a lot and has been a continuous source of inspiration. Working in cancer research has been an honor and a privilege, and this thesis is dedicated to her memory.

Thank you,

Alison